5-1-2010

Development of renewable and hydrolytically degradable polymers from biomass-based monomers

Mathew Dennis Rowe

DEVELOPMENT OF RENEWABLE AND HYDROLYTICALLY DEGRADABLE POLYMERS FROM BIOMASS-BASED MONOMERS

By

Mathew Dennis Rowe

A Dissertation
Submitted to the Faculty of
Mississippi State University
in Partial Fulfillment of the Requirements
for the Degree of Doctor of Philosophy
in Chemical Engineering
in the Swalm School of Chemical Engineering

Mississippi State, Mississippi

May 2010

DEVELOPMENT OF RENEWABLE AND HYDROLYTICALLY DEGRADABLE POLYMERS FROM BIOMASS-BASED MONOMERS

By

Mathew Dennis Rowe

Approved:

_____ Keisha B. Walters Assistant Professor of Chemical Engineering (Director of Dissertation)	_____ Kirk H. Schulz President of Kansas State University (Committee Member)
_____ Judy Schneider Associate Professor of Mechanical Engineering (Committee Member)	_____ Priscilla J. Hill Associate Professor of Chemical Engineering (Committee Member)
_____ Hossein Toghiani Associate Professor of Chemical Engineering (Committee Member)	_____ Bill Elmore Associate Professor and Hunter Henry Chair of Chemical Engineering (Committee Member)
_____ Sarah A. Rajala Dean of the Bagley College of Engineering	_____ Lori M. Bruce Associate Dean for Research and Graduate Studies in the Bagley College of Engineering
_____ Rafael Hernandez Associate Professor of Chemical Engineering (Graduate Coordinator)	

Name: Mathew Dennis Rowe

Date of Degree: May 1st, 2010

Institution: Mississippi State University

Major Field: Chemical Engineering

Major Professor: Dr. Keisha B. Walters

Title of Study: DEVELOPMENT OF RENEWABLE AND HYDROLYTICALLY DEGRADABLE POLYMERS FROM BIOMASS-BASED MONOMERS

Pages in Study: 298

Candidate for Degree of Doctor of Philosophy

Renewable polymers (bioplastics) offer an alternative to petroleum-based polymers and reduced environmental impact through decreased petroleum dependence and a sustainable product lifecycle via renewable, biomass-derived monomers and completely degradable polymers. Applying green chemistry principles, melt polycondensations of 1,3-propanediol with malonic acid and 1,3-propanediol with itaconic acid were performed to produce poly(trimethylene malonte) (PTM) and poly(trimethylene itaconate) (PTI), respectively. Aluminum chloride was used as the catalyst and reaction temperatures from 125-175 °C and reaction times from 2-32 h were attempted in order to produce high yields and molecular weights (Mw). Gravimetric yields ranged from 20-95 wt.% for PTM and 20-85 wt.% for PTI. Both PTM and PTI contained ester and ether backbone bonds, as determined by Fourier transform infrared and nuclear magnetic resonance spectroscopy. Gel permeation chromatography showed both PTM and PTI to have a bi-modal Mw distributions centered at 1.4±0.1 kDa and 35±3 kDa for PTM and 1.0±0.1 kDa and 38±2 kDa for PTI. For PTM, a Tg of -64 °C and a Tm of 29 °C was identified using differential scanning calorimetry (DSC). A crystallization temperature for PTI was found at ~160 °C using DSC. A hydrolytic degradation study was performed at 25 °C on

PTM and PTI in pH 5.4, 7, 9, and 11 aqueous solutions for up to 4 weeks. The introduction of K^+ ions (in the KOH aq. solutions) interfered with the $A_{AC}2$ and $A_{AL}1$ ester hydrolysis mechanisms through acid-base interactions. PTM was found to be susceptible to hydrolytic degradation and lost ~37 wt.% through ester hydrolysis and showed a molecular weight reduction of ~0.8 kDa over 10,000 min for a pH range of 7 to 11. PTI was also found to be susceptible to hydrolytic degradation with ~22 wt.% decrease through ester hydrolysis and molecular weight reduction of ~0.25 kDa over 10,000 min for a pH range of 7 to 11. PTM is a low molecular weight, saturated, linear copolymer and PTI is a low molecular weight, unsaturated, branched copolymer. Both PTM and PTI are renewable copolymers produced using green chemistry and mild reactions conditions and were found to be susceptible to hydrolytic degradation.

Key Words: bioplastics, renewable polymers, polycondensation, hydrolytic degradation

DEDICATION

I would like to dedicate this research to my wife, Megan Rowe, and to my parents, Dennis and Cheryl Rowe, for all of their support.

ACKNOWLEDGEMENTS

The author would like to express gratitude to the people who have helped me through my dissertation and research over the past four years. Most of all, I would like to thank my director of dissertation Dr. Keisha Walters, for all her guidance through my research, and her assistance in editing and writing my dissertation. I would also like thank my committee members for their input on my research and dissertation: Dr. Kirk H. Schulz, Dr. Priscilla J. Hill, Dr. Judy Schneider, Dr. Bill Elmore, and Dr. Hossein Toghiani. This work was partially funded through the Sustainable Energy Research Center at Mississippi State University under U.S. Department of Energy award DE-FG3606GO86025. Financial support was also provided by MSU Bagley Fellowship. Completion of this work in a timely manner would not have been possible without undergraduate researchers Erin Smith and Mitch Wall, and Kimberly Ivey of Clemson University who completed the initial TGA and DSC work.

TABLE OF CONTENTS

APPENDIX

LIST OF TABLES

LIST OF FIGURES

CHAPTER 1

INTRODUCTION

Energy savings, weight savings, and durability of plastic makes it an ideal substitutes for metal, paper, and glass, but petroleum-based plastic lacks the sustainability of renewable plastic. Since 1976 plastics have been the most used material by weight world-wide [Finkelstein 2004]. In 2008, 30.05 million tons plastic waste was generated and only 7.6 wt% was recycled [EPA 2008]. Renewable plastics produced from biomass-derived monomers, known as bioplastics, are sustainable polymeric materials that are also biologically and/or hydrolytically degradable. Polyhydroxyalkanoates, poly(lactic acid) [Williams 2008, Shikanov 2005, van Beilen 2008, Gandini 2008, Phillip 2007], poly(glycolic acid) [Williams 2008, Shikanov 2005, van Beilen 2008, Gandini 2008], polysaccharides [Williams 2008, Shikanov 2005, van Beilen 2008, Gandini 2008], vegetable-derived polymers [Williams 2008, Shikanov 2005, van Beilen 2008, Gandini 2008], and poly(orthester) [Williams 2008, Shikanov 2005, van Beilen 2008, Gandini 2008]are just a few examples of different bioplastic types/classes. From each of these bioplastic classes, polymers with varied properties, cost, and degradation rates can be developed that rival petroleum-based plastics in terms of properties and cost [Phillip 2007, van Beilen 2008, Shikanov 2005, Patel 2005, Ragauskas 2006, Vert 2005, Narayan 2005, Willke 2004, Mohanty 2002, Finkelstein 2004, Okada 2002, Pillai 2009]. Bioplastics sustainability should go beyond just the standard “reduce, reuse, and recycle”, it should include green(er) chemistry to eliminate/reduce the use of organic solvents and hazardous chemicals, toxic by-products, and

energy intensive operations [Anastas 2010, Gaynor 2002]. Green chemistry design principles state that from inception to disposal, chemicals and chemical processes be designed to minimize hazards, maximize product utilization, use inherently less toxic chemistry, and degradation [Anastas 2010, Gaynor 2002, Wilson 2009, Kobayashi 2009, Garcia-Serna 2007, Poliakoff 2002].

Through the careful selection of non/low toxic monomers, catalysts, and organic solvents and careful selection of reaction conditions, green chemistry principals can be applied in the production of bioplastics. Monomer selection is critical to reduce environmental impact and follow green chemistry principals. Most commodity polymers are produced from petroleum-based monomers (a non-renewable resource) and are generally not degradable [Chen 2009, Chiellini 2004, Gandini 2008, Hoffmann 2009, Li 2006]. Biomass-derived monomers are renewable and proper selection can lead to the incorporation of hydrolysable bonds (e.g., anhydride, ester, and ether) to ensure that the resultant bioplastics will be susceptible to hydrolytic degradation, and possibly also biological degradation [Albertsson 2002, Gopferich 2002, Gopferich 1996, Tamada 1993, Helminen 2003]. Catalyst selection can dictate polymerization reaction conditions, reaction by-products, and purification procedures [Okada 2002, Jerome 2008, Sun 2002, Church 2003, Helminen 2003, John 1996, Storey 2001, Teramoto 2004]. Rare-earth metal and heavy metal organometallic catalysts have been proposed as catalysts for polymerization for their high selectivity and reaction yields, but are toxic to humans and the environment [Okada 2002, Jerome 2008, Sun 2002, Church 2003, Sun 2006, Spassky 2000, Morton 1985, Ishihara 2000, Takasu 2003]. Even if the organometallic catalysts do not have to be removed by purification, they become deactivated and need to be recycled or disposed thereby exposing people and the environment. In terms of worker and environmental health, effective no/low toxicity catalysts (homogenous or heterogeneous) should be identified and used. Reaction conditions influence energy usage, by-product production, and solvents

needed for polymerization and purification. Through the appropriate selection of reaction conditions, monomers, and catalysts the polymer chemistry and by-product formation can be controlled, to some degree, in a manner to avoid or minimize energy intensive purifications and solvent usage and yield polymers that can be degraded in a controlled manner using backbone bonds, crystallinity, and molecular weight as variables that can be controlled [Tamada 1993, Qiu 2001, Gouin 2000, Saha 2006, Quynh 2009, Shirahase 2006, El-Hadi 2002, Nostrum 2004]. Biodegradation is the most desirable method of degradation because it degrade polymers to carbon dioxide, water, carbon, and other basic molecules, but it is often possible under very limited conditions and would require specialized industrial composting that many municipalities are currently not equipped to handle [Albertsson 2002, Alvarez 2006, Vert 2005, Pivsa-Art 2002, Chiellini 2004, Nagata 1996, Okada 1996, Scherer 2001]. Abou-Zeid et al. degraded polyhydroxybutyrate and poly(hydroxybutyrate-co-hydroxyvalerate) using four strains of *Clostridum* under anaerobic conditions at 35 °C for 56 days with trace elements and vitamins [Abou-Zeid 2004]. Teramoto et al. biodegraded poly(butylenes succinate)-based polymers at pH 7.4 and 25 °C with $CaCl_2$, $MgSO_4$, NH_4Cl and $FeCl_2$ with activated sludge [Termoto 2005]. Nagata et al. degraded bioplastics based on glycerol and various diacids at 37 °C at pH 7.2 with *Rhizopus delemar* lipase for 24 h [Nagata 1996]. To ensure that bioplastics are degradable under a wide range of conditions, bioplastics need to be hydrolytically degradable, but in a controlled fashion [Albertsson 2002, Gopferich 2002, Satchell 1992, Smith 2007, Bruckner 2002, Saunders 1976]. In an effort to reduce dependence on petroleum-based plastics, green chemistry principles were utilized to produce novel, hydrolytically degradable bioplastics from 1,3-propanediol, malonic acid, and itaconic acid.

1.1. Monomer Selection

The availability of petroleum-based monomers is tied to the availability and price of petroleum, and so they are projected to become scarce and expensive as petroleum reserves dwindle. In 2004, U. S. Department of Energy (DOE) identified 12 building block chemicals having the greatest potential for development due to their functionality, availability, toxicity, and possible derivatives that can be derived from biomass: (1) 1,4 succinic, fumaric, and malic acids, (2) 2,5 furan dicarboxylic acid, (3) 3-hydroxy propionic acid, (4) aspartic acid, (5) glucaric acid, (6) glutamic acid, (7) itaconic acid, (8) levulinic acid, (9) 3-hydroxybutyrolactone, (10) glycerol, (11) sorbitol, (12) xylitol and arabinitol [Werpy 2004]. From these building block molecules, commodity, intermediate, and specialty chemicals can be produced [Committee on Biobased Industrial Products 1999, Werpy 2004]. In terms of polymerization, the selection of monomers from the DOE 12 building blocks list must consider other features besides only the potential for polymerization [Werpy 2004, Anastas 2010, Gaynor 2002, Wilson 2009, Kobayashi 2009, Garcia-Serna 2007, Poliakoff 2002]. Economic cost, availability, toxicity, and degradability of the polymer product have to also be taken into consideration. It is known that certain types of bonds are more susceptible to degradation through hydrolytic or biological degradation. Specifically, the presence of anhydride, ester, ether, and/or amide bonds in the resultant polymer facilitates biodegradation and hydrolytic degradation [Albertsson 2002, Gopferich 2002, Gopferich 1996, Tamada 1993, Helminen 2003]. To obtain these backbone functional groups, the more common polymerization techniques that have been used are polycondensation, ring opening polymerization (ROP), and ring opening metathesis polymerization (ROMP), but these are not the only techniques available [Albertsson 2002, Gopferich 2002, Gopferich 1996, Tamada 1993, Helminen 2003]. Monomers for polycondensation, ROP, or ROMP needs to be poly-functional, cyclic, or able to form a cyclic and

subsequently limit the possible biomass-based monomers from the DOE list because there are an infinite number of monomer from biomass [Odian 1991, Fradet 1982, Daoud 1990, Kuchanov 2004, Flory 1953-A]. In keeping with engineering (waste and energy minimization) and green chemistry principals, ROP and ROMP are not favored mechanisms due to polymerization complexity (need for tightly controlled atmosphere, high-purity solvents and monomers, sensitivity to air, and purification) and required catalysts [Odian 1991, Costa 2005, He 2004]. Selection of biomass-based monomers that can participate in polycondensation is one the simplest and low-cost means to develop novel bioplastics with properties comparable to petroleum-based plastics.

In designing a polycondensation reaction, considerations must be made for the polymer structure (e.g., linear, branched, block, alternating, graft) and polymer chemistry (made from a single monomer or multiple monomers). Linear and branched polymers dominate the petroleum-based plastics market; examples include poly(ethylene), poly(styrene), nylon, and poly(carbonate). In an effort to match properties, biomass-based monomers should be selected that will yield linear or branched polymers. For a linear polymer, any di-functional monomer with end groups susceptible to polycondensation would be acceptable [Odian 1991, Fradet 1982, Daoud 1990, Kuchanov 2004, Flory 1953-B]. A branched polymer requires a minimum of three functional groups present, but not all functional groups have to be susceptible to polycondensation [Odian 1991, Fradet 1982, Daoud 1990, Kuchanov 2004, Flory 1953-C]. In an effort to control branching, unsaturated monomers with two functional groups that can participate in polycondensation could be used [Odian 1991, Fradet 1982, Daoud 1990, Kuchanov 2004, Fardet 1982, Zetterlund 2002]. Using an unsaturated monomer allows for the potential to control branching and cross-linking during polymerization and/or after polymerization and can be used to tune the polymer properties [Fardet 1982, Zetterlund 2002]. In a further effort to be

able to tune polymer properties, copolymerization of two different monomers is preferred over the polymerization of a single monomer [Odian 1991, Costa 2005, He 2004]. By varying the ratio of two monomers, the copolymer properties could be expanded [Bacaloglu 1996, Tserki 2006, Takasu 2003]. To fine potential bioplastics to replace petroleum-based plastics, co-monomers with di-functionality should be selected for linear polymer prodcution, and unsaturated, di-functional co-monomers (or tri-functional monomers, see Appendix C) should be selected to produce branched and cross-linked polymers.

Identification of di-functional monomers available from biomass that are saturated or unsaturated produces an extensive list. In paring down this list, monomer cost and availability is not the only consideration. The amenability of the monomers to polycondensation and the expected final properties of the resultant polymers need to be considered. Polyhydroxyalkanoates and aliphatic polyesters and are the two largest classes of polymers produced from biomass. Polyhydroxyalkanoates are biologically-derived bioplastics [Phillip 2007, Chen 2009, Avella 2000] and do not fit into the goals of this study. Aliphatic polyesters are commonly formed from the monomers lactic acid and glycolic acid. Poly(lactic acid) (PLA) and poly(glycolic acid) (PGA) have been commercialized at various molecular weights despite problems with poor thermal stability and brittleness of the final product [Quynh 2009, Shirahase 2006, Catiker 2000, Hill 2006, Neffe 2010, Hoglund 2007, Ajioka 1997, Maharanan 2009, Moon 2000, Sodergard 1998, Dobrzynaski 2002]. Succinic acid is a building block and has been copolymerized with butylene for an increased melting point to make the commercialized polymer poly(butylene succinate) [Edlund 2003, Okada 2002, Zhu 2003, Takasu 2003]. A derivative of succinic acid, maleic acid, is an unsaturated variant of succinic acid, and it has been copolymerized with 1,3-propylene glycol and 1,4-butylene glycol to produce unsaturated polyesters. With both copolymers, isomerization competes with polymerization giving low

molecular weight polymers [Cristobal 1991, Cristobal 1990]. Attempts have been made at using adipic acid, a chemical from biomass, with diols, 1,3-butanediol and ethylene glycol [Chen 1982, Bacaloglu 1996]. The DOE noted in their "Top Value Added Chemicals from Biomass" publication that adipic acid had been examined previously with minimal success [Werpy 2004].

As mentioned above, a problem encountered with PLA and PGA is poor thermal stability and brittleness [Quynh 2009, Shirahase 2006]. To overcome these shortcomings of PLA and PGA , polymeric blends and copolymers of PLA, PGA, and poly(ε-caprolactone) (PCL) with one another and with other polymers have been attempted to provide better mechanical properties with varying degrees of success [Catiker 2000, Hill 2006, Neffe 2010, Hoglund 2007, Oyama 2009, Quynh 2009]. The use of glycerol, a derivative of biomass and bio-diesel production, dates back to Paul J. Flory and his pioneering work on polycondensation [Flory 1953-C]. Glycerol forms a network polyester under polycondensation conditions making it ideal for studying network polymers, but it has not been commercialized due to network formation and difficulties in processing network polymers [Flory 1953-C, Fu 2003, Kiyotsukuri 1994]. Two interesting derivatives of glycerol are 1,3-propanediol (PDO) and malonic acid (MA). PDO is used in at least two commercially available polymers, Corterra PTT® from Shell Chemical Company and Sorona® from DuPont Chemical Company [Werny 1999]. Research on the polymerization of PDO under a variety of polymerization conditions has been attempted with different comonomers and reaction conditions [Umare 2007, Liu 2002, Ranucci 2000, Witt 1994]. These prior studies with PDO provide a strong literature base from which to build a new series of polymers. MA has not been heavily studied for use in polymerizations. Dogan and Kusefoglu used MA with soy bean oil to produce a polymer with some success [Dogan 2008]. So the polymerization of MA is an area of research that present an opportunity for future research. Itaconic acid (IA) is another monomer from the DOE 12 building block list that could be used to produce an unsaturated

polymer [Willke 2004]. The majority of published research with IA has been in conjunction with acrylonitrile in non-polycondensation reactions [Chen 2007, Devasia 2003]. The di-acid, unsaturated structure of IA makes it a prime candidate for polycondensation with PDO to produce unsaturated polymers. The polycondensation of PDO with MA and IA would produce novel saturated and unsaturated polyesters that have the propensity to be hydrolytically and biologically degradable.

1.2. Catalyst Selection

Polycondensation is traditionally catalyzed by strong acids, which goes against green chemistry principals. For polycondensation to occur, the carbonyl carbon must be protonated through the $A_{AC}2$ or $A_{AL}1$ mechanisms (Figure 1.1 (a) and (b)) that will be discussed in detail in Chapters 2 and 4 [Satchell 1992, Smith 2007, Bruckner 2002, Saunders 1976]. To protonate the carbonyl carbon, a strong electrophile, such as a Lewis acid, is required [Satchell 1992, Smith 2007, Bruckner 2002, Saunders 1976, Odian 1991]. Enzyme-catalyzed polycondensation would follow green chemistry principals, but there is a lack of research with PDO, MA, and IA polycondensaiton with enzymes [Uyama 2001, Uyama 1999, Umare 2007, Metral 2005, Okada 2002, Jerome 2008, Sun 2002, Fu 2003]. If enzymes were used, an extensive research program with a survey of enzymes would be required and would necessitate new infrastructure. A parameter of this study was that bioplastic synthesis, purification, and processing would utilize existing equipment in plants that are currently producing petroleum-based polymers. Catalysts that show high selectivity and are heterogeneous, which would negate a need for catalyst separation from the final products, or homogeneous are rare earth metals and transition metals [Okada 2002, Jerome 2008, Sun 2002, Church 2003, Sun 2006, Spassky 2000, Morton 1985, Ishihara 2000, Takasu 2003]. These catalysts follow green chemistry principals by reducing the

need for solvents and energy intensive separations, but they do have major drawbacks. They are often highly toxic and would require extensive research into which ligands would provide the best selectivity for PDO, MA, and IA polycondensation. For renewable polymers such as PLA and PGA, a large body of work has been done with stannous octoate [Okada 2002, Jerome 2008, Sun 2002, Church 2003, Helminen 2003, John 1996, Storey 2001, Teramoto 2004]. The use of stannous octoate does pose a risk to the environment and is known to be toxic [Li 2004]. Another option is Lewis acids that are known to polymerize poly-acids and poly-alcohols by polycondensation [Ajioka 1997, Kajiyama 2003, Moon 2000, Sodergard 1998, Dobrzynski 2002, Odian 1991]. There is a wide selection of Lewis acids. In selecting a Lewis acid catalyst, the catalyst toxicity and effectiveness can be controlled somewhat by varying the base metal. By restricting the catalyst cost and minimizing toxicity, a limited number of Lewis acids are available for use as polycondensation catalysts.

(a)

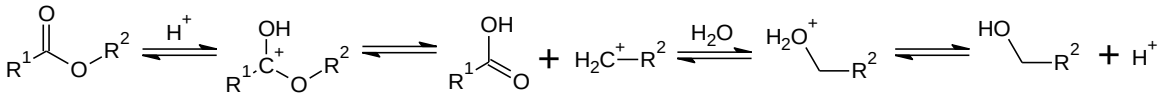

(b)

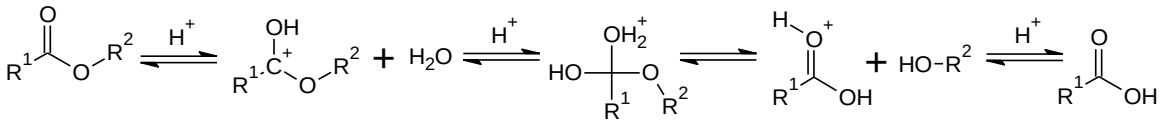

Figure 1.1: The $A_{AC}2$ and $A_{AL}1$ mechanisms for ester formation and hydrolysis [Satchell 1992, Smith 2007, Bruckner 2002, Saunders 1976].

1.3. Reaction Condition Selection

Along with monomer and catalyst selection, the reaction conditions affect the ability and ease to achieve high molecular weights. Melt polycondensation has been used to obtain high molecular weight polymers, and it is a green chemistry method [Odian 1991, Bacaloglu 1996, Olson 2006, Benabdillah 1999, Moon 2000, Lehton 1998, Salmi 2001]. Melt polycondensation avoids the use of solvents that must be removed after the reaction. Residual solvents are a critical concern for medical, food, and food packaging applications. The use of solvents can further complicate polycondensation since interactions between solvent and the monomers and polymers can lead to synergistic or detrimental complications in polymerization [Odian 1991, Kuchanov 2004]. To achieve the high conversions and molecular weights, vacuum is often used during polycondensations to remove low molecular reaction products, such as water and hydrochloric acid, and shift the equilibrium to favor reaction products [Ordelt 1991, Bacaloglu 1996, Olson 2006, Benabdillah 1999, Moon 2000, Lehton 1998, Salmi 2001, Fradet 1982]. Along with vacuum, bioplastics are temperature sensitive and require relatively lower

reaction temperatures [Harrison 2006, Bordes 2009, Zou 2009]. The optimum temperature for a specific polycondensation is dependent on the monomer(s), catalyst, and polymer. Using melt polycondensation with vacuum, the polymerization of PDO-MA and PDO-IA copolymers is expected to be successful.

1.4. Degradation

Along with considerations for catalysts, monomer, and reaction condition selection, the sensitivity of bioplastics to thermal, hydrolytic, and biological degradation is important in the selection of application and processing. Thermal degradation in polyhydroxyalkanoates (PHAs) and aliphatic polyesters occurs at lower temperatures than petroleum-based polyesters [Harrison 2006, Bordes 2009, Zou 2009]. A limited view of thermal degradation under real-world conditions is gained from thermal degradation without elevated pressures (e.g., uptake on roll, stacked sheet storage) and shear (e.g., extrusion). As compared to petroleum-based polyesters, PHAs and aliphatic polyesters exhibit increased rates of thermal degradation at temperatures typically encountered during polymer processing [Harrison 2006, Bordes 2009, Zou 2009]. Thermal degradation of PHAs and aliphatic polyesters, such as PLA, lead to decreases in Mw and mechanical properties and can be attributed to random main-chain scission [Carrasco 2006, Signori 2009]. Other minor pathways also contribute to thermal degradation, including depolymerization, oxidative degradation and transesterification [Signori 2009, Carrasco 2006, Zou 2009, Liu 2006].

Polymers that are classified as being biologically degradable by fungal or bacterial enzymes, such as PLA and PCL, may exhibit no degradation and appear biostable due to lack of any biological activity in the environment and will be further discussed in Chapter 4 [Albertsson 2002, Alvarez 2006, Vert 2005, Pivsa-Art 2002, Chiellini 2004, Nagata 1996, Okada 1996, Scherer

2001]. Incorporation of bonds in the polymer backbone that are acceptable to hydrolytic degradation through the $A_{AC}1$, $A_{AL}2$, and $B_{AC}2$ mechanisms (Figure 1.1 (a)), $A_{AL}2$ (Figure 1.1 (b)), and $B_{AC}2$ (Figure 1.2)mechanisms can overcome the short comings of biologically degradable polymers [Albertsson 2002, Gopferich 2002]. Using anhydride, ester, and ether that can be produced during polycondensation of alcohols and acids, the degradation rate can be controlled under varying pH and temperature conditions [Tamada 1993, Qiu 2001, Gouin 2000]. PHAs and aliphatic polyesters with high concentrations of anhydride bonds exhibit the highest rates of degradation, although the degradation rate can be slowed with the inclusion of ester and ether bonds into the polymer backbone [Gopferich 1996, Tamada 1993, Helminen 2003]. Anhydride modified PCL can be completely hydrolytically degraded in 24h at pH 7.4 and 37 °C, and salicylic acid based polymers experience completed degradation in 24h at pH 10 and 37 °C [Helminen 2003, Erdmann 2000]. Bioplastics containing only ester bonds can retain 50% of their strength for more than 20 days for PGA, or years for PLA [Chu 1981, Henton 2005]. PGA and poly(glycolide-lactide) (PGALA) hydrolytically degraded under pH ranging from 5.25 to 10.09 loss 50 % of breaking strength between 21 and 28 d at 7.44 pH for PGALA, and in comparison, PGA loss 50 % of breaking strength in 7 d at pH 10.09 [Chu 1981]. A change in pH or temperature can affect the rate of degradation by orders of magnitude with complete degradation time changing from under 20 h to over 8,000 h [Vert 1997, Erdmann 2000, Gopferich 1996, Kajiyama 2004, Tomihata 2001, Vasanthan 2009, Shirahase 2006]. In addition to pH affecting the degradation rate, the pH of the solution changes the mechanism by which degradation proceeds. In basic solutions, base mediated ester hydrolysis degradation is dominant and produces stable carboxylate anions by the $B_{AC}2$ (Figure 1.2) with a lack of excess water [Vasanthan 2009, Satchell 1992, Smith 2007, Bruckner 2002, Saunders 1976]. The acid catalyses ester hydrolysis is dominant in acidic solution ($A_{AC}2$ and $A_{AL}1$), and the degradation is driven by excess water and

can come to equilibrium state if degradation products are not removed [Vasanthan 2009, Satchell 1992, Smith 2007, Bruckner 2002, Saunders 1976]. The degradation, whether it be based mediated or acid catalyzed, can be broken down into three steps. The first step is the diffusion of water into the polymer. Second step is the hydrolytic degradation of bonds, and in the third step, degradation products diffusion out of the polymer into solution [Hofmann 2009, Li 1999, Hoglund 2007, Neffe 2010]. Two other factors strongly influence hydrolytic degradation, crystallinity and molecular weight (Mw), and affect the ability of water to diffuse into the polymer is affected by the crystallinity and molecular weight [Saha 2006, Quynh 2009, Shirahase 2006, El-Hadi 2002, Nostrum 2004]. A bioplastic with a high initial Mw decreases the rate of hydrolytic degradation due to the lack of end groups present to interact in the degradation [Li 2006, Alexis 2006, Saha 2006, Quynh 2009, Shirahase 2006, El-Hadi 2002, Nostrum 2004]. With increasing crystallinity and Mw, PLA degradation rate decreases due to changes in the ability of water to diffuse into the matrix [Saha 2006, Quynh 2009, Shirahase 2006, El-Hadi 2002, Nostrum 2004]. A method that has been used to control the degradation rate, by influencing crystallization and water diffusion rate, is cross-linking polymers. There are two effects with cross-linking of polymers, 1) cross-linking reduces crystallinity making the polymer more susceptible to water diffusion, and 2) cross-linking reduces the water permeability into the polymer [Quynh 2009, Hoglund 2007, Neffe 2009, Neffe 2010]. The physical size of the polymer samples affects hydrolytic degradation by increasing the time it takes water to diffuse into and the time it takes degradation products to diffuse out of the polymer sample. If the degradation products are retained in the polymer and are acidic, the polymer can have auto-catalytic degradation due to the increased end groups present [Li 1999]. By controlling the polymer back bond type, crystallinity, Mw, and size, the hydrolytic degradation rate can be varied in accordance to the application.

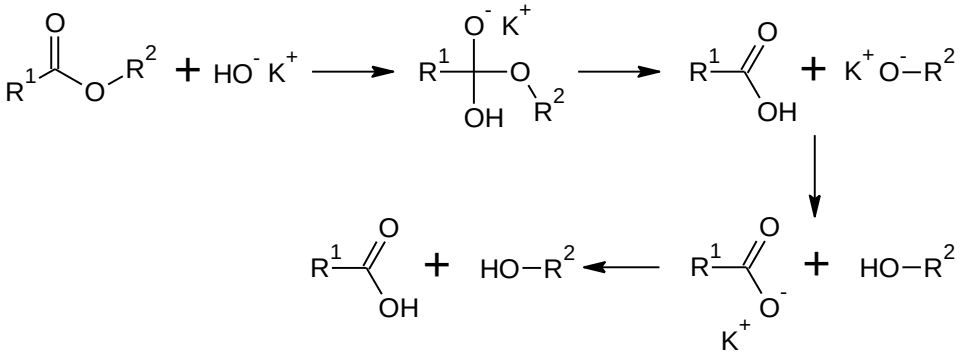

Figure 1.2: $B_{AC}2$ base mediated ester hydrolysis mechanism [Satchell 1992, Smith 2007, Bruckner 2002, Saunders 1976].

1.5. Objectives

The overall research objective is the development of polymers from biomass-derived monomers that are hydrolytically degradable, have potential to replace petroleum-based plastics, and are synthesized and processed following green chemistry principals. This work is specifically focused on determining whether PDO-MA and PDO-IA copolymers can be produced using melt polycondensation under mild conditions and with a no/low toxicity Lewis acid catalyst. The synthesis reactions were carried out under varied reaction times and temperatures and the resultant polymers were characterized to determine if they had sufficient chemical and physical properties to be a useful polymer. Hydrolytic degradation studies were conducted on these copolymers to determine the degradation kinetics, useful lifespan, and dependence of the degradation rate on environmental pH.

1.6. Dissertation Format

This dissertation is comprised of four research chapters: PDO-MA copolymerization and characterization (Chapter 2), PDO-IA copolymerization and characterization (Chapter 3), PDO-MA hydrolytic degradation (Chapter 4), and PDO-IA hydrolytic degradation (Chapter 5). Each of these chapters is formatted to be the basis for a stand-alone manuscript, and it is planned to submit these for publication. Therefore, there is necessarily some redundancy in references, materials and methods, introductions, and figures. Appendix A is a detailed description of all methods and procedures. The other appendices describe research efforts that were conducted but may not fit into individual manuscripts (Chapters 2-5): Appendix B, Examination of Stannous Octoate as a Catalyst; Appendix C, Copolymer from Glycerol and Fumaric Acid; Appendix D, Thermal Degradation of PTM; Appendix E, Alternative Monomer, Catalysts Ratio; Appendix F: PTM Kinetic Modeling, and Appendix G: PTM Atomic Force Microscopy.

1.7 References

Abou-Zeid, D.-M., Rolf-Joachim, M., Wold-Dieter, D., "Biodegradation of aliphatic Homopolyesters and Aliphatic-Aromatic Copolyesters by Anaerobic Microorganisms," Biomacromolecules, 5(5), 1687-1697, 2004.

Ajioka, M., Suizu, H., Higuchi, C., Kashima, T., "Aliphatic Polyesters and their Copolymers Synthesized through Direct Condensation Polymerization," Polymer Degradation and Stability, 59, 137-143, 1998.

Albertsson, A.-C., Varma, I. K., "Aliphatic Polyesters: Synthesis, Properties and Applications," Advances in Polymer Science, 157, 1-40, 2002.

Alexis, F., Venkatraman, S., Rath, S. K., Gan L.-H., "Some Insight into Hydrolytic Scission Mechanisms in Bioerodible Polyesters," Journal of Applied Polymer Science, 102, 3111-3117, 2006.

Alvarez, V. A., Ruseckaite, R. A., Vazquez, A., "Degradation of Sisal Fibre/Mater Bi-Y Biocomposites Buried in Soil," Polymer Degradation and Stability, 91, 3156-3162, 2006.

Anastas, P., Eghbali, N., "Green Chemistry: Principles and Practice," Chemical Society Reviews, 39, 301-312, 2010.

Avella 2000, M., Martuscelli, E., Raimo, M., "Review Properties of blends and Composites Based on Poly(3-Hydroxy)Butyrate (PHB) and Poly(3-Hydroxybutyrate-Hydroxyvalerate) (PHBV) Copolymers," Journal of Materials Science, 35, 523-545, 2000.

Bacaloglu, R., Fish, M., Biesiada, K., "Kinetics of Polyesterification of Adipic Acid," Polymer Engineering and Science, 36(6), 1014-1022, 1996.

Benadbillah, K. M., Coudane, J., Boustta, M., Engle, R., Vert, M., "Synthesis and Characterization of Novel Degradable Polyesters Derived from D-Gluconic and Glyclic Acids," Macromolecules, 32, 8774-8780, 1999.

Bordes, P., Hablot, E., Pollet, E., Averous, L., "Effect of Clay Organomodifiers on Degradation of Polyhydroxyalkanoates," Polymer Degradation and Stability, 94, 789-796, 2009.

Bruckner, R., "Nucleophilic Substitution Reactions on the Carboxyl Carbon (Except Through Enolates)," in Advanced Organic Chemistry, Elsevier, New York, 221-270, 2002.

Carrasco, F. Dionisi, D., Martinelli, A., Majone, M., "Thermal Stability of Polyhydroxyalkanoates," Journal of Applied Polymer Science, 100, 2111-2121, 2006.

Catiker, E., Gumusderelioglu, M., Guner, A., "Degradation of PLA, PLGA homo- and Copolymers in the Presence of Serum Albumin: A Spectroscopic Investigation," Polymer International, 49, 728-734, 2000.Chen, G.-Q., "A Microbial Polyhydroxyalkanoates (PHA) Based Bio- and Materials Industry," Chemistry Society Review, 38, 2434-2446, 2009.

Chen, J., Wang, C., Ge, H., Bai, Y., Wang, Y., "Effect of Coagulation Temperature on the Properties of Poly(Acrylonitrile-Itaconic) Acid Fibers in Wet Spinning," Journal of Polymer Research, 14, 223-228, 2007.

Chen, S.-A., Wu, K.-C., "Kinetics of Polyesterification. II. Foreign Acid Catalyzed Dibasic Acid and Glycol Systems," Journal of Polymer Science: Polymer Chemistry Edition, 20, 1819-1831, 1982.

Chiellini, E. Cinelli, P., Chiellini, F. Iman S. H., "Environmentally Degradable Bio-Based Polymeric Blends and Composites," Macromolecular Bioscience, 4, 218-231, 2004.

Chu, C. C., "Hydrolytic Degradation of Polyglycolic Acid: Tensile Strength and Crystallinity Study," Journal of Applied Polymer Science, 26, 1727-1734, 1981.

Church, A. C., Smith, J. A., Pawlow, J. H., Wagener, K. B., "Nontraditional Step-Growth Polymerization: ADMET," in Synthetic Methods in Step-Growth Polymers, John Wiley & Sons, New York, 431-526, 2003.

Committee on Biobased Industrial Products, Board on Biology, Commission on Life Sciences, National Research Council, "Biobased Industrial Products: Priorities for Research and Commercialization," National Academy Press, Washington, D. C., 1-13, 1999.

Costa, M. R. P. F. N., Bachmann, R., "Poly Condensation," in Handbook of Polymer Reaction Engineering, Wiley-VCH, Weinheim, 57-152, 2005.

Cristobal, J., Larez, V., Mendoza, G. A. P., "Unsaturated Polyesters. III. Polyester from Maleic Anhydride and 1,4-Butylene Glyxol, Journal of Applied Polymer Science, 43, 1605-1607, 1991.

Cristobal, L. V., Mendoza, G. A. P., "Unsaturated Polyester 2. Polyester from Maleic Anhydride and 1,3-Propylene glycol," Polymer Bulletin, 23, 577-581, 1990.

Daoud, M., Lapp, A., "Branched Polymers and Gels," Journal of Physics: Condensed Matter, 2, 4021-4050, 1990.

Devasia, R., Reghunadhan, C. P. Nair, Sivadasan, P., Katherine, B. K., Ninan, K. N., "Cyclization Reaction in Poly(Acrylonitrile/Itaconic Acid) Copolymer: An Isothermal Differential Scanning Calorimetry Kinetic Study," Journal of Applied Polymer Science, 88, 915-920, 2003.

Dobrzynaski, P., Kasperczyk, J., Janeczek, H., Bero, M., "Synthesis of Biodegradable Glycolide/L-Lactide Copolymers using Iron Compounds as Initiators," Polymer, 43, 2595-2601, 2002.

Dogan, E., Kusefoglu, S., “Synthesis and In situ Foaming of Biodegradable Malonic Acid ESO Polymers,” Journal of Applied Polymer Science, 110, 1129-1135, 2008.

Edlund, U., Albertsson, A.-C., “Polyesters Based on Diacid Monomers,” Advanced Drug Delivery Review, 55, 585-609, 2003.

El-Hadi, A., Schnabel, R., Straube, E., Muller, G., Henning, S., “Correlation Between Degree of Crystallinity, Morphology, Glass Temperature, Mechanical Properties and Biodegradation of Poly(3-hydroxyalkanoate) PHAs and their Blends,” Polymer Testing, 21, 665-674, 2002.

Environmental Protection Agency, “Municipal Solid Waste Generation, Recycling, and Disposal in the United States: Facts and Figures for 2008.” Unites States Environmental Protection Agency, 2008.

Erdmann, L., Uhrich, K. E., “Synthesis and Degradation Characteristics of Salicylic Acid-Derived Poly(anhydride-esters),” Biomaterials, 21, 1941-1946, 2000.

Erdmann, L., Uhrich, K. E., “Synthesis and Degradation Characteristics of Salicylic Acid-Derived Poly(anhydride-esters),” Biomaterials, 21, 1941-1946, 2000.

Finkelstein, M., McMillan, J. D., Davison, B. H., Evans, B., “Opportunities in the Industrial Biobased Products Industry,” Applied Biochemistry and Biotechnology, 113-116, 871-885, 2004.

Flory, P. J., Principles of Polymer Chemistry, Cornell University, 29-36, 1953-A.

Flory, P. J., Principles of Polymer Chemistry, Cornell University, 79-82, 1953-B.

Flory, P. J., Principles of Polymer Chemistry, Cornell University, 347-398, 1953-C.

Fradet, A., Marechal, E., “Kinetics and Mechanisms of Polyesterification I. Reactions of Diols with Acids,” Advances in Polymer Science, 43, 51-142, 1982.

Fradet, A., Marechal, E., “Study on Models of Double Bond Saturation During the Synthesis of Unsaturated Polyesters,” Makromolekulare Chemie, 183, 319-329, 1982.

Fu, H., Kulshrestha, A. S., Gao, W. Gross, R. A., “Physical Characterization of Sorbitol or Glycerol Containing Aliphatic Copolyesters Synthesized by Lipase-Catalyzed Polymerization,” Macromolecules, 26, 9804-9808, 2003.

Gandini, A., “Polymers from Renewable Resources: A Challenge for the Future of Macromolecular Materials,” Macromolecules, 41(24), 9491-9504, 2008.

Garcia-Serna, J., Perez-Barrigon, L., Cocero, M. J., “New Trends for Design Towards Sustainability in Chemical Engineering: Green Engineering,” Chemical Engineering Journal, 133, 7-30, 2007.

Gaynor, S., Qiu, J., Matyjaszewski, K., "Using Atom Transfer Radical Polymerization in Environmentally Benign Processes," in Advancing Sustainability through Green Chemistry and Engineering, American Chemical Society, Washington, D.C.,113-204, 2002.

Gopferich, A., "Mechanisms of Polymer Degradation and Erosion," Biomaterials, 17, 103-114, 1996.

Gopferich, A., Tessmar, J., "Polyanhydride Degradation and Erosion," Advanced Drug Delivery Reviews, 54, 911-931, 2002.

Gouin, S., Zhu, X. X., Lehnert, S., "New Polyanhydrides Made from a Bile Acid Dimer and Sebacic Acid: Synthesis, Characterization, and Degradation," Macromolecules, 33, 5379-5383, 2000.

Harrison, G. M., Melik, D. H., "Application of Degradation Kinetics to the Rheology of Poly(hydroxyalkanoates)," Journal of Applied Polymer Science, 102, 1794-1802, 2006.

He, Z., Whale, E. A., Davis, F. J., "Step-Growth Polymerization – Basics and Development of New Materials," Polymer Chemistry: A Practical Approach, Oxford University Press, Oxford, 126-144, 2004.

Helminen, A., O., Korhonen, H., Seppala, J.V., "Crosslinked Poly(ester anhydride)s Based on Poly(ε-caprolactone) and Polylactide Oligomers," Journal of Polymer Science: Part A: Polymer Chemistry, 41, 3788-3797, 2003.

Henton, D. E., Gruber, P., Lunt, J., Randall, J., "Polylactic Acid Technology," Natural Fibers, Biopolymers, and Biocomposites, CRC Press, Boca Raton, FL, 527-577, 2005.

Hill, S. P., de Oca, H. M., Klein, P. G., Ward, I. M., Rose, J., Farrar, D., "Dynamic Mechanical Studies of Hydrolytic Degradation in Isotropic and Oriented Maxon B," Biomaterials, 27, 3168-3177, 2006.

Hofmann, D., Entrialgo-Castano, M., Kratz, K., Lendlein, A., "Knowledge-Based Approach towards Hydrolytic Degradation of Polymer-Based Biomaterials," Advanced Materials, 21, 3237-3245, 2009.

Hoglund, A., Odelius, K., Hakkarainen, M., Albertsson, A.-C., "Controllable Degradation Product Migration from Cross-Linked Biomedical Polyester-Ethers through Predetermined Alterations in Copolymer Composition," Biomacromolecules, 8, 2025-2032, 2007.

Ishihara, K., Ohara, S., Yamamoto, H., "Direct Condensation of Carboxylic Acids with Alcohols Catalyzed by Hafnium(IV) Salts," Science, 290, 1140-1142, 2000.

Jerome, C., Lecomte, P., "Recent Advances in the Synthesis of Aliphatic Polyesters by Ring-Opening Polymerizaiton," Advanced Drug Delivery Reviews, 60, 1056-1076, 2008.

John, G., Tsuda, S., Morita, M., "Synthesis and Modification of New Biodegradable Copolymer: Serine/Glycolic Acid Based Copolymers," Journal of Polymer Science Part A: Polymer Chemistry, 35(10), 1901-1907, 1996.

Kajiyama, T., Kobayashi, H., Taguchi, T., Komatsu, Y., Kataoka, K., Tanaka, J., "Study on the Hydrolytic Degradation of Poly(α,β-Malic Acid) by Direct Polycondensation," Materials Science and Engineering C, 24, 821-825, 2004.

Kajiyama, t., Taguchi, T., Kobayashi, H., Kataoka, K., Tanaka, J., "Synthesis of High Molecular Weight Poly(α,β-malic acid) for Biomedical use by Direct Polycondensation," Polymer Degradation and Stability, 81, 525-530, 2003.

Kiyotsukuri, T., Kanaboshi, M., Tsutsumi, N., "Network Polyester Films from Glycerol and Dicarboxylic Acids," Polymer International, 33, 1-8, 1994.

Kobayashi, S., Makino, A., "Enzymatic Polymer Synthesis: An Opportunity for Green Polymer Chemistry," Chemical Review, 209, 5288-5353, 2009.

Kuchanov, S., Slots, H., Stroeks, A., "Development of a Quantitative Theory of Polycondensation," Progress in Polymer Science, 29, 563-633, 2004.

Lehton, J., Salmi, T., Harju, T., Immonen, K., Paatero, E., Nyholm, P., "Dynamic Modelling of Simultaneous Reaction and Distillation in a Semibatch Reactor System," Chemical Engineering Science, 53(1), 113-121, 1998.

Li, H., Wang C., Bai, F., Yue, J., Woo, H.-G., "Living ring-Opening Polymerizaiton of L-Lactide Catalyzed by Red-Al," Organometallics, 23, 1411-1415, 2004.

Li, S., "Degradation of Biodegradable Aliphatic Polyesters," in Scaffolding in Tissue Engineering, CRC Press, Boca Raton, FL, 335-352, 2006.

Li, S., "Hydrolytic Degradation Characteristics of Aliphatic Polyesters Derived from Lactic and Glycolic Acids, Journal of Biomedical Materials Research," Applied Biomaterials, 48, 342-353, 1999.

Lindblad, M. S., Liu, Y., Albertsson, A.-C., Ranucci, E., Karlsson, S., "Polymers from Renewable Resources," Advances in Polymer Science, 157, 139-161, 2002.

Liu, Y., Rancucci, E., Soderqvist, M., Alvertsson, A.-C., "New Biodegradable Polymers from Renewable Sorces – Segmented Coplyesters of Poly(1,3-propanediol succinate) and Poly(ethylene glycol)., Journal of Bioactive and Compatible Polymers, 17, 209-219, 2002.

Liu, Z., Zou, Y., Li, W., Cao, G., Chen, W., "Kinetics of Thermo-Oxidative and Thermal Degradation of Poly(D,L-Lactide) (PDLLA) at Processing Temperature," Polymer Degradation and Stability, 91, 3259-3265, 2006.

Maharanan, T., Mohanty, B., Negi, Y. S., "Melt-Solid Polycondensation of Lactic Acid and its Biodegradability," Progress in Polymer Science, 34, 99-124, 2009.

Metral, G., Wentland, J., Thomann, Y., Tiller, J., "Biodegradable Poly(ester hydrazide)s via Enzymatic Polymerization," Macromolecular Rapid Communications, 26, 2005, 1330-1335.

Mohanty, A. K., Misra, M., Drzal, L. T., "Sustainable Bio-Composites from Renewable Resources: Opportunities and Challenges in the Green Materials World." Journal of Polymers and the Environment, 10(1/2), 19-26, 2002.

Moon, S, I,. Lee, C. W., Miyamtot, M., Kimura, Y. Melt Polycondensation of L-Lactic acid with Sn(II) Catalysts Activated by Various Proton Acids: A Direct Manufacturing Route to High Molecular Weigh Poly(L-lactic acid), Journal of Polymer Science, Part A: Polymer Chemistry, 38, 1673-1679, 2000.

Morton, M., Wu. M., "Organolithium Polymerization of ε-Caprolactone," in Ring-Opening Polymerization, Washington, D.C., 175-182, 1985.

Nagata, M., Kiyotsukuri, T., Ibuki, H., Tsutsumi, N., Sakai, W., "Synthesis and Enzymatic Degradation of Regular Network Aliphatic Polyesters," Reactive & Functional Polymers, 20, 165-171, 1996.

Narayan, R., "Plastics from Renewable Resources," Global Plastics Environmental Conference, Atlanta, February 23rd-25th, 2005.

Neffe, A. T., hanh, B. D., Steuer, S., Lendlein, A., "Polymer Networks Combining Controlled Drug Release, Biodegradation, and Shape Memory Capability," Advanced Materials, 21, 3394-3398, 2009

Neffe, A. T., Tronci, G. Alteheld, A. Lendlein, A., "Controlled Change of Mechanical Properties during Hydrolytic Degradation of Polyester Urethane Networks," Macromolecular Chemistry and Physics, 211, 182-194, 2010.

Nostrum, C. F. v., Veldhuis, T. F. J., Bos, G. W., Hennink, W. E., "Hydrolytic Degradation of Oligo(Lactic Acid): A Kinetic and Mechanistic Study," Polymer, 45, 6779-6787, 2004.

Odian, G., Principles of Polymerization, 3rd edition, John Wiley & Sons, New York, 41-197, 1991.

Okada, M., "Chemical Syntheses of Biodegradable Polymers," Progress in Polymer Science, 27, 87-133, 2002.

Okada, M., Okada, Y., Tao, A., Aoi, K., "Biodegradable Polymers Based on Renewable Resources: Polyesters Composed of 1,4:3,6-Dianhydroheitol and Aliphatic Dicarboxylic Acid Units," Journal of Applied Polymer Science, 62, 2257-2265, 1996.

Olson, D. A., Sheares, V. V., "Preparation of Unsaturated Linear Aliphatic Polyesters using Condensation Polymerization," Macromolecules, 39, 2808-2814, 2006.

Oyama, H. T., Tanaka, Y., Kadosaka, A., "Rapid Controlled Hydrolytic Degradation of Poly(L-Lactic Acid) by Blending with Poly(Aspartic Acid-co-L-Lactide)," Polymer Degradation and Stability, 94, 1419-1426, 2009.

Patel, M, Narayan, R., "Biobased Products? The Hope, the Doubts, and the Reality," Natural Fibers, Biopolymers and Biocomposites, 833-853, 2005.

Phillip, S., Keshavarz, T., Roy, I., "Review Polyhydroxyalkanoates: Biodegradable Polymers with a Range of Applications," Journal of Chemical Technology and Biotechnology, 82, 233-247, 2007.

Pillai, C. K. S., "Plastic Materials – The Resource Crunch and Transitions: Can Monomers and Polymers from Renewable Resources Meet the Demand?," Popular Plastics & Packaging, 41-54, 2009.

Pivsa-Art, S. Nakayama, A., Kawasaki, N., Yamamoto, N., Aiba, S., "Biodegradability Study of Copolyesteramides Based on Diacid Chlorides, Diamines, and Diols," Journal of Applied Polymer Science, 85, 774-784, 2002.

Poliakoff, M., Fitzpatrick, J. M., Farren, T. R., Anastas, P. T., "Green Chemistry: Science and Politics of Change," Science, 297, 807-825, 2002.

Qiu, L. Y., Zhu, K. J., "Design of a Core-Shelled Polymer Cylinder for Potential Programmable Drug Delivery," International Journal of Pharmaceutics, 219, 151-160, 2001.

Quynh, T. M., Mitomo, H., Yoneyama, M., Hien, N. Q., "Properties of Radiation-Induced Crosslinking Sterocomplexes Derived from Poly(L-Lactide) and Different Poly(D-Lactide)," Polymer Engineering and Science, 970-976, 2009.

Ragauskas, A. J., Williams, C. K., Bavison, B H., Britovsek, G., Cairney J., Eckert, C. A., Frederick, W. J., Hallett, J., P., Leak, D. J., Liotta, C. L., Mielenz, J. R., Murphy, R., Templer, R., Tschaplinski, T., "The Path Forward for Biofuels and Biomaterials," Science, 311, 484-489, 2006.

Ranucci, E., Liu, Y., Lindblad, M. S. L., Albertsson, A.-C., "New biodegradable Polymers from Renewable sources. High Molecular Weight Poly(Ester Carbonate)s From Succinic Acid and 1,3-Propanediol," Macromolecular Rapid Communications, 21, 680-684, 2000.

Saha, S. K., Tsuji, H., "Effects of Molecular Weight and Small Amounts of D-Lactide Units on Hydrolytic Degradation of Poly(L-Lactic Acid)s," Polymer Degradation and Stability, 91, 1665-1673, 2006.

Salmi, T., Paatero, E., Lehtonen, J., Nyholm, P., Harju, T., et al, "Polyesterification Kinetics of Complex Mixtures in Semibatch Reactors," Chemical Engineering Science, 56, 1293-1298, 2001.

Satchell, D. P. N., Satchell, R. S., "Mechanistic Aspects. Recent Developments Concerning Mechanisms of Acylation by Carboxylic Acid Derivatives," in Supplement B: The

Chemistry of Acid Derivatives, Vol. 2, John Wiley & Sons, Ltd., Hoboken, New Jersey, 747-802, 1992.

Saunders, J. H., Dobinson, F., "The Kinetics of Polycondensation Reactions," in Comprehensive Chemical Kinetics, Vol. 15, Bamford, C. H., Tippers, C. F. H., American Elsevier, New York, 473-581, 1976

Scherer, T. M., Rothermich, M. M., Quinteros, R., Poch, M. T., Lenz, R. W., Goodwin, S., "Broad-Based Screening of Polymer Biodegradability," in Polymers from Renewable Resources, American Chemical Society, Washington D. C., 254-280, 2001.

Scholz, C., Gross, R. A., "Biopolyesters and Biocatalysis Introduction," Polymers from Renewable Sources: Biopolyesters and Biocatalysts, Oxford University Press, Oxford, 1-11, 2000.

Scott, G., "Why Degradable Polymers?" Degradable Polymers, 2nd edition, Kluwer Academic Publisher, Dordrecht, Netherlands, 1-15, 2002.

Shikanov, A. Kumar, N., Domb, "Biodegradable Polymers: An Update," Israel Journal of Chemistry, 45, 393-399, 2005.

Shirahase, T., Komatsu, Y., Tominaga, Y., Asai, S., Sumita, M., "Miscibility and Hydrolytic Degradation in Alkaline Solution of Poly(L-Lactide) and Poly(Methyl Methacrylate) blends," Polymer, 47, 4829-4844, 2006.

Signori, F., Coltelli, M.-B., Bronco, S., "Thermal Degradation of Poly(lactic acid) (PLA) and Poly(butylenes adipate-co-terephthalate) (PBAT) and Their Blends upon Melt Processing," Polymer Degradation and Stability, 94, 74-82, 2009.

Smith, M., March, J., "Aliphatic Substitution: Nucleophilic and Organometallic," in March's Advanced Organic Chemistry, 6th ed., Wiley-Interscience, Hoboken, New Jersey, 425-656, 2007.

Sodergard, A., Stolt, M., "Ring-Opening Polymerizaiton of L-lactide by Means of Different Iron Compounds," Macromolecular Symposium, 130, 393-402, 1998.

Spassky, N., Simic, V., "Polymerization and Copolymerization of Lactides and Lactones using Some Lanthanide Initiators," in Polymers from Renewable Resources, American Chemical Society, Washington, DC, 146-159., 2000.

Storey, R. F., Sherman, J. W., "Novel Synthesis of (Carboxylic Acid)-Telechelic Poly(ε-Caprolacton)," Polymer Preprints, 42(2), 2001.

Sun, H., Chen, S., Yao, Y., Shen, Q., Yu, K., "Homoleptic Lanthanide Metallocenes and their Derivatives: Syntheses, Structural Characterization and their Catalysis for Ring-Opening Polymerization of ε-Caprolactone," Applied Organometallic Chemistry, 20, 310-314, 2006.

Sun, J., Shi, W., Chen, D., Liang, C., "The Ring-Opening Polymerization of D,L-Lactide Catalyzed by New Complexes of Cu, Zn, Co, and Ni Schiff Base Derived from Salicylidene and L-Aspartic Acid," Journal of Applied Polymer Chemistry, 86, 3312-3315, 2002.

Takasu, A., Oishi, Y., Iio, Y., Inai, Y., Hirabayashi, Y., "Synthesis of Aliphatic Polyesters by Direct Polyesterificaiton of Dicarboxylic Acids with Diols under Mild conditions Catalyzed by Reusable Rare-Earth Triflate," Macromolecules, 36, 1772-1774, 2003.

Tamada, J. A., Langer, R., "Erosion Kinetics of Hydrolytically Degradable Polymers," Proceedings of the National Academy of Science, 90, 552-556, 1993.

Teramoto, N., Kogure, H., Kimura, Y., Shibata, M., "Thermal Properties and Biodegradability of the copolymers of L-Lactide, ε-Caprolactone, Ethylene Glycol Oligomer with Maleate Units and their Crosslinked Products," Polymer, 45, 7927-7933, 2004.

Tomihata, K., Suzuki, M., Ikada, Y., "The pH Dependence of Monofilament Sutures on Hydrolytic Degradation," Journal of Biomedical Materials Research Part B: Applied Biomaterials, 58(5), 511-518, 2001.

Tserki, V., Matzinos, P., Pavlidou, E., Panayiotou, C., "Biodegradable Aliphatic Polyesters. Part II. Synthesis and Characterization of chain Extended Poly(Butylene Succinate-co-butylene Adipate)," Polymer Degradation and Stability, 91, 377-384, 2006.

Umare, S. S., Chandure, A. S., Pandely, R. A., "Synthesis, Characterization, and Biodegradable Studies of 1,3-Propanediol Based Polyesters, 2007," Polymer Degradation and Stability, 92, 464-497, 2007.

Uyama, H., Inada, K., Kobayashi, S., "Regioselectivity control in Lipase-Catalyzed Polymerization of Divinyl Sebacate and Triols," Macromolecular Bioscience, 1, 4-44, 2001.

Uyama, H., Yaguchi, S., Kobayashi, S., "Lipase-Catalyzed Polycondensation of Dicarboxylic Acid-Divinyl Esters and Glycols to Aliphatic Polyesters," Journal of Polymer Science: Part A: Polymer Chemistry, 37, 2737-2745, 1999.

van Beilen, J., Poirier, Y., "Production of Renewable Polymers from Crop Plants," The Plant Journal, 54, 684-701, 2008.

Vasanthan, N., Ly, O., "Effect of Microstructure on Hydrolytic Degradation Studies of Poly(L-Lactic Acid) by FTIR Spectroscopy and Differential Scanning Calorimetry," Polymer Degradation and Stability, 94, 1364-1372, 2009.

Vert, M., "Aliphatic Polyesters: Great Degradable Polymers that Cannot Do Everything," Biomacromolecules, 6, 538-546, 2005.

Vert, M., Li, S., Garreau, H., Mauduit, J., Boustta, M., Schwach, G., Engel, R., Coudane, J., "Complexity of the Hydrolytic Degradation of Aliphatic Polyesters," Die Angewandte Makromolekulare Chemie, 247, 239-253, 1997.

Werny, F., Chuah, H., “Corterra PTT – A New Polymer for the Carpet Industry”, Shell Chemicals, 1999.

Werpy, T., Petersen, G., “Top Value Added Chemicals from Biomass. Volume I: Results of Screening for Potential Candidates from Sugars and Synthesis Gas,” U.S. Department of Energy, Energy Efficiency and Renewable Energy, 2004.

Williams, C., K., Hillmyer, M. A., “Polymers from Renewable Resources: A Perspective for a Special Issue of Polymer Review,” Polymer Reviews, 48, 1-10, 2008.

Willke, T., Vorlop, K. D., “Industrial Bioconversion of Renewable Resources as an Alternative to Conventional Chemistry,” Applied Microbiology and Biotechnology, 66, 131-142, 2004.

Wilson, M. P., Schwarzman, M. R., “Toward a New U.S. Chemicals Policy: Rebuilding the Foundation to Advance New Science, Green Chemistry, and Environmental Health,” Environmental Health Perspectives, 117(8), 1202-1209, 2009.

Witt, U., Műller, R.-J., Augusta, J., Widdecke, H., Deckwer, W.-D., Synthesis, Properties and Biodegradability of Polyesters based on 1,3-Propanediol, Macromolecular Chemistry and Physics, 195, 793-802, 1994.

Zetterlund, P. B., Weaver, W., Johnson, A. F., “Kinetics of Polyesterification: Modelling of the Condensation of Maleic anhydride, Phthalic Anhydride, and 1,2-Propylene Glycol,” Polymer Reaction Engineering, 10(1&2), 41-57, 2002.

Zhu, C., Zhang, Z. Liu, Q., Wang, Z. Jin, J., “Synthesis and Biodegradation of Aliphatic Polyesters from Dicarboxylic Acids and Diols,” Journal of Applied Polymer Science, 90, 982-990, 2003.

Zou, H., Yi, C., Wang, L., Liu, H., Zu, W., “Thermal Degradation of Poly(Lactic Acid) Measured by Thermogravimetry Couple to Fourier Transform Infrared Spectroscopy,” Journal of Thermal Analytical Calorimetry, 97, 929-935, 2009.

CHAPTER 2

SYNTHESIS AND CHARACTERIZATION OF COPOLYMERS BASED ON RENEWABLY RESOURCED MONOMERS 1,3-PROPANEDIOL AND MALONIC ACID

2.1. Abstract

To reduce our environmental impact and reduce our dependence on petroleum based polymers, renewable based polymers, bioplastics, were polymerized from renewably resourced monomers 1,3-propanediol (PDO) and malonic acid (MA) using green chemistry principals to make poly(trimethylene malonate) (PTM). Reaction time was varied from 2 to 16 h, and reaction temperature was varied from 125 to 175 °C to maximize gravimetric yield and molecular weight using melt polycondensation. Four catalysts were attempted under mass transfer limited conditions, no vacuum or stirring of reaction. The Lewis acids aluminum chloride, iron (III) chloride, tin (II) chloride, and zinc chloride were surveyed over varied reaction temperatures of 125 to 175 °C. The gravimetric yields and attenuated total reflectance Fourier transform infrared (ATR-FTIR) spectroscopy were used to characterize the catalysts survey. Gravimetric yield did not have a dependence on catalysts as a function of reaction temperature and the maximum yield was less than 60 wt.% obtained between 145 and 165 °C. ATR-FTIR showed that aluminum chloride had the highest concentration of ester carbonyls at 1726 and 1749 cm^{-1}. Aluminum chloride was chosen for further study due to its higher reactivity and higher concentration of ester bonds. A second study was performed polymerizing PDO and MA with aluminum chloride with vacuum and stirring with varied reaction temperatures, 125 to 175

°C, and varied reaction time, 2 to 16 h. Gravimetric yield was determined as a function of reaction temperature and time, and it varied from 20 to 95 wt.%. To determine the chemical structure, transmission Fourier transform infrared (FTIR) spectroscopy, proton nuclear magnetic resonance (NMR), and x-ray photoelectron spectroscopy (XPS) were used, and they confirmed the presence of ester and ether bonds with concentrations dependent on reaction time and temperature. Gel-permeation chromatography (GPC) was used to determine molecular weight and polydispersity index. A bi-modal molecular weight distribution was found, and it was dependent on both reaction temperature and time. The high molecular weight ranged from 25 to 45 kDa, and the low molecular weight did not exceed 2.5 kDa. Thermal analysis was performed using thermogravimetic analysis (TGA) and differential scanning calorimetry (DSC). TGA showed that 5 wt.% loss occurred at a minimum of 113 °C and was dependent on reaction temperature. The Tg was found by DSC to vary between -66 and -41 °C and was dependent on reaction temperature. A Tm was present at ~29 °C for PTM polymerized at 135 and 155 °C (4 h, aluminum chloride) by DSC. Copolymers of PDO and IA were made chemical structures and molecular weights dependent on reaction temperature.

2.2. Introduction

From environmental, economic, and political factors, along with the increasing scarcity of petroleum feedstocks, the need has arisen to develop biomass-based plastics (bioplastics) that have equivalent or better properties than petroleum-based plastics. There are currently bioplastics on the market, but the distinct types and subsequently thermal and mechanical properties are limited [Albertsson 2002, Mohanty 2000, Phillip 2007]. With biomass containing thousands of precursors for the production of polymers, monomer options, along with the resultant bioplastics, are numerous. Saturated and unsaturated poly-acids and poly-alcohols can

be derived and separated from wide-ranging biomass feedstocks and used to develop many novel bioplastics with ester, anhydride, and ether linkages that are susceptible to hydrolysis and biodegradation [Ragauskas 2006, Dodds 2007]. Exploration of novel monomers beyond lactic acid, glycolic acid, and 3-hydroxybutyrate acid used in commercial bioplastics is necessary to achieve a greater range of chemical and physical properties, mimicking the wide range of properties found in petroleum-based plastics [Drumright 2000, Phillip 2007, Mohanty 2000, Albertsson 2002]. Bi-functional monomers available in biomass, such as 1,3-propanediol (PDO) and malonic acid (MA), are useful in the production of linear copolymers that may have similar properties to linear petroleum-based polyesters, poly(trimethylene malonate) (PTM). For slightly branched and cross-linked polymers, the unsaturated monomer itaconic acid (IA) can be co-polymerized with PDO. The primary difficulty in synthesizing these polymers is the selection of catalyst and reaction conditions to achieve functional group conversions above 99.5%.

In melt polycondensations, if functional group conversions above 99.5% are not achieved, molecular weight will be below the critical entanglement molecular weight, and the polymer will not have useful properties [Odian 1991]. The selection of catalyst and reaction conditions becomes critical to achieve the necessary yield. Lewis acids are common catalysts in the production of polyesters, with the health and environmental hazards varying substantially with each compound [Ajioka 1998, Kajiyama 2003, Moon 2000, Sodergard 1998, Dobrzynski 2002, Odian 1991]. Stannous octoate is a common catalyst for the production of poly(lactic acid) and produces polymers with useful properties [Okada 2002, Jerome 2008, Sun 2002, Church 2003, Helminen 2003, John 1996, Storey 2001, Teramoto 2004]; however, there are drawbacks when considering leaving stannous octoate in the final product. The possible organotin biodegradation products from stannous octoate can be more toxic than the initial catalyst, which is of concern when producing bioplastics that are susceptible to biodegradation [Li 2004].

Other Lewis acids, such as aluminum chloride, pose less risk to human and environmental health and may be better choices than stannous octoate. Along with the selection of catalyst, the optimization of reaction conditions will dictate whether a polymer has useful thermal and mechanical properties. Controlling reaction conditions (time, temperature, co-monomer molar ratio, catalyst-monomer molar ratio, pressure, and mixing) will allow for manipulation of the bioplastic properties for specific applications, such as packing materials, films, and structural elements. When considering reaction conditions, minimizing the use of energy, solvents, and feedstocks to produce the maximum amount of product is not only economically responsible, but it is also environmentally responsible and will increase the competitiveness of the product with petroleum-based plastics. The manipulation of reaction conditions can also affect the rate of degradation though modification of chemical structure and molecular weight to dictate the useable lifespan of the bioplastic [Gopferich 1996, Tamada 1993, Helminen 2003, Erdmann 2000, Chu 1981, Henton 2005]. The use of different monomers, catalyst, and reaction conditions will allow for tailoring of properties and lifetimes to the specific application.

To predict the chemical structure of bioplastics made through melt polycondensation, an understanding of the basic reaction pathways is needed. Polycondensation involving carboxylic acid and alcohol groups may follow one of four possible reversible acid-catalyzed reaction pathways [Satchell 1992, Smith 2007, Bruckner 2002, Saunders 1976]. In a successful polycondensation reaction, equilibrium is driven to favor products and make the reactions appear irreversible. The irreversibility is usually accomplished by the removal of side products such as water or hydrochloric acid. Four simultaneous reaction pathways have been proposed with the $A_{AC}1$ and $A_{AC}2$ mechanisms starting with the acid and proceeding to an ester with the loss of a low Mw byproduct, and the $A_{AC}2$, Figure 2.1 (a), mechanism is considered the dominant of the two mechanisms [Satchell 1992, Smith 2007, Bruckner 2002, Saunders 1976]. The $A_{AL}1$

and $A_{AL}2$ mechanisms have been theorized, but the $A_{AL}2$ mechanism has not been observed to occur during polycondensation [Satchell 1992, Smith 2007, Bruckner 2002, Saunders 1976]. The $A_{AL}1$ mechanism, Figure 2.1 (b), along with $A_{AC}2$ mechanism is considered the dominant mechanisms in polycondensation. For dilute reactions, monomer and reaction product solubilities and polarities become important and can dictate the Mw and structure of the products.

(a)

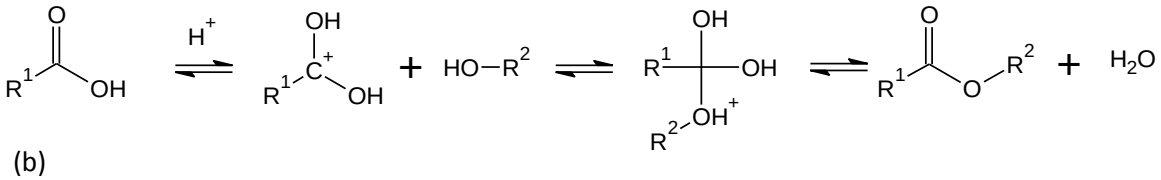

(b)

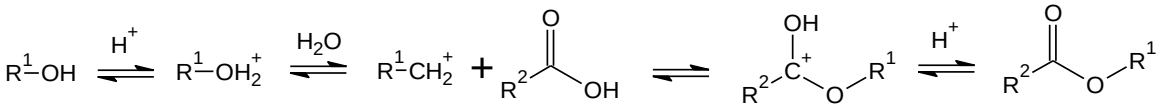

Figure 2.1: Potential reversible di-acid and di-alcohol polycondensation mechanisms: $A_{AC}2$ (a) and $A_{AL}1$ (b) [Satchell 1992, Smith 2007, Bruckner 2002, Saunders 1976].

The polycondensation mechanisms shown in Figure 2.1 and discussed above are valid for a step growth model of polycondensation, but polycondensation can also follow a chain growth mechanism. Within a given system, polycondensation generally follows both chain and step growth paths simultaneously, making the system description difficult [Kricheldorf 2003]. Flory defined step growth polymerization as involving equal end group reactivity, reactivities unaffected by molecular size, and the elimination of small by-products in every propagation step [Flory 1953].

It also has been shown with matrix-assisted laser desorption-ionization time-of-flight (MALDI-TOF) that cyclic molecules with molecular weights of 55 kDa easily cyclize at any concentration, and the cyclization reaction can compete with the polycondensation reaction [Krichldorf 2003]. Furthermore, Flory did not differentiate between kinetically-controlled and thermodynamically-controlled polycondensation reactions [Krichldorf 2003]. Kinetics also affects the feasibility and stability of ring formation with the thermodynamically controlled polycondensation reaction. The product of a kinetically controlled polymerization may be unstable and may change its structure to become thermodynamically stable [Krichldorf 2007, Kuchanov 2004]. Furthermore, a thermodynamically controlled reaction is reversible and is also able to form ring structures. However, cyclics from a thermodynamically controlled reaction are limited in size by ring strain and are most favored to form five, six, and seven member rings. Flory's treatment of only ideal polycondensation leaves out several reactions, including cyclization. While Flory considered only the reaction of direct esterification, at least five other reactions can be considered (Table 1) [Flory 1946, Odian 1991, Saunders 1976].

Table 2.1: Flory's direct esterification reaction and five other reactions that need to be considered during polycondensation [Odian 1991, Saunders 1976, Flory 1946].

Direct Esterification	$ROH + R_1COOH \leftrightarrow R_1COOR + H_2O$
Alcoholysis	$ROH + R_1COOR_2 \leftrightarrow R_1COOR + R_2OH$
Acidolysis	$RCOOH + R_1COOR_2 \leftrightarrow RCOOR_2 + R_1COOH$
Double Ester Interchange	$R_1COOR_2 + R_3COOR_4 \leftrightarrow R_1COOR_4 + R_3COOR_2$
Self-Condensation of Hydroxy Acids	$nHORCOOH \leftrightarrow (HORCOO)_n + nH_2O$
Schotten-Baumann Reaction	$R_1COCl + R_2OH \leftrightarrow R_1COOR_2 + HCl$

The catalysts used for renewable copolymer production need to be environmentally benign, biocompatible, easily handled, and low cost. Aluminum, iron, zinc, and tin, for the most part, are environmentally benign, biocompatible, easily handled, and low cost [Ajioka 1998, Kajiyama 2003, Moon 2000, Sodergard 1998, Dobrzynski 2002, Odian 1991]. While these metals may not perfectly fit the criteria outlined above, they are good starting catalyst components for renewable copolymer development. The reaction of these elements with hydrogen chloride leads to strong Lewis acids, which have been shown to be good catalysts for the cationic polymerization of lactones and derivatives of glycerol [Kricheldorf 1984, Abraham 2000, Moon 2000]. The catalysts selected for this study include aluminum chloride, iron(III) chloride, tin(II) chloride, and zinc chloride.

1,3-Propanediol (PDO) and malonic acid (MA) copolymer bioplastics were produced using aluminum chloride, iron(III) chloride, tin(II) chloride, and zinc chloride under melt polycondensation conditions. Variable chemical structure and molecular weights were obtained and monitored as a function of reaction time, reaction temperature, molar ratio of catalyst to monomer, and molar ratio of acid to alcohol functional groups. Selection of reaction conditions to achieve maximum molecular weights was use of aluminum chloride as the catalyst, a 2 to 32 h reaction time, 125 to 175 °C reaction temperature, vacuum of 25 torr, and stirring with a magnetic stir bar.

2.3. Experimental Materials and Methods

Reagents. Malonic acid (MA, 99%, Figure 2.2) and chloroform (98%) were used as received from VWR. 1,3-Propanediol (PDO, 98%, Figure 2.2), $AlCl_3$ (98%), $ZnCl_2$ (98%), $FeCl_3$ (98%), $SnCl_2$ (98%), and diethyl ether (>99%) were used as received from Sigma-Aldrich.

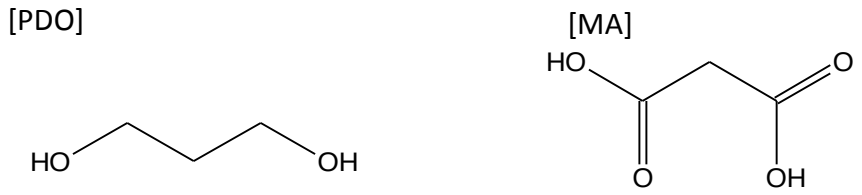

Figure 2.2: PDO and MA monomer chemical structures.

Copolymerization of 1,3-propanediol (PDO) and malonic acid (MA). The melt polycondensation of PTM was investigated using two experimental set-ups. Small scale polymerizations were run in 10 mL test tubes (~5 g monomer) without stirring or vacuum (mass transfer limited conditions) and vented to the atmosphere. PDO with MA were fed in a 1:1 mole ratio with a 100:1 monomer to catalyst (M/C) ratio, and the test tubes were immediately placed into an oil bath and allowed to react for 24 h. These reactions were carried out from 125-175 °C at 10 °C intervals. The second set of experiments were performed in a 100 mL round bottom flask (~ 50 g monomer) for 2-16 h at 155 °C and 4 h at 125-175 °C at 25 torr with mixing using a magnetic stir bar. A 100:1 M/C ratio and a 1:1 alcohol:acid molar ratio was maintained for all reactions.

Polymer separation. Excess monomer and catalyst were removed from the reaction products by dissolving in chloroform and then poured into diethyl ether. Precipitated polymer was then filtered using Whitman (grade 40) filter paper. For each reaction, this separation procedure was repeated until precipitated polymer could no longer be visually identified. The filtered polymer was dried in a vacuum oven at 15 torr and 20 °C for 24 h and then weighed.

Characterization. A Bruker AMX-300 NMR instrument was used to collect H^1 spectra at 300 MHz. Samples were dissolved into deuterated chloroform and tetramethylsilane (TMS)

added as an internal standard. Based on the reaction mechanisms discussed previously, options for the PTM repeat unit were determined. NMR chemical shifts were determined using literature references [Mahdavian 2007, Spyrous 1996, Chikh 2007, Kohut 2009, BRUNO 2003, Silverstein 2005]. A PHI 1600 Electron Scanning Chemical Analysis (ESCA) instrument with PHI 10-360 spherical detector and achromatic Mg K_α X-ray source (300 W, 15 kV) was used to gather additional information on the chemical composition and repeat unit structure. The spectrum were collected with PHI Surface Analysis Software for windows version 3.0 copyright 1994 Physical electronics Inc. and analyzed with CasaXPS version 2.2.88. The C-H peak for in the carbon high resolution scan was shifted to 285 eV as a reference. The polymer was also characterized by transmission FTIR spectroscopy using a Thermo Electron 6700 instrument purged with dry air. Samples were either smeared or solution cast with THF onto potassium bromide crystals. Attenuated total reflectance FTIR was performed using a Pike VeeMax II accessory with a zinc-selenide crystal with a 60 ° face. Gravimetric product yields were calculated using the limiting monomer to determine theoretical yields based on complete conversion. The recovered polymer weight was divided by the theoretical weight and then converted to percent yield. Differential scanning calorimetry (DSC) was performed on a TA Instruments Q1000 DSC using Therma Advanted for Q series version 2.8.0.392 version 4.8.2 with aluminum hermetic pans, purged with helium at 20 mL/min, and a heating rate of 5 °C/min from -40 °C to 200 °C or 400 °C. Thermalgravimetric analysis (TGA) was performed on a TA Instruments Q5000 with the same instrument control and data analysis software as the DSC. Samples were analyzed from room temperature to 400 °C at 10 °C/min under nitrogen using Al_2O_3 pans. A Waters gel permeation chromatograph (GPC) with RI detector, 4E and 5E (polystyrene-divinylbenzene, 4.6 x 300 mm) Styragel® columns, 0.3 mL/min THF effluent, and a 10-point polystyrene calibration was used to determine molecular weights and polydispersities.

2.4. Results and Discussion

2.4.1. Preliminary Catalyst and Temperature Screening

An initial catalyst screening was performed for the PTM polymerization using aluminum chloride ($AlCl_3$), zinc chloride ($ZnCl_2$), tin (II) chloride ($SnCl_2$), and iron (III) chloride ($FeCl_3$) at 1:100 M/C ratio. Reactions were performed from 125 °C to 175 °C under mass transfer limited conditions (no stirring and no vacuum). At temperatures above 135 °C, the four catalysts tested did showed a negative trend in yield with a maximum average of ~37.3 % w/w from 135 to 155 °C to a minimum of ~29 % w/w for 175 °C(Figure 2.3). Lower PTM yields were observed (11.1 ± 1.7 % w/w) when the reaction temperature was below the melting point of MA (133 °C) [Snell 1972]. Between 135 °C and 155 °C, the yields remain constant at ~36 % w/w. As the reaction temperature was raised above 155 °C, the yields decreased. The reaction is thermodynamically controlled, allowing for the reverse reaction. If the reaction was kinetically controlled, the reaction yields would continue to increase with increasing temperature. With only heat used to drive water from the polymerization, limitations on water diffusion from the mixture impeded the progression of the reaction. Although only a small amount of product was obtained for these reactions, FTIR characterization was performed to provide more insight into the chemical structure of the polymer produced

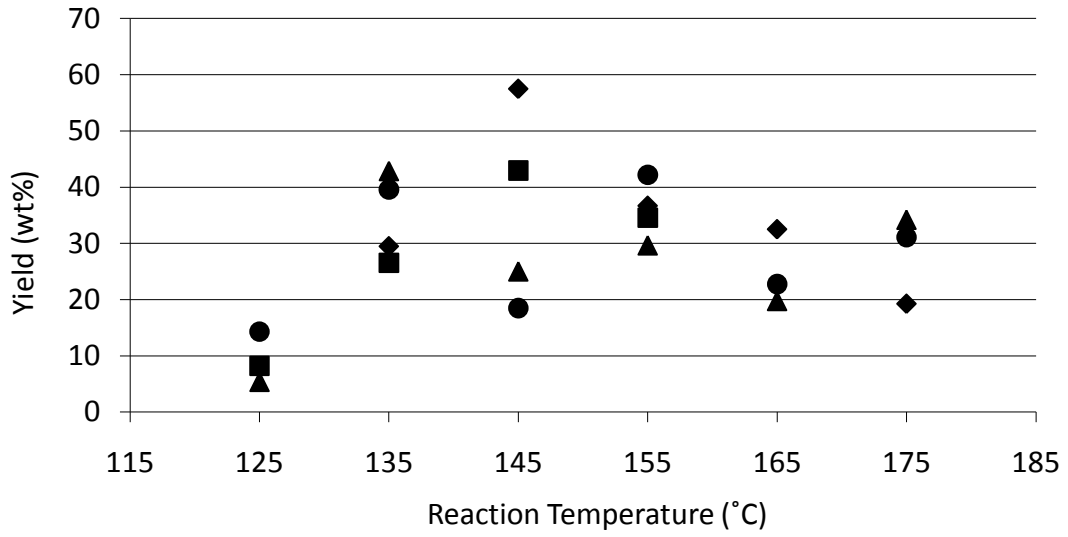

Figure 2.3: PTM gravimetric yields for small volume reactions using Lewis acid catalysts (■: $FeCl_3$, ◆: $AlCl_3$, ●: $ZnCl_2$, ▲: $SnCl_2$; reaction conditions: 5 mL volume, no vacuum or stirring, 24 h). Error bars represent 95% confidence intervals.

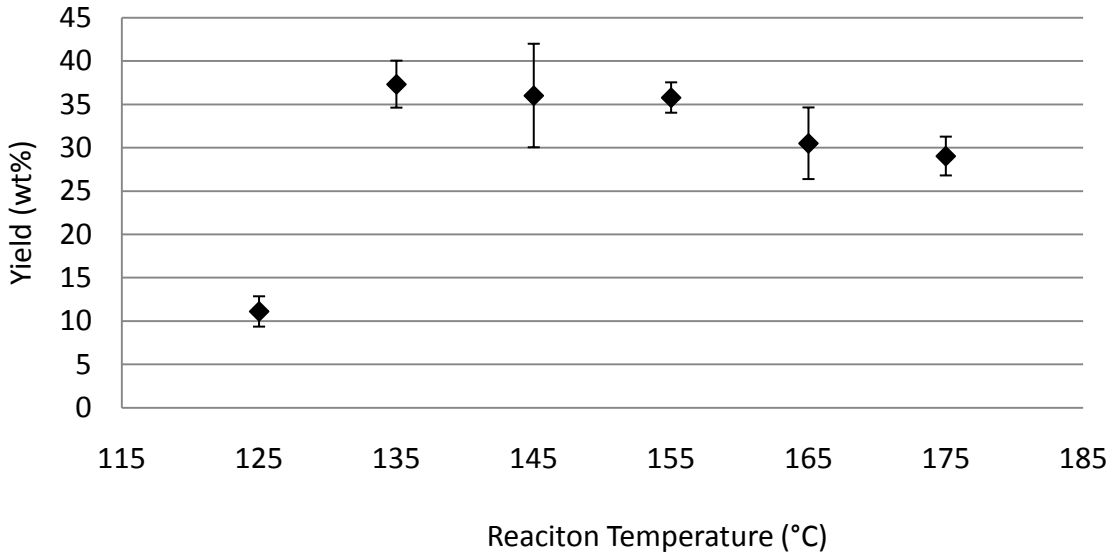

Figure 2.4: PTM gravimetric yields averaged over all Lewis acid catalysts tested in small volume reactions (reaction conditions: 5 mL volume, no vacuum or stirring, 24 h). Error bars represent 95% confidence intervals.

While there were no significant differences observed in the gravimetric yields of the four Lewis acid catalysts examined as part of the screening reactions, using attenuated total reflectance (ATR) FTIR spectroscopy differences were seen in the chemical structure of the PTM copolymer formed. ATR-FTIR spectra are shown in Figures 2.5 and 2.6 for PTM synthesized at 155 °C for 24 h without vacuum or stirring using $AlCl_3$, $FeCl_3$, $ZnCl_2$, and $SnCl_2$ with a reaction volume of 5 mL. Peaks can be identified for the large cyclic or low molecular ester carbonyl at 1749 cm^{-1}, high molecular weight ester carbonyl at 1726 cm^{-1}, low molecular weight cyclic ester carbonyl at 1777 cm^{-1}, and the ether C-O stretch at 1151 cm^{-1} in all of the spectra [Dell'Erba 1997, Silverstein 1991, Dean 1992, Caitker 2000, Sutton 2006, Gulmine 2006, Zhou 2009]. When examining the region from 1800 to 800 cm^{-1} in more detail (Figure 2.6), spectral differences can be more easily distinguished; these positions are numbered in Figure 2.6. In Figure 2.6 at position (1), there is a noticeable change in peak shape as a function of catalyst. It is apparent that the different type of catalyst affected the concentration of the anhydride. At position (2) in Figure 2.6, the C-C stretching can be seen at 1465 cm^{-1}. A change in the peak strength for the C-O-C of an ether as a function of catalyst can be seen at position (3) in Figure 2.6 at 1097 cm^{-1}. The C-O stretch at 1050 cm^{-1} of a primary alcohol, C-C(=O)-C(=O)-C stretch at 1040 cm^{-1}, and the C-O-C stretch at 1020 cm^{-1} changing as a function of catalyst can be seen at position (4) in Figure 2.6.

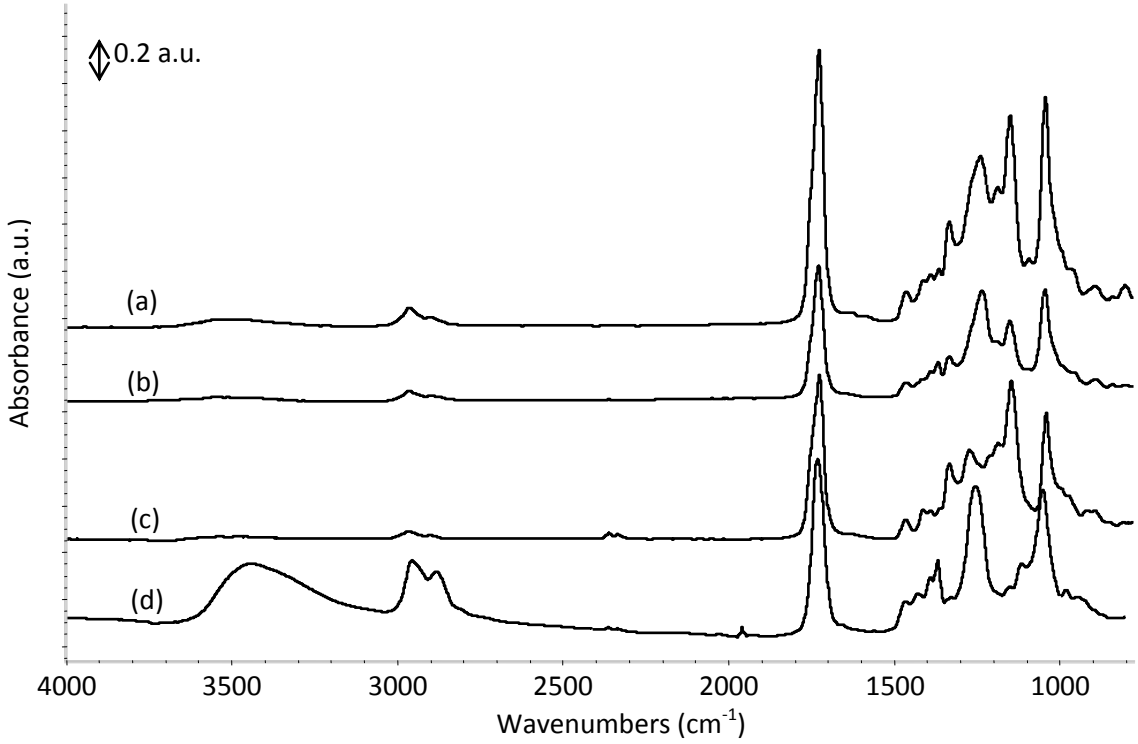

Figure 2.5: ATR-FTIR spectra of PTM reacted for 24 h at 155 °C with (a) $AlCl_3$, (b) $FeCl_3$, (c) $SnCl_2$, and (d) $ZnCl_2$ (with no vacuum or stirring, 5 mL reaction volume).

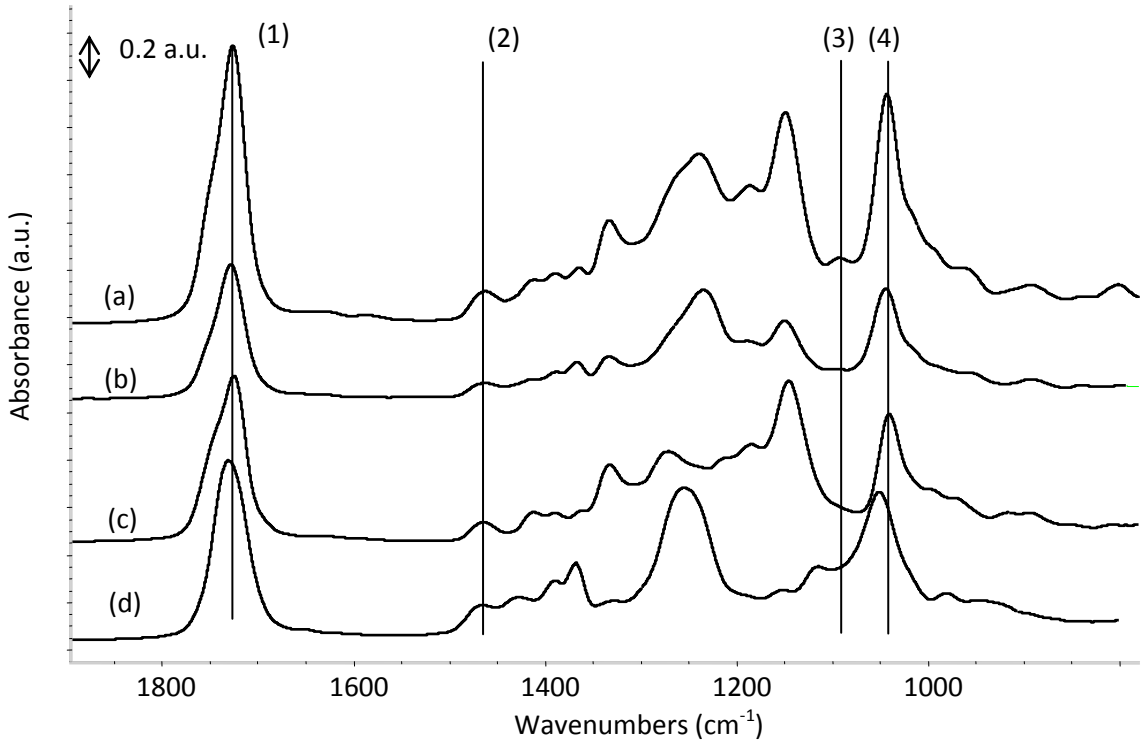

Figure 2.6: ATR-FTIR spectra of PTM synthesized using (a) $AlCl_3$, (b) $FeCl_3$, (c) $SnCl_2$, and (d) $ZnCl_2$ [no vacuum or stirring, 155 °C, 24 h, 5 mL reaction volume].

Qualitative spectral changes give an indication of chemical differences, but do not give a clear picture of the chemical structure as a function of catalyst and reaction conditions. Peak height ratio (PHR) analysis was used as a semi-quantitative measure of functional group concentration for the carboxylic acid carbonyl at 1702 cm^{-1}, high molecular weight ester carbonyl at 1726 cm-1, large cyclic or low molecular ester carbonyl at 1749 cm^{-1}, low molecular weight cyclic ester carbonyl at 1777 cm^{-1}. The peak assignments will be discussed in detail in section 2.4.2.2. With PHR, a ratio is calculated between the height of a peak of interest and the peak height for a functional group that is expected to remain relatively constant in the samples. The peak at 1465 cm^{-1} corresponding to the C-H scissoring of the methylene (CH_2) group was chosen as the 'constant' functional group in this study using the equation $PHR = \frac{Peak\ Height_{Target\ \ Functional\ \ \ Group}}{Peak\ Height_{CH_2\ Scissoring\ \ \ (1465\ cm^{-1})}}$ [Silverstein 1991]. In Figure 2.7, the PHR of the

carbonyl of the esters and carboxylic acids as a function of catalyst for single samples. Aluminum chloride has the highest concentration of esters at 1726 and 1749 cm^{-1}. Zinc chloride had the lowest concentration of ester bonds. For all of the catalysts, the relative concentration of carboxylic acids and low molecular cyclic esters for all catalysts was low when compared to the major ester peaks. The four catalysts produce different chemical structures with relatively the same yield, Figure 2.4 and 2.7.

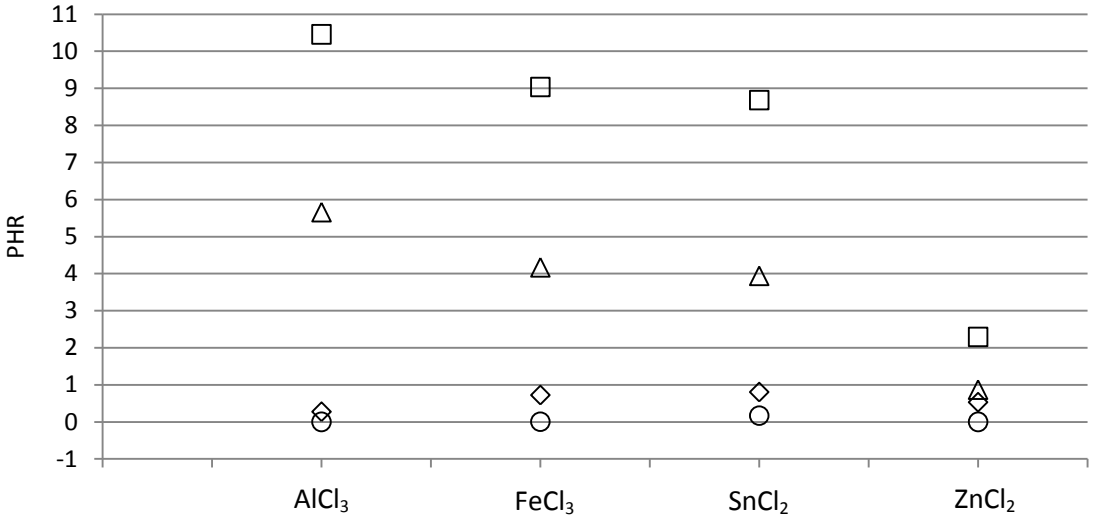

Figure 2.7: FTIR PHR for carboxylic acid carbonyl (1702 cm^{-1}, ◇), high molecular weight ester carbonyl (1726 cm^{-1}, □), low molecular weight ester or large cyclic ester carbonyl (1749 cm^{-1}, △), and low molecular weight cyclic ester carbonyl (1777 cm^{-1}, ○) for PTM made with $AlCl_3$, $FeCl_3$, $SnCl_2$, and $ZnCl_2$ catalysts with single data points (155 °C, 24 h, no vacuum or stirring).

Out of the four catalysts studied under mass transfer limited conditions (5 mL reaction volume without stirring), aluminum chloride was chosen for further study due to its higher reactivity and higher concentration of ester bonds. Aluminum chloride is relatively low cost when compared to zeolites, transition metal catalysts, and rare earch catalysts. With the low environmental impact of aluminum chloride, the polymerization will follow green chemistry principals [Anastas 2010, Wilson 2009, Kobayashi 2009, Garcia-Serna 2007, Poliakoff 2002].

Aluminum chloride was used in the second set of PTM polymerizations conducted over the 125 – 175 °C temperature range with a larger reaction volume (~50 mL), stirring, and vacuum.

2.4.2. PTM Copolymerization Expanded Study

Using $AlCl_3$ as the catalyst due to its higher reactivity, economic cost, and toxicity, the PTM polymerizations were scaled up (monomer mass increased from 5 to 50 g), providing sufficient polymer product to conduct more extensive characterizations. Reactions were run from 125 to 175 °C and 2 to 16 h with stirring and vacuum. Chemical structure was examined with FTIR, NMR, and XPS, and the molecular weights (Mw) and polydispersities (PDI) were examined with GPC. Thermal properties of the PTM copolymer was characterized using TGA and DSC to determine thermal properties.

2.4.2.1. Gravimetric Yields

As shown in Figure 2.8, melt polycondensation yields of PTM decreased from 75 to 62 % over the 2 to 16 h reaction time studied. With longer reactions times, PTM can experience a reduced water diffusion rate leading to an increased reverse reaction rate or equilibrium in the $A_{AC}2$ and $A_{AL}1$ mechanisms. From 4 to 16 h in Figure 9, the samples showed less variation in yield, which is attributed to steady state conditions with the removal of water and other small by-products by vacuum. By 4 h, the reaction mixtures were highly viscous, leading to the reduction or stoppage of stirring and the entrainment of low Mw products, water and hydrochloric acid from the decomposition of the aluminum chloride. The reduction in yield seen in Figure 2.8 with increasing reaction time is evidence of a thermodynamically controlled reaction. If the polycondensation reaction is thermodynamically controlled, water in the system will limit the progress of the forward reaction and catalyze the reverse reaction, both serving to

prevent yields in excess of 99.5%. The maximum yield for PTM at 155 °C is considered to happen near 4 h in Figure 9; it is difficult to determine a more exact reaction time that maximizes gravimetric yield due to the large variance in yield at 2 h. By 4 h, the system is at equilibrium with by-product removal visibly slowed and minimal change in the appearance of the reaction mixture as a function of reaction time, as seen in Figure 15. However, differences are seen in Mw and chemical structure with time, which will be discussed later

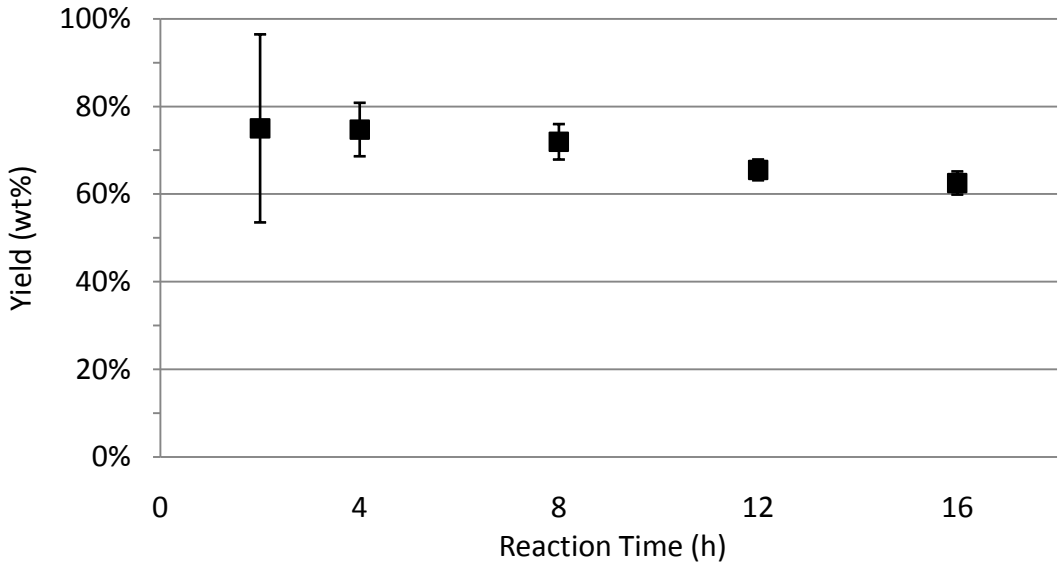

Figure 2.8: PTM gravimetric yield dependence on reaction time, 2 to 16 h, (155 °C reaction temperature, $AlCl_3$ catalyst) with 95% confidence intervals.

Gravimetric yields were also determined as a function of temperature for PTM (Figure 2.9). PTM appears to have a random yield. At 125 °C in Figure 2.9, the reaction is being attempted below the melting point of MA. Due to the high viscosity of the reaction products, the reaction products could not be passed through a 45 micron filter during the purification process, which artificially inflated the gravimetric yield value to ~ 70%. The end product of the 125 °C reaction is expected to be primarily a hydrogen bonded mixture of PTM oligomers and

the PDO and MA monomers, with only minimal polymeric material of substantial Mw. The 135 °C reaction product showed a considerably lower viscosity. The reaction temperature was now above the melting point of MA, and a soft, waxy solid was produced. The maximum yield of ~78% for PTM occurred between 145 °C and 155 °C as seen in Figure 10, and then decreased with increasing temperature. At 175 °C, black and brown discoloration, due to thermal degradation, are noticeable by visual inspection at approximately 2 h and increase in size with reaction time. The relatively low yields (< 99.5%) are due to thermodynamic control of the reactions, which allow the reverse reaction being prevalent in the reaction, and the entrainment of low Mw products in the reaction mixture. Furthermore, the reverse reaction becomes more dominant at temperatures above 155 °C, further limiting the reaction yields.

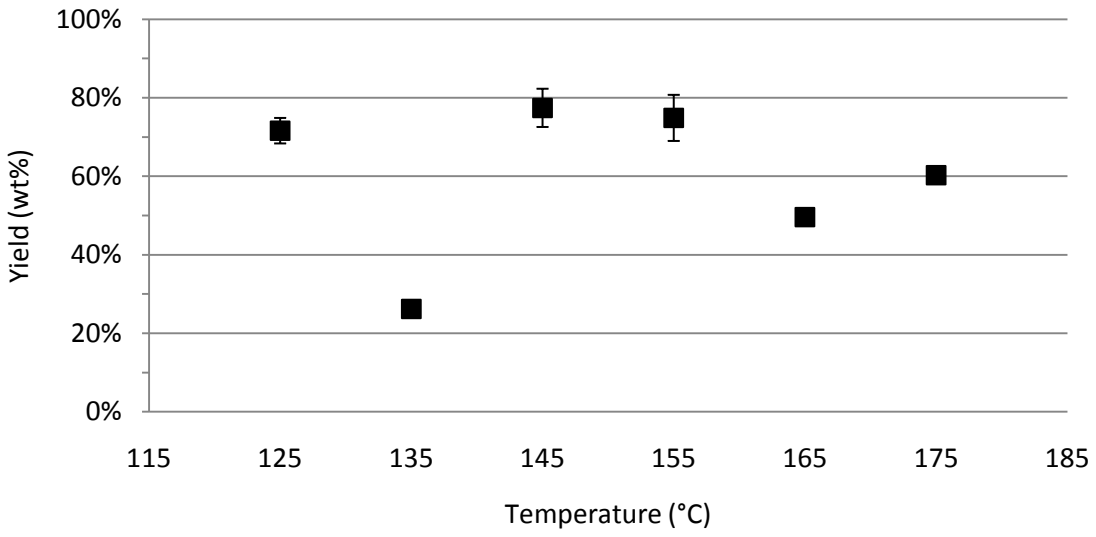

Figure 2.9: PTM gravimetric yield dependence on reaction temperature, 125 to 175 °C, (4 h reaction time, $AlCl_3$) with 95% confidence intervals.

2.4.2.2. FTIR Spectroscopy

Transmission FTIR spectra were taken of all resultant polymers in the condensed state to determine chemical composition and functional group concentration. In addition to general chemical characterization, the relative concentrations of ester groups were determined by spectral analysis for PTM polymers produced under different reaction conditions. Carbonyl peak height ratio was used to determine semi-quantitative concentrations of the ester and carboxylic acid functional groups. Spectral analysis for the PTM copolymers provided key information regarding the chemical structure and, therefore, the reaction mechanisms involved.

FTIR spectrum of PTM is shown in Figure 2.10 and 2.11. For PTM, major features include a broad O-H stretch peak from approximately 3680 to 3135 cm^{-1}, peaks for C-H stretching from 3135 to 2800 cm^{-1}, a broad peak from 3200 to 2600 caused by the carboxylic acid O-H stretch, and the carbonyl C=O stretch around 1730 cm^{-1} [Dell'Erba 1997, Silverstein 1991, Dean 1992]. Closer inspection of the carbonyl peak revealed multiple peaks from the carbonyl of esters and carboxylic acid groups (Figure 2.11). Three peaks were identified and attributed to ester carbonyls through peak deconvolution, 1726, 1749, and 1777 cm^{-1} were determined by spectral analysis and literature review of literature, Figure 2.12 [Dell'Erba 1997, Silverstein 1991, Dean 1992, Caitker 2000, Sutton 2006, Gulmine 2006, Zhou 2009]. An ester cyclic with increasing ring strain will shift the ester carbonyl range from 1725 to 1750 cm^{-1} to 1760 to 1785 cm^{-1} [Dell'Erba 1997, Silverstein 1991, Dean 1992]. Kricheldorf demonstrated that large cyclic rings do exists in polymers, and it has been theorized by others that cyclization is a competing reaction during polymerization [Deans 2007, Caitker 2000, Sutton 2006, Gulmine 2006, Zhou 2009]. It cannot be conclusively determined if the peak at 1749 cm^{-1} is a large cyclic or a low molecular weight polymer without the use of techniques such as MALDI-ToF, but a hydrolytic study that was performed on PTM has a degradation pattern that supports that the

carbonyl peak at 1749 cm-1 is a type of low molecular weight ester and the carbonyl at 1726 cm-1 is a higher molecular weight ester [Chapter 4]. Two peaks were identified for carboxylic acid carbonyls, one peak was at 1702 cm^{-1}, and it was identified as dimerized carboxylic acid carbonyl. The second peak related to carboxylic acids was identified at 1587 cm^{-1} as a carboxylate anion carbonyl. During FTIR characterization of preliminary experiments, the acid chloride carbonyl was identified at 1785 cm^{-1} and provided evidence that the carboxylic acid groups were converted into acid chlorides, but this peak was not found in the final products. Examination of the spectrum below 2000 cm^{-1} reveals a noticeable peak at 1633 cm^{-1} that is indicative of the formation of alkene double bonds that can be explained by the acid catalyzed alcohol dehydration of PDO [Dell'Erba 1997, Silverstein 1991, Dean 1992]. The ester and carboxylic acid carbonyls had a dependence on reaction time and temperature and the changes in ester and carboxylic acid concentration give information into reaction mechanisms.

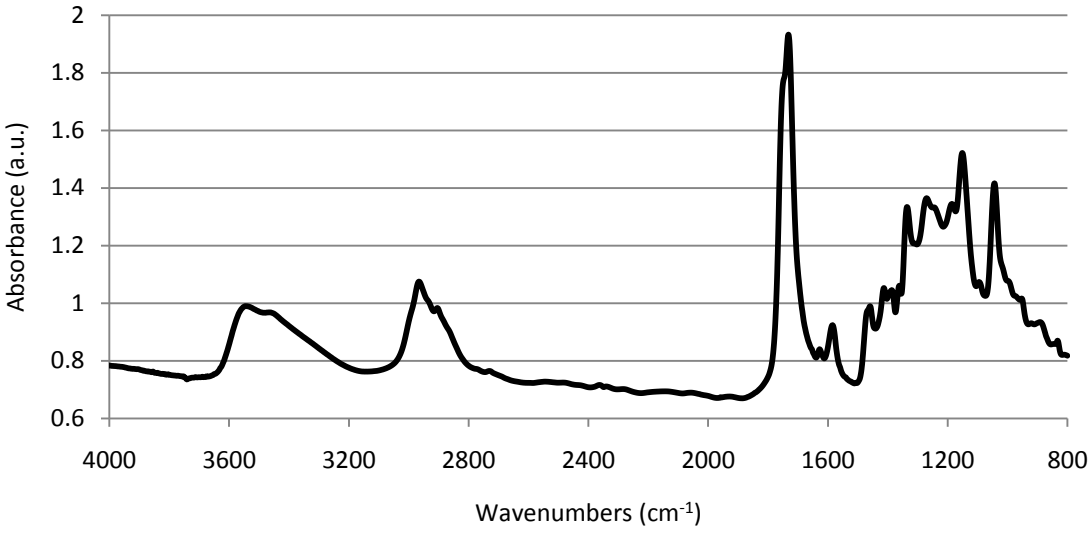

Figure 2.10: Representative transmission FTIR spectrum of PTM made at 155 °C for 4 h with aluminum chloride catalyst.

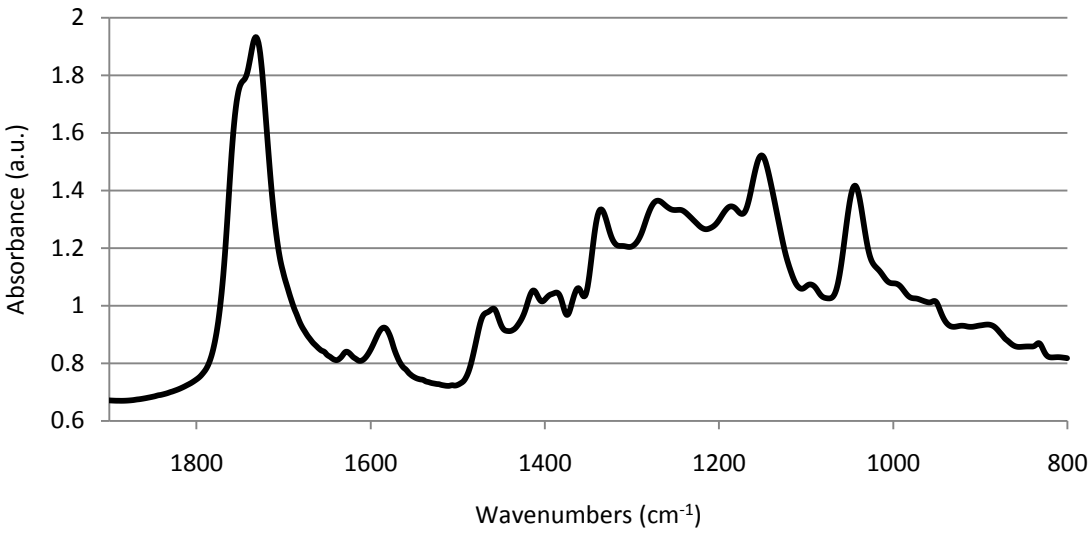

Figure 2.11: Representative transmission FTIR spectrum of PTM made at 155 °C for 4 h with aluminum chloride catalyst from 800 to 1900 cm^{-1}.

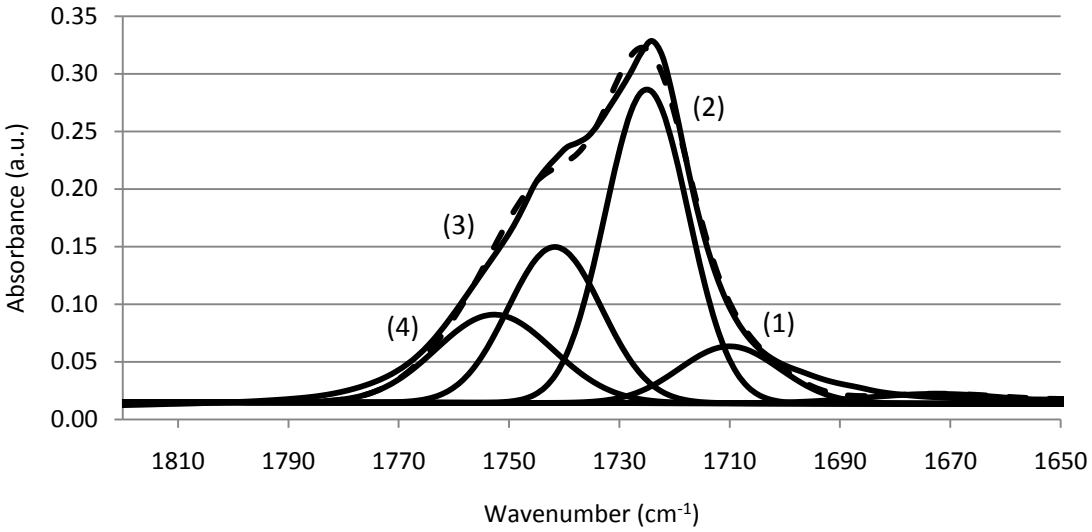

Figure 2.12: Representative transmission FTIR spectrum of PTM from 1820 cm^{-1} to 1650 cm^{-1} with peak fitting showing four major peaks of interest: (1) 1710 cm^{-1}, carboxylic acid carbonyl stretch, (2) 1725 cm^{-1}, high Mw ester carbonyl stretch, (3) 1742 cm^{-1}, low Mw ester carbonyl stretch, and (4) 1753 cm^{-1}, cyclic ester carbonyl stretch. The dashed line represents the composite curve of the fitted peaks.

Changes in the relative concentrations of the ester linkages and carboxylic acids as a function of reaction time and temperature were examined using peak height ratio. Using Equation 1.1, the PHR of esters and carboxylic acid carbonyl was determined for each sample. The trends in 1726 and 1749 cm^{-1} PHR (Figure 2.13) match the trends seen in the yield, Figure 2.8. With increasing reaction time there is a reduction in the ester bonds present due to increased $A_{AC}2$ and $A_{AL}2$ reverse reactions due to increased entrained water at longer reaction times. 1726 and 1749 cm^{-1} PHRs appear to reach a maximum value around 2 to 4 h of ~3.5 (1726 cm^{-1}) and ~4.5 (1749 cm^{-1}), before decreasing to between 2 and 3 at longer reaction times. The $A_{AC}2$ and $A_{AL}1$ mechanisms are proceeding forward dominantly through 4 h as water readily diffuses out of the vessel. After 4 h, there was a noticeable increase in viscosity that coincides with the reduction in 1726 and 1749 cm^{-1} PHR as the reverse $A_{AC}2$ and $A_{AL}1$ mechanisms negatively impact the polymerization. The carboxylate anion PHR, 1587 cm^{-1} (Figure 2.13), decreases with increasing reaction time, which is contrary to what was expected as the ester carbonyl's decreased. It was expected that as the ester carbonyl's PHR decreased there would be an increase in carboxylate anions' PHR. While the ester and carboxylate anion carbonyl's PHR decrease with increasing reaction time, the carboxylic acid carbonyl, 1702 cm^{-1}, increases and appears to be competing with the cyclic ester carbonyl, 1777 cm^{-1}, from 8 to 16 h. As the carboxylic acid carbonyl PHR decreases from 8 to 12 h, ~1.1 to ~0.9, and increases from 12 to 16 h, ~0.9 to ~1, the cyclic ester carbonyl has the opposite trends, increasing from ~0.3 to 0.9 from 8 to 12 h and decreasing from ~0.9 to ~0.4 from 13 to 16 h. Further study is needed to explain the relationship between carbocylic acid and cyclic ester formation. The decrease in 1726 and 1749 cm^{-1} PHR and the decrease in yield from 4 to 16 h indicates that the PTM melt polycondensation is thermodynamically controlled. If PTM polycondensation was kinetically controlled, 1726 and 1749 cm^{-1} PHR would continue to increase with increasing reaction time.

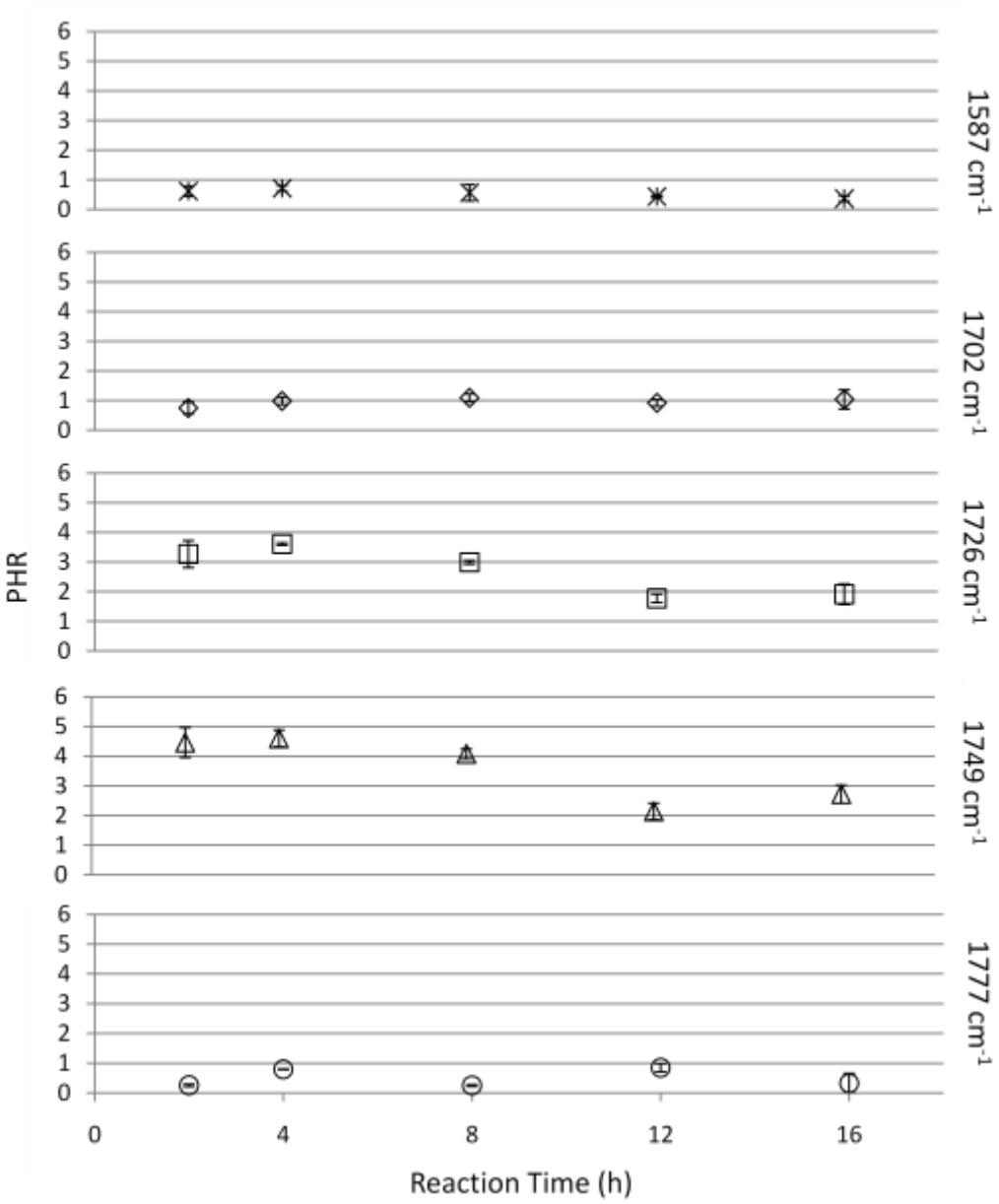

Figure 2.13: PTM PHR for carboxylic acid carbonyl (1702 cm^{-1}, ◇), high molecular weight ester carbonyl (1726 cm^{-1}, □), low molecular weight ester or large cyclic ester carbonyl (1749 cm^{-1}, △), and low molecular weight cyclic ester carbonyl (1777 cm^{-1}, ○) at variable reaction time with bars indicating 95% confidence intervals (155 °C reaction temperature, $AlCl_3$ catalyst).

The ester carbonyls at 1726 and 1749 cm^{-1} showed a strong dependence on reaction temperature, Figure 2.14. At 125 °C, the yield was at ~70 wt.%, Figure 2.9, the ester carbonyls, 1726 and 1749 cm^{-1}, PHR were ~1 and significantly lower 155 °C ester carbonyls PHR, ~3.7 and ~4.5, with a comparable yield and PHR for carboxylate anion, carboxylic acid, and cyclic ester carbonyl. It is not known why 125 °C has a comparable yield to 155 °C with low concentration ester carbonyls, but it is theorized it is related to hydrogen bonding and the 125 °C reaction being performed below the melting point of MA, 133 °C. Further study needs to be completed to fully understand the PTM polymerization results at 125 °C. From 135 to 175 °C, 1726 and 1749 cm^{-1} PHR increases from ~1.3 to ~4.2 and ~2 to ~5.3 as 1702 PHR decreases ~1 to ~0.5. As ester bonds are created, the carboxylic acid end groups should decrease, which is seen in the PHRs. 1777 cm^{-1} cyclic ester carbonyl PHR showed no dependence on reaction temperature from 125 to 175 °C and maintained a value of ~0.6. Carboxylate anion, 1587 cm-1, PHR, also, did not demonstrate a dependence on reaction temperature and varied between 0.5 and 0.7 from 125 to 175 °C. 1726 and 1749 cm^{-1} ester carbonyl PHR increased from 155 to 175 °C indicating an increase in ester bonds in PTM, while yield decreased; this was unexpected. Monomer evaporation at temperatures above 155 °C was not taken into account in the yield and may be causing the yields to appear artificially depressed. Temperatures above 175 °C were not attempted due to the thermal degradation of aluminum chloride at temperatures above 177 °C [Lange's Handbook]. The PTM ester carbonyls' increased significantly with increasing reaction temperature from 125 to 175 °C.

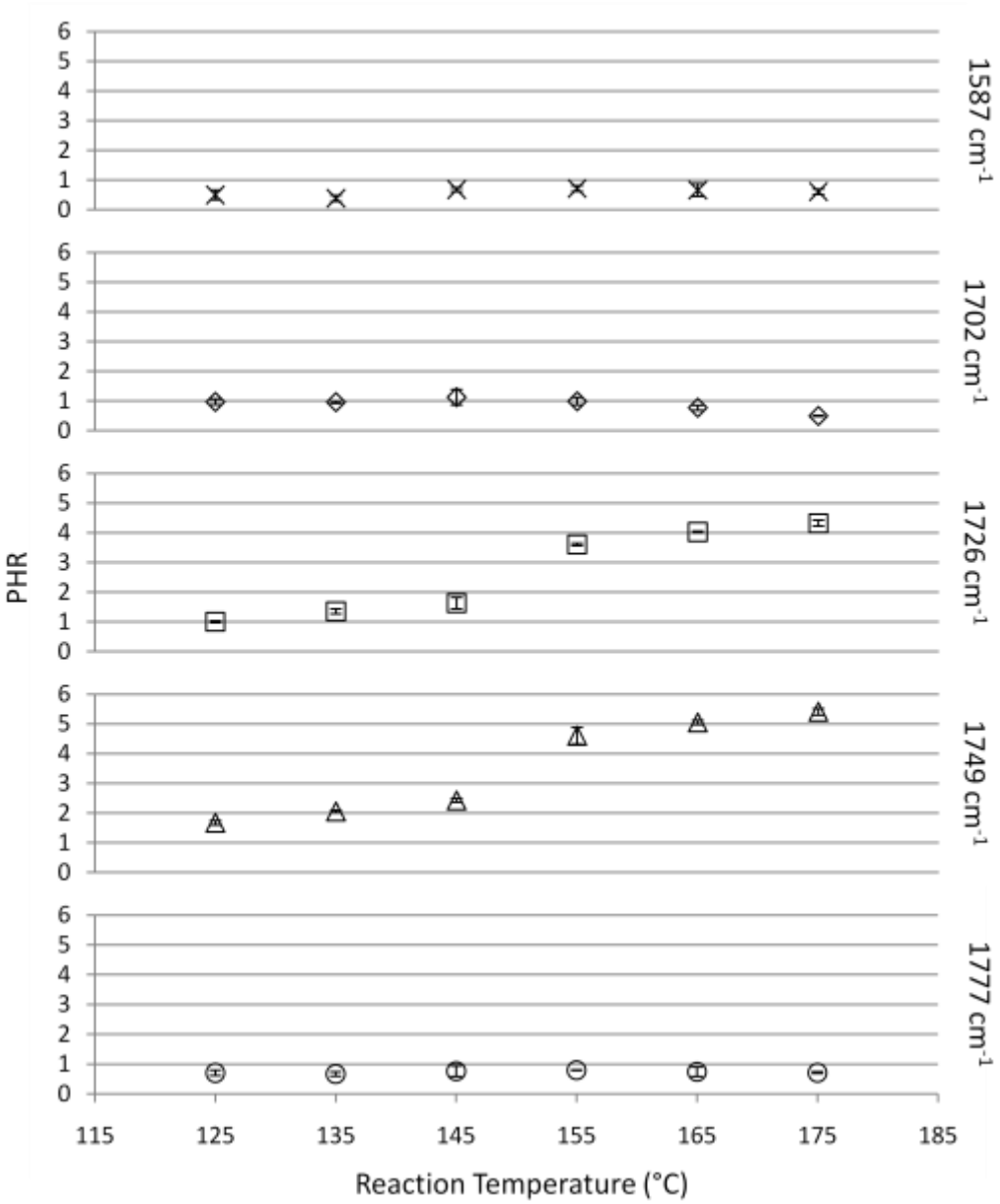

Figure 2.14: PTM PHR for carboxylic acid carbonyl (1702 cm^{-1}, ◇), high molecular weight ester carbonyl (1726 cm^{-1}, □), low molecular weight ester or large cyclic ester carbonyl (1749 cm^{-1}, △), and low molecular weight cyclic ester carbonyl (1777 cm^{-1}, ○) at variable reaction temperature with bars indicating 95% confidence intervals (4 h reaction time, $AlCl_3$ catalyst).

2.4.2.3. Nuclear Magnetic Resonance (NMR) Spectroscopy

Proton NMR analysis showed that the PTM copolymer backbone contained a mixture of alkane, ester, and ether bonds. Experimental shifts were determined though literature, Figure 2.15 and Table 2.2 [Agraw 1993, Qian 2007, Pretsch 2000]. The $A_{AC}2$ and $A_{AL}1$ reactions are occurring, allowing for the ester and ether formation as formally found by FITR.

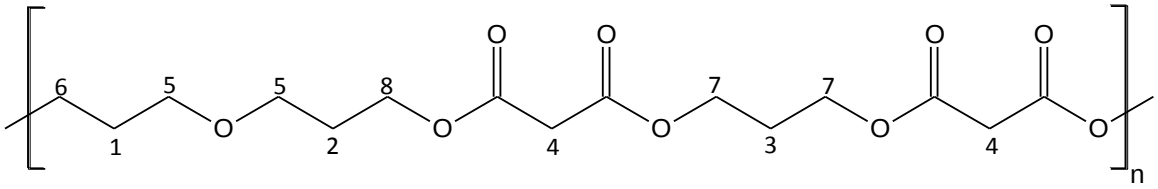

Figure 2.15: Representative PTM structure with ester and ether bonds.

Table 2.2: Peak shifts for PTM (4 h, 155 °C, aluminum chloride) from proton NMR.

Functional Group	Experimental Shift (ppm)
1	1.667
2	1.872
3	1.996
4	3.379
5	3.671
6	3.690
7	4.209
8	4.287

2.4.2.4. X-ray Photoelectron Spectroscopy (XPS)

To verify the FTIR analysis , XPS was used to characterize PTM made 155 °C for 4 h using aluminum chloride. The survey scan revealed only the presence of carbon and oxygen, and, as expected, the carbon and oxygen atomic concentrations were not in the correct ratio for PTM made of 1:1 ratio of PDO and MA units, Table 2.3. The low concentration of oxygen and high concentration of carbon indicate that PDO is preferentially being added to the polymer. FTIR

could only show the relative concentration of functional groups, and it could not show if one monomer was being preferentially being added to the polymer. With XPS, the concentration of carbon and oxygen show that one monomer is being preferentially reacted, PDO. Under acidic conditions, alcohols can react with other alcohols to form ether bonds [Dell'Erba 1997, Silverstein 1991, Dean 1992]. Since PDO repeat unit has a lower concentration of oxygen (25 at.%) and a higher carbon content (75 at.%) than MA (50 at.% oxygen, 50 at.% carbon), the preferential addition of PDO would cause the lower than expected oxygen content of the polymer.

Table 2.3: Comparison of experimental atomic concentrations of carbon and oxygen in PTM, as determined by XPS, to theoretical concentrations for an equimolar polymerization of PDO and MA.

	Percent Atomic Concentration	
Atom	Experimental	Theoretical
O	36.57 ± 0.72	40
C	64.43 ± 0.72	60

Peak fitting of the high resolution C 1s scan for the C-H, C-O- and C=O functional groups allowed for an accurate determination of the fractions of PDO and MA repeat units, Figure 2.16 [Sabbatini 1996, Louette 2006 69-73, Louette 2006 38-43, Cossement 2006, Nanse 1997]. The peaks were identified as C-H at 285 eV (36.5 % ±1.2 % area), C-O at 286.5 eV (37.5 % ±1.8 % area), and C=O at 289.2 eV (25.6 % ±0.2 % area). Determination of C-O and C=O participating in ester bonds could not be determined from the XPS results. The results show a high concentration of C-O in PTM that should have been closer to 25% area for agreement with

theoretical results. The increased C-O concentration is due to a higher concentration of PDO in PTM as the survey scan results suggest.

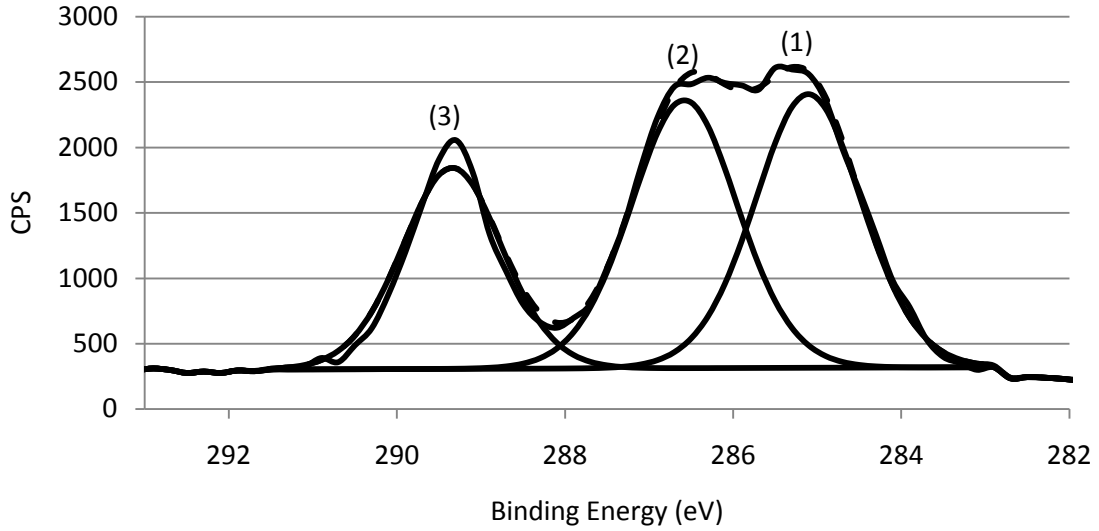

Figure 2.16: Peak fitting of a high resolution C 1s XPS scan for PTM (155 °C, 4 h, $AlCl_3$ catalyst). The peaks were identified as (1) C-H at 285 eV (36.5±1.2 % area), (2) C-O at 286.5 eV (37.5±1.8 % area), and (3) C=O at 289.2 eV (25.6±0.2 % area).

2.4.2.5. Gel Permeation Chromatography (GPC)

After the chemical composition of the PTM copolymer was characterized with FTIR and XPS, the molecular weights and polydispersity index were examined with GPC. It was noticed on all of the GPC traces for PTM that there was a bimodal molecular weight, Mw, distribution, with a peak above 10 kDa, HMw, and a peak below 10 kDa, LMw. The HMw constituted <5% of the area under the curve and the LMw accounted the remainder of the area under the curve. For the PTM samples, GPC analysis was a relatively simple task, as they were readily soluble in THF. The low Mw distribution was indicative of step growth polymerization since high molecular weights would only occur above yields of 99.5 %, and PTM yield was not above 99.5% [Odian 1991]. The higher Mw distribution in PTM could not initially be explained. A second type of polymerization existed concurrently in the reaction vessel or a side reaction that could produce

moderate Mw products needed to be considered. A possibility for a concurrent polymerization pathway for the moderate Mw material was chain growth polymerization; chain growth polycondensation has been developed for some time and could explain the HMw's at low yields [Odian 1991, Voit 2000, Yokoyama 2007]. PTM polymer was mainly low Mw material and was a waxy solid.

One of the objectives throughout the project has been to make a usable polymer by achieving a usable Mw. Whether this was done by maximizing the Mw achieved though step or chain growth polymerization was not a consideration; the end product needed to be a usable polymer. The problem with maximizing chain-growth polymerization reactions is chain-growths sensitivity to reaction conditions, and the problem with step-growth polymerization reactions is achieving the necessary yields to obtain high Mw material [Odian 1991]. Two main variables were identified as having the highest impact on yield and Mw, reaction temperature and reaction time, through literature. The HMw of PTM was not initially expected and had Mws ranging from 42 kDa to 29 kDa when only reaction time was considered. PTM showed no dependence on reaction time, Figure 2.17. The lack of dependence on reaction time is due to the reaction reaching an equilibrium of all reactions present after the first two hours of the reaction. The LMw of PTM had a Mw ranging from 1 kDa to 2.5 kDa over reaction time of 2 to 16 h, Figure 2.18. The LMw did not achieve a usable Mw of 10 kDa due to the reaction not reaching a yield greater than 99.5%. The Mw of the PTM's LMw increased with reaction time, which was in line with step growth polymerization theory. The interaction between the chain growth and step growth polymerization and the reverse reactions maintains the yield, but allows for the Mw of the step growth polymer to continue to increase in weight; this interaction was not examined further during this study. Reaction temperature appears to have a larger effect on the Mw of PTM than reaction time, Figure 2.19. The HMw that was contributed to the

chain growth polymerization increased ~15 kDa with temperature increasing from 125 °C to 165 °C, and then the Mw decreased after 165 °C as the polymer started to show visible signs of degradation, yellow to black coloration from an initially white mixture. The LMw increases with increasing temperature, with the largest increase from 165 °C to 175 °C when degradation begins and HMw is decreasing , Figure 2.20. The degradation products of HMw may be adding to the increase in LMw. Furthermore, the increase in LMw with increasing temperature is indicative of a thermodynamically controlled reaction that allows the reverse reaction to occur. The LMw of PTM showed a dependence on both reaction temperature and time, while the HMw only showed a dependence on reaction temperature.

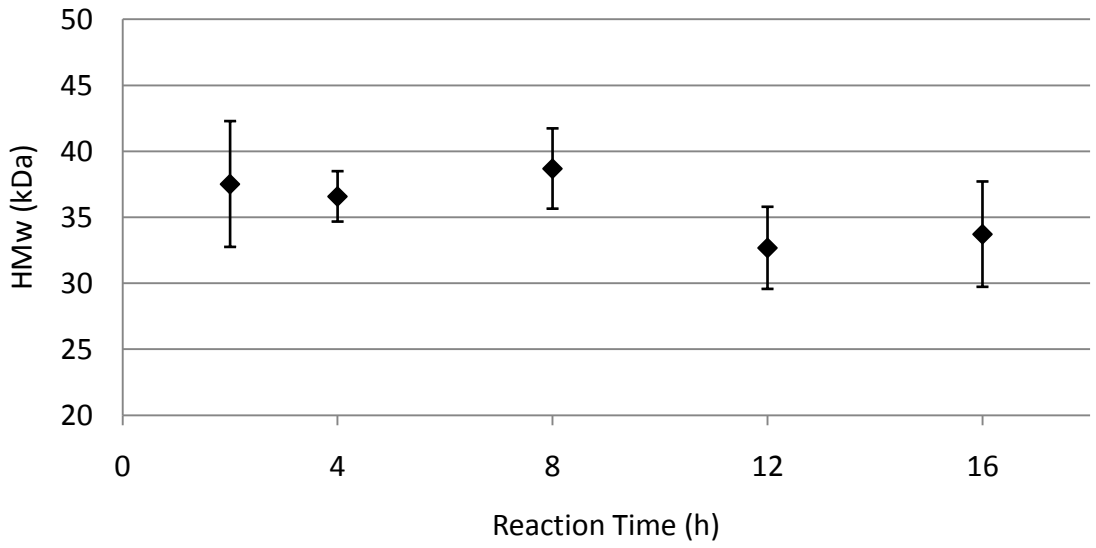

Figure 2.17: PTM HMw plotted versus reaction time (2-16 h) with 95% confidence interval error bars. Reaction conditions were 155 °C with aluminum chloride as the catalyst.

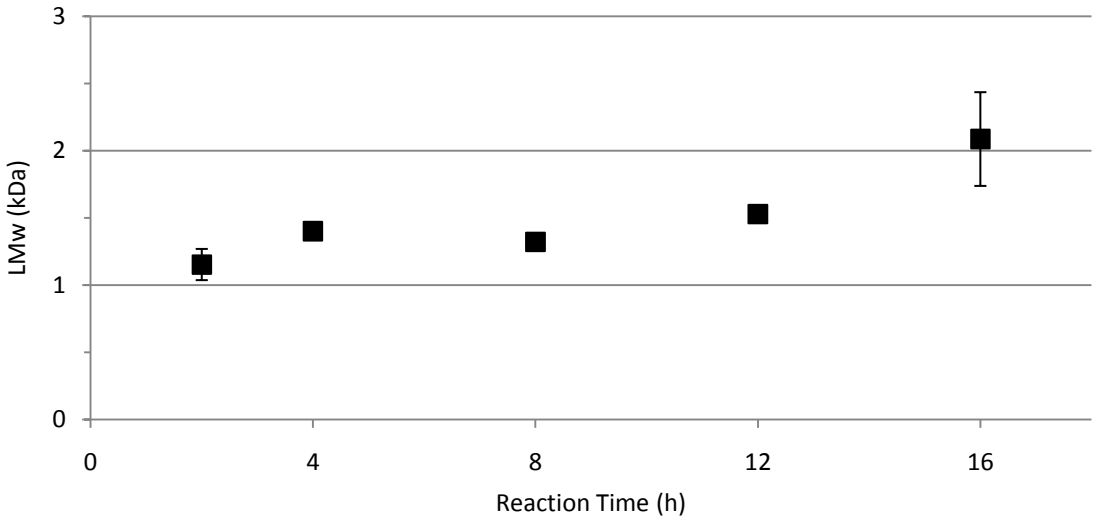

Figure 2.18: PTM LMw plotted versus reaction time (2-16 h) with 95% confidence interval error bars. Reaction conditions were 155 °C with aluminum chloride as the catalyst.

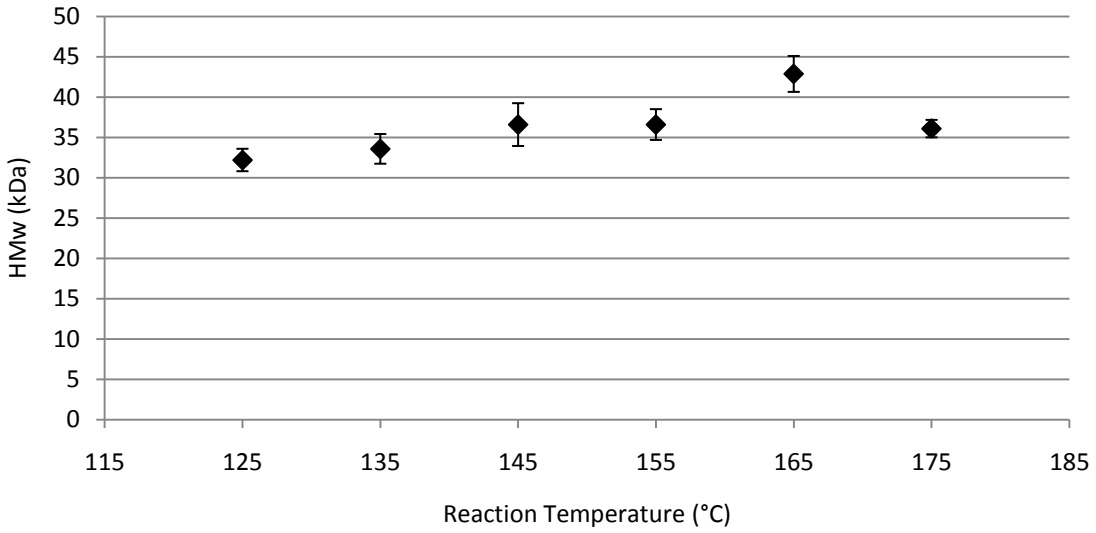

Figure 2.19: HMw PTM plotted versus reaction temperature (125 to 175 °C) with 95% confidence interval error bars. Reactio conditions were 4 h with aluminum chloride as the catalyst.

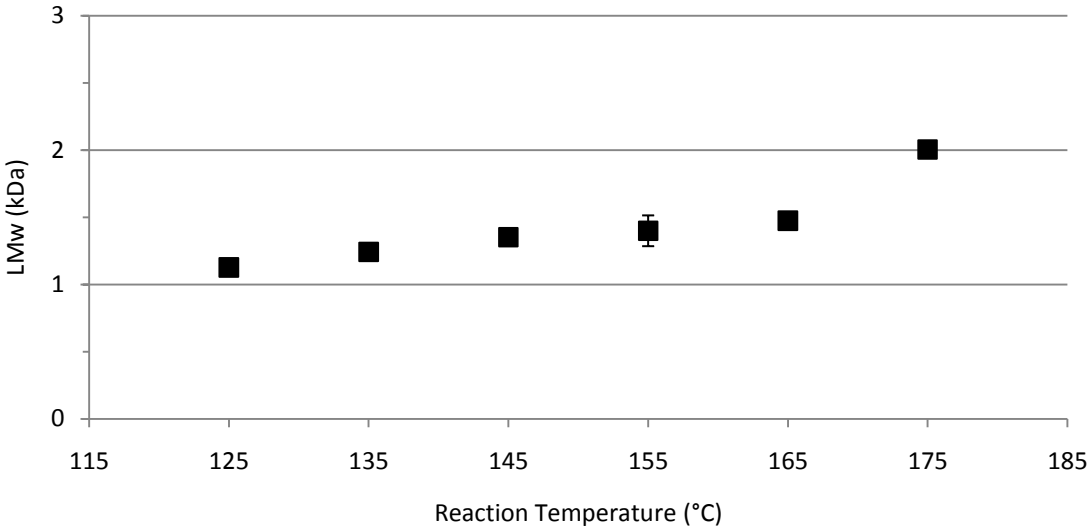

Figure 2.20: LMw PTM versus reaction temperature with 95% confidence interval error bars. Reaction conditions: 125 to 175 °C, 4 h reaction time, and aluminum chloride as the catalyst).

2.4.2.6. Thermogravimetric Analysis (TGA)

TGA was performed on several representative samples from PTM samples made at 135, 155, and 175 °C with aluminum chloride, for 4 h, and with stirring and vacuum. The 135 °C sample lost 5 wt.% by 113 °C, which may have been due to loss of oligomers, water, and other solvents, Table 2.5. PTM samples made at 155 and 175 °C 5 wt.% loss at approximately 175-176 °C (Table 2.4), which is below the boiling point of PDO and above the boiling points of fluids that the polymer has come into contact with, including water, ether, and chloroform. In the TGA graph (Figure 2.21), an increase in the slope occurs around 210 °C, which is the boiling point of PDO, and would indicate that PDO or PDO oligomers are present in the polymer. There are no other readily discernable features above 220 °C, and by 400 °C, the sample is thermally decomposed.

Table 2.4. TGA-determined 5% weight loss temperatures for PTM synthesized at 135, 155, and 175 °C for 4 h using aluminum chloride with vacuum and stirring.

Reaction Temperature	5% Weight Loss Temperature
135 °C	113 °C
155 °C	175 °C
175 °C	176 °C

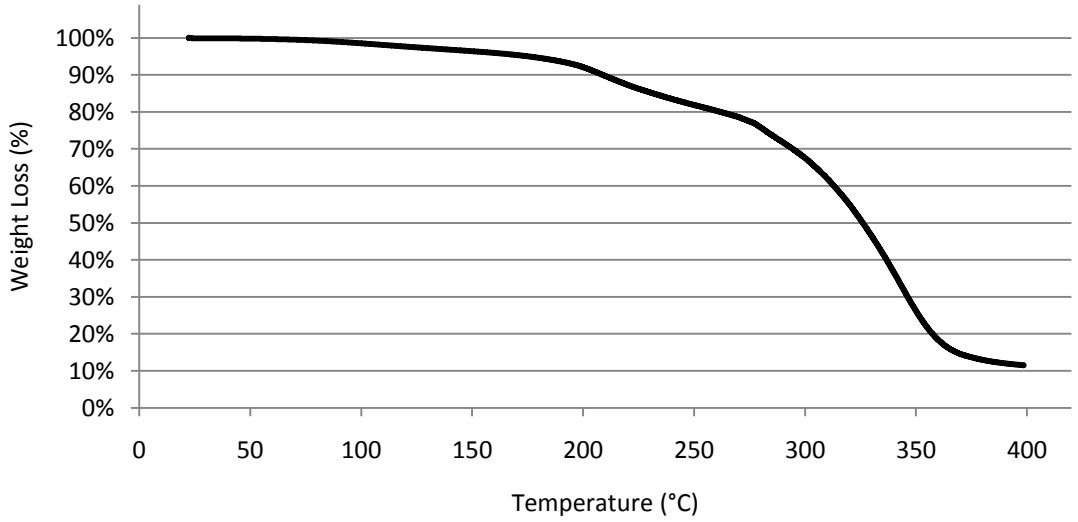

Figure 2.21: TGA weight loss versus temperature from TGA for PTM made 155 °C for 4 h using aluminum chloride with vacuum and stirring.

2.4.2.6. Differential Scanning Calorimetry (DSC)

Initial experiments were performed to 400 °C to ensure that the glass transition and melting temperatures were captured, and later experiments were performed only to 175 °C. For a representative samples made from PTM at 155 °C for 4 h with aluminum chloride, vacuum and stirring, the glass transition temperature is believed to lie at approximately -65.2 °C, seen in Figure 2.22. However, the location of the glass transition temperature needs to be verified by replication. The most notable feature of the experiments is the melting point seen between 25

°C and 40 °C. The melting point is at approximately 28.7 °C with an onset temperature of 26.6 °C. Two other representative samples were run on DSC to examine Tg and Tm as a function of reaction temperature. PTM polymerized at 135 and 175 °C with aluminum chloride, with vacuum and stirring, for 4 h, Table 2.5. For the 135 °C PTM sample, the Tg and Tm were similar to the 155 °C sample, -65.2 and 29.3 °C respectively. The Tg for the 175 °C sample was at approximately 42.3 °C and had no distinguishable Tm. No trend was notable with the limited amount of data available. The low melting point of PTM makes it useful for low temperature applications, but not for normal consumer use.

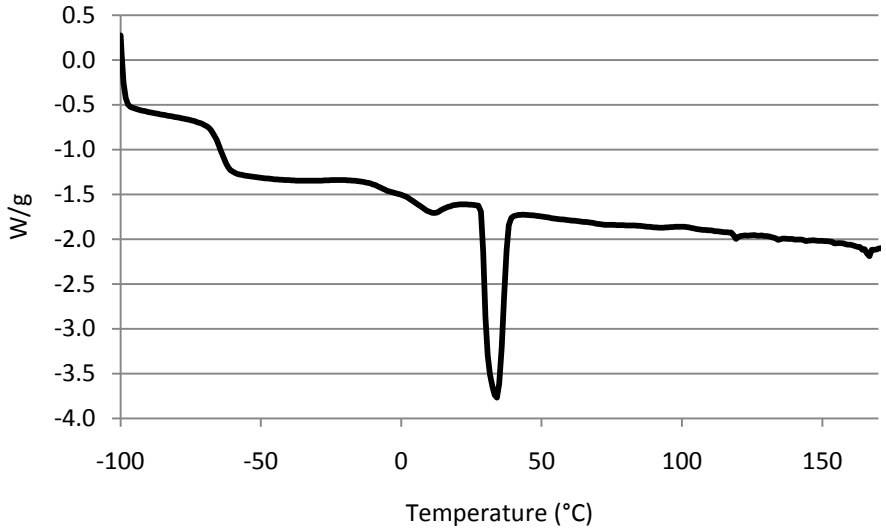

Figure 2.22: Heat flow versus temperature from DSC for PTM polymerized under vacuum with stirring and aluminum chloride catalysts for 4 h at 155 °C.

Table 2.5: Melting and glass transition temperatures for PTM samples synthesized at 135, 155, and 175 °C with aluminum chloride catalyst at 4 h with vacuum and stirring.

Reaction Temperature (°C)	Tg (°C)	Tm (°C)
135	-65.2	29.3
155	-64.6	28.7
175	-42.3	N/A

2.5. Conclusions

A bioplastics was produced from renewable monomers, PTM , with varying chemical structures and Mw. The yield, Mw, and chemical structures of PTM, a linear copolymer, depended on reaction time and temperature. The four different Lewis acids used, aluminum chloride, iron(III) chloride, tin(II) chloride, and zinc chloride, provided varying chemical structures when used to polymerize PTM. Gravimetric and GPC measurements showed substantial changes in yield and Mw with the use of larger reaction volumes and vacuum. Using FTIR, proton NMR, and XPS, it was determined that both polymers had ester and ether linkages present in PTM's backbone. The ester carbonyls had reaction times under 8 h at 155 °C and at reaction temperatures above 155 °C at 4 h reaction time. For polymerization in which vacuum and stirring were used, yields were never achieved above 99.5%, limiting the achievable Mw of the polymers through step-growth polymerization to under 2.5 kDa. The high Mw material present due to chain-growth polymerization was only present in relatively small amounts, less than 5 wt.%. Thermal analysis revealed that PTM is readily susceptible to thermal degradation and has a melting temperature of ~29 °C. Research with these polymers will continue with future hydrolytic and enzymatic degradation studies.

2.6. Recommended Future Work

As a comparison against this work, a set of experiments using no catalysts need to be performed to determine the extent of the catalyst effect. PTM polymerizations need to be performed at temperatures below 125 °C and at reaction times longer than 4 h to avoid thermodynamic effects of monomer melting and to follow green chemistry principals. Alternative chemical analysis methods need to be performed on PTM to determine if the cyclic esters are present in the final product as theorized. MALDI-ToF would be ideal for the determination of cyclic products. GC-MS would also provide information on cyclic products. More extensive thermal analysis would provide greater insight into the processing parameters of PTM. To prove that PTM is degradable, hydrolytically and bio-degradation studies need to be performed on PTM.

2.7. Acknowledgements

This work was partially funded through the Sustainable Energy Research Center at Mississippi State University under the Department of Energy award DE-FG3606GO86025. Financial support was also provided by MSU Bagley Fellowship. Completion of this work in a timely manner would not have been possible without undergraduate researchers Erin Smith, Mitch Wall, Zach Wynne, and Phillip Jamison. TGA and DSC was completed by Kimberly Ivey of Clemson University.

2.8. Disclaimer

responsibility for the accuracy, completeness, or usefulness of any information, apparatus, product, or process disclosed, or represents that its use would not infringe privately owned rights. Reference herein to any specific commercial product, process, or service by trade name, trademark, manufacturer, or otherwise does not necessarily constitute or imply its endorsement, recommendation, or favoring by the United States Government or any agency thereof. The views and opinions of authors expressed herein do not necessarily state or reflect those of the United States Government or any agency thereof.

2.9. References

Abraham, G. A., Gallardo, A., Lozano, A. E., Roman, J. S., "ε-Caprolactone/ZnCl2 Complex Formation: Characterization and Ring-Opening Polymerization Mechanism," Journal of Polymer Science, Part A: Polymer Chemistry, 38, 1355-1365, 2000.

Agrawal, J. P., "Structural Aspects of novel Unsaturated Polyesters," Pure Applied Chemistry, A30(1), 59-73, 1993.

Ajioka, M., Suizu, H., Higuchi, C., Kashima, T., "Apliphatic Polyesters and their Copolymers Synthesized through Direct Condensation Polymerizaiton," Polymer Degradation and Stability, 59, 137-143, 1998.

Albertsson, A.-C., Varma, I. K., "Aliphatic Polyesters: Synthesis, Properties and Applications," Advances in Polymer Science, 157, 1-40, 2002.

Anastas, P., Eghbali, N., "Green Chemistry: Principles and Practice," Chemical Society Reviews, 39, 301-312, 2010.

Bruno, T. J., Svoronos, P. D. N., Handbook of Basic Tables for Chemical Analysis, 2nd ed., CRC Press, Boca Raton, FL, 405-448, 2003.

Catiker, E., Gumusderelioglu, M., Guner, A., "Degradation of PLA, PLGA homo- and Copolymers in the Presence of Serum Albumin: A Spectroscopic Investigation," Polymer International, 49, 728-734, 2000.

Chen, S.-A., Wu, K.-C., "Kinetics of Polyesterification. II. Foreign Acid Catalyzed Dibasic Acid and Glycol Systems," Journal of Polymer Science: Polymer Chemistry Edition, 20, 1819-1831, 1982.

Chu, C. C., "Hydrolytic Degradation of Polyglycolic Acid: Tensile Strength and Crystallinity Study," Journal of Applied Polymer Science, 26, 1727-1734, 1981.

Cossement, D., Gouttebaron, R., Cornet, V., Viville, P., Hecq, M., Lazzaroni, R., "PLA-PMMA blends: A Study by XPS and ToF-SIMS," Applied Surface Science, 252, 6636-6639, 2006.

Dean, J. A., Lange's Handbook of Chemistry, 14th ed., McGraw-Hill, Inc., 7.42-7.71, 1992.

Dell'Erba, R., Martuscelli, E., Musto, P., Ragosta, G., "Unsaturated Polyester Resins: a Study of the Mechanism and kinetics of the Curing Process by FTIR Spectroscopy," Polymer Networks and Blends, 7(1), 1-11, 1997.

Dobrzynaski, P., Kasperczyk, J., Janeczek, H., Bero, M., "Synthesis of Biodegradable Glycolide/L-Lactide Copolymers using Iron Compounds as Initiators," Polymer, 43, 2595-2601, 2002.

Dodds, D. R., Gross, R. A., "Chemicals from Biomass," Science, 318, 1250-1251, 2007.

Drumright, R. E., Gruber, P. R., Henton, D. E., "Polylactic Acid Technology", Advanced Materials,, 12, 1841-1846, 2000.

Erdmann, L., Uhrich, K. E., "Synthesis and Degradation Characteristics of Salicylic Acid-Derived Poly(anhydride-esters)," Biomaterials, 21, 1941-1946, 2000.

Flory, P. J., "Fundamental Principles of Condensation Polymerization," Chemical Review, 39, 137-197, 1946.

Flory, P. J., Principles of Polymer Chemistry, Cornell University, 29-36, 1953.

Garcia-Serna, J., Perez-Barrigon, L., Cocero, M. J., "New Trends for Design Towards Sustainability in Chemical Engineering: Green Engineering," Chemical Engineering Journal, 133, 7-30, 2007.

Gopferich, A., "Mechanisms of Polymer Degradation and Erosion," Biomaterials, 17, 103-114, 1996.

Gulmine, J. V., Akcelrud, L., "FTIR Characterization of Aged XLPE," Polymer Testing, 25, 932-942, 2006.

Helminen, A., O., Korhonen, H., Seppala, J.V., "Crosslinked Poly(ester anhydride)s Based on Poly(ε-caprolactone) and Polylactide Oligomeers," Journal of Polymer Science: Part A: Polymer Chemistry, 41, 3788-3797, 2003.

Henton, D. E., Gruber, P., Lunt, J., Randall, J., "Polylactic Acid Technology," Natural Fibers, Biopolymers, and Biocomposites, CRC Press, Boca Raton, FL, 527-577, 2005.

Jerome, C., Lecomte, P., "Recent Advances in the Synthesis of Aliphatic Polyesters by Ring-Opening Polymerizaiton," Advanced Drug Delivery Reviews, 60, 1056-1076, 2008.

John, G., Tsuda, S., Morita, M., "Synthesis and Modification of New Biodegradable Copolymer: Serine/Glycolic Acid Based Copolymers," Journal of Polymer Science Part A: Polymer Chemistry, 35(10), 1901-1907, 1996.

Kajiyama, t., Taguchi, T., Kobayashi, H., Kataoka, K., Tanaka, J., "Synthesis of High Molecular Weight Poly(α,β-malic acid) for Biomedical use by Direct Polycondensation," Polymer Degradation and Stability, 81, 525-530, 2003.

Kobayashi, S., Makino, A., "Enzymatic Polymer Synthesis: An Opportunity for Green Polymer Chemistry," Chemical Review, 209, 5288-5353, 2009.

Kricheldorf, H. R., "Polycondensation of 'a-bn' or 'a2 ++ bn' Monomers – A Comparison," Macromolecular Rapid Communications, 28, 1839-1870, 2007.

Kricheldorf, H. R., "What does Polycondensation Mean?" Macromolecular Symposium, 199, 1-13, 2003.

Kricheldorf, H. R., Mang, T., Jonte, J. M., "Polylactones. 1. Copolymerization of Glycolide and e-Caprolactone," Macromolecules, 17, 2173-2181, 1984.

Kuchanov, S., Slots, H., Stroeks, A., "Development of a Quantitative Theory of Polycondensation," Progress in Polymer Science, 29, 563-633, 2004.

Li, H., Wang C., Bai, F., Yue, J., Woo, H.-G., "Living ring-Opening Polymerizaiton of L-Lactide Catalyzed by Red-Al," Organometallics, 23, 1411-1415, 2004.

Louette, P., Bodino, F., Pireaux, J.-J., "Poly(dimethyl siloxane) (PDMS) XPS Reference Core Level and Energy Loss Spectra," Surface Science Spectra, 12, 38-43, 2005.

Louette, P., Bodino, F., Pireaux, J.-J., "Poly(methyl methacrylate) (PMMA) XPS Reference Core Level and Energy Loss Spectra," Surface Science Spectra, 12, 69-73, 2005.

Mahdavian, A. R., Abdollahi, M., "Kinetic Study of Radical Polymerization. VII. Investigation into the Solution copolymerization of Acrylonitrile and Itaconic Acid by Real-Time ^{1}H NMR Spectroscopy," Journal of Applied Polymer Science, 103, 3253-3260, 2007.

Mohanty, A. K., Misra, M., Hinrichsen, G., "Biofibres, Biodegradable Polymers and Biocomposites: An Overview, Macromolecular Materials and Engineering," 276-277, 1-24, 2000.

Moon, S, I,. Lee, C. W., Miyamtot, M., Kimura, Y., "Melt Polycondensation of L-Lactic acid with Sn(II) Catalysts Activated by Various Proton Acids: A Direct Manufacturing Route to High Molecular Weigh Poly(L-lactic acid)," Journal of Polymer Science, Part A: Polymer Chemistry, 38, 1673-1679, 2000.

Nanse, G., Papirer, E., Fioux, P., Moguet, F., Tressaud, A., "Fluorination of Carbon Blacks. An X-Ray Photoelectron Spectroscopy Study. Part II. XPS Study of a Furnace Carbon Black treated with Gaseous Fluorine at Temperatures below 100 °C. Influence of the Reaction Parameters and of the Activation of the Carbon Black on the Fluorine Fixation," Carbon, 35(3), 371-388, 1997.

Odian, G., Principles of Polymerization 3rd ed., John Wiley & Sons, New York, 41-197, 1991.

Okada, M., "Chemical Synthesis of Biodegradable Polymers," Progress in Polymer Science, 27, 87-133, 2007.

Phillip, S., Keshavarz, T., Roy, I., "Review Polyhydroxyalkanoates: Biodegradable Polymers with a Range of Applications," Journal of Chemical Technology and Biotechnology, 82, 233-247, 2007.

Poliakoff, M., Fitzpatrick, J. M., Farren, T. R., Anastas, P. T., "Green Chemistry: Science and Politics of Change," Science, 297, 807-825, 2002.

Pretsch, E., Buhlmann, P., Affolter, C., Structure Determination of Organic Compounds, Tables of Spectral Data, Springer, Berlin, 161-244, 2000.

Qian, H., Mathiowitz, E., "Acyl Chloride –Facilitated Condensation Polymerization for the Synthesis of Heat-Sensititve Poly(anhydride-ester)s," Journal of Polymer Science: Part A: Polymer chemistry, 45, 5899-5915, 2007.

Ragauskas, A. J., Williams, C. K., Bavison, B H., Britovsek, G., Cairney J., et al, "The Path Forward for Biofuels and Biomaterials," Science, 311, 484-489, 2006.

Sabbatini, L., Zambonin, P. G., "XPS and SIMS Surface Chemical Analysis of some Important Classes of Polymeric Biomaterials," Journal of Electron Spectroscopy and Related Phenomena, 81, 285-301, 1996.

Satchell, D. P. N., Satchell, R. S., "Mechanistic Aspects. Recent Developments Concerning Mechanisms of Acylation by Carboxylic Acid Derivatives," Supplement B: The Chemistry of Acid Derivatives, Vol. 2, Johy Wiley & Sons, Ltd., Hoboken, New Jersey, 747-802, 1992.

Saunders, J. H., Dobinson, F., "The Kinetics of Polycondensation Reactions," Comprehensive Chemical Kinetics, 473-581, 1976.

Saunders, J. H., Dobinson, F., "The Kinetics of Polycondensation Reactions," in Comprehensive Chemical Kinetics, Vol. 15, Bamford, C. H., Tippers, C. F. H., American Elsevier, New York, 473-581, 1976.

Silverstein, R. M., Blassler, G., C., Morrill, T. C., iSpectrometric Identification of Organic Compounds, 5th ed., John Wiley & Sons, Inc., Hoboken, NJ, 102-133, 1991.

Silverstein, R. M., Webster, F. X., Kiemle, D. J., Spectrometric Identification of Organic Compounds, 7th ed., John Wiley & Sons, Hoboken, NJ, 127-203, 2005

Smith, M., March, J., "Aliphatic Substitution: Nucleophilic and Organometallic," March's Advanced Organic Chemistry, 6th ed., Wiley-Interscience, Hoboken, New Jersey, 425-656, 2007.

Snell, F. D., Ettre, L. S., "Malonic Acid and Derivatives," Encyclopedia of Industrial Chemical Analysis, Interscience Publishers, New York, 15, 929-945, 1972.

Sodergard, A., Stolt, M., "Ring-Opening Polymerizaiton of L-lactide by Means of Different Iron Compounds," Macromolecular Symposium, 130, 393-402, 1998.

Storey, R. F., Sherman, J. W., "Novel Synthesis of (Carboxylic Acid)-Telechelic Poly(ε-Caprolacton)," Polymer Preprints, 42(2), 2001.

Sun, J., Shi, W., Chen, D., Liang, C., "The Ring-Opening Polymerization of D,L-Lactide Catalyzed by New Complexes of Cu, Zn, Co, and Ni Schiff Base Derived from Salicylidene and L-Aspartic Acid," Journal of Applied Polymer Chemistry, 86, 3312-3315, 2002.

Sutton, D., Durand, R., Shuai, X., Gao, J., "Poly(D,L-Lactide-co-Glycolide)/Poly(Ethylenimine) Blend Matrix System for pH Sensitive Drug Delivery," Journal of Applied Polymer Science, 100, 89-96, 2006.

Tamada, J. A., Langer, R., "Erosion Kinetics of Hydrolytically Degradable Polymers," Proceedings of the National Academy of Science, 90, 552-556, 1993.

Teramoto, N., Kogure, H., Kimura, Y., Shibata, M., "Thermal Properties and Biodegradability of the copolymers of L-Lactide, ε-Caprolactone, Ethylene Glycol Oligomer with Maleate Units and their Crosslinked Products," Olymer, 45, 7927-7933, 2004.

Wilson, M. P., Schwarzman, M. R., "Toward a New U.S. Chemicals Policy: Rebuilding the Foundation to Advance New Science, Green Chemistry, and Environmental Health," Environmental Health Perspectives, 117(8), 1202-1209, 2009.

Zhou, Y., Wy, G.-L., Zhou, R.-X., Liu, Z.-L., "Synthesis and Properties of Novel Aliphatic Poly(Carbonate-Esters)s," European Polymer Journal, 45, 1868-1872, 2009.

CHAPTER 3

SYNTHESIS AND CHARACTERIZATION OF COPOLYMERS BASED ON 1,3-PROPANEDIOL AND ITACONIC ACID RENEWABLY RESOURCED MONOMERS

3.1. Abstract

To reduce our environmental impact and reduce our dependence on petroleum based polymers, renewable based polymers, bioplastics, were polymerized from renewably resourced monomer 1,3-propanediol (PDO) and itaconic acid (IA) using green chemistry principals to produce poly(trimethylene itaconate) (PTI). Reaction time was varied from 2 to 32 h, and reaction temperature was varied from 125 to 175 °C to maximize gravimetric yield and molecular weight using melt polycondensation using aluminum chloride as the catalyst with vacuum and stirring. Gravimetric yield was determined as a function of reaction temperature and time, and it varied from 20 to 85 wt.%. To determine the chemical structure, transmission Fourier transform infrared (FTIR) spectroscopy, proton nuclear magnetic resonance (NMR), and x-ray photoelectron spectroscopy (XPS) were used, and they confirmed the presence of ester and ether bonds with concentrations dependent on reaction time and temperature. Gel-permeation chromatography (GPC) was used to determine molecular weight and polydispersity index. A bi-modal molecular weight distribution was found, and it was dependent on both reaction temperature and time. The high molecular weight ranged from 25 to 50 kDa, and the low molecular weight did not exceed 3 kDa. Thermal analysis was performed using

thermogravimetic analysis (TGA) and differential scanning calorimetry (DSC). TGA showed that 5 wt.% loss occurred at a minimum of 190 °C and was dependent on reaction temperature. A cold crystallization peak was found at ~160 °C by DSC. Copolymers of PDO and IA were made chemical structures and molecular weights dependent on reaction temperature.

3.2. Introduction

For the introduction and background on monomer and catalyst selection, comparable bioplastics, and reactions, referrer to Chapter 2. For unsatureated monomers, there are reactions that occur due to the presence of alkenes. Ordelt saturation needs to be considered for the unsaturated monomers. Ordelt saturation is defined as the electrophilic addition of hydroxyl group to a carbon double bond. Under acidic conditions, a double bond can be saturated by an alcohol group leading to polymer branching and possible formation of an infinite network. The degree of saturation is dependent on the acidity, temperature, and alcohol concentration of the reaction mixture and can lead to a reduction of 10 to 20% of the C-C double bonds under thermodynamically controlled conditions [Fardet 1982-A, Fardet 1982-B, Zetterlund 2002]. In Figure 3.1, the addition of an alcohol to fumaric acid is shown as a representative mechanism for Ordelt saturation. With maleic acid and fumaric acid, this reaction is difficult to avoid, and with other unsaturated linear monomers, this reaction should be considered, as it will affect the final products, mechanical properties and chemical structure [Fardet 1982-B].

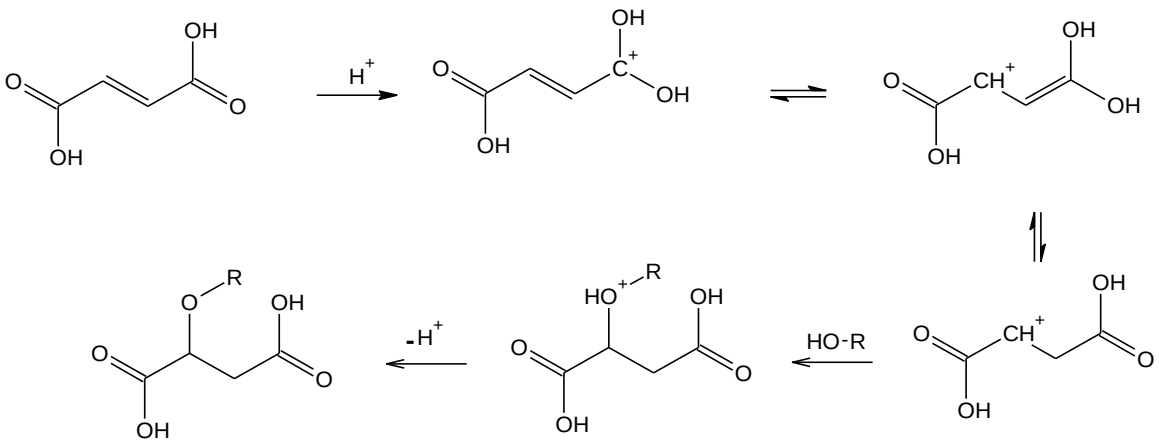

Figure 3.1: Mechanism for the Ordelt saturation of fumaric acid [Fardet 1982-B].

Since the polycondensation reaction being studied is acid catalyzed, electrophilic addition reactions with the unsaturated monomers which occur under acidic conditions and are similar to Ordelt saturation need to be considered, Figure 3.2. Electrophilic addition does differ from Ordelt saturation in that a proton and a halide is used to saturate the double bond. If R_1 and R_2 are CH_2, the chlorine will add without any preference to location. When using catalysts such as Lewis acids, it is not unusual to have an acid side-product present that will support electrophilic addition.

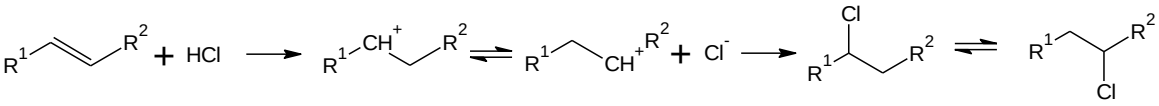

Figure 3.2: Mechanism for the electrophilic addition of a chlorine to an unsaturated carbon chain [Saunders 1976].

The chlorination of the double bond could lead to additional branching and cross-linking within the polymer. The chlorinated product of the electrophilic addition can have the chlorine replaced by an alcohol, leading to branching in a similar fashion as the Ordelt saturation, Figure

3.3. If a methylene group is present, the electrophilic addition of the double bond will preferentially place the chlorine on the more substituted carbon because the carbon cation is more stable. This will lead to the formation of methyl group on the carbon chain as seen in Figure 3.3. When a double bond is present on one of the monomers during polycondensation under acidic conditions, reactions are possible at the double bond and should be considered during characterization.

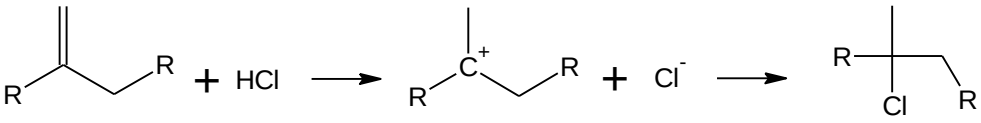

Figure 3.3: Generic reaction scheme for the electrophilic addition of a chlorine to a methylene group [Saunders 1976].

Because of branching and cross-linking, the molecular weight (Mw) determined by GPC can have significant error and the effective molecular weight (EMw) of a polymer may differ from the Mw. When a monomer with more than two function groups is used for polycondensation, branching and cross-linking can occur and distort the polymer shape and thus change the radius of gyration [Odian 1991, Buchard 1999]. A branched and cross-linked polymer will have a smaller radius of gyration than a linear polymer due to restrictions polymer chain movement by the additional bonds [Daoud 1990, Buchard 1999]. The smaller radius gyration of a branched and cross-linked polymer reduces the apparent Mw when using GPC with a refractive index detector that is calibrated with linear standards, such as polystyrene standards. The EMw of a polymer increases with increasing branching and cross-linking due to polymer entanglement. The increase in polymer entanglement is due to increased topological interaction of the polymers chain giving them properties similar to linear polymers of higher Mw

[Doi 1996, Rubinstein 2003]. Branching and cross-linking of a polymer decreases the radius of gyration and increases the EMw.

3.3. Experimental Materials and Methods

Reagents. 1,3-Propane diol (PDO, 98%, Sigma Aldrich, Figure 3.4), itaconic acid (IA, 99%, VWR, Figure 3.4), $AlCl_3$ catalyst (98%, Sigma Aldrich), Optima tetrahydrofuran (Fisher Scientific, +99.9%), chloroform (VWR, 98%), diethyl ether (VWR, >99%) were used as received.

Figure 3.4: PDO and MA monomer chemical structures.

Copolymerization of 1,3-propanediol (PDO) and itaconic acid (IA). Experiments were performed in a 100 mL round bottom flask (~ 50 g monomer) for 2-32 h at 155 °C and 16 h at 125-175 °C and 25 torr with mixing using a magnetic stir bar. A 100:1 M/C ratio and a 1:1 acod:alcohol monomer ratio was maintained for all reactions.

Polymer separation. Excess monomer and catalyst were removed from the reaction products by dissolving in chloroform and then poured into diethyl ether. Precipitated polymer was then filtered using Whitman (grade 40) filter paper. For each reaction, this separation procedure was repeated until precipitated polymer could no longer be visually identified. The filtered polymer was dried in a vacuum oven at 15 torr and 20 °C for 24 h and then weighed.

Characterization. A Bruker AMX-300 NMR instrument was used to collect H^1 spectra at 300 MHz. Samples were dissolved into deuterated chloroform and tetramethylsilane (TMS)

added as an internal standard. Based on the reaction mechanisms discussed previously, options for the PTM repeat unit were determined. NMR chemical shifts were determined using literature references [Mahdarian 2006, Spyrous 1996, Chikh 2007, Kohut 2009, Bruno 2003, Silverstein 2005]. A PHI 1600 Electron Scanning Chemical Analysis (ESCA) instrument with PHI 10-360 spherical detector and achromatic Mg K_α X-ray source (300 W, 15 kV) was used to gather additional information on the chemical composition and repeat unit structure. The spectrum were collected with PHI Surface Analysis Software for windows version 3.0 copyright 1994 Physical electronics Inc. and analyzed with CasaXPS version 2.2.88. The C-H peak for in the carbon high resolution scan was shifted to 285 eV as a reference. The polymer was also characterized by transmission FTIR spectroscopy using a Thermo Electron 6700 instrument purged with dry air. PTI was solution coated onto KBr crystal using tetrahydrofuran (THF) as the solvent. Gravimetric product yields were calculated using the limiting monomer to determine theoretical yields based on complete conversion. The recovered polymer weight was divided by the theoretical weight and then converted to percent yield. Differential scanning calorimetry (DSC) was performed on a TA Instruments Q1000 DSC using Therma Advanted for Q series version 2.8.0.392 version 4.8.2 with aluminum hermetic pans, purged with helium at 20 mL/min, and a heating rate of 5 °C/min from -40 °C to 200 °C or 400 °C. Thermalgravimetric analysis (TGA) was performed on a TA Instruments Q5000 with the same instrument control and data analysis software as the DSC. Samples were analyzed from room temperature to 400 °C at 10 °C/min under nitrogen using Al_2O_3 pans. A Waters gel permeation chromatograph (GPC) with RI detector, 4E and 5E (polystyrene-dinvinylbenzene, 4.6 x 300 mm) Styragel® columns, 0.3 mL/min THF effluent, and a 10-point polystyrene calibration was used to determine molecular weights and polydispersities. A Rigaku SmartLab X-ray diffraction (XRD) system was used with a 2.2 kW

long-fine focus x-ray tube, Bragg-Brentano para-focusing optics, and GE (220) 4-bounce incident beam monochromator with 2θ varying from 3° to 153° using somesort of software.

3.4. Results and Discussion

Using aluminum chloride for the reasons discussed in Chapter 2, PDO and IA were polymerized to make poly(trimethylene itaconate) (PTI). The reactions were performed using 50 g of monomer with reaction temperature ranging from 125 to 175 °C and reaction time ranging from 2 to 32 h. Chemical structure was examined with FTIR, NMR, and XPS, and the molecular weights (Mw) and polydispersities (PDI) were examined with GPC. Thermal properties of the PTM copolymer was characterized using TGA and DSC to determine thermal properties.

3.4.1. Gravimetric Yields

As shown in Figure 3.5, PTI demonstrated steady yield increases from 20% at 125 °C to a maximum of 78% at 155 °C. A dip in yield to 52% occurs at 165 °C due to energy being used to melt IA, and then the yield increases back to the maximum at 175 °C. The PTI reaction is thermodynamically controlled in the same manner as the PTM reaction, Chapter 2. As the reaction progresses and the system increases viscosity until it becomes a gel and stirring ceases, the diffusion rate of water decreases, leading to the entrapment of water. The entrapped water reduces the driving force of the reaction to produce polymeric products and increases the reverse reaction, hydrolytic scission of the polymeric chains. The reverse reaction limits the gravimetric yields to < 90%.With a strict step-growth polymerization and a linear PTI polymer structure, it would be necessary to obtain yields greater than 99% for usable polymer molecular weights. Since PTI polymer is a branched polymer, the conversion necessary to achieve a usable Mw is lowered as the gel is formed, producing an insoluble infinite networked polymer. With

Ordelt saturation being temperature dependent, higher reaction temperatures will produce polymers with increasing numbers of branch points [Fradet 1982]. The increase in Ordelt saturation may overcome the hydration reaction by adding an addition reaction pathway besides $A_{AC}2$ and $A_{AL}1$. With increasing reaction temperature, Ordelt saturation will be become more prevalent countering the $A_{AC}2$ and $A_{AL}1$ reverse reaction that will increase with increasing reaction temperature.

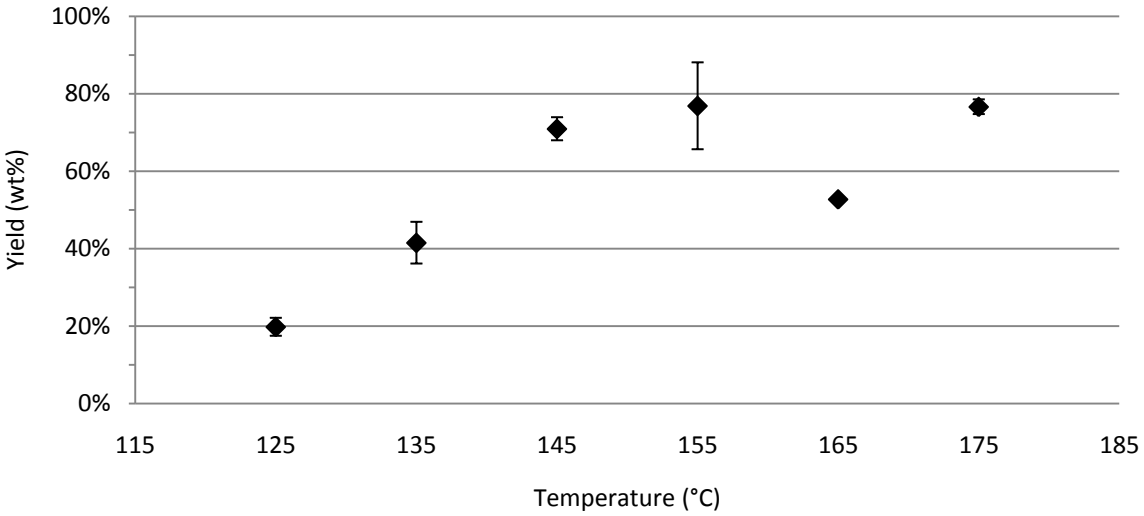

Figure 3.5: PTI gravimetric yield dependence on reaction temperature, 125 to 175 °C, (16 h reaction time and aluminum chloride catalyst) with 95% confidence intervals.

Shown in Figure 3.6, the yield for PTI is dependent on reaction time and has a parabolic shape with a maximum between 8 and 24 h. The parabolic response is related to viscosity changes and small molecule entrapment. Through visual inspection, during the first 8 h, the viscosity of the mixture increased dramatically. After 8 h there was not a noticeable change in the viscosity of the mixture followed by degradation and a resulting significant decrease in viscosity at reaction times greater than 20 h. The system does appear to reach a plateau in gravimetric yield from 8 to 24 h. By classical theory, the rate at which the yield increases should

reduce as the reaction approaches a yield of 100%. For the PTI system, it appears that the limit of reaction yield is 99.5%. The decrease in yield above 20 h in Figure 3.6 is also in conflict with classical theory of step-growth polymerization. The yield should increase continuously with increasing reaction time unless a side reaction, such as hydrolysis, is causing the reaction to proceed in reverse. A fraction of all reaction products was insoluble in tetrahydrofuran and chloroform at temperatures from 145 to 175 °C and 8 h to 32 h. The insoluble fraction is assumed to be branched or cross-linked PTI. Since the starting material was unsaturated, Ordelt saturation and electrophilic addition of hydrochloric acid are likely occurring to produce a branched structure, which is supported by gel formation during the reaction. Whether Ordelt saturation of the electrophilic addition is dominant during synthesis is not known and was not further investigated. With Ordelt saturation, the carbon cation that the alcohol will react with will be at the more substituted carbon. This will lead to the branch coming off the carbon that the methylene group is attached to and not the methylene carbon for the majority of the products. Gravimetric yields alone do not give a good perspective on the best temperature conditions; however, it does narrow the temperature range to be investigated further. Based on Mw and the desired chemical and physical properties, optimum reaction conditions can be determined.

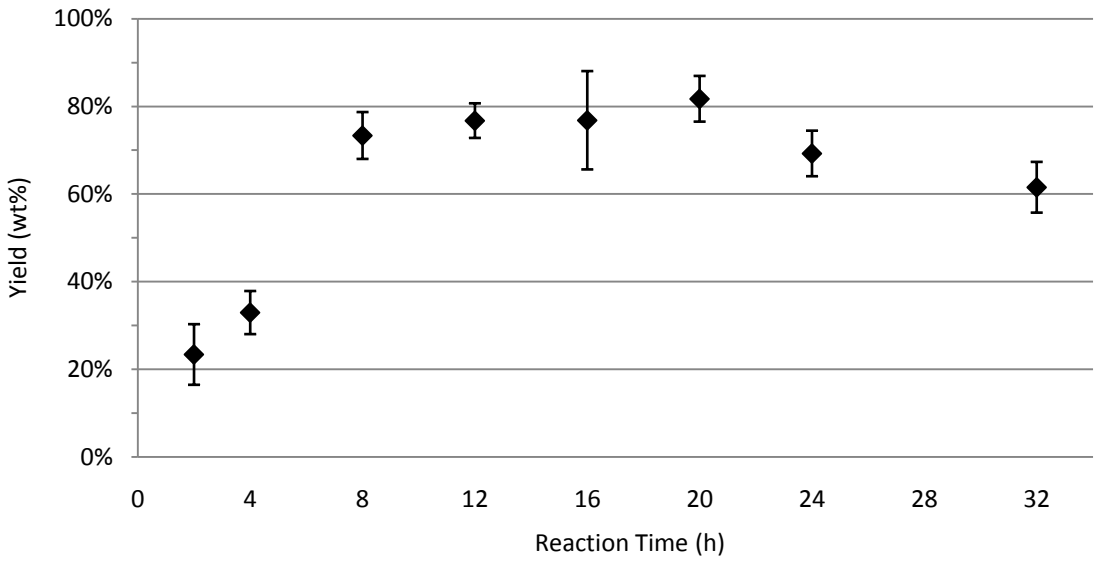

Figure 3.6: PTI gravimetric yield dependence on reaction time, 2 to 32 h, (155 °C reaction temperature and aluminum chloride catalyst) with 95% confidence intervals.

3.4.2. Transmission FTIR Spectroscopy

Transmission FTIR spectra were taken of all resultant polymers in the condensed state to determine chemical composition and functional group concentration. Solution coating KBr crystals may have resulted in selective FTIR analysis of the PTI THF soluble fraction. In addition to general chemical characterization, the relative concentrations of ester groups were determined by spectral analysis for PTI polymers produced under different reaction conditions. Carbonyl peak height ratio was used to determine semi-quantitative concentrations of the anhydride, ester, and carboxylic acid functional groups. Spectral analysis for the PTM copolymers provided key information regarding the chemical structure and, therefore, the reaction mechanisms involved.

Representative PTI FTIR spectrum shown in Figures 3.7 and 3.8 have major features including a very broad peak from 3700 to 2200 cm^{-1} from the C-H stretch of carboxylic acid, a C-H stretch peak for CH_X from 3050 to 2780 cm^{-1}, a strong peak for the C=O stretch from 1865 to

1680 cm^{-1}, and a peak for the C=C stretch at 1637 cm^{-1} [Dell'Erba 1997, Silverstein 1991, Dean 1992]. Peak fitting of the carbonyl and alkene stretch region, 1865 to 1520 cm-1, revealed seven peaks, Figure 3.9. The seven peaks were identified as 1587 cm^{-1} carboxylate anion carbonyl stretch (1), 1639 cm^{-1} vinylidine stretch (2), 1673 cm^{-1} trans-substituted alkenes or tri-/quad-substituted alkenes stretch (3), 1704 cm^{-1} dimerized carboxylic acid carbonyl stretch (4), 1744 cm^{-1} ester carbonyl stretch (5), 1786 cm^{-1} cyclic anhydride carbonyl symmetric stretch (6), and 1822 cm^{-1} cyclic anhydride carbonyl asymmetric stretch (7) [Dell'Erba 1997, Silverstein 1991, Dean 1992, Helminen 2003]. PTI synthesis followed the $A_{AC}2$ and $A_{AL}1$ mechanism with the formation of both ester linkages. The peaks below 1,000 cm^{-1} are from different cis-trans double bonds configurations, which shows that there was bonding at the double bonds. The saturation of double bonds, shown by a decrease in PHR of the peak at 1650 cm^{-1}, is from saturation by hydrogen or Ordelt saturation leading to branching of the polymer. The ester carbonyl showed a dependence on both time and temperature. Furthermore, the saturation of the double bond also showed dependence on time and temperature. The chemical structure of PTI was dependent on reaction temperature and time, leading to different degrees of double bond saturation and changes in concentration of ester functional groups.

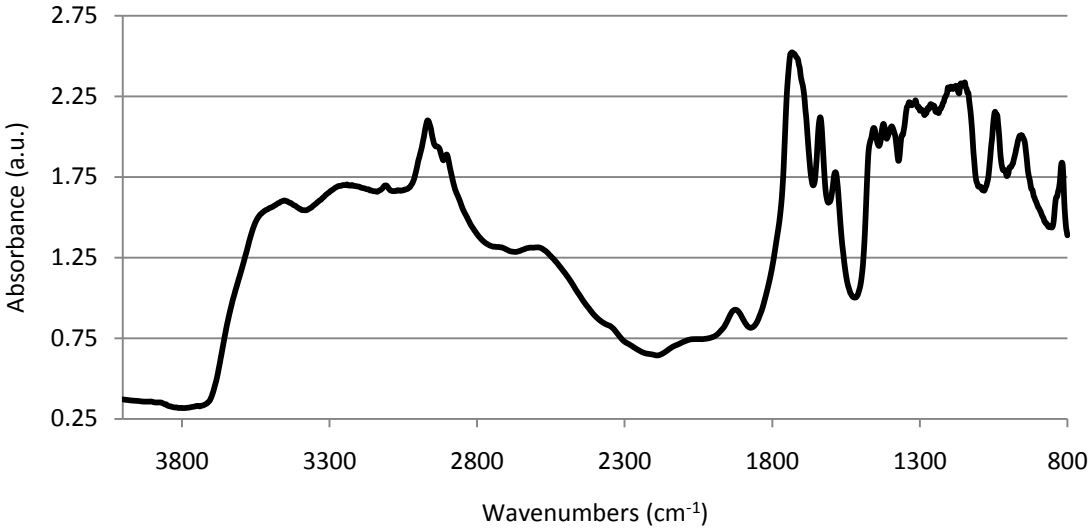

Figure 3.7: Representative transmission FTIR spectra of PTI made at 155 °C for 16 h with aluminum chloride catalyst.

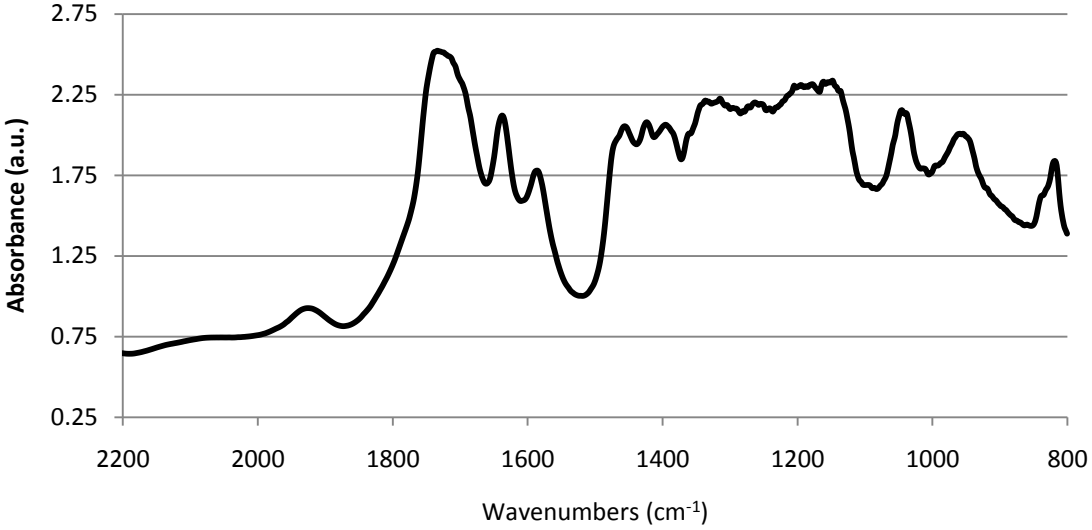

Figure 3.8: Representative transmission FTIR spectra of PTI made at 155 °C for 16 h with aluminum chloride catalyst from 800 to 2200 cm^{-1}.

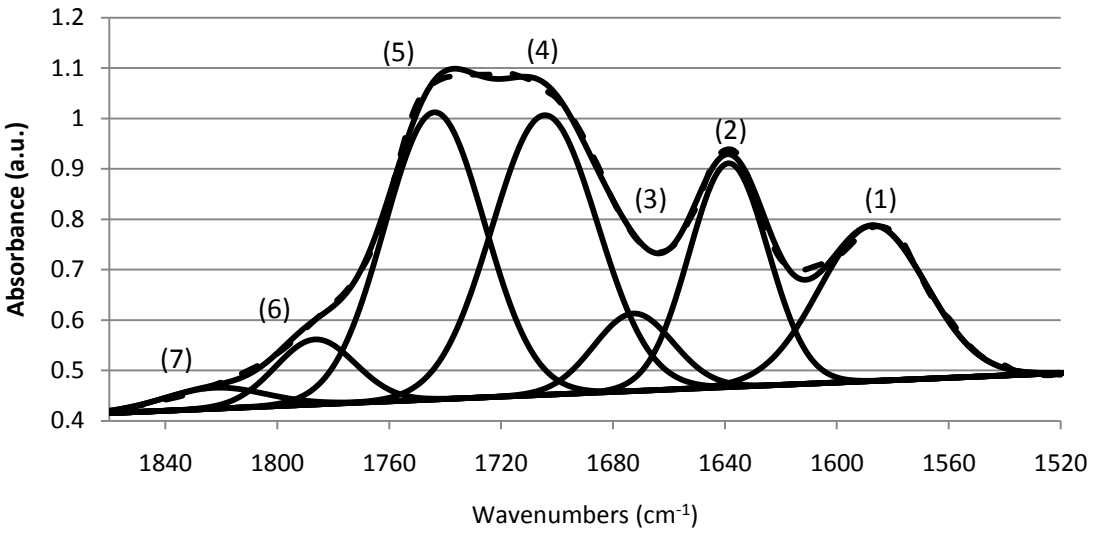

Figure 3.9: Representative transmission FTIR spectrum of 1520 to 1860 with fitting of 1587 cm^{-1} carboxylate anion carbonyl stretch (1), 1639 cm^{-1} vinylidine stretch (2), 1673 cm^{-1} trans-substituted alkenes or tri-/quad-substituted alkenes stretch (3), 1704 cm^{-1} dimerized carboxylic acid carbonyl stretch (4), 1744 cm^{-1} ester carbonyl stretch (5), 1786 cm^{-1} cyclic anhydride carbonyl symmetric stretch (6), and 1822 cm^{-1} cyclic anhydride carbonyl asymmetric stretch (7) .

In Figure 3.10 using Equation 1.1, the PHRs as a function of reaction temperature are shown for carboxylate anion, vinylidene, carboxylic acid, ester, cyclic anhydride symmetric and asymmetric carbonyl stretch. The carboxylic acid, 1704 cm^{-1}, and ester, 1743 cm^{-1}, carbonyl PHR changes provide the most information into reaction temperature impact on polymerization. Ester formation, through the $A_{AC}2$ and $A_{AL}1$ mechanisms, will decrease carboxylic acid carbonyl PHR, increase ester carbonyl PHR, and increase PTI Mw. With increasing reaction temperature from 125 to 155 °C, the ester PHR increases from ~1.5 to ~3.8, and over the same temperature range, the carboxylic acid carbonyl decreases from ~3 to ~1.5. The yield, Figure 3.5, increases from ~20 wt.% to ~76 wt.% from 125 to 155 °C reaction temperature. The increase in ester carbonyls and gravimetric yield indicates that the $A_{AC}2$ and $A_{AL}1$ reaction are favoring ester formation over ester hydrolysis. The increase in yield cannot be completely contributed to ester bond formation from 125 to 155 °C. The vinylidene PHR, 1639 cm-1, decreased from ~1.3 to

~0.9 with reaction temperature increasing from 125 to 155 °C indicating that Ordelt saturation was occurring and forming branch and cross-links. Ordelt saturation increasing with increased reaction temperature was expected because Ordelt saturation is endothermic [Fardet 1982]. When the reaction temperature was increased from 155 to 165 °C, the reaction reached IA's melting point range, 165 to 169 °C, which may have influence the system's thermodynamics [MSDS]. The carboxylic acid carbonyl PHR increased from ~1.5 to ~2.8, ester carbonyl PHR decreased from ~3.8 to ~2.8, and the yield decreased from ~76 wt.% to ~53 wt.%. The increased in reaction temperature to 165 °C caused a change in thermodynamics due to IA melting and shifted the $A_{AC}2$ and $A_{AL}1$ equilibrium towards ester hydrolysis. When the reaction temperature is increased to 175 °C, carboxylic acid PHR increases to ~3.2 and ester carbonyl PHR decreases to ~2.2 as ester hydrolysis becomes dominant. Another reason for the decrease in ester carbonyl is the rate of deactivation of aluminum chloride increases with increasing reaction temperature. More study would be needed to confirm whether thermodynamic changes or catalyst deactivation is the reason for reduced ester carbonyl PHR. From 165 to 175 °C, the reaction yield increased due to Ordelt saturation. The vinylidene PHR decreased from ~0.9 to ~0.7 as branching increased causing the yield to increase from 165 to 175 °C. From 125 to 175 °C, the carboxylate anion PHR decreased from ~1.2 to ~0.7 as IA preferred to form cyclic anhydrides with increasing temperature. The symmetric and asymmetric cyclic anhydride PHR increased from 0 to ~0.7 and 0 to ~0.4 as the carboxylate anion PHR decreased from 125 to 175 °C. Ester formation is favored by the $A_{AC}2$ and $A_{AL}1$ mechanisms until IA melting temperature is reached at 165 °C, and Ordelt saturation increases with increasing reaction temperature.

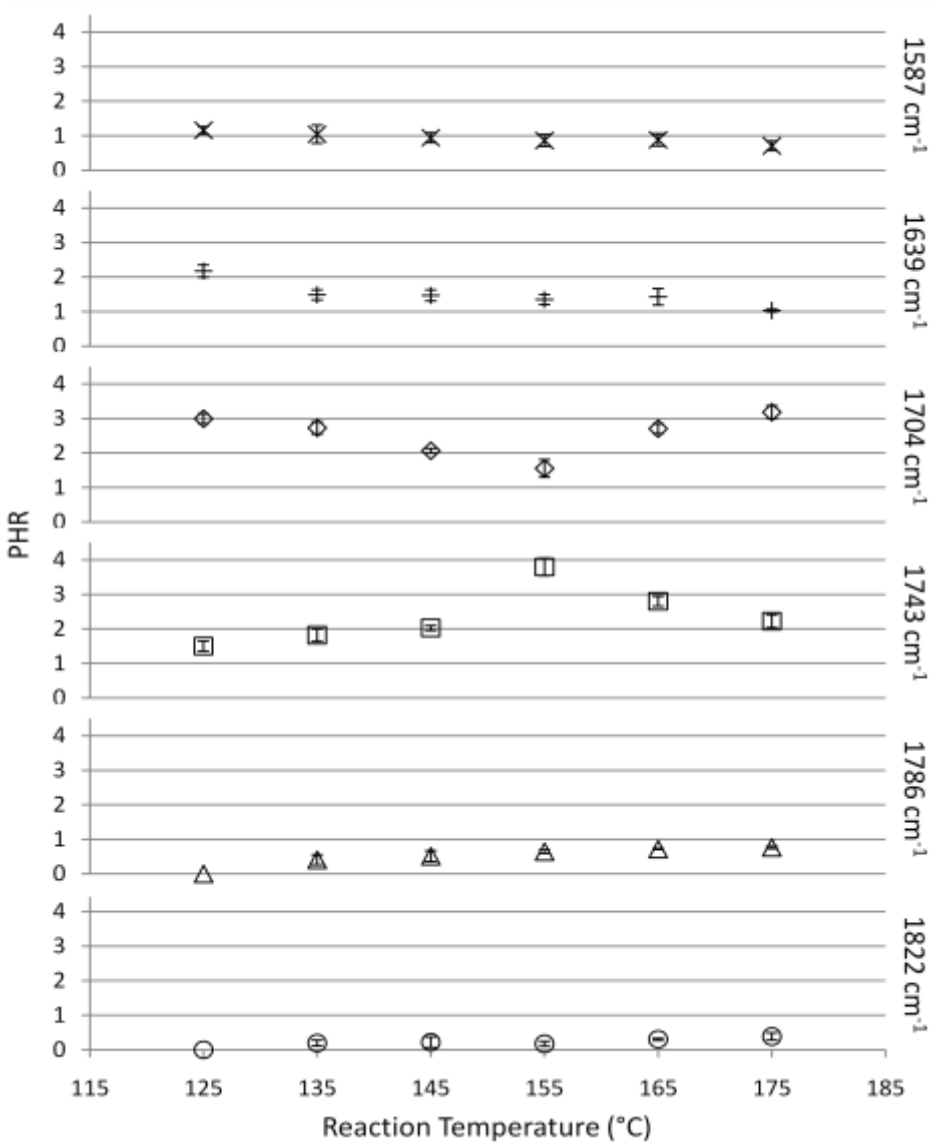

Figure 3.10: Representative transmission FTIR spectrum of 1520 to 1860 with fitting of 1592 cm^{-1} carboxylate anion carbonyl stretch, ×; 1639 cm^{-1} vinylidine stretch, +; 1704 cm^{-1} dimerized carboxylic acid carbonyl stretch, ◇, 1744 cm^{-1} ester carbonyl stretch, □; 1786 cm^{-1} cyclic anhydride carbonyl symmetric stretch, △; and 1822 cm^{-1} cyclic anhydride carbonyl asymmetric stretch ○, at variable reaction temperature with bars indicating 95% confidence intervals (16 h reaction time and aluminum chloride).

PTI chemical structure showed a dependence on reaction time from 2 to 32 h, Figure 3.11. The carboxylic anion (1587 cm^{-1}, ~0.7) and asymmetric and symmetric cyclic anhydride (1786 and 1822 cm^{-1}, ~0.4 and ~0.2) carbonyl PHR showed no dependence on reaction time from 2 to 24 h. The carboxylate anion and cyclic anhydride come to equilibrium in the first 2 h at 155 °C, and they stay at equilibrium until PTI begins to carbonize. At 32 h, PTI started to carbonize as indicated by the appearance of black spots. The asymmetric and symmetric cyclic anhydride peaks did not appear in the 32 h spectra and the carboxylate anion PHR decreased from ~0.7 to ~0.5. As ester carbonyl PHR increases from ~1.2 to ~3.8 over the reaction time 2 to 16 h, the carboxylic acid carbonyl PHR decreases from ~2.9 to ~1.5. At 16 h an 155 °C, PTI reaches the maximum ester carbonyl PHR and minimum carboxylic acid carbonyl PHR in both the temperature and time varied studies. From 16 to 32 h, the ester carbonyl PHR decreases from ~3.8 to ~2.5, and the carboxylic acid carbonyl PHR increases from ~1.5 to ~2.9. The decrease in ester carbonyl is accompanied by a decrease in yield from ~76 wt.% to ~62 wt.%. At longer reaction times, catalyst deactivation could be shifting $A_{AC}2$ and $A_{AL}1$ equilibrium to favor the monomers. Another reason is an increase water concentration with increasing reaction time. The deactivation of catalyst theory is favored. When aluminum chloride decomposes, it produces hydrochloric acid gas at the PTI polymerization conditions, 155 °C and 40 torr, and the condensate coming off of the reactor has a -2 pH. To prove this theory, additional catalyst would have to be added during the reaction, which was not done during these experiments.

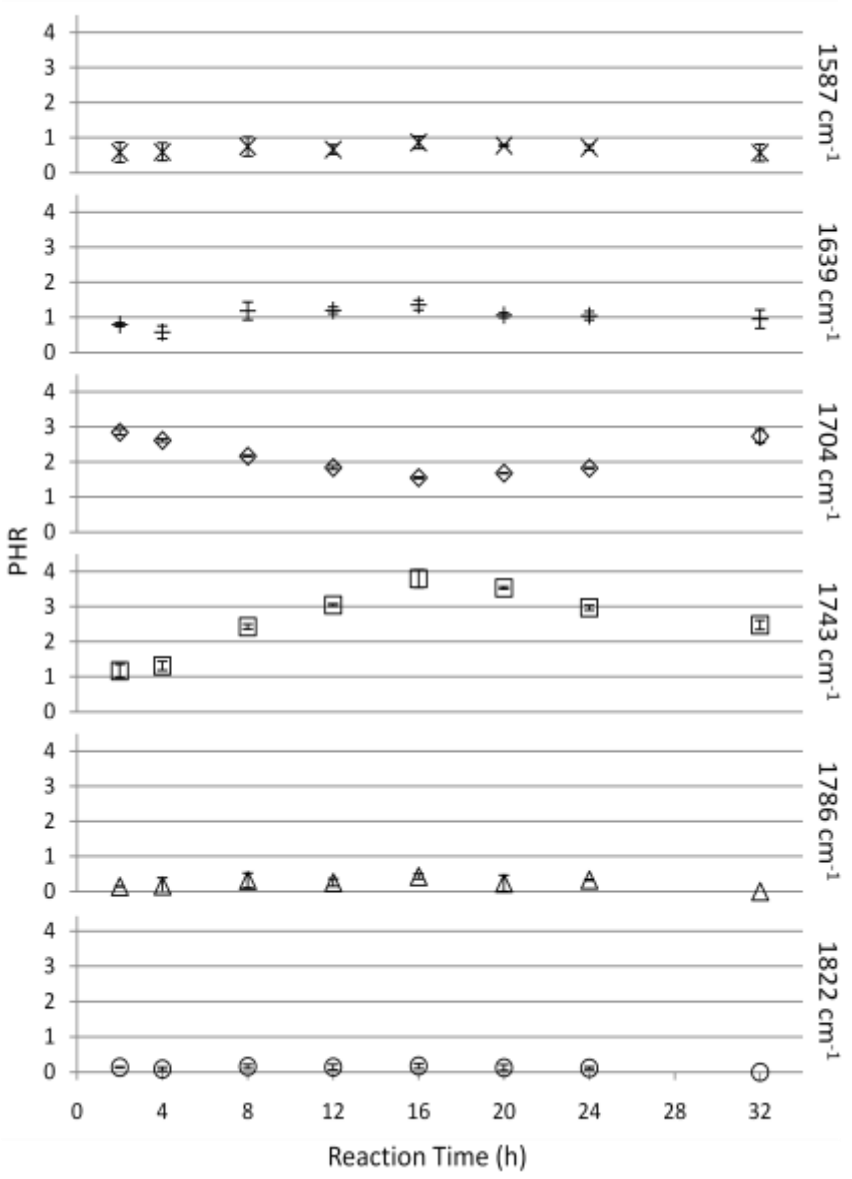

Figure 3.11: Representative transmission FTIR spectrum of 1520 to 1860 with fitting of 1592 cm^{-1} carboxylate anion carbonyl stretch, ×; 1639 cm^{-1} vinylidine stretch, +; 1704 cm^{-1} dimerized carboxylic acid carbonyl stretch, ◇, 1744 cm^{-1} ester carbonyl stretch, □; 1786 cm^{-1} cyclic anhydride carbonyl symmetric stretch, △; and 1822 cm^{-1} cyclic anhydride carbonyl asymmetric stretch ○, at variable reaction time with bars indicating 95% confidence intervals (155 °C reaction temperature and aluminum chloride).

3.4.3. Nuclear Magnetic Resonance (NMR) Spectroscopy

The proton NMR analysis of PTI presented some difficulties due to low solubility in deuterated chloroform. The model structure for the prediction of shifts can be seen in Figure 3.12, and Table 3.1 shows the experimental shifts [Agraw 1993, Qian 2007, Pretsch 2000]. The multiplet splitting of the hydrogen overlapped in the areas around 3.7 ppm, making it difficult to determine the chemical structure from the spectrum. NMR did indicate that branching was occurring in the polymer. The peaks for branching, 3.28 and 3.614 ppm, were relatively weak, indicating a low concentration of branch points.

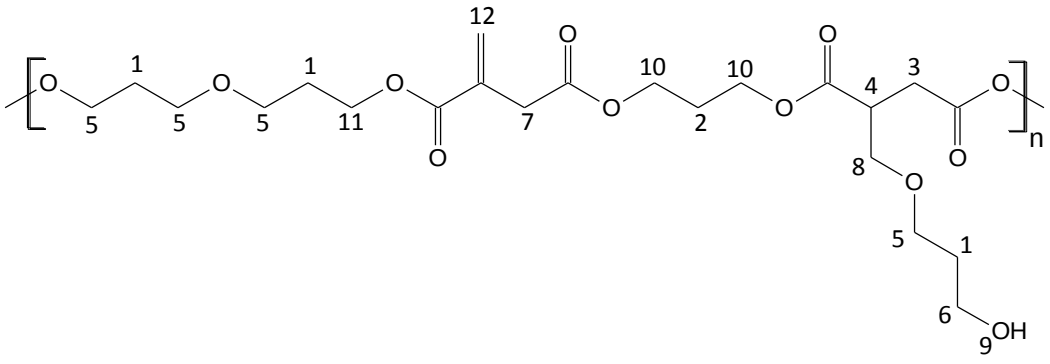

Figure 3.12: Model PTI structure used to predict 1H NMR chemical shifts of different bonds.

Table 3.1: Comparison of theoretical and experimental 1H NMR chemical shifts for PTI.

Functional Group	Experimental Shift (ppm)	Functional Group	Experimental Shift (ppm)
1	1.77	7	3.56
2	1.905	8	3.614
3	2.56	9	3.77
4	3.28	10	4.197
5	3.37	11	4.264
6	3.5	12	5.808, 6.433

3.4.4. X-ray Photoelectron Spectroscopy (XPS)

To verify the FTIR analysis , XPS was used to characterize PTI made 155 °C for 16 h using aluminum chloride. The survey scan revealed only the presence of carbon and oxygen, and, as expected, the carbon and oxygen atomic concentrations were in the correct ratio for PTI made of 1:1 ratio of PDO and IA units, Table 3.2. With XPS, the concentration of carbon and oxygen show that one monomer was not being preferentially reacted. It was expected that PDO and IA would not be in the correct concentration due to branching. For PTI made 155 °C for 16 h using aluminum chloride, branching does not appear to affect the atomic concentration of O and C. It is expected, if the extreme conditions were analyzed, that the atomic concentration of O would increase with branching.

Table 3.2: Comparison of experimental atomic concentrations of carbon and oxygen in PTM, as determined by XPS, to theoretical concentrations for an equimolar polymerization of PDO and IA.

Atom	Percent Atomic Concentration	
	Experimental	Theoretical
O	29.99 ±1.97%	31.25%
C	70.01 ±1.97%	68.75%

Peak fitting of the high resolution C 1s scan for the C-H, C-O- and C=O functional groups allowed for an accurate determination of the fractions of PDO and IA repeat units, Figure 3.13[Sabbatini 1996, Louette 2006 69-73, Louette 2006 38-43, Cossement 2006, Nanse 1997]. The peaks were identified as C-H at 285 eV (53.68 % ±1.56 % area), C-O at 286.6 eV (28.51 % ±1.56 % area), and C=O at 289.2 eV (17.81 % ±1.21 % area). The theoretical calculations for C-H (54.4 % area), C-O (27.27 % area), and C=O at 289.2 eV (18.18 %) were in close agreement with experimental results. Branching did not appear to affect functional groups concentration.

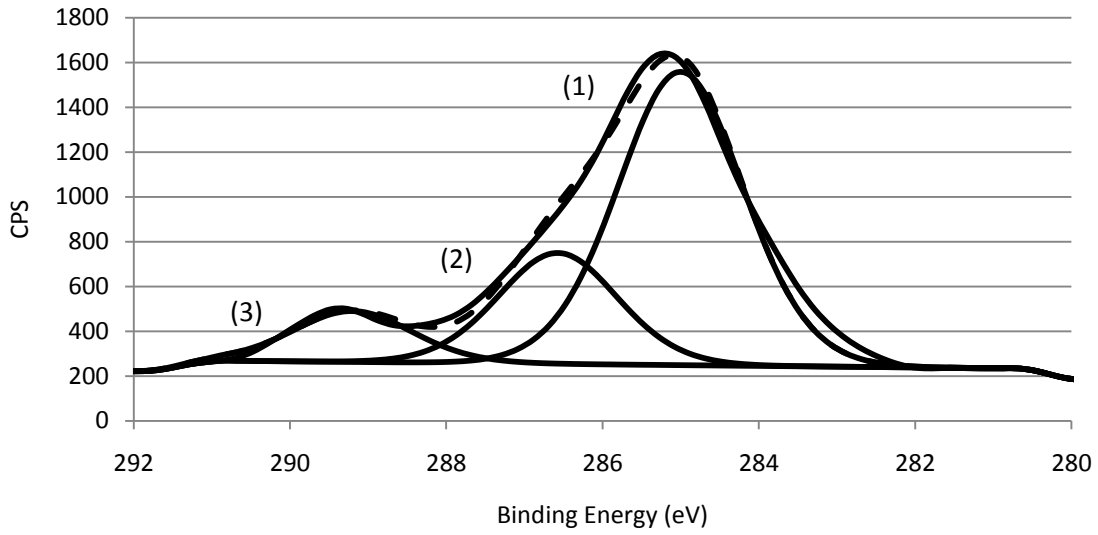

Figure 3.13: High resolution C 1s XPS scan for PTI (155 °C, 16 h, $AlCl_3$ catalyst) with peak fitting: (3) C-H at 285 eV (53.68±1.56 % area), (2) C-O at 286.6 eV (28.51±1.56 % area), and (1) C=O at 289.2 eV (17.81±1.21 % area).

3.4.5. Gel Permeation Chromatography (GPC)

After the chemical composition of the PTI copolymers was characterized with FTIR and XPS, the molecular weights and polydispersity index were examined with GPC. It was noticed on all of the GPC traces for PTI, except for the temperature extremes on PTI, that there was a bimodal molecular weight, Mw, distribution, with a peak above 10 kDa, HMw, and a peak below 10 kDa, LMw. The HMw constituted <5% of the area under the curve and the LMw accounted the remainder of the area under the curve. For the PTM samples, GPC analysis was a relatively simple task, as they were readily soluble in THF. The low Mw distribution was indicative of step growth polymerization since high molecular weights would only occur above yields of 99.5 %, and PTI yield was not above 99.5% [Odian 1991]. The higher Mw distribution in PTI could not initially be explained. A second type of polymerization existed concurrently in the reaction vessel or a side reaction that could produce moderate Mw products needed to be considered. A possibility for a concurrent polymerization pathway for the moderate Mw material was chain

growth polymerization; chain growth polycondensation has been developed for some time and could explain the HMw's at low yields [Odian 1991, Voit 2000, Yokoyama 2007]. For PDO-IA, though the THF soluble material had a low concentration in the GPC results, the polymer produced was elastic to stiff and brittle due to cross-linking and branching of the polymer.

PTI showed a dependence on temperature and time, Figure 3.14 to 3.17. The GPC data reported for PTI's higher Mw material is skewed to lower values due to the cross-linking and branching, which decreases the radius of gyration of the molecule, or are skewed because the cross-linked and branched material is insoluble in THF. Step and chain growth polymerization was expected for PTI, and Ordelt saturation was also a possibility, with a methylene group on the second carbon. For PTI's HMw at 2 h reaction time, the large 95% confidence interval is indicative of the reaction not having reached equilibrium, Figure 3.14. From 2 h to 24 h, the HMw increases in Mw by ~17 kDa. After 24 h, there is no statistically significant change in the Mw of HMw, seen in Figure 3.14. PTI's HMw dependence on reaction time is in contrast to PDO-MA's HMw lack of dependence on reaction time. The full extent of the HMw dependence on reaction time cannot be explored due of the difficulties in solvating PTI because of cross-linking and branching . The concentration of double bonds decreased from a PHR of 1.5 to 1.2 while the Mw increased by 17 kDa. The decrease in the concentration of double bonds that is associated with Ordelt saturation accounts for some of the increase in the Mw. The rest of the change in Mw can be attributed to an increase in the Mw from the chain growth polymerization as the reaction time becomes longer. The LMw from the step growth polymerization increases Mw from 2 to 20 hrs by 0.6 kDa, and after 20 h, there is no significant change in the LMw, Figure 3.15. The lack of change after 20 h shows that the step growth polymerization has reached equilibrium of the forward and reverse reactions. For the variation of reaction temperature, PTI showed a strong dependence on the reaction temperature for both HMw and LMw, Figure 3.16

and 3.17. HMw appears for this system from 135 °C to 165 °C with vacuum and stirring, Figure 3.17. Chain growth polymerization was not detected at 125 °C and 175 °C, and Ordelt saturation does not appear to significantly contribute to the changes in Mw. When a decrease in the LMw occurs from 125 °C to 135 °C, the product of chain growth polymerization is detected, which may be competing for monomers with step growth polymerization. At 175 °C, HMw becomes undetectable, the yield increases, and the LMw increases significantly, demonstrating a dependence between competing reaction pathways, Mw, and yield of PTI.

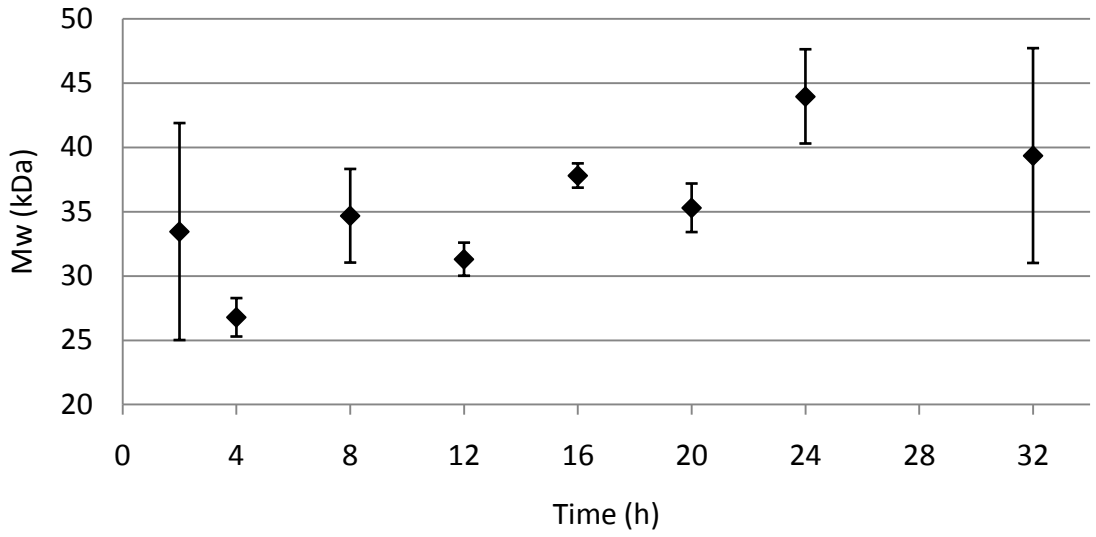

Figure 3.14: PTI HMw plotted versus reaction temperature (2-16 h) with 95% confidence interval error bars (reaction conditions: 155 °C, $AlCl_3$ catalyst).

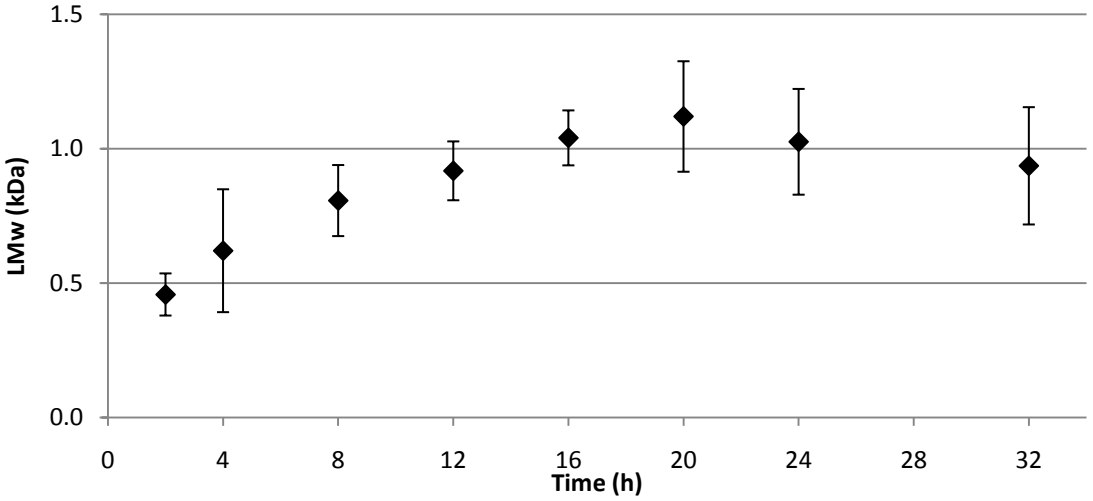

Figure 3.15: PTI LMw plotted versus reaction temperature (2-32 h) with 95% confidence interval error bars (reaction conditions: 155 °C, $AlCl_3$ catalyst).

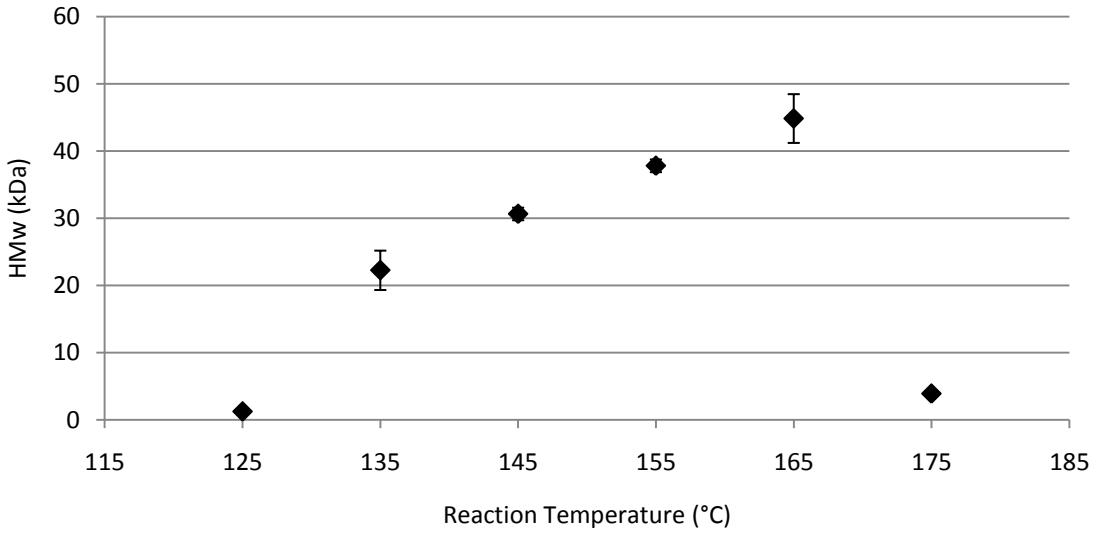

Figure 3.16: HMw PTI versus reaction temperature (125 to 175 °C) with 95% confidence interval error bars (reaction conditions: 16 h, $AlCl_3$ catalyst).

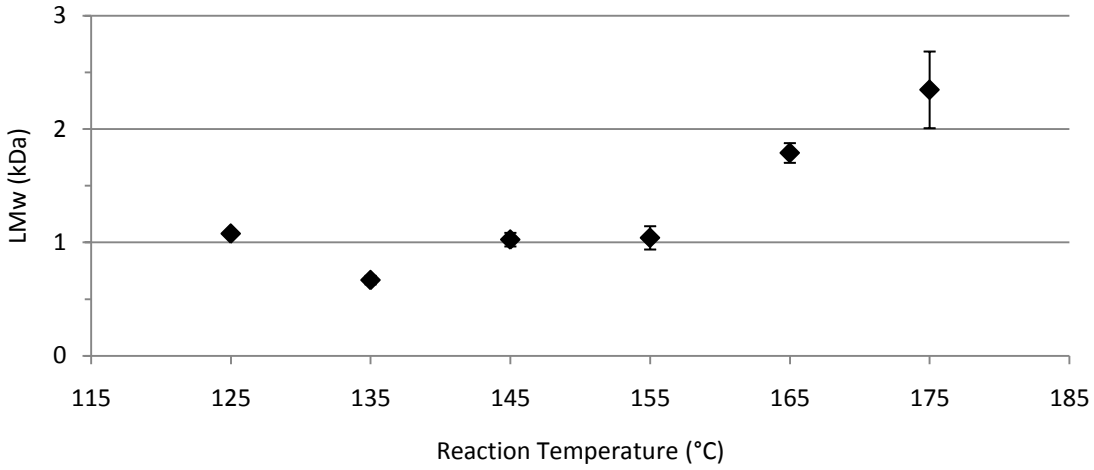

Figure 3.17: LMw PTM versus reaction temperature (125 to 175 °C) with 95% confidence interval error bars (reaction conditions: 4 h, $AlCl_3$ catalyst).

3.4.6. Thermal Gravimetric Analysis (TGA)

PTI samples made at 135, 155, and 175 °C with aluminum chloride, for 16 h, and with stirring and vacuum were chosen as representative samples. Loss of weight due to thermal decomposition was much slower than PTM (Chapter 2), Figure 3.18. The 135 °C PTI sample did not lose 5 wt.% until 192 °C, which is substantially below PDO's boiling point and well above the solvents used in processing, chloroform and ether, boiling point. PTI 155 and 175 °C samples did not have 5 wt.% loss until 235 and 227 °C, respectively, Table 2.4. The higher Mw of PTI due to cross-linking and branching led to more thermally stable than PTM.

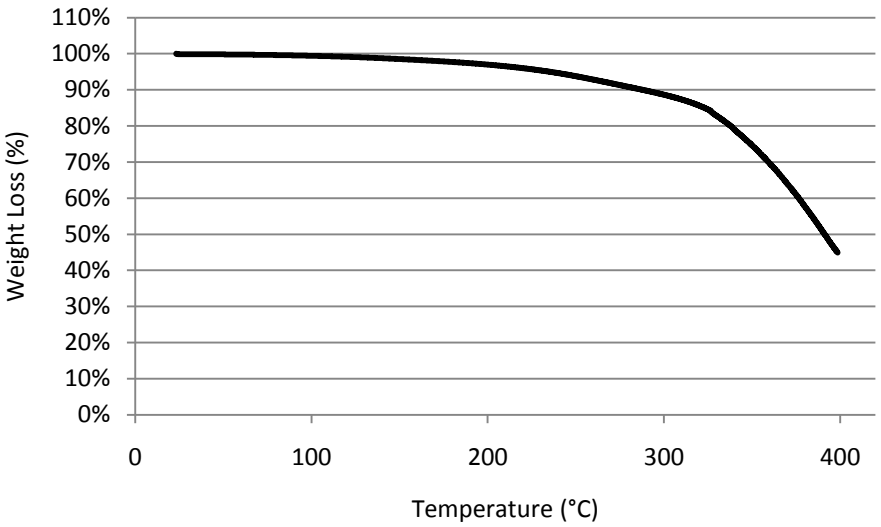

Figure 3.18: TGA weight loss versus temperature from TGA for PTI made 155 °C for 16 h using aluminum chloride with vacuum and stirring.

Table 3.3: Temperature at which PTI made at 135, 155, and 175 °C for 16 h using aluminum chloride with vacuum and stirring achieved 5% weight loss.

Sample	5% Weight Loss
135	192
155	235
175	227

3.4.7. Differential Scanning Calorimetry (DSC)

For a representative sample made from PTI at 155 °C for 16 h with aluminum chloride, vacuum and stirring, no Tg or Tm could be clearly defined, seen in Figure 3.19, but a clearly defined crystallization peak was noted at 126.2 °C. The lack of a Tg and Tm may be due to the cross-linked and branched structure of the polymer. Two other representative samples were also examined for PTI, samples made at 135 and 175 °C for 16 h with aluminum chloride, vacuum and stirring. For the 135 °C, there was an apparent Tg at -34.4 °C and a crystallization at

166.6 °C, Table 3.4. The 175 °C PTI sample had a similar DSC curve as 155 °C PTI with a crystallization peak at 120.4 °C, Table 3.4. The PTI polymer demonstrated more superior thermal properties than PDO-MA and may be better suited for commercial application.

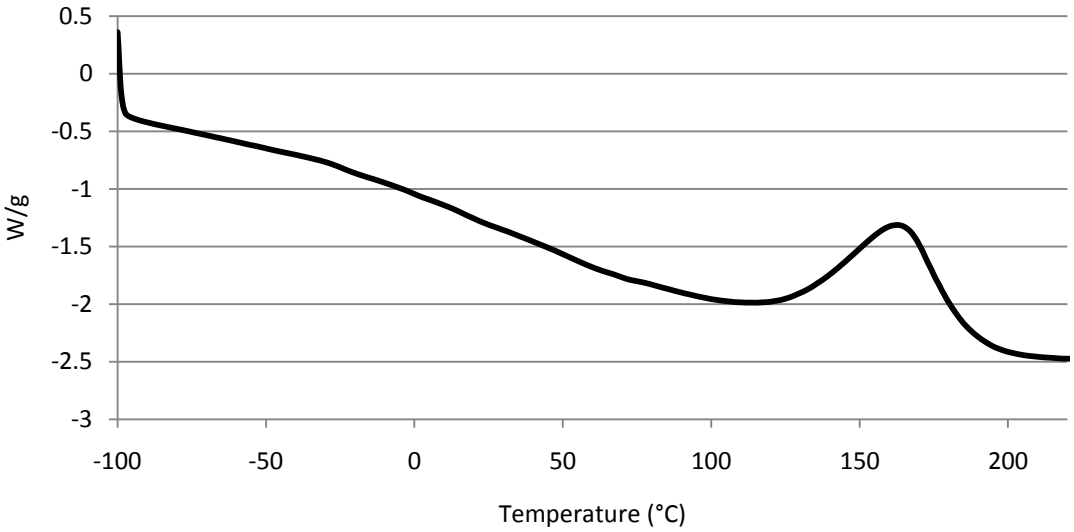

Figure 3.19: Heat flow versus temperature from DSC for PTI polymerized under vacuum with stirring and aluminum chloride catalysts for 16 h at 155 °C.

Table 3.4: Glass transition and crystallization temperatures determined by DSC for PTI samples produced at 135, 155, and 175 °C with aluminum chloride catalyst at 16 h with vacuum and stirring.

Reaction Temperature (°C)	Tg (°C)	Tc (°C)
135	-34.4	166.6
155	N/A	126.2
175	N/A	120.4

3.4.8. X-ray Diffraction (XRD)

In preparation for XRD, a PTI sample ($AlCl_3$, 155 °C, 16 h) was ground into a powder using a mortar and pestle. As shown in Figure 3.20, the XRD pattern for PTI contains a sharp crystalline peak. A rounded peak would indicate the absence of crystalline material, and this is

not the case for this PTI sample. However, the broadness of the peak indicates that there are crystalline, semi-crystalline, and amorphous regions in PTI. A purely crystalline material is expected to have a peak width of less than 5 degrees. PTI has a peak width of ~15 degrees indicating that the polymer does have crystalline regions [Roe 2000].

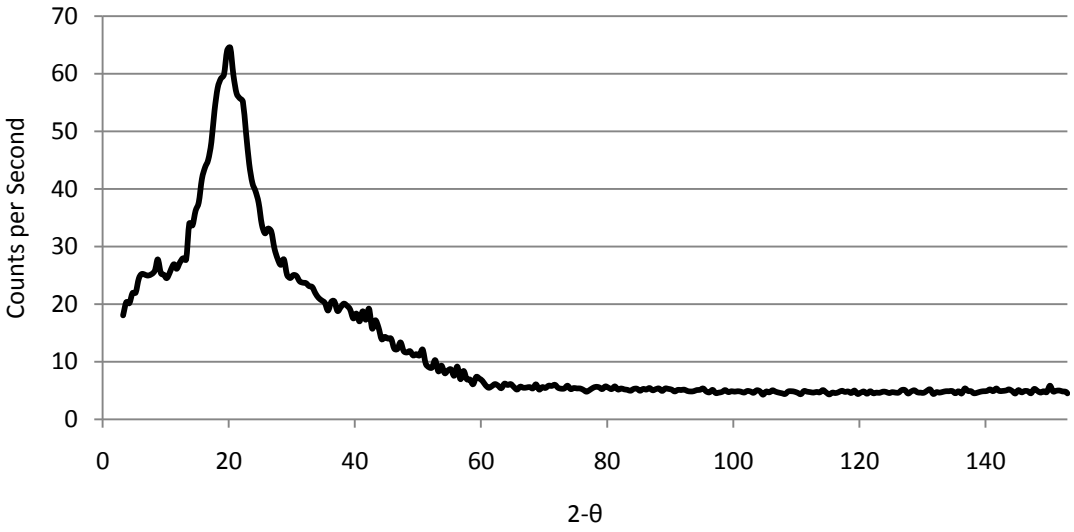

Figure 3.20: XRD pattern for powder PTI sample (155 °C, 16 h, $AlCl_3$).

3.5. Conclusions

A bioplastic was produced with varying chemical structure and Mw, PTI. Gravimetric yield did not achieve the necessary 99.5% yield to obtain high Mw polymer and was maximized around 155 °C and 16 h using aluminum chloride. Using FTIR, it was determined that maximum ester content was achieved at 16 h and 155 °C. Ordelt saturation was found to increase with increasing reaction temperature, and it caused the yield to significantly increase from 53 wt.% to 77 wt.% when reaction temperature was increased from 165 to 175 °C. Proton NMR confirmed that branching was occurring by saturation of the vinylidene and that only ester and ether bonds were present. PDO and IA were confirmed to adding in a 1:1 ratio by XPS survey and C 1s high resolution analysis of PTI (155 °C, 16 h, $AlCl_3$). GPC showed that both chain and step-growth

polymerization was occurring during polycondensation giving a bi-modal Mw distribution. The LMw was limited to Mw under 3 kDa due to the reaction not achieving a yield greater than 99.5%, and HMw did not account for more than 5 wt.% of the final product. The T 5% wt. loss was dependent on reaction temperature as shown by TGA, and a cold crystallization peak around 160 °C was found by DSC. Research with these polymers will continue with future hydrolytic and enzymatic degradation studies.

3.6. Recommended Future Work

As a comparison against this work, a set of experiments using no catalysts need to be performed to determine the extent of the catalyst effect. The addition of catalyst during the polymerization needs to be attempted to determine if the deactivation of the catalyst is hindering the reaction. The impact of OrdeIt saturation needs to be further explored to determine if it can be controlled. In addition, reactions at temperatures below 125 °C and reaction times greater than 16 h need to be attempted to see if OrdeIt saturation can be avoided and a higher Mw can be achieved. To prove that PTI is degradable, hydrolytically and bio-degradation studies need to be performed on PTI.

3.7. Acknowledgements

This work was partially funded through the Sustainable Energy Research Center at Mississippi State University under the Department of Energy award DE-FG3606GO86025. Financial support was also provided by MSU Bagley Fellowship. Completion of this work in a timely manner would not have been possible without undergraduate researchers Erin Smith, Mitch Wall, Zach Wynne, and Phillip Jamison. TGA and DSC was completed by Kimberly Ivey of Clemson University.

3.8. Disclaimer

This report was prepared as an account of work sponsored by an agency of the United States Government. Neither the United States Government nor any agency thereof, nor any of their employees, makes any warranty, express or implied, or assumes any legal liability or responsibility for the accuracy, completeness, or usefulness of any information, apparatus, product, or process disclosed, or represents that its use would not infringe privately owned rights. Reference herein to any specific commercial product, process, or service by trade name, trademark, manufacturer, or otherwise does not necessarily constitute or imply its endorsement, recommendation, or favoring by the United States Government or any agency thereof. The views and opinions of authors expressed herein do not necessarily state or reflect those of the United States Government or any agency thereof.

3.9. References

Agrawal, J. P., "Structural Aspects of novel Unsaturated Polyesters," Pure Applied Chemistry, A30(1), 59-73, 1993.

Bruno, T. J., Svoronos, P. D. N., Handbook of Basic Tables for Chemical Analysis, 2nd ed., CRC Press, Boca Raton, FL, 405-448, 2003.

Buchard, W., "Solution Properties of Branched Macromolecules," in Advances in Polymer Science, Springer-Verlag, Berlin, 143, 1999.

Cossement, D., Gouttebaron, R., Cornet, V., Viville, P., Hecq, M., Lazzaroni, R., "PLA-PMMA blends: A Study by XPS and ToF-SIMS," Applied Surface Science, 252, 6636-6639, 2006.

Daoud, M., Lapp, A., "Branched Polymers and Gels," Journal of Physics: Condensed Matter, 2, 4021-4050, 1990.

Dean, J. A., Lange's Handbook of Chemistry, 14th ed., McGraw-Hill, Inc., 7.42-7.71, 1992.

Dell'Erba, R., Martuscelli, E., Musto, P., Ragosta, G., "Unsaturated Polyester Resins: a Study of the Mechanism and kinetics of the Curing Process by FTIR Spectroscopy," Polymer Networks and Blends, 7(1), 1-11, 1997.

Doi, M., Introduction to Polymer Physics, Clarendon Press, Oxford, 89-113, 1996.

Fradet, A., Marechal, E., "Kinetics and Mechanisms of Polyesterification I. Reactions of Diols with Acids," Advances in Polymer Science, 43, 51-142, 1982-A.

Fradet, A., Marechal, E., "Study on Models of Double Bond Saturation During the Synthesis of Unsaturated Polyesters," Makromol. Chem., 183, 319-329, 1982-B.

Helminen, A., O., Korhonen, H., Seppala, J.V., "Crosslinked Poly(ester anhydride)s Based on Poly(ε-caprolactone) and Polylactide Oligomeers," Journal of Polymer Science: Part A: Polymer Chemistry, 41, 3788-3797, 2003.

Louette, P., Bodino, F., Pireaux, J.-J., "Poly(dimethyl siloxane) (PDMS) XPS Reference Core Level and Energy Loss Spectra," Surface Science Spectra, 12, 38-43, 2005.

Louette, P., Bodino, F., Pireaux, J.-J., "Poly(methyl methacrylate) (PMMA) XPS Reference Core Level and Energy Loss Spectra," Surface Science Spectra, 12, 69-73, 2005.

Nanse, G., Papirer, E., Fioux, P., Moguet, F., Tressaud, A., "Fluorination of Carbon Blacks. An X-Ray Photoelectron Spectroscopy Study. Part II. XPS Study of a Furnace Carbon Black treated with Gaseous Fluorine at Temperatures below 100 °C. Influence of the Reaction Parameters and of the Activation of the Carbon Black on the Fluorine Fixation," Carbon, 35(3), 371-388, 1997.

Odian, G., Principles of Polymerization 3rd ed., John Wiley & Sons, New York, 41-197, 1991.Pretsch, E., Buhlmann, P., Affolter, C., Structure Determination of Organic Compounds, Tables of Spectral Data, Springer, Berlin, 161-244, 2000.

Qian, H., Mathiowitz, E., "Acyl Chloride –Facilitated Condensation Polymerization for the Synthesis of Heat-Sensititve Poly(anhydride-ester)s," Journal of Polymer Science: Part A: Polymer chemistry, 45, 5899-5915, 2007.

Rubinstein, M., Colby, R. H., Polymer Physics, Oxford University Press, New York, 361-422, 2003.

Sabbatini, L., Zambonin, P. G., "XPS and SIMS Surface Chemical Analysis of some Important Classes of Polymeric Biomaterials," Journal of Electron Spectroscopy and Related Phenomena, 81, 285-301, 1996.

Saunders, J. H., Dobinson, F., "The Kinetics of Polycondensation Reactions," Comprehensive Chemical Kinetics, 473-581, 1976.

Silverstein, R. M., Blassler, G., C., Morrill, T. C., Spectrometric Identification of Organic Compounds, 5th ed., John Wiley & Sons, Inc., , Hoboken, NJ, 102-133, 1991.

Silverstein, R. M., Webster, F. X., Kiemle, D. J., Spectrometric Identification of Organic Compounds, 7th ed., John Wiley & Sons, Hoboken, NJ, 127-203, 2005.

Zetterlund, P. B., Weaver, W., Johnson, A. F., "Kinetics of Polyersterification: Modelling of the Condensation of Maleic Anhydride, Phthalic Anhydride, and 1,2-propylene Glycol," Polymer Reaction Engineering, 10(1-2), 41-57, 2002.

CHAPTER 4

HYDROLYTIC DEGRADATION OF POLY(TRIMETHYLENE-MALONATE)

4.1. Abstract

Poly(trimethylene-malonate) (PTM) was produced from 1,3-propandiol (PDO) and malonic acid (MA) to reduce our impact on the environment through the use renewable polymers through with green chemistry. PTM was made to be hydrolytically degradable by incorporating ester bonds into the polymer backbone. Before hydrolytic degradation, experimentation was performed to determine the solubility of PTM. The solubility testing was performed in DI water, toluene and ethanol to cover a spectrum of polarities. PTM was most soluble in ethanol and toluene, and it had the low molecular weight polymer solbulize before the high molecular weight polymer. The first hydrolytic degradation study was performed for 672 h with pH 2 HCl/DI water, pH 4, 7, and 10 phosphate buffer solution (PBS), and pH 12 NaOH/DI water solution. PTM was readily degradable over the pH range. PTM was degraded and loss 50 to 90 wt.% at 672 h due to diffusion and degradation making characterization on the solid material difficult. Attenuated total relectance-Fourier transform infrared spectroscopy (ATR-FTIR) did not provide insight into the degradation mechanism. Using gel permeation chromatography (GPC), the remaining solid material maintined the same molecular weight, ~1.9 kDa, for the 672 h aging. It was determined that exchanging the fluid every 24 h increased PTM diffusion and made it difficult to determine if pH had an affect on PTM.

A second solubility test was performed to determine MA and PDO solubility and interaction with DI water and phosphate buffer solutions (PBSs). PDO interacted with PBS, and PBS was determined to be not to be usable during this study due to the interaction. PTM was placed in DI water, pH 7, 9, and 11 KOH adjusted DI water, and a control with no fluid for 10 to 10,000 min. Weight change was monitored as a function of aging time to determine if degradation was taking place and if the PTM degradation products were water soluble by a monitoring for reduction in weight. Weight loss varied from 20 to 37 wt.% as a function of aging time and initial pH. To monitor changes in chemical structure, ATR-FTIR spectroscopy was used to analyize samples from various pH solutions and aging times, and it was determined that PTM in DI water had the most ester hydrolysis by the reduction in the ester carbonyl from 10 to 10,000 min. Gel-permeation chromatography (GPC) was used to determine molecular weight and polydispersity index. PTM in pH 11 solution maintained the highest molecular weight over 10 to 10,000 min aging time. The addition of K^+ ion reduced ester hydrolysis, and pH 11 solutions had the highest concentration of K^+ ions and experienced the least degradation throughout the study.

4.2. Introduction

Over the past 15 years there has a 3.5 fold increase in the published research on biologically degradable polyhydroxyalkanoates (PHAs). Biodegradation is limited to specific temperatures, moisture, oxygen, and nutrient where the enzymes can function [Albertsson 2002, Alvarez 2006, Vert 2005, Pivsa-Art 2002, Chiellini 2004, Nagata 1996, Okada 1996, Scherer 2001]. Abou-Zeid et al. degraded polyhydroxybutyrate and poly(hydroxybutyrate-co-hydroxyvalerate) using four strains of Clostridum under anaerobic conditions at 35 °C for 56 days with trace elements and vitamins [Abou-Zeid 2004]. Teramoto et al. biodegraded

poly(butylenes succinate) based polymers at pH 7.4 and 25 °C with $CaCl_2$, $MgSO_4$, NH_4Cl and $FeCl_2$ with activated sludge [Termoto 2005]. Nagata et al. degraded bioplastics based on glycerol and various diacids at 37 °C at pH 7.2 with Rhizopus delemar lipase for 24 h [Nagata 1996]. Hydrolytically degradable materials require only the presence of (liquid) water. Along with biological and hydrolytic degradation, thermal degradation of polymers during processing and in elevated temperature environments (as can occur during processing, storage or use) will limit the applications for degradable polymers. It has been shown with PHAs that thermal degradation occurs at lower temperatures than in similar petroleum-based polymers [Harrison 2006, Bordes 2009, Zou 2009]. The synthesis and chemical and physical characterization of poly(trimethylene-malonate) (PTM) has been examined in a prior chapter. Here, a study of the hydrolytic degradation of PTM as a function of pH and time is described.

Polymers that are classified as being biologically degradable by fungal or bacterial enzymes, such as polylactic acid (PLA) and poly(ε-caprolactone) (PCL), may exhibit no degradation and appear biostable due to the lack of any biological activity in the environment. The incorporation of hydrolytically degradable bonds into the backbone of the polymer allow for an addition degradation route besides biologically degradation [Albertsson 2002, Gopferich 2002]. Through the incorporation of hydrolytically degradable bonds in the polymer backbone, such as anhydride, ester, and ether, the degradation rate can be controlled under varying pH and temperature conditions [Tamada 1993, Qiu 2001, Gouin 2000]. PHAs and PHBs with high concentrations of anhydride bonds exhibit the highest rates of degradation, although the degradation rate can be slowed with the inclusion of ester and ether bonds into the polymer backbone [Gopferich 1996, Tamada 1993, Helminen 2003]. Polyanhydrides can be completely hydrolytically degraded in 24h at pH 7.4 and 37 °C for anhydride modified PCL and in 24h for salicylic acid based polymers at pH 10 and 37 °C [Helminen 2003, Erdmann 2000]. In contrast,

PLA and poly(glycolic acid) (PGA), that contain only ester backbone bonds, can retain 50% of their strength for more than 20 days (PGA) or years (PLA) [Chu 1981,Henton 2005]. In a study by Chu, PGA and poly(glycolide-lactide) (PGALA) were examined under variable pH conditions ranging from 5.25 to 10.09 [Chu 1981]. PLGA showed a 50 % reduction in breaking strength between 21 and 28 d at 7.44 pH. In comparison, PGA showed a 50 % reduction in breaking strength in 7 d at pH 10.09. Another factor in hydrolytic degradation is waters ability to diffuse into the polymer, which is affected by the molecular weight and crystallinity [Saha 2006, Quynh 2009, Shirahase 2006, El-Hadi 2002, Nostrum 2004]. For Mw influence, a high initial Mw decreases the rate of hydrolytic degradation due to the reduced number of end groups [Li 2006, Alexis 2006, Saha 2006, Quynh 2009, Shirahase 2006, El-Hadi 2002, Nostrum 2004]. With increasing crystallinity, water diffusion to the polymer back bone is hindered [Saha 2006, Quynh 2009, Shirahase 2006, El-Hadi 2002, Nostrum 2004]. Environmental pH and temperature have been found to impact the degradation rate by orders of magnitude, hours to months, to complete degradation [Vert 1997, Erdmann 2000, Gopferich 1996, Kajiyama 2004, Tomihata 2001, Vasanthan 2009, Shirahase 2006]. In basic solutions, the degradation is mediated by the basic solution and produces carboxylate anions. With the base mediated degradation, there is no need for an excess of water because the formation of stable carboxylate anions drives the reaction to completion [Vasanthan 2009, Satchell 1992, Smith 2007, Bruckner 2002, Saunders 1976]. When the degradation is acid catalyzed by an acidic solution, the degradation is driven by excess water and can come to equilibrium state if degradation products are not removed [Vasanthan 2009, Satchell 1992, Smith 2007, Bruckner 2002, Saunders 1976]. The degradation, whether it be based mediated or acid catalyzed, can be broken down into three steps. The first step is the diffusion of water into the polymer. Second step is the hydrolytic degradation of bonds. And the third step, degradation products diffusion out of the polymer into solution

[Hofmann 2009, Li 1999, Hoglund 2007, Neffe 2010]. With larger samples, the degradation products diffusion can be hindered. If the degradation products are retained in the polymer and are acidic, the polymer can have auto-catalytic degradation due to the increased end groups present [Li 1999]. High degradation rates, complete degradation or substantial loss of mechanical properties, are desirable in only select applications, such as drug release, sensors, and specialty packaging. Polymers exhibiting a controlled degradation and complete degradation or substantial loss of mechanical properties (dependent on application) between 6 to 36 months could be used in a large number of disposable or short-term use product applications. The working assumption is that if the chemical structure of the polymer can be controlled then the degradation (rate and total time) can be tailored for specific applications.

PTM, developed as part of this study, belongs to the PHA family and exhibit the same tendencies to hydrolytically as is seen in other PHAs. The solubility of PTM was examined to aide in differentiating between diffusion and degradation. Hydrolytic degradation of PTM was examined under variable pH conditions. Changes in gravimetric weight were monitored, molecular weight was monitored by gel-permeation chromatography (GPC), chemical functionality was monitored by Fourier transform infrared (FTIR) spectroscopy, and the thermal properties were monitored by differential scanning calorimetry and thermal gravimetric analysis. There were two hydrolytic degradation and solubility studies performed on PTM.

4.3. PTM Hydrolytic Degradation using Phosphate Buffer Solutions over 4 Weeks

4.3.1. Introduction

A hydrolytic degradation study was performed on compression molded PTM samples under variable pH, time, and temperature conditions. The pH of the degradation fluid ranged

from 2-12 and samples were aged for 6 h, 24 h, 168 h, or 672 h. Solubility, weight change, FTIR spectroscopy, and GPC were used to examine the chemical and physical changes occurring in these PTM samples as a function of degradation pH and time.

4.3.2. Experimental Materials and Methods:

Materials. The PTM sample used for the degradation study was bulk polymerized from 1,3-propane diol (PDO, 98%, Sigma Aldrich) and malonic acid (MA, 99%, VWR) using $AlCl_3$ catalyst (98%, Sigma Aldrich) with a 100:1 monomer to catalyst ratio at 155 °C for 4 h. Additional detail on the PTM synthesis and characterization of the neat material is provided in Chapter 2. Note that the PTM, as prepared, contained a bi-modal MW distribution and both the high and low MW components were monitored during the study. PTM: 64,150 ± 1,909 Da (with 1.82 ± 0.15 PDI, DP 891.7 ± 2.1, 1.2 ± 0.4 wt.%) and 1,401 ± 51 Da (with 1.81 ± 0.07 PDI, DP 19.4 ± 0.2, 98.8 ± 0.4 wt.%). The high Mw component will be referred to as HMw, and the low Mw component will be referred to as LMw. pH 4, 7, and 10 phosphate buffer solutions (PBS) were purchased from VWR. , HCl (Fisher Scientific, 1N), and NaOH (Fisher Scientific, 99%) were used to prepare aqueous solutions. Optima Tetrahydrofuran (Fisher Scientific, +99.9%) was used as the effluent in gel-permeation chromatography. All chemicals purchased were used as received.

Compression Molding. In order to keep the surface area and mass of each sample consistent, coupons of the PTM materials were made. PTM was first compression molded into a 12 cm x 12 cm x 0.318 cm sheet using a 12 ton press hydraulic press at 17 MPa and 30 °C for 10 min. The sheet was then cut into 1 cm x 0.5 cm x 0.318 cm individual samples (coupons) with individual physical dimensions and mass collected. Each sample was then placed into individual, labeled vials.

Polymer Dissolved in Solvents. To be able to differentiate between solubilization and degradation, a solubility experiment was under taken. Into a 16 mL vial, 1 g of PTM was placed along with 10 mL of each of the following solvents: DI water, toluene, and ethanol. As a control, a set of samples was also placed into vials without a liquid (air control). Samples were allowed to sit for 1 h and were then removed. Excess solvent was removed, samples were weighed, and the weight change recorded as the wet weight change. Samples were then placed into a vacuum oven (25 torr) at room temperature for 24 h, their weights recorded, and the weight change recorded as the wet weight change and recorded as the dry weight change.

Polymer Hydrolysis (Degradation Procedure). For the initial hydrolysis experiment, vials containing individual compression molded PTM coupons had 10 mL of either pH 2 aqueous solutions (HCl), pH 4 PBS, DI water (measured 5.4 pH), pH 7 PBS, pH 10 PBS, or pH 12 aqueous solution (NaOH). Samples were placed in a vacuum over at 25 torr for 24 h to remove excess water before degradation. One set of vials had no liquid added as an 'air' control, to attempt to take into account any changes due to aging alone. All work was done in triplicate. All of the sealed sample vials were then placed into a 25 °C water bath for 6 h, 24 h, 168 h, or 672 h. For pH 2 and 12, only one set of samples were made and analyzed for 672 h. The fluid in the samples was changed every 24 h to prevent the system from coming to equilibrium. At each pre-designated time, the samples were removed from solution, blotted with a KimWipe®, and the wet weights were recorded. They were then vacuum dried (25 torr) at room temperature for 24 h and the dry sample weights were recorded. All chemical and physical characterization was performed samples after vacuum drying. Samples will be referred to by their initial pH (pH 2, 4, 5.4, 7, 10, and 12) or as the air control (no liquid added).

Gravimetric weight. At the end of the allotted aging time, the samples were removed from their vials, excess water was removed by gently blotting with a KimWipe®, and the polymer

samples were weighed. The difference in the 'wet weight' minus the initial weight was divided by the initial weight to give the wet weight change. The samples were then vacuum dried at room temperature for 24 h and weighed again. The difference between the 'dry weight' minus the initial weight was divided by the initial weight to give the dry weight change.

Chemical and physical characterization. The polymer samples were also characterized by attenuated total reflectance (ATR) FTIR spectroscopy at discrete times during the degradation study using a Thermo Electron 6700 instrument (DTGS detector , room temperature, dry air purge, ZnSe crystal with a 60° angle of incidence). The peaks were fitted with PeakSolve in Thermo Scientific Omnic 8.1.10. Gaussian peaks were fitted at specific wavenumbers to minimize standard error. A peak height ratio (PHR) calculation was used in the quantitative analysis of FTIR spectra. PHR uses the height of the C-C rocking at 1465 cm^{-1} as the denominator and the height of the peak of interest as the numerator to form a ratio. Solution pH was determined using Seven Easy pH meter by Mettler Toledo that was calibrated every 30 min at 3 points (using PBS of pH 4, 7, and 10). The pHs of experimental solutions were examined after vacuum filtration with a Buchner funnel and Whitman Grade 40 filter paper. Gel permeation chromatography (GPC) data was collected with a Waters GPC with RI detector, 4E and 5E (polystyrene-dinvinylbenzene, 4.6 x 300 mm) Styragel® columns, Optima THF as the effluent at 0.3 mL/min, and a ten-point polystyrene calibration. For the degradation solids, 6 to 8 mg was weighed out and dissolved in Optima THF for at least 4 h. The samples were then filtered through a 0.45 µm expanded PTFE syringe filter before being analyzed with GPC. The degradation solutions were subjected to room temperature vacuum (25 torr) for seven days to evaporate the water. If there were no visibly discernable solids left after evaporation, 2 mL of Optima THF was added. The solution was allowed to dissolve for at least 4 h and then was filtered with 0.45 µm expanded PTFE syringe filter before being analyzed with GPC. If there

were discernable solids after evaporation, the solid sample GPC procedure (as described above) was followed.

4.3.3. Results and Discussion

4.3.3.1. PTM Dissolved in Solvents

Dissolving PTM into Solvents affect on pH testing was conducted for only 1 h to avoid degradation and determine if PTM would dissolve into DI water, ethanol, or toluene. As shown in Figure 4.1, there was no significant deviation from initial sample weight for the control sample (air), either before or after being 'dried' (only water is from atmosphere) under vacuum. The wet weight for DI water also showed no significant deviation from initial weight. This indicates one of two possible scenarios: (1) neither sample dissolution (indicated by negative deviation) nor swelling or water absorption (positive deviation) occurred or (2) some material dissolved into solution and the remaining sample swelled with water such that the net wet weight change was negligible. From an examination of the dry weight change, it can be seen that approximately 3 wt.% of the solid sample was dissolved into the DI water after only 1 h. For toluene, a weight loss can be seen in both the wet (~ 2 wt.%) and dry (~6.5 wt.%) data. Similar results were obtained for ethanol with wet (~ 2.5 wt.%) and dry (~7 wt.%) weight loss. It was expected that, if soluble, PTM would be more soluble in more polar solvents due to the acid and alcohol end groups. However, that is not the case. The dry weight decrease in DI water, ethanol, and toluene is likely due to the loss of lower Mw materials from this sample since there was a substantial increase in the low Mw fraction for all samples in solvents. The higher Mw fraction maintained its Mw in all solvents (Figure 4.2). Low Mw PTM diffuses into water causing significant decreases in weight and PTM does have an affinity for water (Figure 4.3).

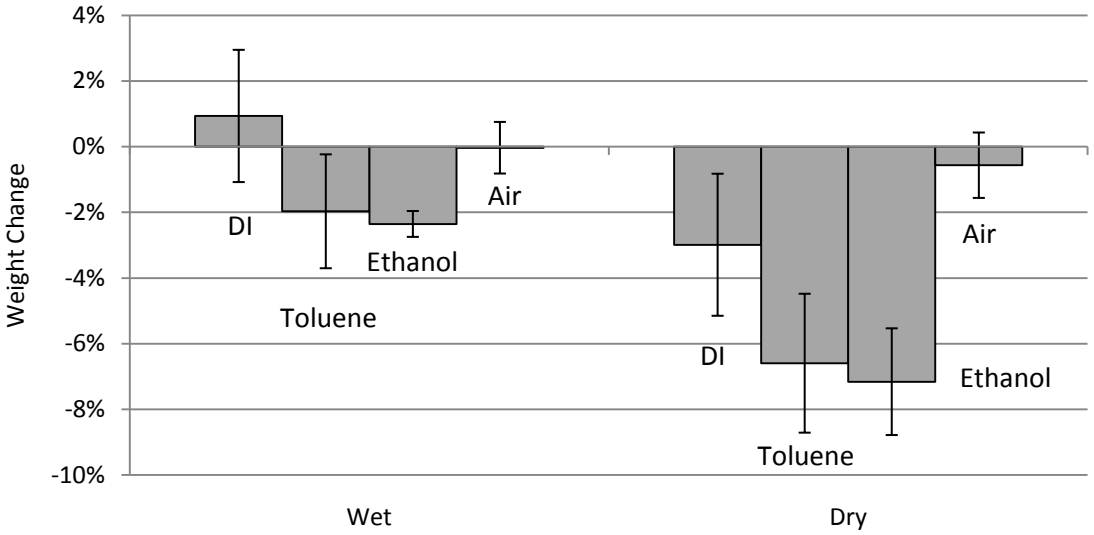

Figure 4.1: Percent weight change of PTM after exposure to DI water, toluene, ethanol, and air for 1 h. Wet weight change was measured with only excess solvent removed and dry weight change was measured after vacuum drying for 24 h. Data is averaged over 3 samples and the error bars represent 95 % confidence intervals.

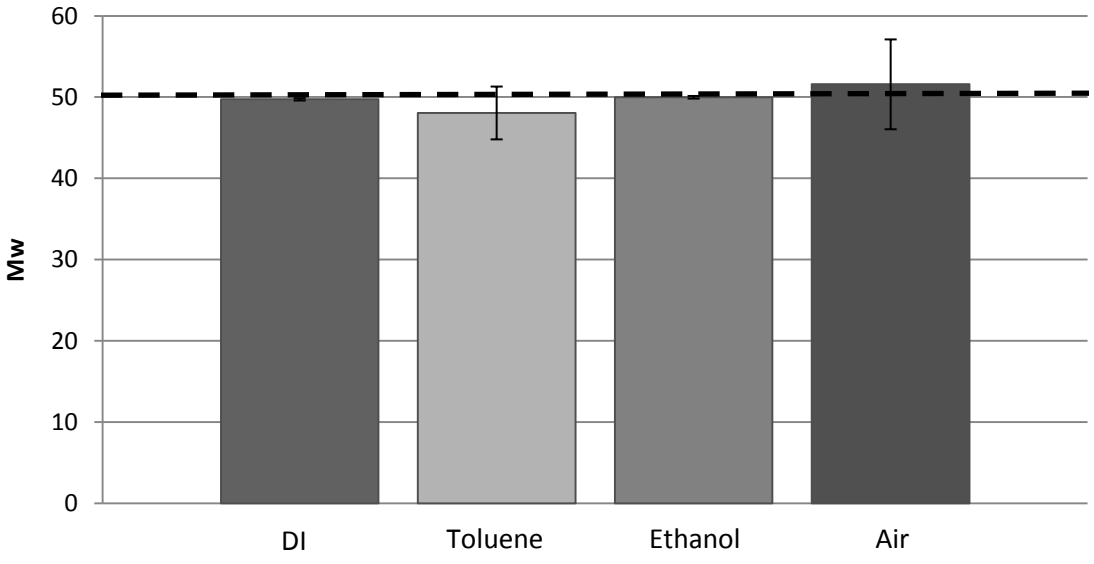

Figure 4.2: Low Mw of PTM after exposure to DI water, toluene, ethanol, and air for 1 h. Data is averaged over 3 samples and the error bars represent 95 % confidence intervals. The dashed line represents the initial molecular weight.

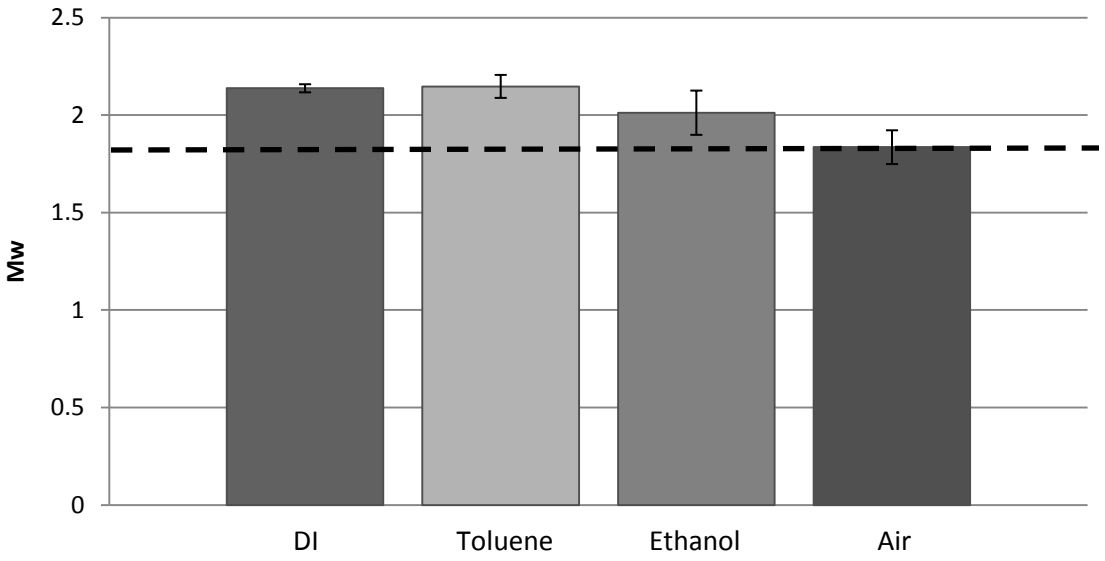

Figure 4.3: High Mw of PTM after exposure to DI water, toluene, ethanol, and air for 1 h. Data is averaged over 3 samples and the error bars represent 95 % confidence intervals. The dashed line represents the initial molecular weight.

4.3.3.2. Hydrolytic Degradation.

A hydrolytic degradation study was performed on compression molded PTM samples under variable pH and time conditions. The initial pH of the degradation fluid ranged from 2-12 and samples were aged for 6 h, 24 h, 168 h, or 672 h. Samples will be referred to by their initial pH of pH 2, 4, 7, 10 or 12, for DI water as DI, and for the control with no fluid as Air throughout the results and discussion. Weight change, FTIR spectroscopy, and GPC were used to examine the chemical and physical changes occurring in these PTM samples as a function of degradation pH and time.

4.3.3.2.1. Gravimetric Analysis

Wet sample weights were measured for all pH conditions over the 672 h duration of the study (Figure 4.4). As expected, the air control did not show statistically significant weight loss, and the pH 7, 10, and 12 samples did not change significantly. There was a trend in the wet

weights that with increasing aging time, the data broadened (as is shown by the 95% CI error bars). DI and pH 4 PBS did have significant wet weight decrease. The PTM samples showed average losses of 29 wt.% and 35 wt.% in DI water at 168 h and 679 h, respectively. At 672 h, approximately ~18 % weight loss was seen in PTM degraded in both pH 4 and pH 2 PBS. The reduction in wet weight as a function aging time for the acidic solutions (DI water, pH 4 PBS, and pH 2 PBS) can be attributed to two related sources. The first is the diffusion of low Mw material out of the polymer, which was demonstrated in the PTM solubility experiment. Simultaneously, hydrolytic degradation produces low Mw material that can diffuse out and further contribute to the PTM weight loss.

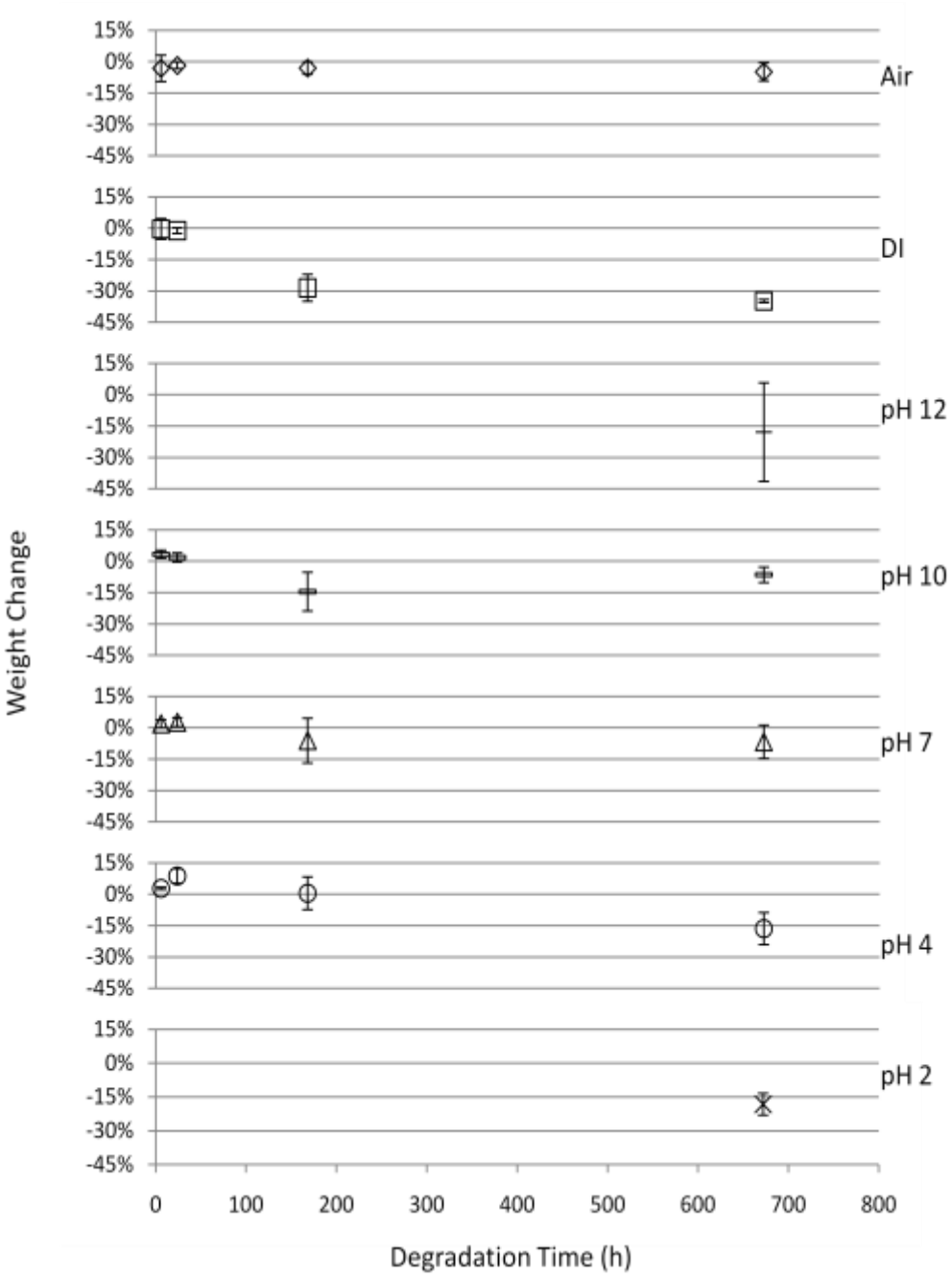

Figure 4.4: Percent weight change of PTM as a function of aging time at RT in PTM when wet (◇ air; □ DI; ⌖ pH 12 (single point); ⎓ pH 10; △ pH 7; ○ pH 4; X pH 2 (single point)). Error bars represent 95% confidence intervals of 3 replicates.

There are three main mechanisms by which hydrolytic degradation will proceed. Two mechanisms, $A_{AC}2$ and $A_{AL}1$, are acid-catalyzed and go to completion only in the presence of excess water (Figure 4.5 a,b) [Satchell 1992, Smith 2007, Bruckner 2002, Saunders 1976]. A third mechanism, $B_{AC}2$, is base-mediated and can go to completion with an excess of water (Figure 4.5 c) [Satchell 1992, Smith 2007, Bruckner 2002, Saunders 1976]. $A_{AC}2$ and $A_{AL}1$ are assumed to drive degradation in DI water, pH 2 PBS, and pH 4 PBS due to the acidic pH and the excess of water. Note that it is not known whether ionic concentration or the specific salts in the PBS solution have a positive or negative impact on the degradation mechanism. In addition, the fluid exchange every 24 h could possibly be driving or hindering hydrolytic degradation by allowing for a buildup of phosphate ions inside the PTM samples. These questions are not part of the current effort, but could be answered with additional studies.

(a)

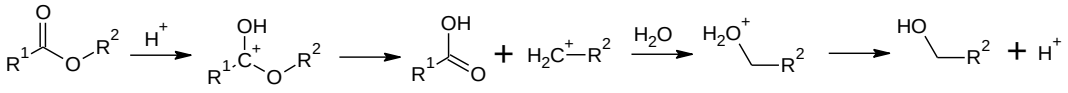

(b)

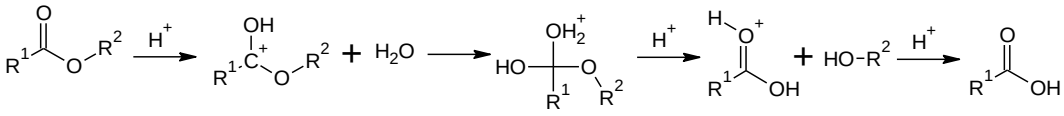

(c)

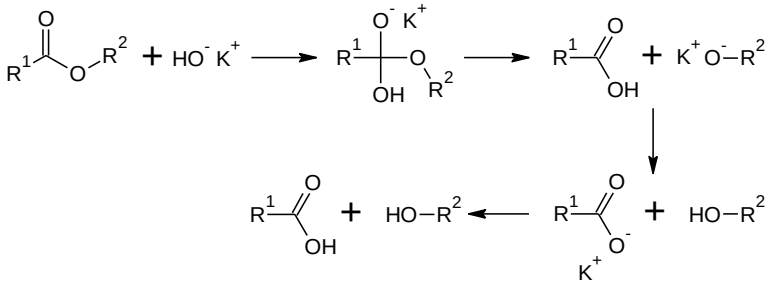

Figure 4.5: The $A_{AC}2$ (a), $A_{AL}1$ (b), and $B_{AC}2$ (c) ester hydrolysis reaction mechanisms with K^+ ions from KOH [Satchell 1992, Smith 2007, Bruckner 2002, Saunders 1976].

As shown in Figure 4.6, all of the dry samples exhibited significant weight loss. Significant weight loss (~ 8 %) was seen the vacuum dried air control sample, which was not expected. It is speculated that some amount of degradation can occur due to the inherent moisture in the sample. It was expected that PTM would degrade at a rapid rate due to its relatively low Mw and the water solubility of the PDO and MA monomers. Indeed, all of the samples aged in liquid showed significant weight loss. The average sample weight loss for the DI water and pH 2, 4, 7, 10, and 12 solutions was -4.76 wt.% ±1.50 wt.% for 6 h, -17.65 wt.% ±6.44wt.% for 24 h, -44.42 wt.% ±7.17 wt.% for 168 h, and -61.99 wt.% ±12.85 wt.% for 672 h. However, the samples showed approximately the same weight loss regardless of the solution pH. This was not expected. If the acid-catalyzed mechanisms, $A_{AC}2$, $A_{AL}1$, and $B_{AC}2$, are involved then the degradation (as measured by weight loss) was expected to be increased at lower pH. From this experiment, only time was found to have a considerable impact on the measured sample weights. It is speculated that the reason solution pH did not impact weight change is that a low pH is created locally (within and in near proximity to the sample) due to the auto-catalytic effect from the increased concentration of carboxylic acid group upon degradation. Therefore, once the sample has been placed in an aqueous environment, the end group present assist in creating a local low pH environment within and around the sample allowing for acid-catalyzed degradation to take place. This theory will be discussed further in the FTIR analysis [Li 1999].

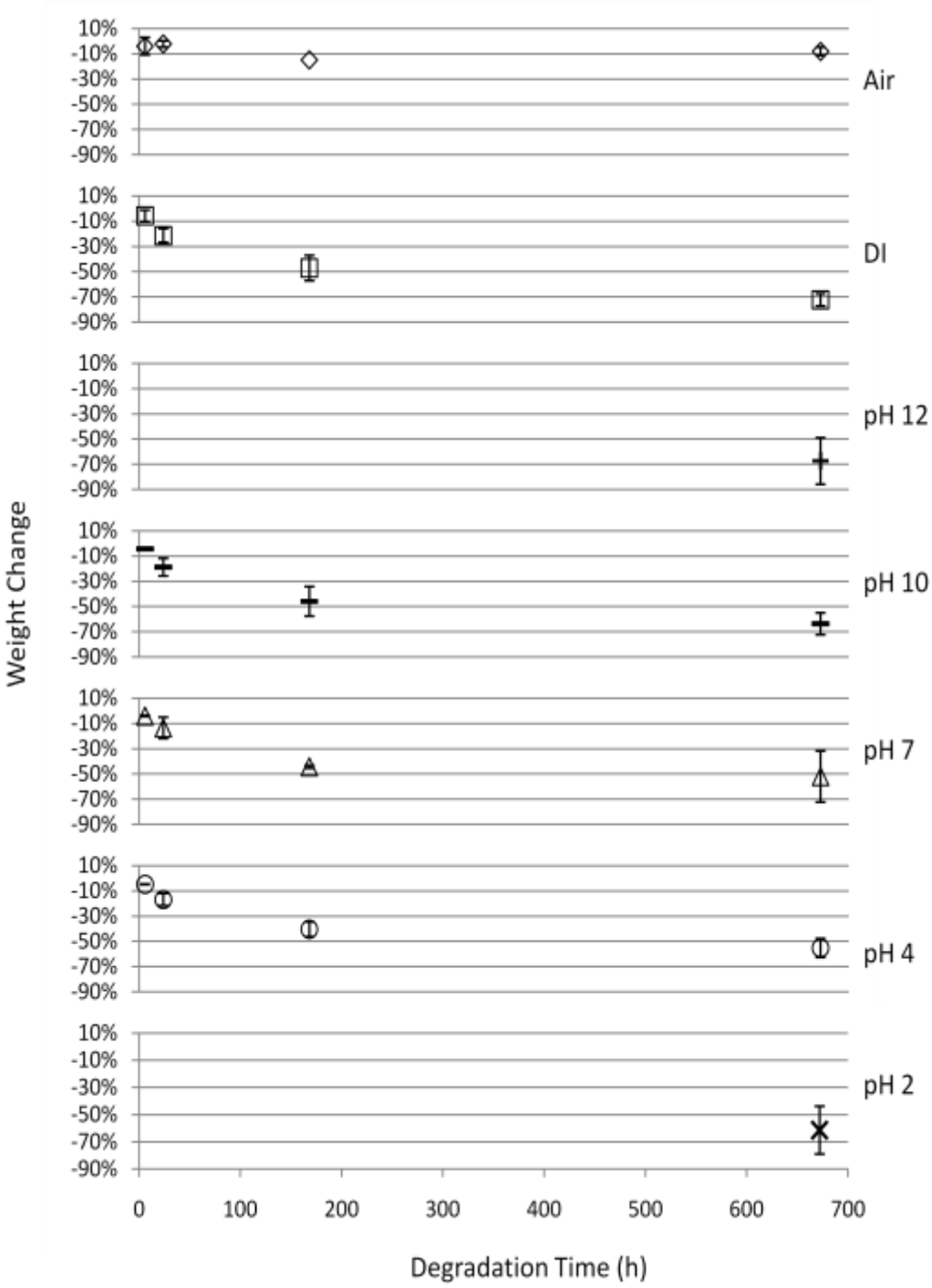

Figure 4.6: Percent weight change as a function of aging time for PTM after drying in air (◇: air; □: DI; ⌖: pH 12 (single point); ╍: pH 10; △: pH 7; ○: pH 4; X: pH 2 (single point)). Error bars represent 95% confidence intervals for 3 replicates.

4.3.3.2.2. Fourier Transform Infrared Spectroscopy

Using attenuated total reflectance (ATR) FTIR spectroscopy, ester bond concentrations in the PTM samples. Spectra were collected both before and after the compression molding (to examine for pressure and temperature effects) and also over the course of the hydrolytic degradation experiment. Peak height ratios (PHR) were used to obtain a semi-quantitative measure of the ester and carboxylic acid carbonyl concentrations. A representative ATR-FTIR spectrum of PTM after compression molding is shown in Figure 4.7. The carbonyl stretch can range from ~1900 to 1500 cm^{-1}, but the area of interest for PTM is 1820 cm^{-1} to 1650 cm^{-1} (Figure 4.8). In this region, four major peaks have been resolved through peak fitting and are labeled in Figure 4.8: (1) 1710 cm^{-1}, carboxylic acid carbonyl stretch; (2) 1725 cm^{-1}, high Mw ester carbonyl stretch; (3) 1742 cm^{-1}, low Mw ester carbonyl stretch; (4) 1753 cm^{-1}, cyclic ester carbonyl stretch [Dell'Erba 1997, Silverstein 1991, Dean 1992, Caitker 2000, Sutton 2006, Gulmine 2006, Zhou 2009]. The PHR of these four peaks was determined before and after compression molding and as a function of aging time and pH.

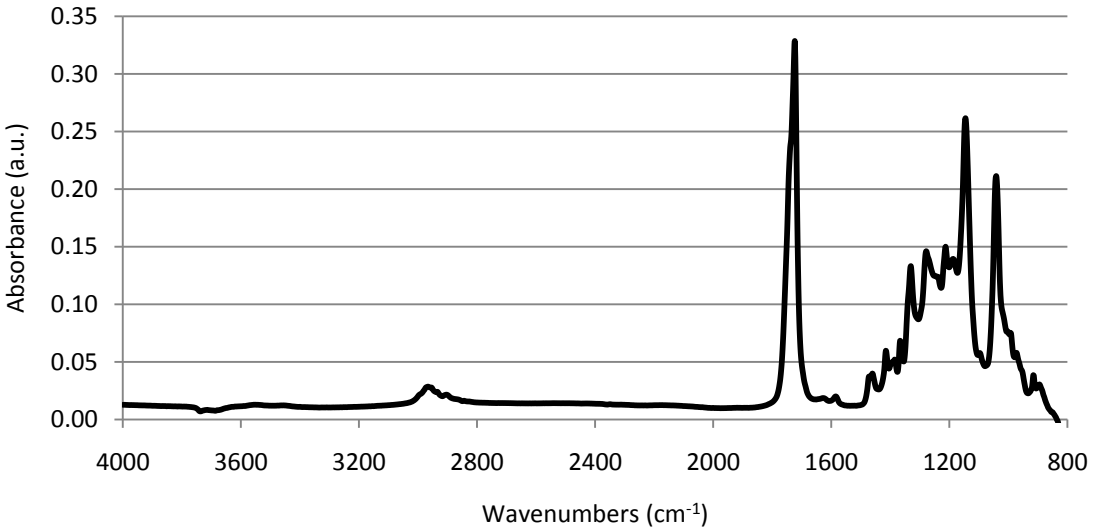

Figure 4.7: Representative ATR-FTIR spectrum of PTM after compression molding.

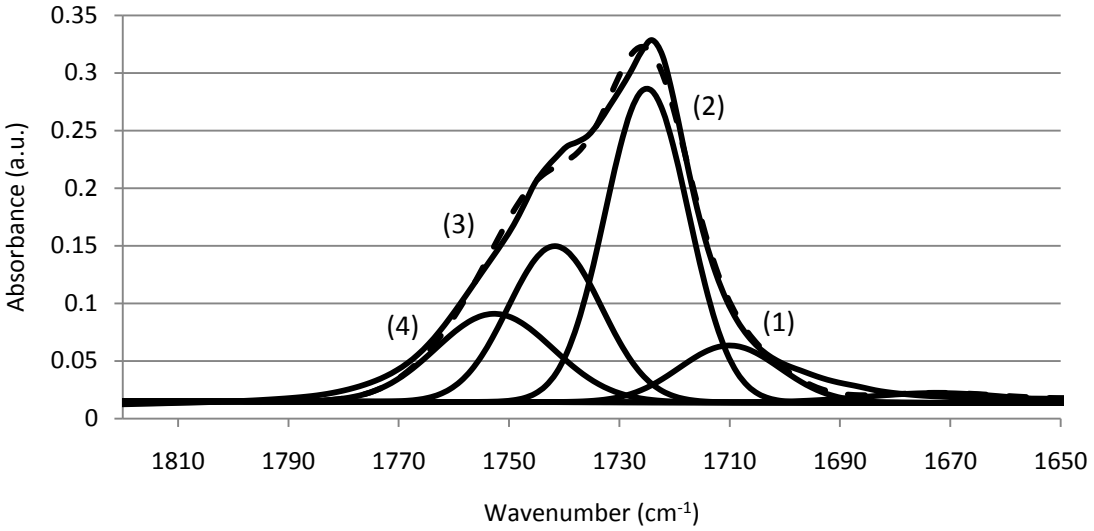

Figure 4.8: Representative ATR-FTIR spectrum of PTM from 1820 cm^{-1} to 1650 cm^{-1} with peak fitting showing four major peaks of interest: (1) 1710 cm^{-1}, carboxylic acid carbonyl stretch, (2) 1725 cm^{-1}, high Mw ester carbonyl stretch, (3) 1742 cm^{-1}, low Mw ester carbonyl stretch, and (4) 1753 cm^{-1}, cyclic ester carbonyl stretch. The dashed line represents the composite curve of the fitted peaks.

Compression molding (30 °C, 17 MPa) in preparation for making coupons caused a change in the initial PHR of 1725 cm^{-1} and 1742 cm^{-1} (Figure 4.9). The ester carbonyl composition shifted during compression molding; the 1725 cm^{-1} PHR increased from 9.6 to 14.3 and the 1742 cm^{-1} PHR decreased from 9.0 to 6.3. This PHR change is not thought to be due to degradation, but from temperature and/or pressure-induced polymerization that will be discussed further in the GPC section.

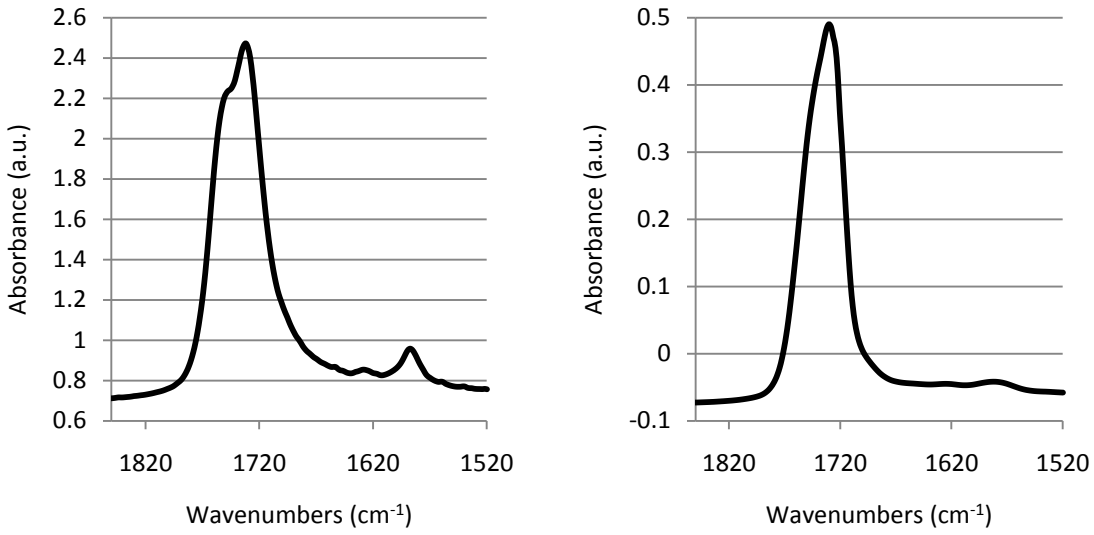

Figure 4.9: Carbonyl peak before compression molding, left, and after compression molding, right, for PTM (155 °C, 4 h, aluminum chloride).

For the degradation experiment, the PHR for the carboxylic acid carbonyl (1710 cm^{-1}) and carboxylic anion carbonyl are shown in Figures 4.10 4.11. If PTM is experiencing degradation by $A_{AC}2$, $A_{AC}1$, or $B_{AC}2$ ester hydrolysis mechanism, there should be an increase in carboxylic acid and carboxylic acid anion carbonyls. The air controls PHR appear to decrease with increased aging time, but the deviations from the neat material appear systematic and not from degradation. For the first 168 h, the concentration of carboxylic acid groups appears to decrease in PTM, which initially appears contradictory to ester hydrolysis. When the solubility (Figure 4.1) and weight change (Figure 4.6) data are considered, it is likely that hydrolytic degradation is taking place with the low Mw products diffusing into solution thereby reducing the carboxylic acid carbonyl PHR in the solid sample.

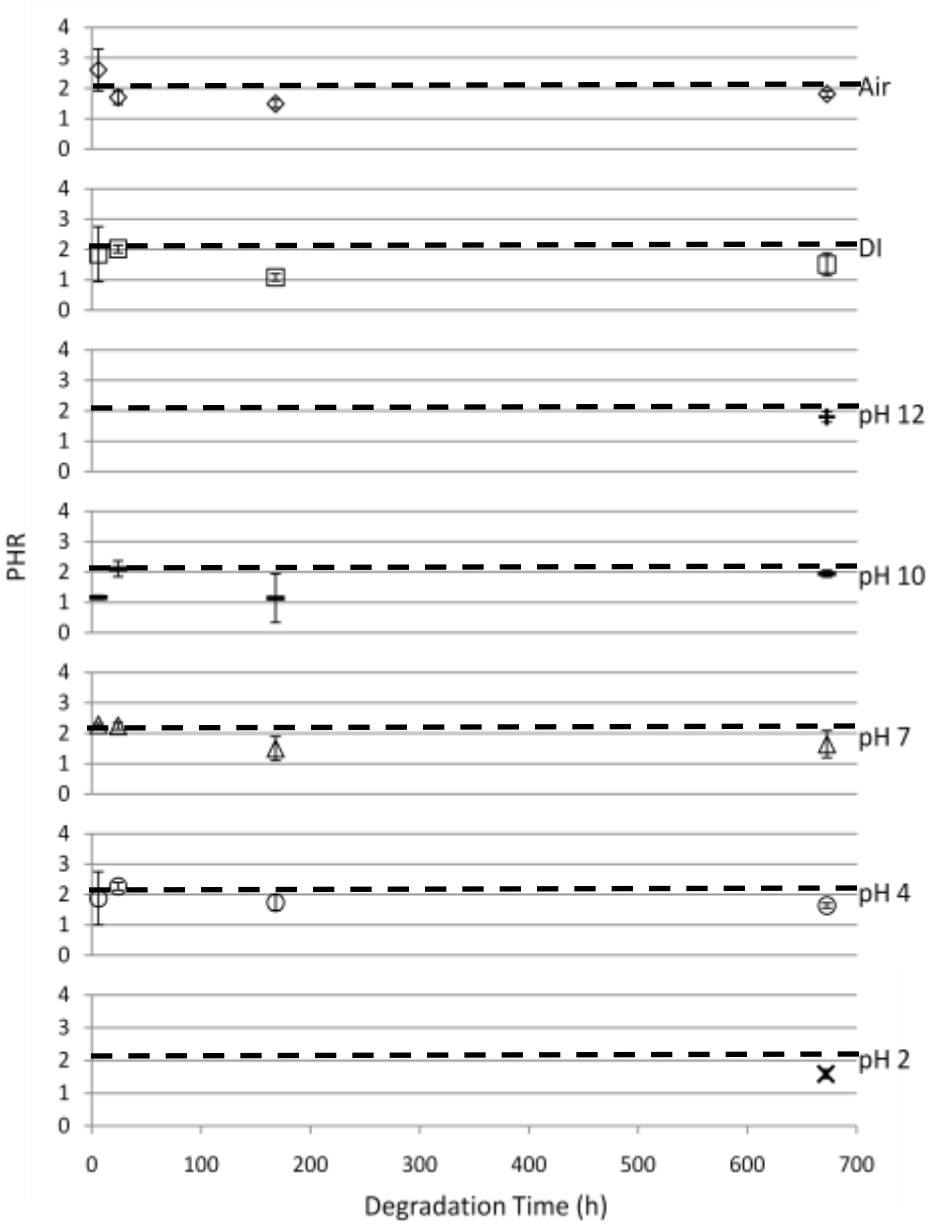

Figure 4.10: PHR for the peak at 1702 cm^{-1}, carboxylic acid carbonyl stretch, as a function of aging time for PTM (◇ air; □ DI; ⌖ pH 12 (single point); ┄ pH 10; △ pH 7; ○ pH 4; X pH 2 (single point)). Error bars represent 95% confidence intervals for 3 replicates. Dashed line shows the PHR for the neat material (before compression molding).

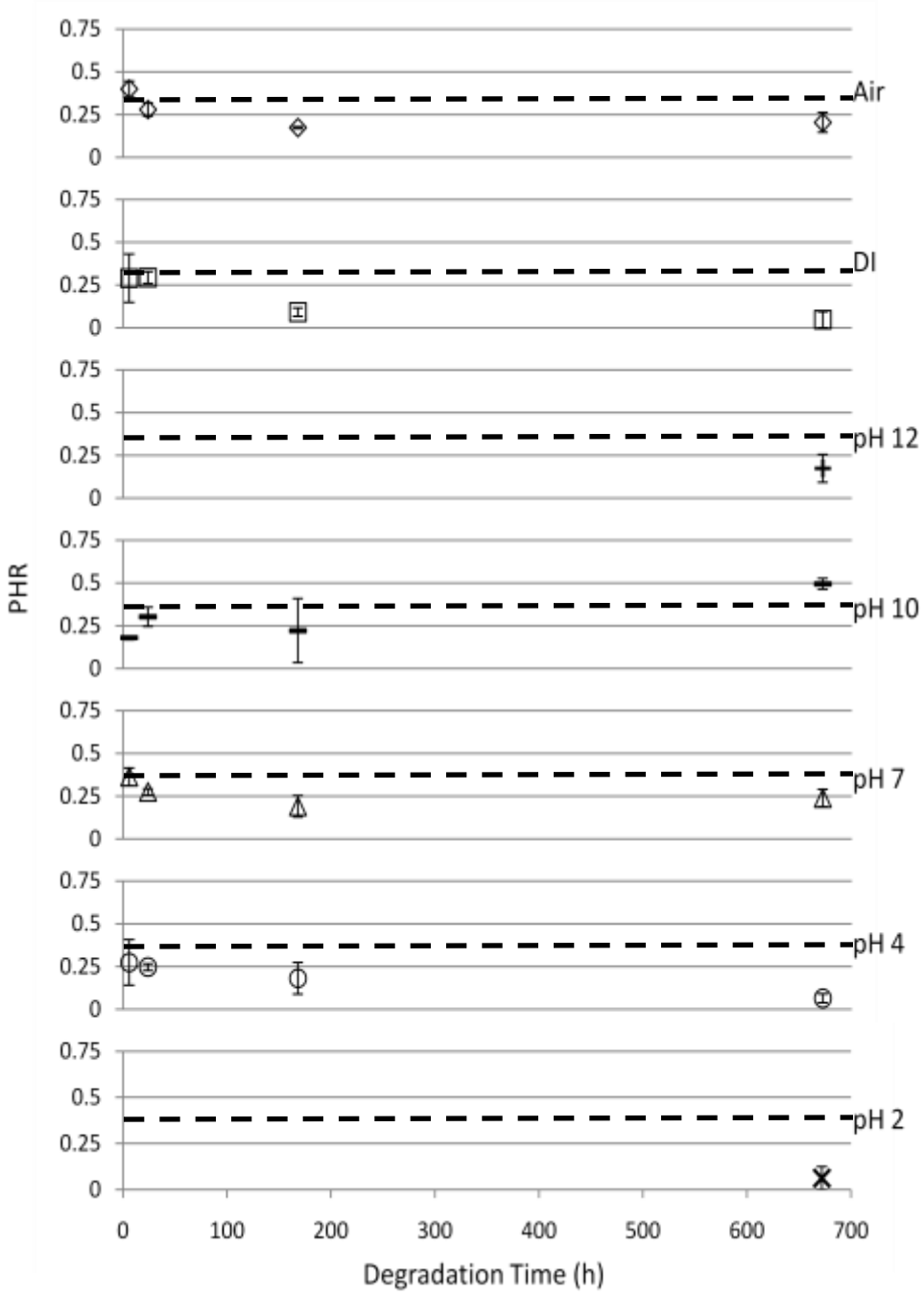

Figure 4.11: PHR of the peak at 1583 cm^{-1}, carboxylic acid anion carboxyl stretch, as a function of aging time for PTM (◇ air; □ DI; ⌖ pH 12 (single point); ⋯ pH 10; △ pH 7; ○ pH 4; X pH 2 (single point)). Error bars represent 95% confidence intervals for 3 replicates. Dashed line shows the PHR for the neat material (before compression molding).

The PHR of 1725 cm^{-1} initially are dependent on the fluid present, Figure 4.12. DI, pH 4, and pH 10's 1725 cm^{-1} PHR increases from 6 to 24 h and then decreases from 24 to 168 h. For air and pH 7, 1725 cm^{-1} PHR decreases from 6 to 168 h. PHR trend increases from 168 to 672 h for all samples, Figure 4.12. Over the 6 to 672 aging time, DI, pH 10, and pH 4 1742 cm^{-1} PHR increase as the samples lose 50-90% of their initial mass. For Air, the PHRs appear to have trends that are of the same magnitude as samples in solution with minimal weight change. The changes in PHR have to be evaluated carefully since it is giving a measure of the chemical functionality in the remaining solid. It does not give an indication of the chemical composition of the material that has diffused out of the solid, either initially or upon degradation, and that is not an insignificant portion of the sample. It should be recalled that all of the samples, except the air control, lost 50-90% of their initial mass over 672 h in solution.

The fluid in all vials being changed every 24 h does not allow for the degradation product accumulation in the fluid driving the degradation reactions and degradation reaction product diffusion into solution leading to a decrease trend in PHR for all peaks of interest, Figures 4.10 – 4.13. The diffusion of degradation reaction product is affected by distance from the surface of the polymer and by the size of the products. Higher Mw degradation products, that are closer to the center of the sample, will become entrapped and facilitate auto-catalysis of the sample, Figure 4.14. The auto-catalysis produces a hollow shell as degradation continues. The shell does not degrade as quickly as the interior of the sample because the low Mw products that have acid end groups can diffuse into solution quickly from the surface.

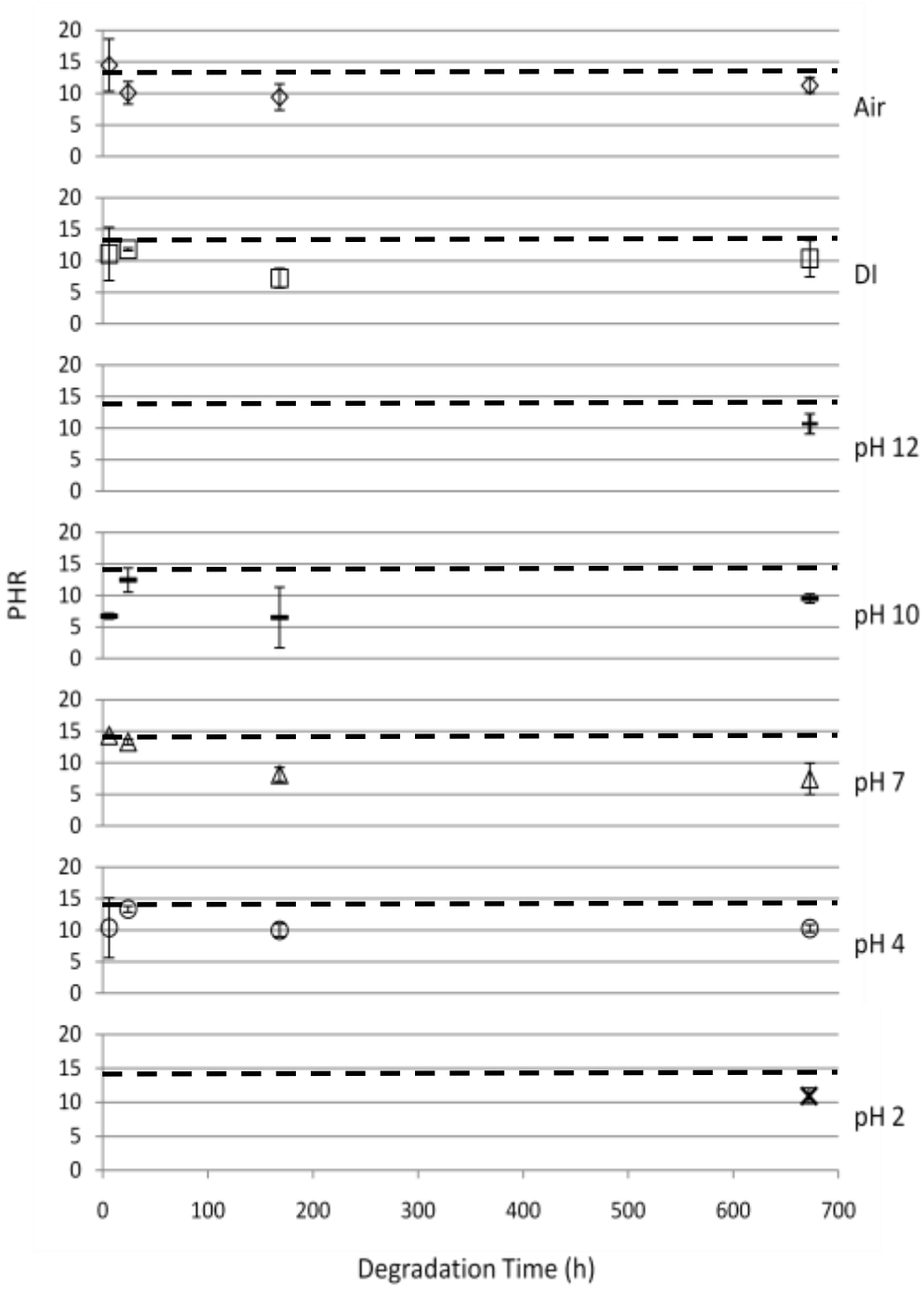

Figure 4.12: PHR of the peak at 1725 cm^{-1}, ester carbonyl stretch, as a function of aging time for PTM (◇ air; □ DI; ⌖ pH 12 (single point); ⋯ pH 10; △ pH 7; ○ pH 4; X: pH 2 (single point)). Error bars represent 95% confidence intervals for 3 replicates. Dashed line shows the PHR for the neat material (before compression molding).

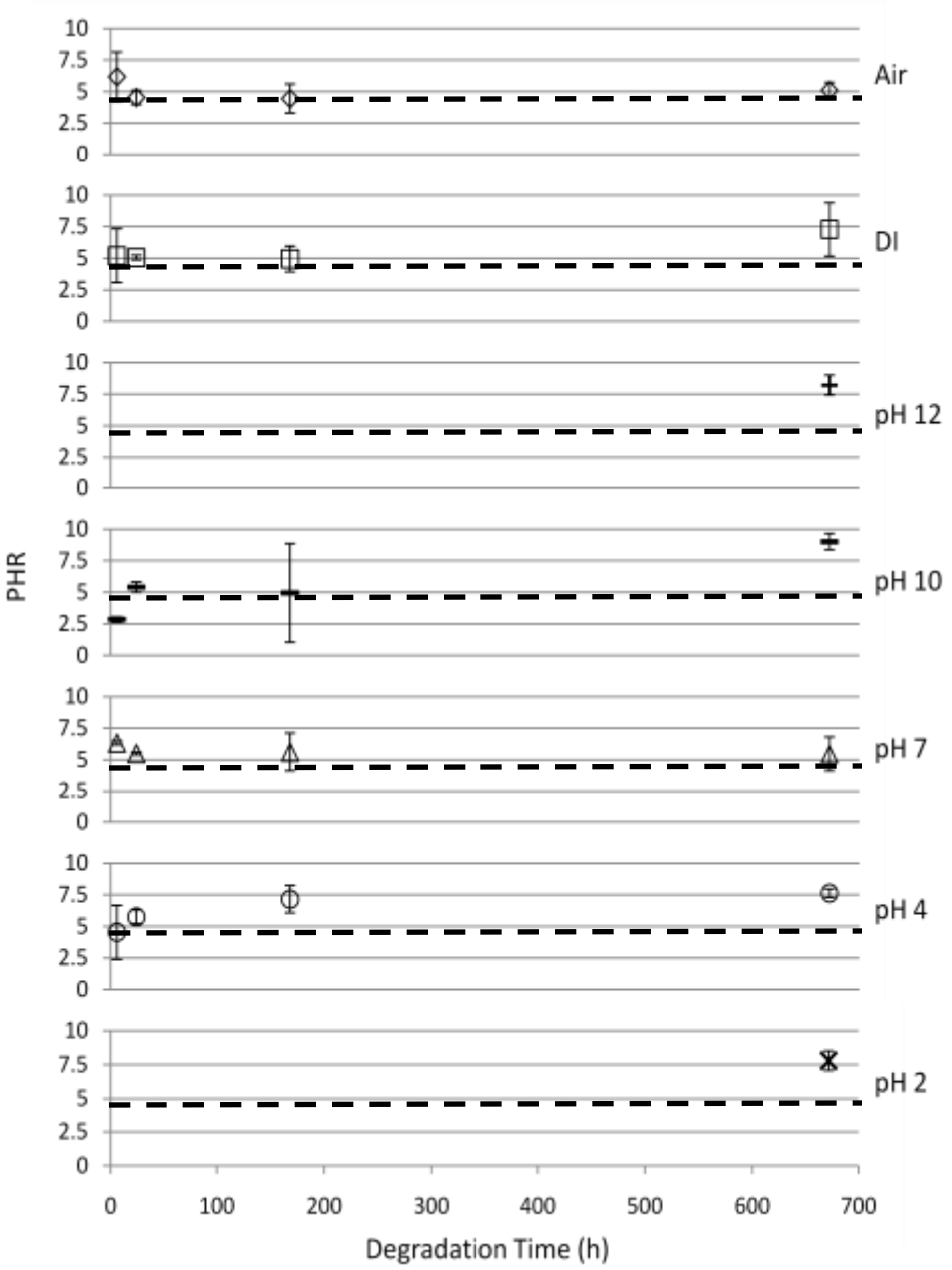

Figure 4.13: PHR of the peak at 1742 cm^{-1}, ester carbonyl stretch, as a function of aging time for PTM (◇ air; □ DI; + pH 12 (single point); -- pH 10; △ pH 7; ○ pH 4; X pH 2 (single point)). Error bars represent 95% confidence intervals for 3 replicates. Dashed line shows the PHR for the neat material (before compression molding).

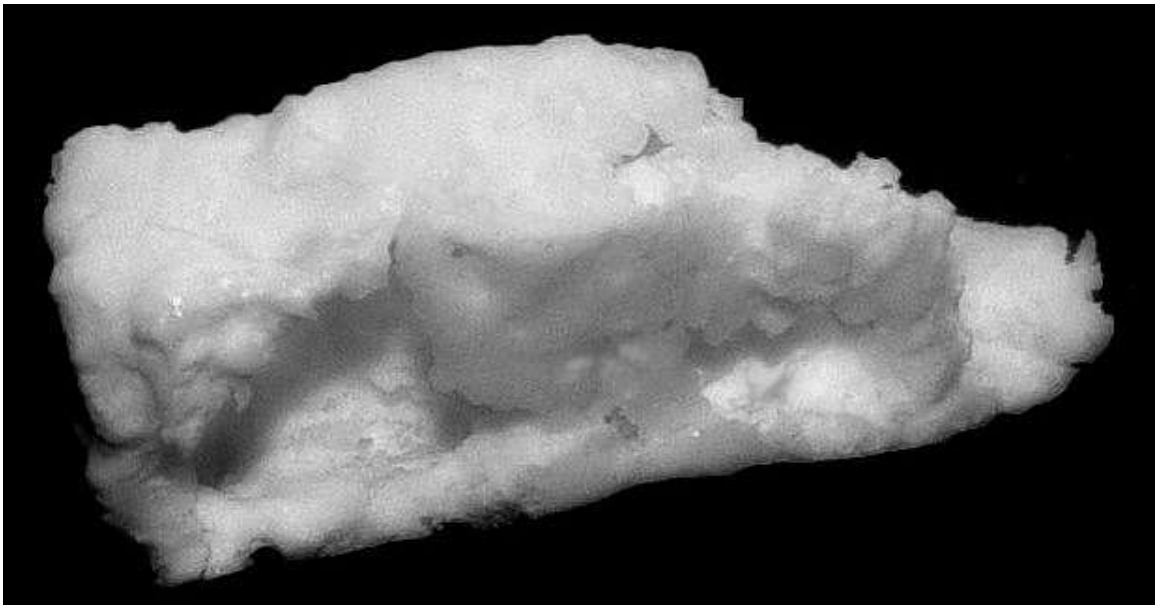

Figure 4.14: Photo of hydrolytically degraded PTM (168 h, pH 4) showing the shell that remains after after auto-catalyzation of interior material.

4.3.3.2.3. Gel Permeation Chromatography (GPC)

GPC was also used to examine the hydrolytically degraded PTM samples. Note that the PTM, as prepared, contained a bi-modal MW distribution and both the high and low MW components were monitored during the study. The high Mw component (greater than 10 kDa) will be referred to as HMw, and the low Mw component (less than 10 kDa) will be referred to as LMw. The GPC-determined average Mw and relative high Mw composition data are shown in Figures 4.15 and 4.16. Neither the average HMw nor the relative HMw and LMw composition of the air control changed with time. The air control does appear to change as a function of aging time. The change appears to systematic and not due to degradation. The samples in pH 7 and DI still showed HMw for the first 6 h, but at times greater than 6 h no HMw material was detected. The pH 4 and pH 10 samples had a HMw component through 168 h. pH 10 had no significant change in the H Mw components, Figure 4.15, and any significant changes in

composition, Figure 4.16. The pH 10 sample lost 45 % of its initial weight over 168 h. For the Mw composition to be maintained while the sample lost significant weight, the degradation rates and diffusion rates of the LMw and HMw material must be comparable for this sample as a function of aging time. For pH 4, a reduction in both the average HMw and relative concentration in the sample was seen with time. pH 4 was the most acidic solution for aging times less than 168 h. pH 2 and pH 12 were run only at 672 h, and they did not have a HMw component. The solution pH does have an effect on the HMw degradation, but there is not a consistency in the affect as a function of pH.

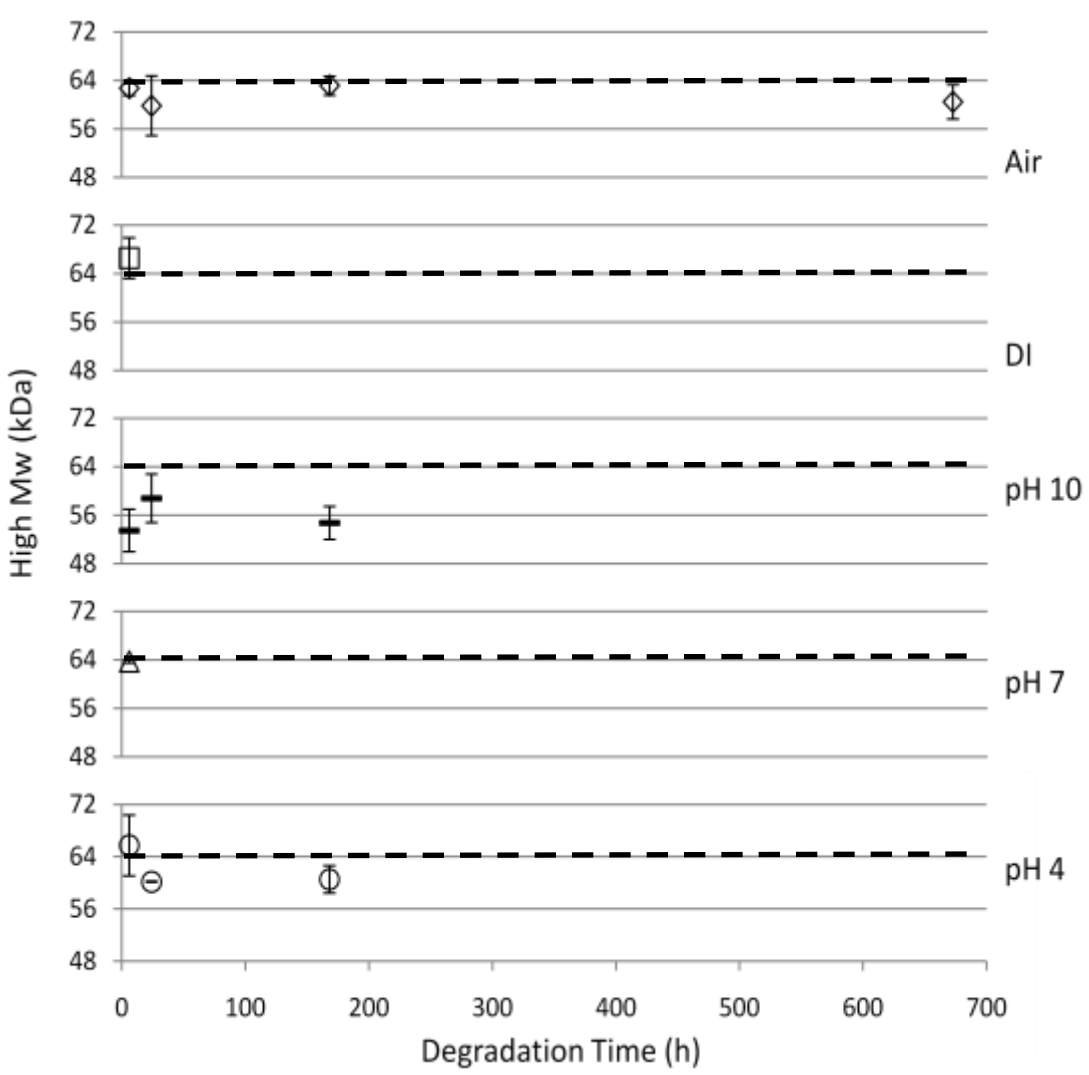

Figure 4.15: High Mw as a function of aging time for PTM (◇ air; □ DI; ⋯ pH 10; △ pH 7; ○ pH 4). Error bars represent 95% confidence intervals. Dashed line shows the PHR for the neat material (before compression molding).

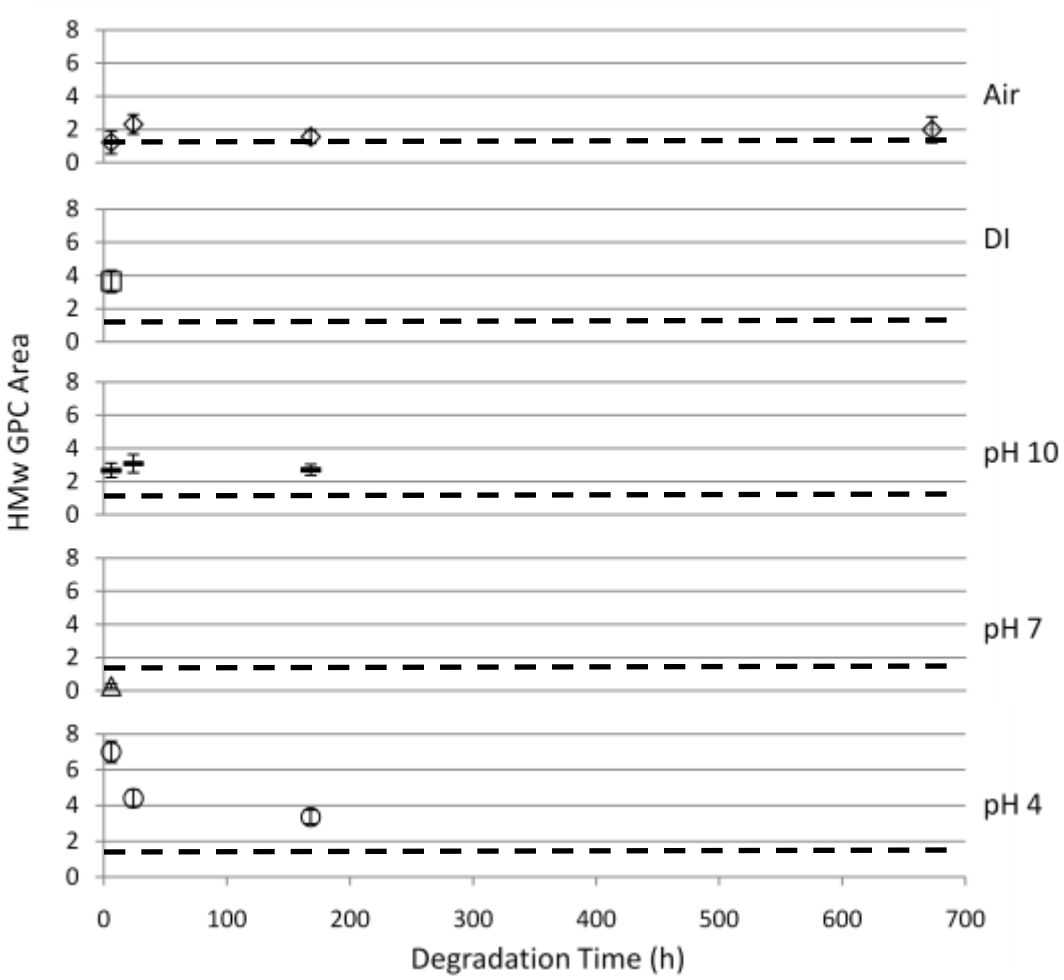

Figure 4.16: High Mw GPC percent area as a function of aging time for PTM (◇ air; □ DI; -- pH 10; △ pH 7; ○ pH 4). Error bars represent 95% confidence intervals. Dashed line shows the PHR for the neat material (before compression molding).

In contrast to the HMw component, the LMw component showed minimal change in average Mw during the hydrolytic degradation experiments for any of the samples (Figure 4.17). For the average Mw of the LMw component to remain constant with time, the degradation reaction products must be readily diffused out of the solid PTM sample. Since PTM and the surrounding solution are not allowed to come to equilibrium or only to a quasi-equilibrium (due to the solution being refreshed every 24 h). All samples showed no change or a slight increase in 672 h. With the samples losing 50 to 90 wt.% over 672 h, the outer shell material was only

left and it had a higher LMw than the neat material, 1.4 kDa. The outer shell had the degradation products diffuse out before auto-catalyzation could take place and were able to maitian their LMw. If the solution was not refreshed every 24 h, PTM and the surrounding solutions would come to equilibrium or quasi- equilibrium and the LMw component may reduce as a function of time.

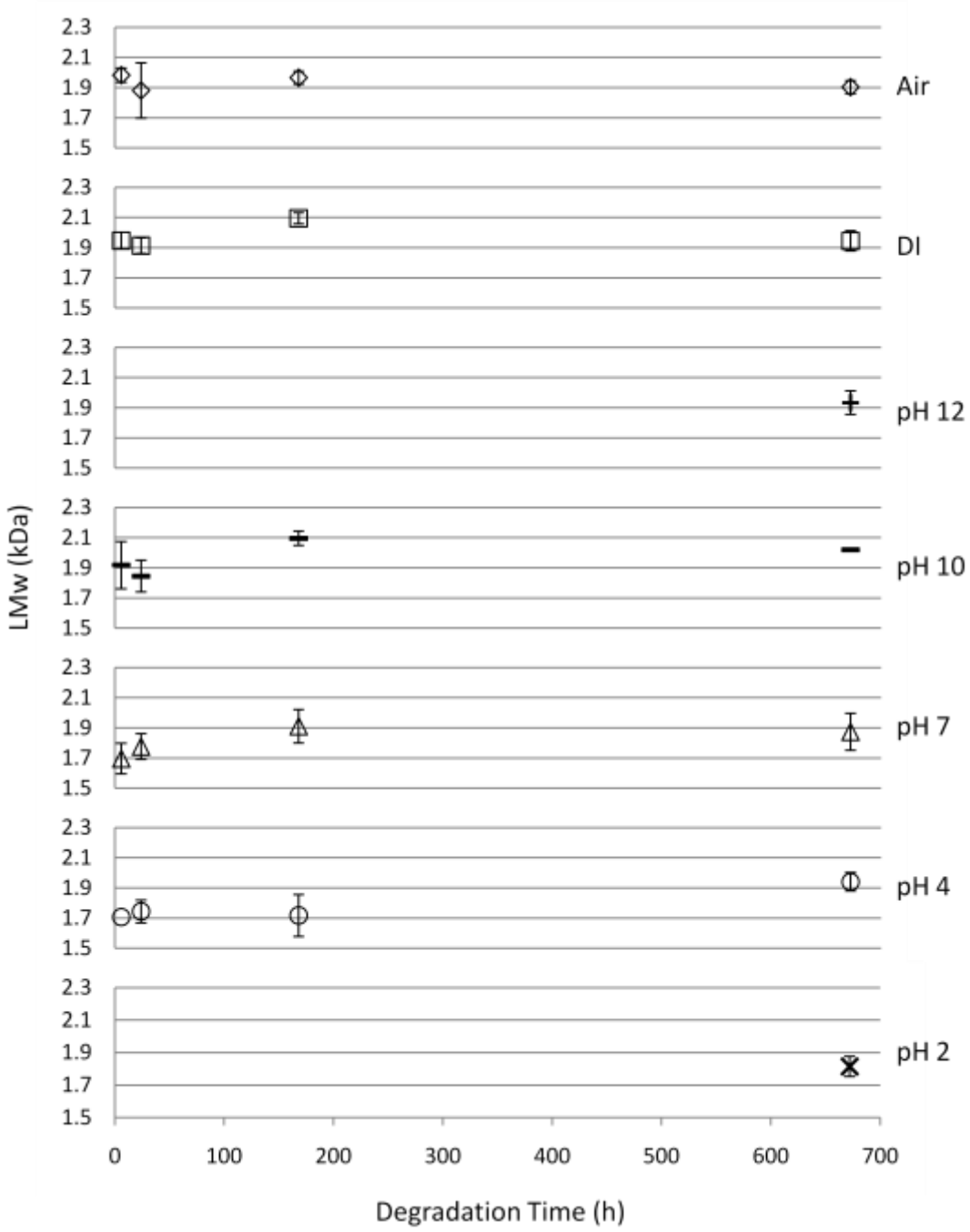

Figure 4.17: Low Mw as a function of aging time for PTM (◇: air; □: DI; ⌖: pH 12; ⎓: pH 10; △: pH 7; ○: pH 4; X: pH 2). Neat material had a LMw of 1.4 kDa. Error bars represent 95% confidence intervals.

The degradation fluid from all samples was analyzed by GPC to determine the Mw of any materials lost from the PTM samples to the aqueous phase (Figure 4.18). The measured Mw ranged broadly from ~1 kDa to the minimum detectable Mw on the GPC. In Figure 4.18, Air is presented for reference, and there was no liquid for Air sample to be analyzed. For 6 h and 24 h solutions, there had been no exchanging of the solutions. For 168 h and 672 h, the solutions had been exchanged 7 and 28 times, respectfully, and only the 7^{th} or 28^{th} solution was analyzed. The pH 10 samples showed the most significant decrease in Mw from approximately 1 to 0.5 kDa from 6 to 168 hours. The pH 4 Mw had a small dependence on aging time reducing from ~0.28 to ~0.14 kDa. PTM in pH 7 PBS solution consistently had the lowest Mw over all time for all samples, ~0.11. The PDI for all aqueous solutions was ~3.5, and it did not show any trends based on aging time or pH. There is significant degradation through $A_{AC}2$, $A_{AL}1$, and $B_{AC}2$ mechanisms for all polymers in solution, but the solution degradation cannot be decoupled from diffusion. Since the minimum Mw of any degradation product is ~0.06 kDa, the PDI indicates that there is a broad range of higher Mw products in solution. These higher Mw products are being degraded to monomers. The exchanging of fluids every 24 h allowed for analysis of only the previous 24 h of diffusion and degradation products in solution. At 672 h for pH 4, pH 7, and DI, the Mw in the solution is approximately the same as it is after 6 h, ~0.2 kDa, with equivalent or higher LMw (Figure 4.15). It can be concluded from these samples that degradation is occurring at an equivalent rate for all times and driven to an equilibrium or quisi-equlibrium state. The pH 10 sample may give a little insight into the diffusion and degradation interaction. From 6 h to 24 h for pH 10, the LMw decreased by ~0.05, Figure 4.15, HMw increased ~4 kDa with minimal compositional change from ~3%, Figures 4.15 and 4.16, the dry weight decreased by 20 wt.%, Figure 4.6, and the solution Mw decreased ~0.3 kDa and was the highest Mw found in solution over that time period for all samples. pH 10 over a 18 h period had no significant

change in it Mw composition with 20 wt.% dry weight loss and significant degradation in solution shown by the decrease in solution Mw. It would appear that PTM is almost water soluble in pH 10 solution from the lack of change in Mw and is very susceptible to hydrolytic degradation in solution.

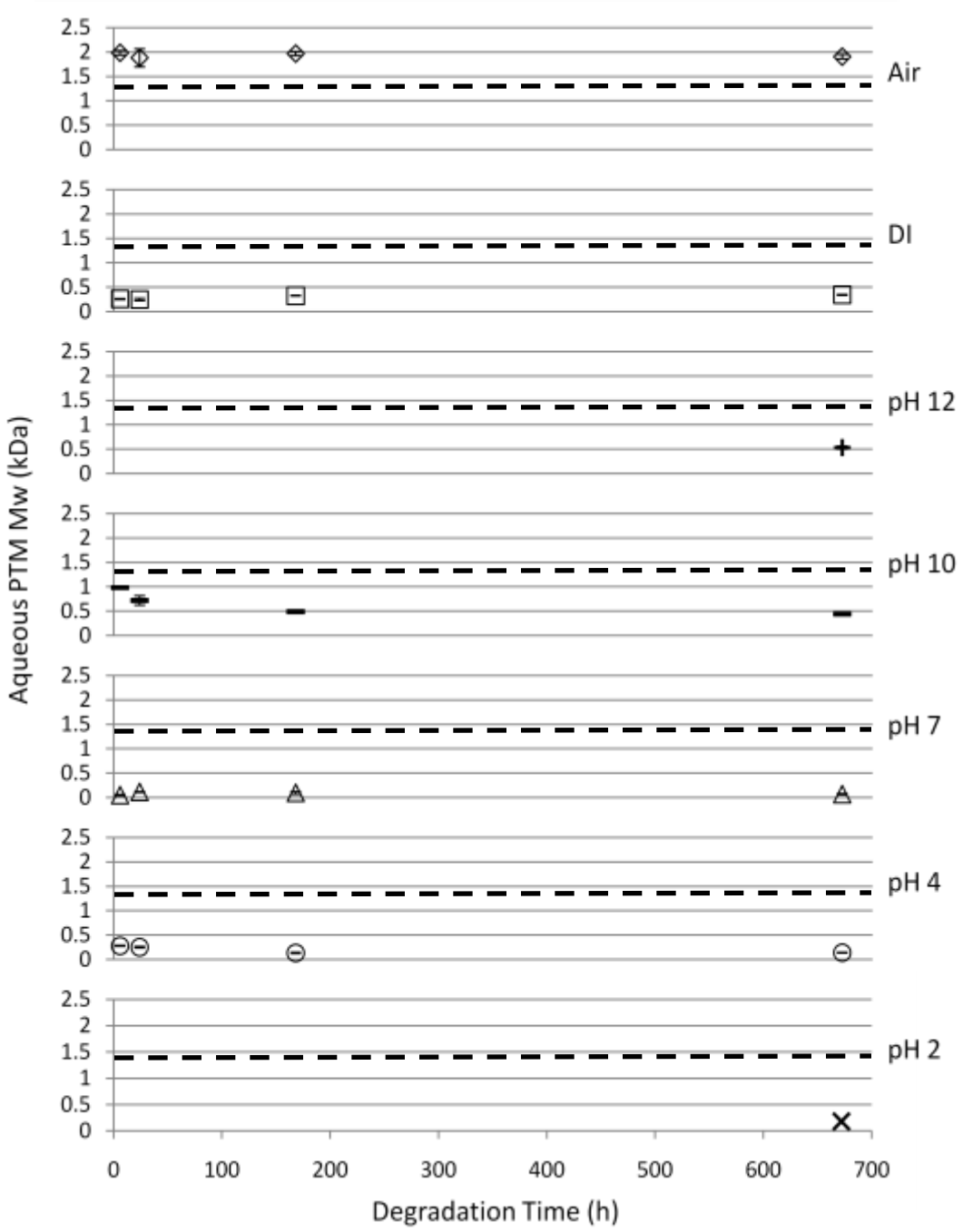

Figure 4.18: Water soluble PTM Mw as a function of aging time for PTM (□: DI; ⌖: pH 12; ⧟: pH 10; △: pH 7; ○: pH 4; X: pH 2). The air control, ◇, is shown as a reference. Error bars represent 95% confidence intervals. Dashed line shows the PHR for the neat material (before compression molding).

4.3.4. Conclusions

PTM was readily hydrolytically degraded by solutions with pHs raging from 2 to 12. The low Mw component of PTM dissolves in DI water, toluene, and ethanol before the higher Mw component. During degradation, hydrolytic degradation and diffusion decrease the PTM by 50 to 90 wt.% aft 672 days. Both the diffusion and degradation are increased by changing the fluid every 24 h that removed all PTM dissolved in solution. Due to the loss of up to 90 wt.% weight loss during the experiment, ATR-FTIR analysis did not provide insight into the degradation mechanism. The LMw remained relatively constant for all samples with aging with weight loss of 50 to 90 wt.%, and the HMw was completely degraded after 168 h for all samples. GPC analysis of PTM dissolved in the solutions surrounding the samples showed that PTM was rapidly degraded in solution. In addition to degradation, ATR-FTIR analysis showed that compression molding was polymerizing PTM and changing PTM's chemical composition. GPC confirmed that compression molding was polymerizing PTM by an increase in the LMw from ~1.4 kDa to ~1.9 kDa.

4.4. PTM Hydrolytic Degradation using KOH Solutions over 1 Week

4.4.1. Introduction

A hydrolytic degradation study was performed on compression molded PTM samples under variable pH and time. The pH of the degradation fluid ranged from 7 to 11 and samples were aged for 10 h, 100 h, 1,000 h, or 10,000 h. Solubility, weight change, FTIR spectroscopy, GPC, DSC, and SDT was used to examine the chemical and physical changes occurring in these PTM samples as a function of degradation pH and time.

4.4.2. Experimental Materials and Methods

Materials. The PTM sample used for the degradation study was bulk polymerized from 1,3-propane diol (PDO, 98%, Sigma Aldrich) and malonic acid (MA, 99%, VWR) using $AlCl_3$ catalyst (98%, Sigma Aldrich) with a 100:1 monomer to catalyst ratio at 155 °C for 4 h. Additional detail on the PTM synthesis and characterization of the neat material is provided in Chapter 2. Note that the PTM, as prepared, contained a bi-modal MW distribution and both the high and low MW components were monitored during the study. PTM: 62,950 ± 504 Da (with 1.82 ± 0.15 PDI, DP 874.3 ± 0.9, 1.6 ± 0.3 wt.%) and 1791 ± 62 Da (with 1.83 ± 0.04 PDI, DP 24.9 ± 0.3, 98.4 ± 0.3 wt.%). The high Mw component will be referred to as HMw, and the low Mw component will be referred to as LMw. pH 4, 7, and 10 phosphate buffer solutions (PBS) were purchased from VWR. , HCl (Fisher Scientific, 1N), and NaOH (Fisher Scientific, 99%) were used to prepare aqueous solutions. Optima Tetrahydrofuran (Fisher Scientific, +99.9%) was used as the effluent in gel-permeation chromatography. All chemicals purchased were used as received.

Compression Molding. PTM (PDO-MA, 155 °C, 4 h) was compression molded into a 12 cm x 12 cm x 0.159 cm sheet using a Carver 15 ton floor stand press at 6.9 MPa for 10 min at 30 °C. The sheet was cut into 1 cm x 0.318 cm x 0.318 cm samples, dimensions and weights were collected, and each sample was placed into individual vials.

pH Response to Monomer in DI water and pH 7 Phosphate Buffer Solution. Monomer solubility was examined using pH 7 phosphate buffer solutions (PBS) and DI water. 1 g of 1,3-propanediol or malonic acid was placed into a 16 mL vial with 10 mL of solution. The vials were allowed to sit for 3 days before being examined by measuring pH.

Polymer Hydrolysis (Degradation Procedure). For the initial hydrolysis experiment, vials containing individual compression molded PTM coupons had 10 mL of DI water (measured 5.4 pH), pH 7 KOH, pH 9 KOH, or pH 11 KOH aqueous solutions. Samples were placed in a vacuum

over at 25 torr for 24 h to remove excess water before degradation. One set of vials had no liquid added as an 'air' control, to attempt to take into account any changes due to aging alone. All work was done in triplicate. All of the sealed sample vials were then placed into a 25 °C water bath for 10 min, 100 min, 1,000 min, or 10,000 min. At each pre-designated time, the samples were removed from solution, blotted with a KimWipe®, and the wet weights were recorded. They were then vacuum dried (25 torr) at room temperature for 24 h and the dry sample weights were recorded. All chemical and physical characterization was performed samples after vacuum drying. Samples will be referred to by their initial pH (pH 7, 9, or 11), DI for DI water, or as the air control (no liquid added).

Gravimetric weigh. At the end of the allotted aging time, the samples were removed from their vials, excess water was removed by gently blotting with a KimWipe®, and the polymer samples were weighed. The difference in the 'wet weight' minus the initial weight was divided by the initial weight to give the wet weight change. The samples were then vacuum dried at room temperature for 24 h and weighed again. The difference between the 'dry weight' minus the initial weight was divided by the initial weight to give the dry weight change.

Chemical and physical characterization. The polymer samples were also characterized by attenuated total reflectance (ATR) FTIR spectroscopy at discrete times during the degradation study using a Thermo Electron 6700 instrument (DTGS detector , room temperature, dry air purge, ZnSe crystal with a 60° angle of incidence). The peaks were fitted with PeakSolve in Thermo Scientific Omnic 8.1.10. Gaussian peaks were fitted at specific wavenumbers to minimize standard error. A peak height ratio (PHR) calculation was used in the quantitative analysis of FTIR spectra. PHR uses the height of the C-C rocking at 1465 cm^{-1} as the denominator and the height of the peak of interest as the numerator to form a ratio. Solution pH was determined using Accumet Basic AB15 pH meter from Fisher Scientific that was calibrated every

30 min at 5 points (using PBS of pH 2, 4, 7, 10, and 12). The pHs of experimental solutions were examined after vacuum filtration with a Buchner funnel and Whitman Grade 40 filter paper. Gel permeation chromatography (GPC) data was collected with a Waters GPC with RI detector, 4E and 5E (polystyrene-dinvinylbenzene, 4.6 x 300 mm) Styragel® columns, Optima THF as the effluent at 0.3 mL/min, and a ten-point polystyrene calibration. For the degradation solids, 6 to 8 mg was weighed out and dissolved in Optima THF for at least 4 h. The samples were then filtered through a 0.45 µm expanded PTFE syringe filter before being analyzed with GPC. The degradation solutions were subjected to room temperature vacuum (25 torr) for 24 h to evaporate the water. If there were no visibly discernable solids left after evaporation, 2 mL of Optima THF was added. The solution was allowed to dissolve for at least 4 h and then was filtered with 0.45 µm expanded PTFE syringe filter before being analyzed with GPC. If there were discernable solids after evaporation, the solid sample GPC procedure (as described above) was followed.

4.4.3. Results and Discussion

4.4.3.1. pH Response to Monomer in DI water and pH 7 Phosphate Buffer Solution

PDO and MA were completely soluble in DI water and pH 7 PBS, which was expected. MA reduced DI water and pH 7 PBS pH significantly from pH ~5.4 to pH ~1.7 for DI water and from pH 7 to pH ~2 for pH 7 PBS, Figure 4.19. DI water pH was reduced by the addition of PDO, but it was not mathematically significant. PDO did interact with pH 7 PBS and increase the pH from 7 to ~7.6. MA had the expected effect on pH, and PDO had little or a positive effect on the solutions' pH. PDO interaction with the PBS indicated PBS should not be used further in the study as it would interact with PDO.

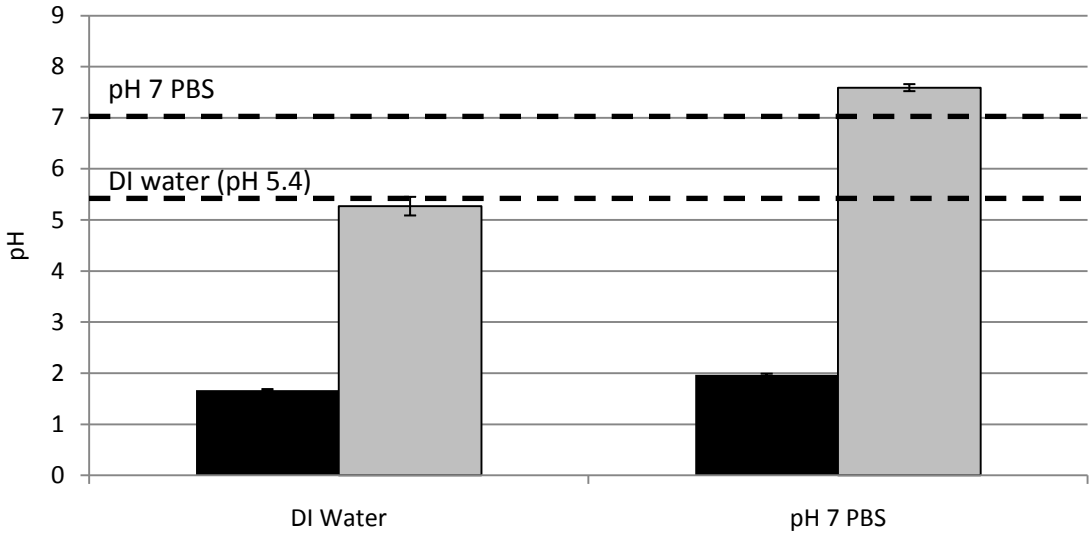

Figure 4.19: Measured pH values after 72 h for DI water (black filled columns) and pH 7 PBS (grey filled columns) after the addition of 1 g of MA and PDO with error bars representing 95 % confidence intervals. Dashed lines show the initial pH of DI water (bottom line) and pH 7 PBS (top line).

4.4.3.2. Gravimetric Analysis and pH

Degradation of PTM was carried out in aqueous solutions adjusted by KOH to pH 7, 9, and 11, DI water with an initial pH of 5.4, and a control with no fluid referred to as air at 25 °C for 10, 100, 1,000, 10,000 min. Samples will be referred to by their initial pH 7, 9, or 11, DI, or Air throughout the results and discussion. The wet weight of samples removed from their fluid, excess fluid removed, and before vacuum drying had a negative trend in weight as a function of aging time, Figure 4.20. Samples reduced in weight less than 1.5 wt.% when still wet. From previous experience with PTM, it was expected that PTM would absorb water and maintain a weight near the initial weight even as degradation proceeded. When comparing the samples from before and after drying, Figures 4.20 and 4.21, the samples absorbed up ~35 wt.% water at 10,000 min for DI and diffused ~35 wt.% of material into solution. The amount of absorbed water may be artificially high due the PTM becoming a porous, hollow structure at longer aging

times and being able to retain excess water in hollow spaces. All samples do not show significant weight loss during the first 10 min of degradation, Figure 4.22. Even though there is a significant weight loss rate initially, it appears that there is an induction period before degradation products can diffuse out of the polymer and cause a significant change in DI and pH 7's dry weight. In the first 100 min as water diffuses into the DI and pH 7, the $A_{AC}2$ and $A_{AL}1$ reaction rates are increasing as there is an increased excess of water to shift the reactions equilibrium to products, Figure 22. The reaction mechanisms for $A_{AC}2$ and $A_{AL}1$ can be seen in Figure 4.23 (a) and (b) and require an excess of water to drive the reactions to completion. DI and pH 7 dry weights decrease and become significantly different at 10,000 min. DI is significantly more acidic initially, pH 5.4, than pH 7, which had its pH adjusted by the addition of KOH. DI is assumed to only follow $A_{AC}2$ and $A_{AL}1$ due to the lack of the addition of a base, such as KOH, to the solution, which does not allow DI's degradation mechanisms to following $B_{AC}2$ kinetics, Figure 4.23 (c). It is assumed that the KOH is affecting pH 7 degradation rate by interfering with the $A_{AC}2$ and $A_{AL}1$ mechanisms. KOH could be stabilizing the carboxylate anion in pH 7 and hinder the protonation of carbonyl carbon in the $A_{AC}2$ and $A_{AL}1$ mechanisms, which is assumed to be happening in all solutions with KOH added. pH 11 and pH 9 initially started as base-mediated degradation through $B_{AC}2$ hydrolysis mechanisms, and as aging time precedes, the pH of the surrounding solutions decrease to acidic conditions, seen in Figure 4.24, where $A_{AC}2$ and $A_{AL}1$ mechanisms dominate the hydrolysis of pH 11 and pH 9 and $B_{AC}2$ mechanism does not occur. It is not known why all sample solutions are driven to the same pH, and theories for why the solutions are being driven to similar pHs will be discussed in the GPC section. pH 11 and pH 9 had significant amounts of KOH initially added to adjust the pH, and the K^+ ion had significant affect on the degradation of pH 11 and pH 9. With increasing K^+ ion content from pH 7 to pH 11 samples, there is a decrease in weight change as the K^+ ion inhibits $A_{AC}2$ and $A_{CL}1$

mechanisms even under acidic conditions at longer aging times. The degradation rates for pH 11 and pH 9, Figures 4.20 and 4.21, do not have an increase from 10 to 100 min in an opposite tend to the degradation rates of DI and pH 7. Even though pH 11 and pH 7 are under acidic conditions from 10 to 100 min, the $A_{AC}2$ and $A_{CL}1$ mechanisms are not as effective at degrading PTM. The increased concentration of K^+ ions with increasing initial solution basicity reduces pH 11 and pH 9 weight change and weight change rate over 10,000 min aging time. The major influence on weight change and weight change rate is the concentration of ions in the initial solution for the degradation of PTM through carboxylate anion stabilization by K^+ acid-base interaction.

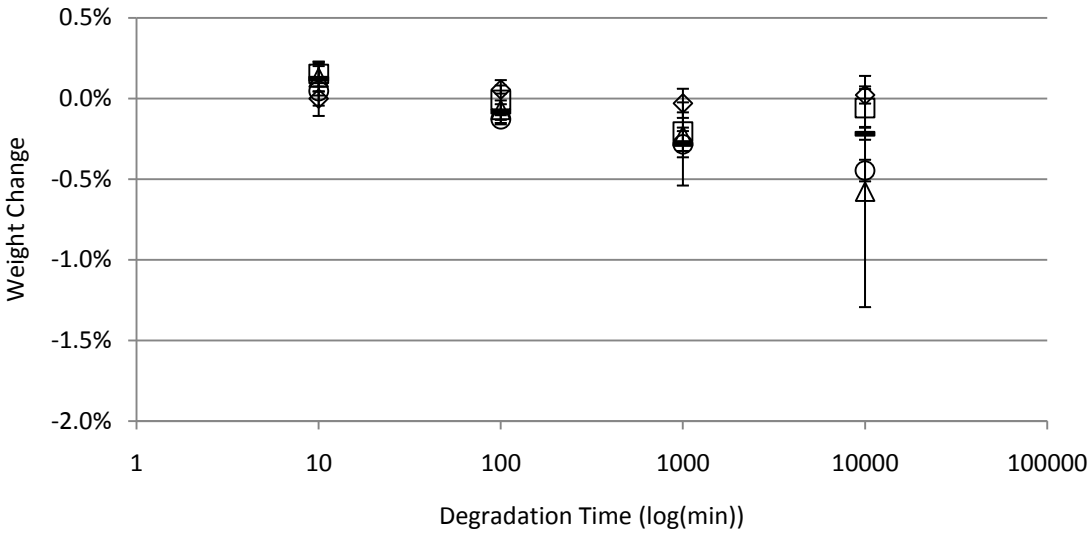

Figure 4.20: Percent weight change as a function of aging time for PTM when wet (◇ air; □ DI water; △ pH 7; -- pH 9; ○ pH 11). Error bars represent 95% confidence intervals for 3 replicates.

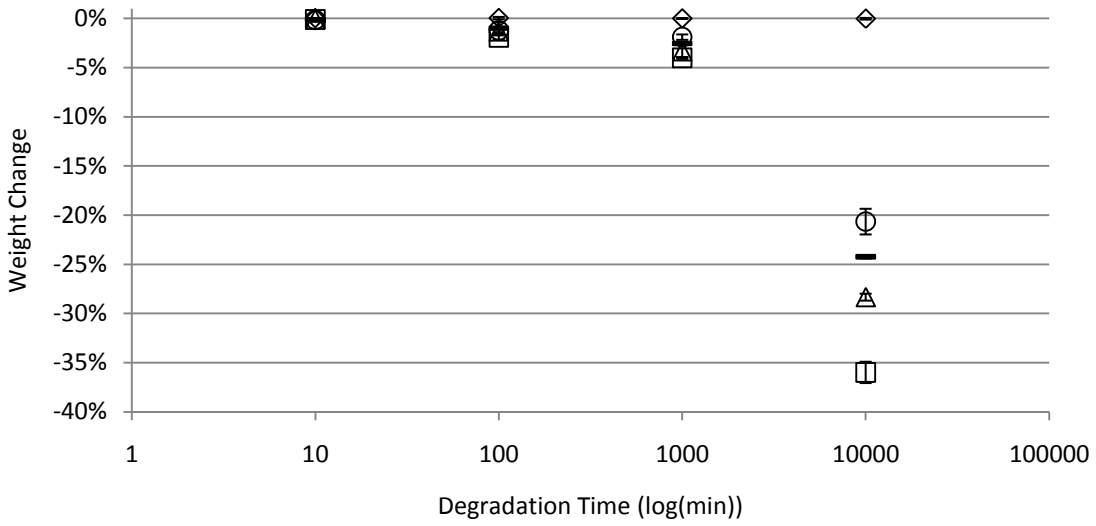

Figure 4.21: Percent weight change as a function of aging time for PTM after drying in air (◇ air; □ Div water; △ pH 7; -- pH 9; ○ pH 11). Error bars represent 95% confidence intervals for 3 replicates.

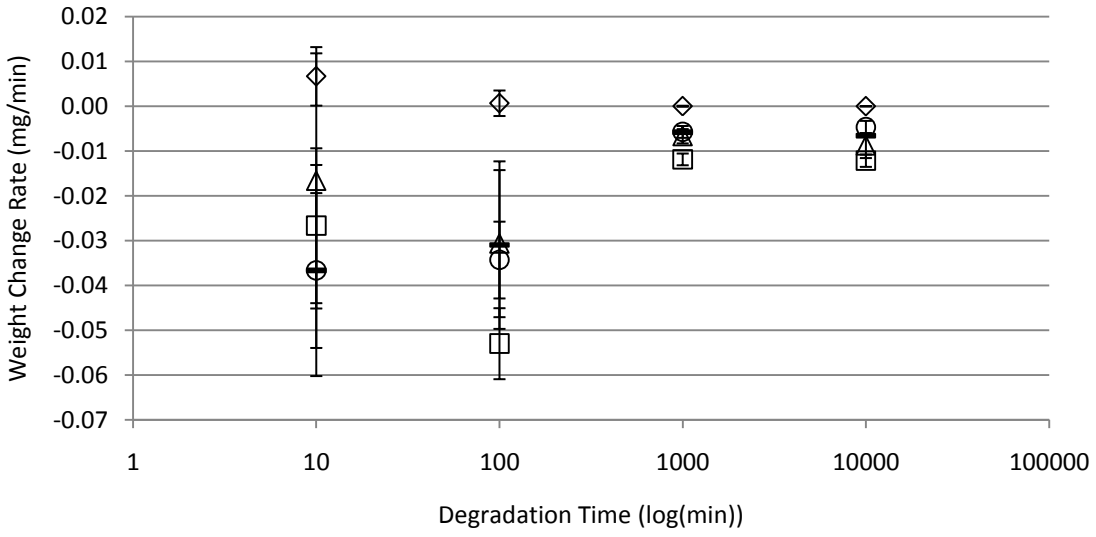

Figure 4.22: Weight loss rate as a function of aging time for PTM (◇ air; □ DI water; △ pH 7; -- pH 9; ○ pH 11). Error bars represent 95% confidence intervals for 3 replicates.

(a)

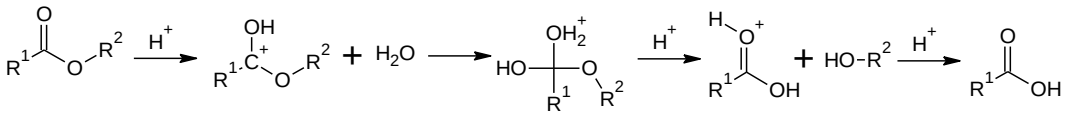

(b)

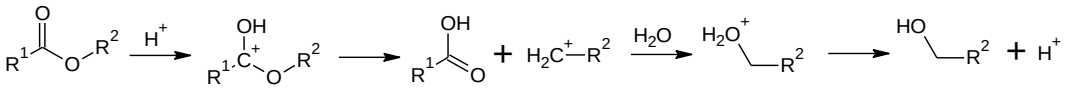

(c)

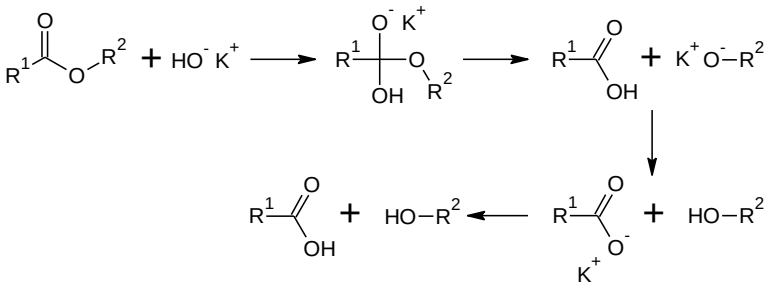

Figure 4.23: The $A_{AC}2$ (a), $A_{AL}1$ (b), and $B_{AC}2$ (c) ester hydrolysis reaction mechanisms.

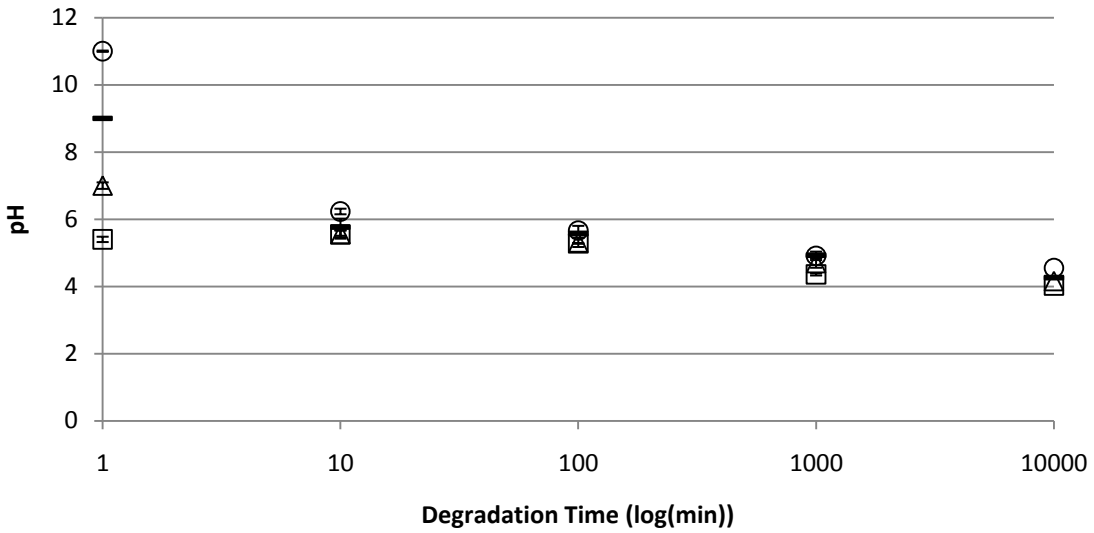

Figure 4.24: pH of aqueous solutions from PTM degradation from 100 to 10,000 min in DI water, and pH 7, 9, and 11 KOH aqueous solutions at 25 °C (□ DI; △ pH 7; -- pH 9; ○ pH 11). Error bars represent 95% confidence intervals for 3 replicates.

4.4.3.3. Attenuated Total Reflectance Fourier Transform Infrared Spectroscopy

The degraded material from pH 7, 9, and 11, DI, and Air was examined using ATR-FTIR to monitor changes in functional group concentration as a function of aging time. A representative spectrum can be seen in Figure 4.25. The area of interest on all spectra was the carbonyl stretch region from 1500 to 1900 cm^{-1}. The ester carbonyl degradation could be monitored by peak fitting the carbonyl stretch and monitoring the change in PHR. The peak fitting was performed on the region of 1500 to 1870 cm^{-1}, Figure 4.26. Seven peaks were identified in this region as 1587 cm^{-1} carboxylate anion carbonyl stretch(1), 1633 cm^{-1} cis-alkene stretch (2), 1672 cm^{-1} trans-alkene, vinylidiene, tri or tetra-substituted alkene stretch (3), 1702 cm^{-1} dimerized carboxylic acid carbonyl stretch (4), 1726 cm^{-1} ester carbonyl stretch (5), 1749 cm^{-1} ester carbonyl stretch (6), and 1777 cm^{-1} cyclic ester carbonyl stretch (7). There are two ester carbonyl peaks identified in the region of 1725 to 1750 cm^{-1} where ester carbonyls are present. It is theorized that there are two different types of esters present in PTM. The first type of ester

at 1726 cm^{-1} is a higher Mw ester carbonyl, and the second type of ester at 1749 cm^{-1} is either a large cyclic ester or low Mw ester carbonyl. The peak identification of two ester carbonyls will not be discussed in this paper, but it is discussed in Chater 2 [Dell'Erba 1997, Silverstein 1991, Dean 1992, Caitker 2000, Sutton 2006, Gulmine 2006, Zhou 2009].

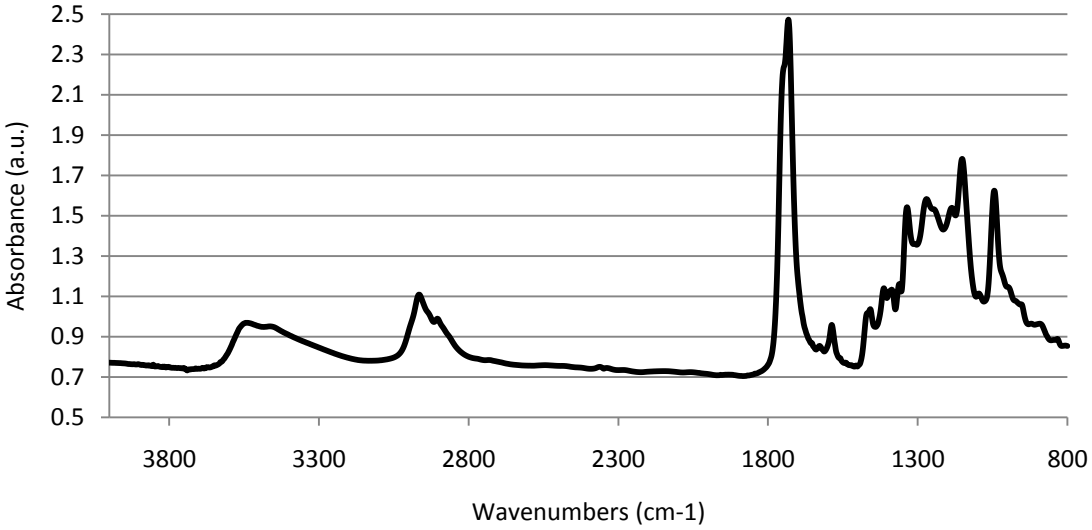

Figure 4.25: Representative ATR-FTIR spectrum for PTM used in the degradation study (1,000 min, air).

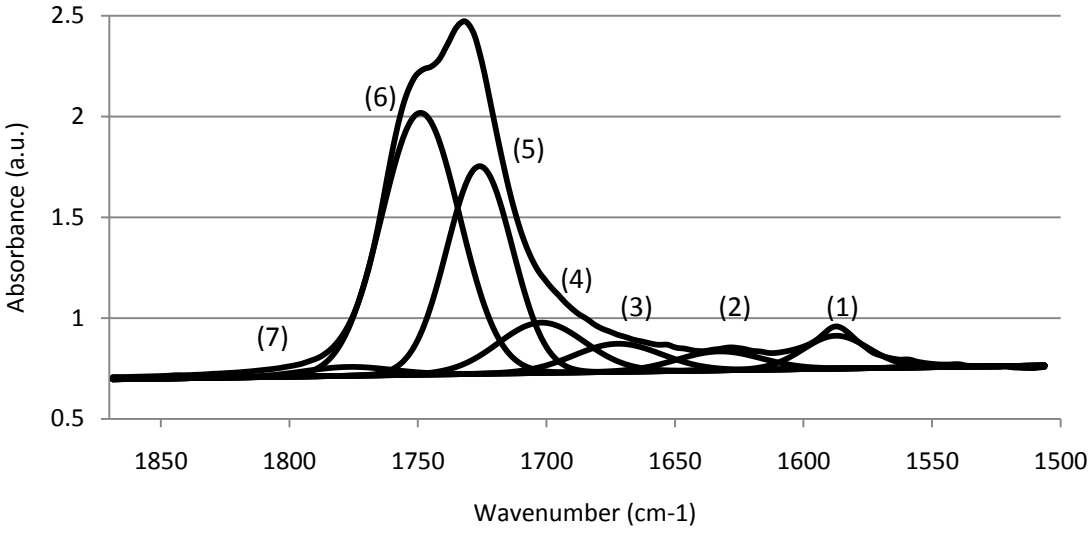

Figure 4.26: Representative peak fitting of PTM with seven peaks identified: 1587 cm^{-1} carboxylate anion carbonyl stretch(1), 1633 cm^{-1} cis-alkene stretch (2), 1672 cm^{-1} trans-alkene, vinylidiene, tri or tetra-substituted alkene stretch (3), 1702 cm^{-1} dimerized carboxylic acid carbonyl stretch (4), 1726 cm^{-1} ester carbonyl stretch (5), 1749 cm^{-1} ester carbonyl stretch (6), and 1777 cm^{-1} cyclic ester carbonyl stretch (7).

pH 7, 9, and 11 and DI solids had varying degrees of ester hydrolysis based on PHR changes of peaks at 1726 cm^{-1} and 1749 cm^{-1} with Air remaining constant. The 1726 cm^{-1} PHR tended to increase for all samples from 10 to 1,000 min, Figure 4.27. PHR is a semi-quantitative measure of concentration of a peak of interest. As the samples weight decreases over the first 1,000 min, the ester associated with 1726 cm^{-1} PHR increases or remains constant. The first 1,000 min could be considered an induction time for 1726 cm^{-1} before it reduces from 1,000 to 10,000 min for all samples in solution. The majority of weight loss for all samples occurs between 1,000 and 10,000 min when all samples, except Air, lose between 19 and 38% of their mass. The 1726 cm^{-1} ester carbonyl could be hydrolytically degrading, but it also may be diffusing into solution leading to a reduction in the PHR. The subject of whether it is degrading or diffusing out of PTM will be discussed with the GPC results later in the paper. 1749 cm^{-1} was identified as low Mw esters or large cyclic esters and appear to be readily hydrolytically

degraded in all solutions, Figure 4.28. Another reason for 1726 cm^{-1} PHR not to decrease in the same manner as 1749 cm^{-1} PHR is that the low Mw esters are more readily accessible by the diffusion of water into PTM. Whether it is diffusion of water into PTM or low Mw esters are more susceptible to hydrolytic degradation is outside the scope of this work. It is going to be assumed that the lower Mw polymer is more susceptible to degradation for this research, and 1749 cm^{-1} will be the focus of the ATR-FTIR discussion.

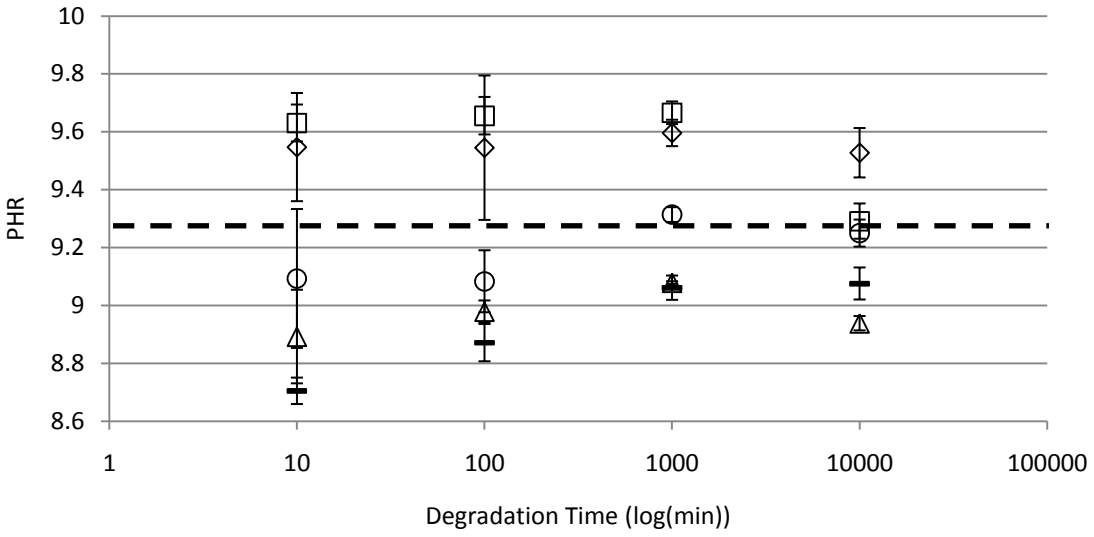

Figure 4.27: 1726 cm^{-1} ester carbonyl, PHR change as a function of aging time for PTM (◇ air; □ DI water; △ pH 7; -- pH 9; ○ pH 11). Error bars represent 95% confidence intervals for 3 replicates. Dashed line represents neat material before compression molding.

The ester carbonyl at 1749 cm^{-1} decreased by a maximum of ~2 during degradation as ester hydrolysis reduced the concentration of ester groups in PTM for all samples in solution, Figure 4.28. Air maintained ~8.8 over the 10,000 min as it experienced no degradation at 25 °C. DI and pH 7 had the largest decrease in PHR, ~2, over 10,000 min. The $A_{AC}2$ and $A_{AL}1$ mechanisms are driven by an excess of water present, and comparing the difference in pH 7 and DI weight before and after drying at 10,000 min, water accounts for 33 to 38 wt.% of the

samples. There is an excess of water at 10,000 min, at 1,000 min DI and pH 7 are retaining less than 5 wt.% water inside of PTM with ~1.5 decrease in PHR for both. DI and pH 7 are hydrolytically degrading during 10,000 aging time, and degradation products or water soluble polymer diffusion out of PTM lags the rate of hydrolytic degradation. For pH 11 and pH 9, 1749 cm^{-1} PHR decreases ~1.2 over the same time period that DI and pH 7 decreases ~2. The increase in K^+ ions in pH 11 and pH 9 interfere with the $A_{AC}2$ and $A_{AL}1$ mechanisms, even in acidic solutions. For pH 11, the PHR change over the first 1,000 min is not statistically significant, but PHR is trending negatively. From 1,000 to 10,000 min for pH 11, there is a statistically significant decrease in PHR. For the first 1,000 min, there is minimal change in pH 11 dry weights, and it appears that once the solution pH becomes negative the $B_{AC}2$ mechanism has minimal effect on pH 11 until excess water can penetrate and the $A_{AC}2$ and $A_{AL}1$ mechanisms can overcome the carboxylate ion stabilization effects of the K^+ ion. Water penetration and the addition of K^+ ions to the solution are the major factors in controlling the ester hydrolysis degradation of PTM.

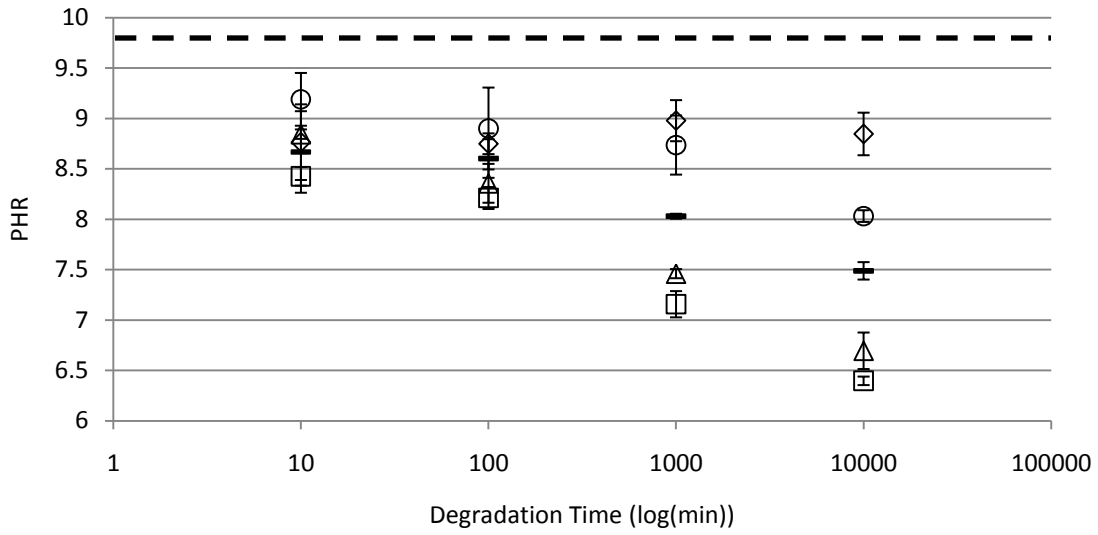

Figure 4.28: 1749 cm^{-1} ester carbonyl, PHR change as a function of aging time for PTM (◇ air; □ DI water; △ pH 7; -- pH 9; ○ pH 11). Error bars represent 95% confidence intervals for 3 replicates. Dashed line represents neat material before compression molding.

The dimerized carboxylic acid carbonyl stretch PHR at 1702 cm^{-1} increased with increasing aging time for DI and pH 7, 9, and 11 in the solid state, Figure 4.29. As ester hydrolysis takes place, carboxylic acid carbonyls will be produced increasing their concentration in the solid. If the carboxylic acid carbonyl PHR did not increase, it would indicate that either cyclization is occurring, the degradation products were diffusing out of the solid as fast as they were produced, or a peak was miss identified. Cyclization may be occurring, but it is not having a substantial effect on 1702 cm^{-1} PHR. The degradation products are diffusing into solution, which will be shown by GPC below, and are of varying Mw. The higher Mw degradation products will diffuse slower out of PTM and lead to an increase in the concentration of carboxylic acids. The peak identification is discussed in a previous paper, and will not be discussed here.

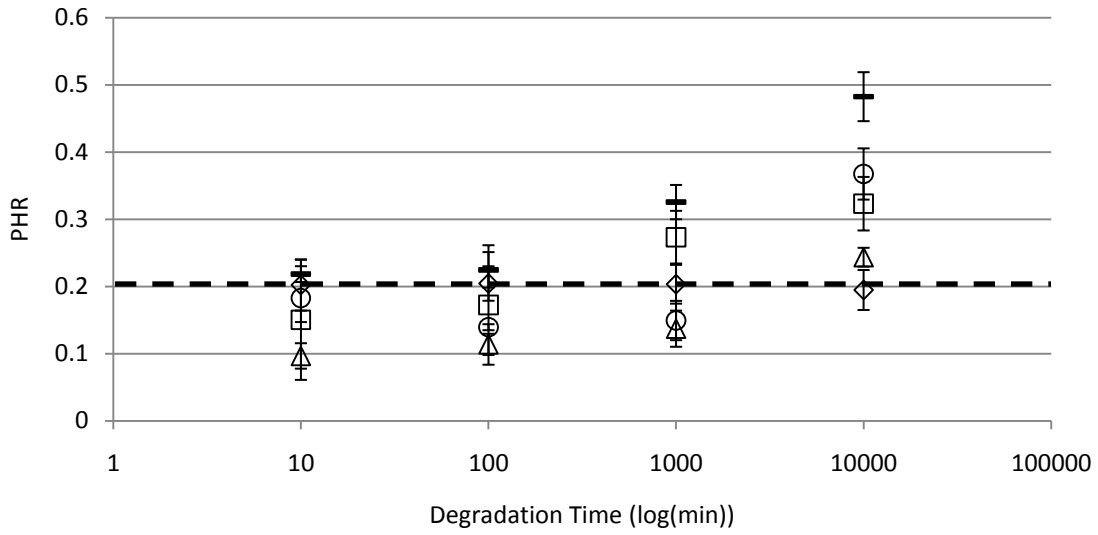

Figure 4.29: 1702 cm^{-1} carboxylic acid carbonyl, PHR change as a function of aging time for PTM (◇ air; □ DI water; △ pH 7; -- pH 9; ○ pH 11). Error bars represent 95% confidence intervals for 3 replicates. Dashed line represents neat material before compression molding.

4.4.3.4. Gel Permeation Chromatography (GPC)

PTM experienced significant decreases in Mw as a function of time of DI and pH 7, 9, and 11 with DI decreasing 800 Da in Mw, Figure 4.30. For no significant decrease in Mw and a significant decrease in 1749 cm^{-1} PHR for DI and pH 7, Figure 4.28, in the first 10 min to occur, low Mw material needs to diffuse out of PTM. If low Mw PTM was diffusing out of DI and pH 7, the PDI should have decrease, Figure 4.31, which does occur. By 100 min for DI and pH 7, there is a significant increase in PDI as the $A_{AC}2$ and $A_{AL}1$ mechanisms degrade ester bonds and decrease 1749 cm^{-1} PHR, Figure 4.26, with a lack of degradation product diffusion out of the samples. At 1,000 and 10,000 min for DI and pH 7, the solid phase Mw significantly decreases from ~2100 to less than 1800 Da and 1400 Da, respectively. The decrease in Mw is accompanied by significant decreases in dry weight and 1749 cm^{-1} PHR for DI and pH 7 as degradation of the bulk material occur. The DI and pH 7's PDI decrease at 1,000 and 10,000 min as diffusion is able to remove degradation products and decrease the PDI. The GPC system is

only calibrated down to a Mw of 240 (approximately 3 polymer repeat units), which cuts off any Mw below this point making for a artificially low PDI. pH 11 and pH 9 have no significant changes in dry weight, 1749 cm^{-1}, or Mw during the first 100 min, Figures 4.28 and 4.39. The PDI initially decrease from the control, Air, during the first 10 min as low Mw material diffuses out of the material, and at 100 min, the PDI increases by ~0.1 degradation does occur without significant impact on any other parameter, Figure 4.31. Starting at 1,000 min, the Mw for each sample becomes distinct from any other sample for the solid phase, Figure 4.30. It becomes apparent at 1,000 min that the ester hydrolysis is preceding at different rates based on the initial pH of the solutions as the change in 1749 cm^{-1} PHR and Mw are decreasing uniquely for each condition. All solution become acidic in the initial 10 min as low Mw material diffuses into the solution, and the acidic solution facilitates the acid catalyzed ester hydrolyses through the $A_{AC}2$ and $A_{AL}1$ mechanisms. The pH 11 and pH 9 transition from a base mediated ester hydrolyses medium to an acid catalyzed ester hydrolyses medium as the pH shifts from a basic solution to an acidic solution. Even though the solution switches from a basic to an acid medium, the concentration of K^+ ions does not change. The K^+ ion will stabilize the carboxylate anions and hinder the carbonyl carbon protonation in the $A_{AC}2$ and $A_{AL}1$ mechanisms. pH 11, with the highest concentration of K^+ ions, only has a Mw decrease of 200 Da and compared to DI decrease of 800 Da at relatively the same final pH, the K^+ ions are significantly impacting the $A_{AC}2$ and $A_{AL}1$ mechanisms during acid catalyzed ester hydrolyses. The pH 11 PDI increases over the aging time and pH 9 PDI does not change from 100 to 10,000 min with a significant decrease in Mw. For pH 11, ester hydrolyses is occurring and producing degradation products that are too large to diffuse out leading to an increasing in PDI with a decreasing Mw from 10 to 10,000 min. pH 9 maintains a constant PDI with a decreasing Mw and dry weight, Figure 4.19, from 100 to 1,000 min. pH 9 has ester hydrolyses as shown by the decreasing Mw and 1749 cm^{-1} PHR,

and considering the constant PDI and decreasing dry weight together, pH 9 degradation products are diffusing out of PTM at a rate that causes the PDI to be maintained as pH 9 decreases in Mw. Two major factors are affecting PTM's Mw and PDI during degradation, concentration of K^+ ions and diffusion of low Mw material into solution, which was characterized by GPC.

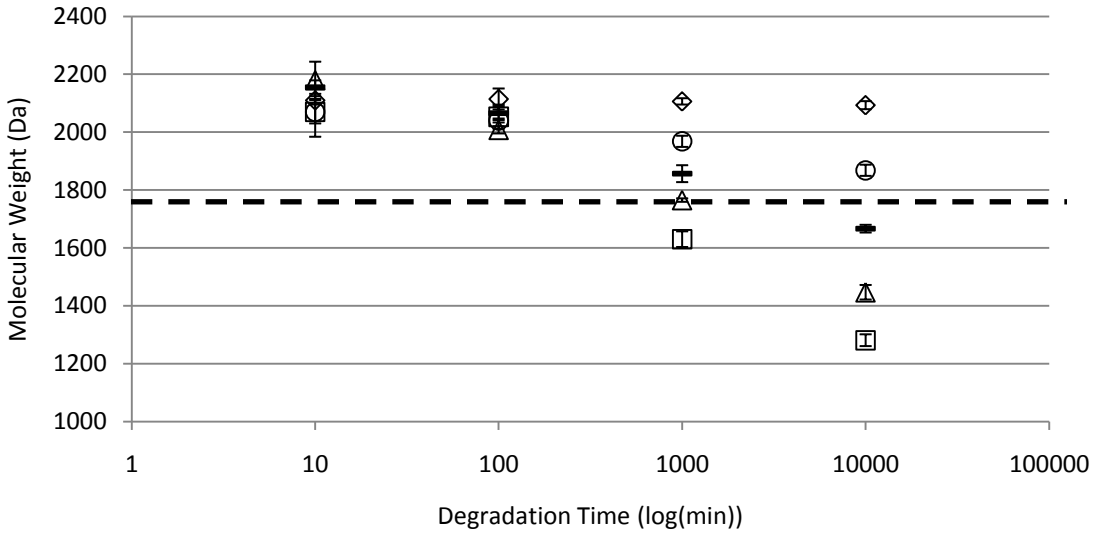

Figure 4.30: Degraded solid phase Mw as a function of aging time for PTM (◇: air; □: DI water; △: pH 7; ╍: pH 9; ○: pH 11). Error bars represent 95% confidence intervals for 3 replicates. Dashed line represents neat material before compression molding.

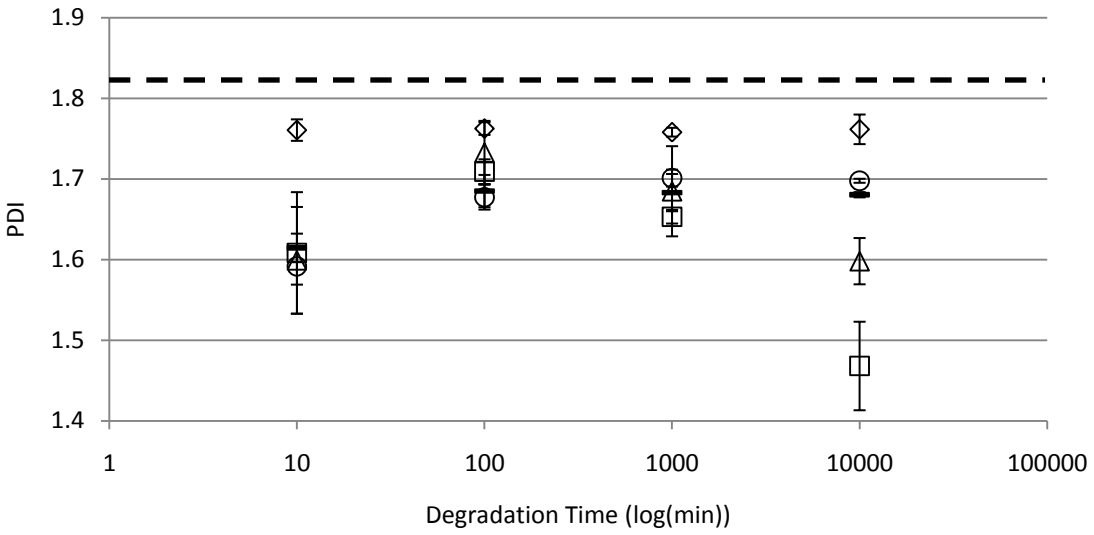

Figure 4.31: Low Mw solid phase PDI as a function of aging time for PTI (◇ air; □ DI water; △ pH 7; ⋯ pH 9; ○ pH 11). Error bars represent 95% confidence intervals for 3 replicates. Dashed line represents neat material before compression molding.

PTM dissolved in solution hydrolytically degraded under acidic conditions following the $A_{AC}2$ and $A_{AL}1$ mechanisms for all solutions leading to a decrease in Mw, Figure 4.32. All solutions became acidic with in the first 10 min as PTM dissolved into solution, Figure 4.24. The $B_{AC}2$ mechanism for pH 11 and pH 9 samples could be still active, though under acidic conditions it would have minor impact, because of the presence of K^+ ions present. The $A_{AC}2$ and $A_{AL}1$ are the dominant mechanisms in solution as there is an excess of water to drive the reactions to completion. In solution, PTM appears to be readily degradable regardless the initial conditions. DI exhibited the greatest degree of degradation in solution with a Mw decrease of ~400 Da, Figure 4.32. The change in Mw cannot be completely attributed to degradation in solution. DI loss ~36 wt.% of its dry weight during degradation from 1,000 to 10,000 min, Figure 4.21, DI solid degradation and degradation products diffusion into solution influenced the solution Mw. The DI solid would be diffusing material of various Mw that could have a positive or negative

effect on the solutions' Mw. Whether it is a positive or negative effect cannot be answered with the data present for DI or any other sample.

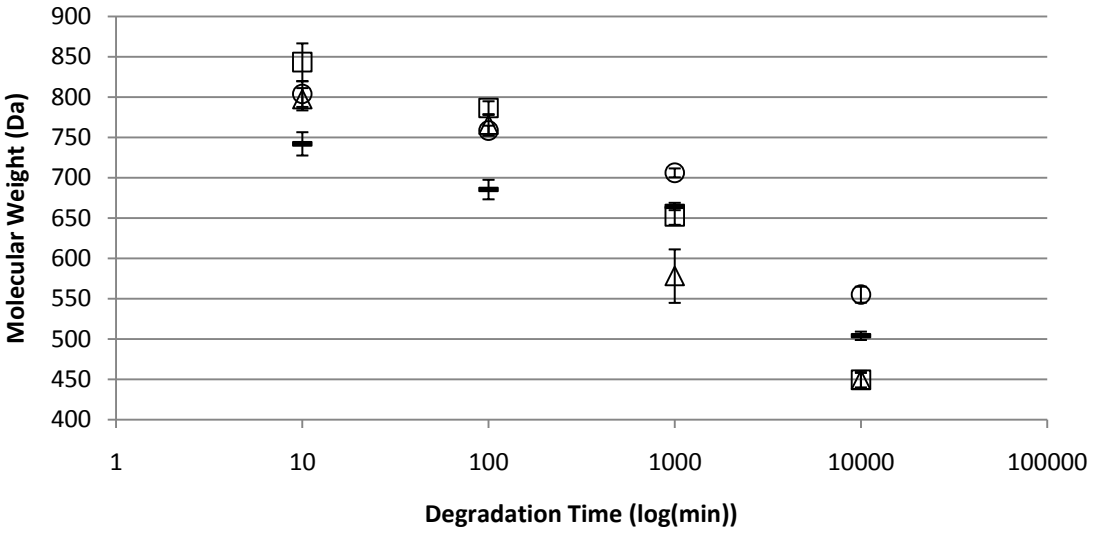

Figure 4.32: Aqueous phase Mw as a function of aging time for PTM (◇ air; □ DI water; △ pH 7; -- pH 9; ○ pH 11). Error bars represent 95% confidence intervals for 3 replicates. Dashed line represents neat material before compression molding.

PDI of the solutions (Figure 4.33) does give insight into whether solid degradation and subsequent diffusion is having a positive or negative impact on the solutions' Mw. For DI, the degradation product diffusion is causing parabolic trend in PDI, Figure 4.33. DI PDI initially decreases, ~0.15, from 10 to 100 min and then plateaus from 100 to 10,000 min. For the higher PDI to be maintained by DI at 10,000 min, while all others samples decrease, the DI solid is diffusing higher Mw material into solution. For all other samples, the weight loss is less than DI, reducing diffusion, and that allows the $A_{AC}2$, $A_{AL}1$, and $B_{AC}2$ mechanisms to drive the degradation to completion and reduce the PDI.

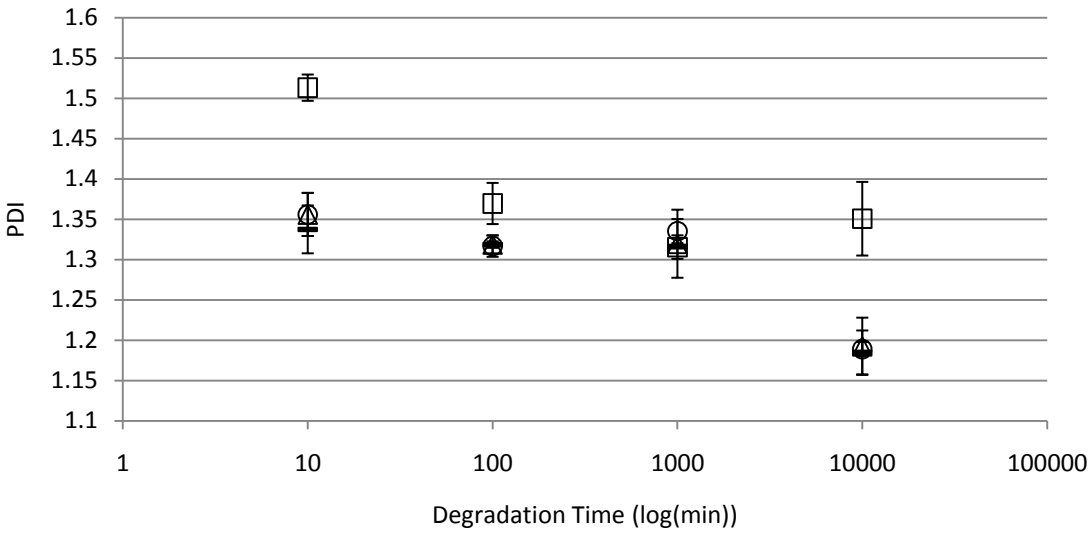

Figure 4.33: Aqueous phase PDI as a function of aging time for PTM (◇ air; □ DI water; △ pH 7; -- pH 9; ○ pH 11). Error bars represent 95% confidence intervals for 3 replicates. Dashed line represents neat material before compression molding.

4.4.4. Conclusion

Hydrolytic degradation of PTM does take place over a varied range of pHs. PTM in DI water has the highest degradation rate in solid state as it only follows the $A_{AC}2$ and $A_{AL}1$ mechanisms and has no K^+ ions to inhibit protonation of carbonyls or to stabilize carboxylate anions. The diffusion of PTM into DI water masks the PTM degradation in the aqueous phase. PTM in KOH pH adjusted solutions have reduced degradation in solid state due to stabilization of carboxylate anions by K^+ ions. In aqueous solution, the $A_{AC}2$, $A_{AL}1$, and $B_{AC}2$ mechanisms drive the degradation and significantly reduce the Mw of solubilized PTI.

4.5. Conclusions

PTM degradation products diffusion and low Mw PTM diffusion are the major driving forces to the reduction in PTM weight over all pH. A non-stagnant fluid system has degradation products removed shifting the $A_{AC}2$ and $A_{AL}1$ equilibrium and increasing the PTM concentration

gradient to increase ester hydrolysis and drive the low Mw material out of the solids leading to an increased degradation rate. The addition of K^+ ions and lower concentration gradient between solid and fluid for stagnant fluid, decreases ester hydrolysis of PTM. With increasing K^+ ion concentration, PTM degradation is inhibited in the solid and solution. With larger samples from the initial study, PTM showed it was susceptible to auto-catalysis by the formation of shell like structures during longer aging times. PTM is a hydrolytically degradable polymer that can have 50 wt.% loss in 1 week in a driven system or more than a week in a non-driven system. In a non-driven system, PTM has increasing degradation with increasing pH, but pH dependence is not apparent in a driven system.

4.6. Recommended Future Work

The effects of ionic concentration and type of salt used during hydrolytic degradation needs to be examined. Thermal analysis needs to be utilized to monitor change in thermal properties and to give further insight into the degradation mechanism. Hydrolytic degradation under elevated temperatures and the use of shorter time periods need to be examined. To prove that PTM is completely renewable, a biological degradation experimental study needs to be undertaken.

4.7. References

Albertsson, A.-C., Varma, I. K., "Aliphatic Polyesters: Synthesis, Properties and Applications," Advances in Polymer Science, 157, 1-40, 2002.

Alexis, F., Venkatraman, S., Rath, S. K., Gan L.-H., "Some Insight into Hydrolytic Scission Mechanisms in Bioerodible Polyesters," Journal of Applied Polymer Science, 102, 3111-3117, 2006.

Alvarez, V. A., Ruseckaite, R. A., Vazquez, A., "Degradation of Sisal Fibre/Mater Bi-Y Biocomposites Buried in Soil," Polymer Degradation and Stability, 91, 3156-3162, 2006.

Bordes, P., Hablot, E., Pollet, E., Averous, L., "Effect of Clay Organomodifiers on Degradation of Polyhydroxyalkanoates," Polymer Degradation and Stability, 94, 789-796, 2009.

Catiker, E., Gumusderelioglu, M., Guner, A., "Degradation of PLA, PLGA homo- and Copolymers in the Presence of Serum Albumin: A Spectroscopic Investigation," Polymer International, 49, 728-734, 2000.

Chiellini, E. Cinelli, P., Chiellini, F. Iman S. H., "Environmentally Degradable Bio-Based Polymeric Blends and Composites," Macromolecular Bioscience, 4, 218-231, 2004.

Chu, C. C., "Hydrolytic Degradation of Polyglycolic Acid: Tensile Strength and Crystallinity Study," Journal of Applied Polymer Science, 26, 1727-1734, 1981.

Dean, J. A., Lange's Handbook of Chemistry, 14th ed., McGraw-Hill, Inc., 7.42-7.71, 1992.

Dell'Erba, R., Martuscelli, E., Musto, P., Ragosta, G., "Unsaturated Polyester Resins: a Study of the Mechanism and kinetics of the Curing Process by FTIR Spectroscopy," Polymer Networks and Blends, 7(1), 1-11, 1997.

El-Hadi, A., Schnabel, R., Straube, E., Muller, G., Henning, S., "Correlation between degree of Crystallinity, Morphology, Glass Temperature, Mechanical Properies and Biodegradaiton of Poly(3-hydroxyalkanoate) PHAs and their Blends," Polymer Testing, 21, 665-674, 2002.

Erdmann, L., Uhrich, K. E., "Synthesis and Degradation Characteristics of Salicylic Acid-Derived Poly(anhydride-esters)," Biomaterials, 21, 1941-1946, 2000.

Gopferich, A., “Mechanisms of Polymer Degradation and Erosion,” Biomaterials, 17, 103-114, 1996Gopferich, A., Tessmar, J., “Polyanhydride Degradation and Erosion,” Advanced Drug Delivery Review, 54, 911-931, 2002.

Gouin, S., Zhu, X. X., Lehnert, S., “New Polyanhydrides made from a Bile Acid Dimer and Sebacic Acid: Synthesis, Characterization, and Degradation,” Macromolecules, 33, 5379-5383, 2000.

Gulmine, J. V., Akcelrud, L., “FTIR Characterization of Aged XLPE,” Polymer Testing, 25, 932-942, 2006.

Harrison, G. M., Melik, D. H., “Application of Degradation Kinetics to the Rheology of Poly(hydroxyalkanoates),” Journal of Applied Polymer Science, 102, 1794-1802, 2006.

Helminen, A. O., Korhonene, H., Seppala, J. V., “Crosslinked Poly(ester anhydride)s based on Poly(ε-caprolactone) and Polylactide Oligomers,” Journal of Polymer Science: Part A: Polymer Chemistry, 41, 3788-3797, 2003.

Hofmann, D., Entrialgo-Castano, M., Kratz, K., Lendlein, A., “Knowledge-Based Approach towards Hydrolytic Degradation of Polymer-Based Biomaterials,” Advanced Materials, 21, 3237-3245, 2009.

Hoglund, A., Odelius, K., Hakkarainen, M., Albertsson, A.-C., “Controllable Degradation Product Migration from Cross-Linked Biomedical Polyester-Ethers through Predetermined Alterations in Copolymer Composition,” Biomacromolecules, 8, 2025-2032, 2007.

Li, S., “Degradation of Biodegradable Aliphatic Polyesters,” in Scaffolding in Tissue Engineering, CRC Press, Boca Raton, FL, 335-352., 2006.

Nagata, M., Kiyotsukuri, T., Ibuki, H., Tsutsumi, N., Sakai, W., “Synthesis and Enzymatic Degradation of Regular Network Aliphatic Polymesters,” Reactive & Functional Polymers, 20, 165-171, 1996.

Neffe, A. T., hanh, B. D., Steuer, S., Lendlein, A., “Polymer Networks Combining Controlled Drug Release, Biodegradation, and Shape Memory Capability,” Advanced Materials, 21, 3394-3398, 2009.

Nostrum, C. F. v., Veldhuis, T. F. J., Bos, G. W., Hennink, W. E., “Hydrolytic Degradation of Oligo(Lactic Acid): A Kinetic and Mechanistic Study,” Polymer, 45, 6779-6787, 2004.

Okada, M., Okada, Y., Tao, A., Aoi, K., “Biodegradable Polymers Based on Renewable Resources: Polyesters Composed of 1,4:3,6-Dianhydroheitol and Aliphatic Dicarboxylic Acid Units,” Journal of Applied Polymer Science, 62, 2257-2265, 1996.

Qiu, L. Y., Zhu, K. J., “Design of a Core-Shelled Polymer Cylinder for Potential Programmable Drug Delivery,” International Journal of Pharmaceutics, 219, 151-160, 2001.

Quynh, T. M., Mitomo, H., Yoneyama, M., Hien, N. Q., "Properties of Ratiation-Induced Crosslinking Sterocomplexes Derived from Poly(L-Lactide) and Different Poly(D-Lactide)," Polymer Engineering and Science, 970-976, 2009.

Saha, S. K., Tsuji, H., "Effects of Molecular Weight and Small Amounts of D-Lactide Units on Hydrolytic Degradation of Poly(L-Lactic Acid)s," Polymer Degradation and Stability, 91, 1665-1673. 2006.

Satchell, D. P. N., Satchell, R. S., "Mechanistic Aspects. Recent Developments Concerning Mechanisms of Acylation by Carboxylic Acid Derivatives," in Supplement B: The Chemistry of Acid Derivatives, Vol. 2, Johy Wiley & Sons, Ltd., Hoboken, New Jersey, 747-802, 1992.

Saunders, J. H., Dobinson, F., "The Kinetics of Polycondensation Reactions," in Comprehensive Chemical Kinetics, Vol. 15, Bamford, C. H., Tippers, C. F. H., American Elsevier, New York, 473-581, 1976.

Scherer, T. M., Rothermich, M. M., Quinteros, R., Poch, M. T., Lenz, R. W., Goodwin, S., "Broad-Based Screening of Polymer Biodegradability," in Polymers from Renewable Resources, American Chemical Society, Washington D. C., 254-280, 2001.

Shirahase, T., Komatsu, Y., Tominaga, Y., Asai, S., Sumita, M., "Miscibility and Hydrolytic Degradation in Alkaline Solution of Poly(L-Lactide) and Poly(Methyl Methacrylate) blends," Polymer, 47, 4829-4844, 2006.

Silverstein, R. M., Blassler, G., C., Morrill, T. C., Spectrometric Identification of Organic Compounds, 5th ed., John Wiley & Sons, Inc., , Hoboken, NJ, 102-133, 1991.

Smith, M., March, J., "Aliphatic Substitution: Nucleophilic and Organometallic," March's Advanced Organic Chemistry, 6th ed., Wiley-Interscience, Hoboken, New Jersey, 425-656, 2007.

Sutton, d., Durand, R., Shuai, X., Gao, J., "Poly(D,L-Lactide-co-Glycolide)/Poly(Ethylenimine) Blend Matrix System for pH Sensitive Drug Delivery," Journal of Applied Polymer Science, 100, 89-96, 2006.

Tamada, J. A., Langer, R., "Erosion Kinetics of Hydrolytically Degradable Polymers," Proceedings of the National Academy of Science, 90, 552-556, 1993.

Vasanthan, N., Ly, O., "Effect of Microstructure on Hydrolytic Degradation Studies of Poly(L-Lactic Acid) by FTIR Spectroscopy and Differential Scanning Calorimetry," Polymer Degradation and Stability, 94, 1364-1372, 2009.

Vert, M., Li, S., Garreau, H., Mauduit, J., Boustta, M., Schwach, G., Engel, R., Coudane, J., "Complexity of the Hydrolytic Degradation of Aliphaic Polyesters," Die Angewandte Makromolekulare Chemie, 247, 239-253, 1997.

Zhou, Y., Wy, G.-L., Zhou, R.-X., Liu, Z.-L., “Synthesis and Properties of Novel Aliphatic Poly(Carbonate-Esters)s,” European Polymer Journal, 45, 1868-1872, 2009.

Zou, H., Yi, C., Wang, L., Liu, H., Zu, W., “Thermal Degradation of Poly(Lactic Acid) Measured by Thermogravimetry Couple to Fourier Transform Infrared Spectroscopy,” Journal of Thermal Analytical Calorimetry, 97, 929-935, 2009.

CHAPTER 5

POLY(TRIMETHYLENE ITACONATE) HYDROLYTIC DEGRADATION WITH VARIABLE PH

5.1. Abstract

To reduce our impact on the environment using renewable polymers with green chemistry, poly(trimethylene itaconate) was hydrolytically degraded under variable pHs and aging times at 25 °C. An initial solubility test was performed to determine itaconic acid (IA) and 1,3-propanediol (PDO) solubility and interaction with DaI water and phosphate buffer solutions (PBSs). PDO interacted with PBS, and PBS was determined to be not to be usable during this study due to the interaction. PTI was placed in DI water, pH 7, 9, and 11 KOH adjusted DI water, and a control with no fluid for 100 to 10,000 min. Weight change was monitored as a function of aging time to determine if degradation was taking place and if the PTI degradation products were water soluble by a monitoring for reduction in weight. Weight loss varied from 7 to 21 wt.% as a function of aging time and initial pH. To monitor changes in chemical structure, Diffused reflectance infrared Fourier transform (DRIFT) spectroscopy was used to analyize samples from various pH solutions and aging times, and it was determined that PTI in DI water had the greatest ester hydrolysis by the reduction in the ester carbonyl from 100 to 10,000 min. Gel-permeation chromatography (GPC) was used to determine molecular weight and polydispersity index. A bi-modal molecular weight distribution was found, and it was dependent on both aging time and pH. PTI in pH 11 solution maintained the highest molecular weight over 100 to 10,000 min aging time. Differential scanning calorimetry found that the cold

crystalliztion energy reduced by as much as 50 J/g as a function temperature. The addition of K^+ ion reduced ester hydrolysis, and pH 11 solution had the highest concentration of K^+ ions and experienced the least degradation throughout the study.

5.2. Introduction

There are several types of hydrolytically degradable polymers, poly(anhydrides), poly(orthoesters), poly(depsipeptides), poly(ether esters), and poly(esters) that are currently being researched as replacements for non-hydrolytically degradable petroleum-based polymers [Neffe 2010]. Poly(esters) have shown the most promise for commercialization and replacement of petroleum-based polymers with the development of poly(lactic acid) (PLA), poly(glycolic acid) (PGA), and poly(ε-caprolactone) (PCL). In the 1960s and 1970s, PGA was the first bio-compatible and hydrolytically degradable synthetic polymers and was commercialized as dissolvable suture material [Chu 1982]. This advance spurred research into other bio-compatible polymers and into other applications for these polymers. However, performance issues encountered with PLA and PGA are poor thermal stability and brittleness [Quynh 2009, Shirahase 2006]. To overcome the thermal and mechanical short comings of PLA, PGA, and PCL, polymeric blends and copolymers of PLA, PGA, and PCL with one another and with other polymers are used to modulate the properties have had varying degrees of success [Catiker 2000, Hill 2006, Neffe 2010, Hoglund 2007, Oyama 2009, Quynh 2009]. In past 10 years, interest has increased in bio-based polymer materials -- either naturally occurring or synthetic -- and their methods of degradation with 14 fold increase in publications since 2000.

A novel branched/cross-linked, unsaturated polyester was made by the copolymerization of itaconic acid (IA) and 1,3-propanediol (PDO) to make poly(trimethylene itaconate) (PTI). The polymer backbone of PTI contains ester bonds that are susceptible to

hydrolysis, but the specific factors that may influence PTI degradation are unknown. In general, molecular weight (Mw) and crystallinity have been shown to have the largest impact on polyester degradation. With increasing crystallinity and Mw, the rate of PLA degradation decreases due to a hindrance in water being able to diffuse into the matrix; therefore, water is not in proximity to the polymer backbone and so hydrolysis is hindered [Saha 2006, Quynh 2009, Shirahase 2006, El-Hadi 2002, Nostrum 2004]. Excess water forces ester hydrolysis to break ester bonds in acidic conditions that are found in polyesters, such as PLA [Vasanthan 2009, Satchell 1992, Smith 2007, Bruckner 2002, Saunders 1976]. If the system is basic, the driving force for hydrolytic degradation changes to the formation of stable carboxylate anions [Vasanthan 2009, Satchell 1992, Smith 2007, Bruckner 2002, Saunders 1976]. Varying the solution pH in which aliphatic polyesters are laced can have a range of effects on degradation. Saha and Tsuji discussed the contradictory results for PLA degraded under different pH conditions [Saha 2006]. It is generally agreed that pH affects the rate of degradation of bioplastics [Vert 1997, Kajiyama 2004, Tomihata 2001, Vasanthan 2009, Shirahase 2006]. For polyesters like PLA and PGA, hydrolytic degradation is considered bulk degradation with two steps. The first step is the uptake of water into the polymer. The second step is the ester cleavage, and diffusion of low Mw products out of the polymer [Hofmann 2009, Li 1999, Hoglund 2007, Neffe 2010]. If the polymer is sufficiently large that degradation product diffusion is slow, the increased number of end groups leads to auto-catalyzation conditions in which the interior of the polymer degrades at a faster rate than the surface of the polymer [Li 1999]. A method that has been used to control the degradation rate by influencing the crystallization and water diffusion rate is polymer cross-linking [Saha 2006, Quynh 2009, Shirahase 2006, El-Hadi 2002, Nostrum 2004]. There are two primary effects from the cross-linking of polymers: (1) cross-linking reduces crystallinity making the polymer more susceptible

to water diffusion; (2) cross-linking reduces the permeability of water in the polymer by reducing polymer movement and the path-ways for water to diffuse through [Quynh 2009, Hoglund 2007, Neffe 2009, Neffe 2010]. By controlling the Mw, crystallinity, and cross-link density, the degradation rate of a hydrolytically degradable polymer can be controlled.

PTI is a partially crystalline, unsaturated, branched/cross-linked copolymer of PDO and IA with ester linkages in the backbone. The bi-modal Mw distribution will give insight into the Mw dependence of hydrolytic degradation in PTI. In addition, PTI's semi-crystalline structure will give insight into crystallinities affect on hydrolytic degradation rate. PTI was subjected to hydrolytic degradation over a range of pH conditions for up to 10,000 h. Gravimetric analysis, gel-permeation chromatography (GPC), Fourier transform infrared (FTIR) spectroscopy, thermal gravimetric analysis (TGA), and differential scanning calorimetry (DSC) was conducted on the PTI solids. For the degradation solution, pH and GPC analysis were performed.

5.3. Experimental Materials and Methods

Materials. The PTI sample used for the degradation study was bulk polymerized from 1,3-propanediol (PDO, 98%, Sigma Aldrich) and itaconic acid (IA, 99%, VWR) using AlCl3 catalyst (98%, Sigma Aldrich) with a 100: 1 monomer to catalyst ratio at 155 °C for 16 h. Additional detals on the PTI synthesis and characterization of the neat material is provided in Chapter 3. pH 2, 4, 7, 10, and 12 phosphate buffer solution were purchased from VWR. KOH (99%) and Optima tetrahydrofuran (+99.9%) were purchased from Fisher Scientific. All chemicals were used as received. It should be noted that PTI was produced with a bi-modal Mw distribution: 50,650 ± 2,953 Da (with 1.71 ± 0.17 PDI, DP 588.9 ± 1.4, 1.5 ± 0.2 wt.%) and 1,379 ± 9 Da (with 1.78 ± 0.05 PDI, DP 16.0 ± 0.1, 98.5 ± 0.2 wt.%).

PTI Grinding. PTI was ground by hand into a powder using a pestle and mortar until all particles could easily sift through 18 x 18 mesh stainless steel wire cloth. PTI samples before and after grinding were tested and there was no impact seen on the Mw or chemical structure from grinding. These results are presented in Appendix F.

pH Response to Monomer in DI water and pH 7 Phosphate Buffer Solution . Monomer solubility was examined using pH 7 phosphate buffer solution and DI water. Into a 16 mL vial, 1 g of 1,3-propanediol or itaconic acid was added along with 10 mL of solvent. The vials were allowed to sit without mixing for 3 days. After 3 days, the solution pH was measured and the IA fluid was vacuum filtered using Whitman 40 filter paper with a Buckner funnel to remove the insoluble material. The filter and solids were then dried in a vacuum oven (25 Torr) at room temperature for 24 h, and the final dry weight was measured. This dry weight was subtracted from the initial weight to determine the monomer solubility.

Polymer Hydrolysis Procedure. Hydrolysis was performed in DI water and in basic aqueous solutions formed by adjusting the pH of DI water (pH 5.4) to pH 7, 9, and 11 using a concentrated DI-KOH solution. DI water was chosen as a control, and pH 7, 9, and 11 were chosen based on a literature review that showed bioplastics had faster hydrolysis rates at basic pHs. For each sample, 0.75 g of PTI powder was placed into a 16 mL clear vial and 10 mL of the aqueous solution was added. One set of samples had no solution added as a control, referred to as 'air'. The sealed vials were then placed into a 25 °C water bath for 100, 1,000, or 10,000 min. All data was collected in triplicate for statistical analysis.

Characterization. At the end of the allotted degradation time, excess water was removed by gently blotting with a KimWipe® and the polymer samples were weighed. The difference in the wet weight and initial weight was divided by the initial weight to give the wet weight change. The samples were then vacuum dried (25 torr) at room temperature for 24 h

and weighed again. The difference between the dry weight and initial weight was divided by the original weight to give the dry weight change.

The solid polymer samples and degradation solutions were characterized by diffuse reflectance infrared Fourier transform spectroscopy (DRIFTS) using a Thermo Electron 6700 instrument with a He-Ne laser, liquid nitrogen-cooled MCT-A* detector, and EasyDiff accessory (Pike Technologies) at room temperature using a dry air purge. Samples were mixed with KBr powder at 5 wt.% PTI and 100% KBr was used for the sample spectra background. Peak height ratios (PHR) were used in the quantitative analysis of the FTIR spectra. In this study, PHR was calculated using the height of the peak corresponding to C-H scissoring of CH_2 at 1465 cm^{-1} as the denominator and the height of the peak of interest as the numerator to form a ratio. A Bruker AMX-300 NMR instrument was used to collect ^1H spectra at 300 MHz in deuterated chloroform. GPC data was collected with a Waters GPC with 4E and 5E (polystyrene-dinvinylbenzene, 4.6 x 300 mm) Styragel® columns, Optima THF as the effluent at 0.3 mL/min, and a ten-point polystyrene calibration. For the solid samples, 6 to 8 mg was weighed out and dissolved in X mL Optima THF for at least 4 h. These samples were then filtered through a 0.45 µm expanded PTFE syringe filter before being analyzed with GPC. The aqueous solutions remaining after the solid samples were removed were evaporated under vacuum (40 torr) at room temperature for seven days. If there were no visibly discernable solids evident after solvent evaporation, 2 mL of Optima THF was added. The solution was allowed to dissolve for at least 4 h and was then filtered with a 0.45 µm expanded PTFE syringe filter before being analyzed with GPC. If there were visible solids after solvent evaporation, the same GPC procedure as described above for the solid samples was followed. The solution pH was determined by Accumet Basic AB15 pH meter from Fisher Scientific using a 5 point calibration

with phosphate buffers of pH 2, 4, 7, 10, and 12 at the end of each degradation time after solid material was removed by filtration.

A TA Instruments Q-600 simultaneous DSC/TGA (SDT) and Q-2000 modulated DSC (mDSC) with a nitrogen purge was used for thermal analysis with the TA Universal Analysis 2000 software (v4.7A). SDT samples were analyzed from 25 to 400 °C at 5 °C/min under 50 mL/min of nitrogen. mDSC samples were analyzed from -90 to 250 °C under 50 mL/min of nitrogen with a ramp rate of 5 °C/min.

5.4. Results and Discussion

5.4.1. Monomer Solubility and pH

PDO was completely soluble in DI water and pH7 PBS at 75 mg/mL and IA was only partially soluble in both fluids. It was gravimetrically determined that IA was soluble at approximately 8 ± 1.2 mg/mL in both DI water and pH7 PBS by vacuum filtering the fluid, vacuum drying the solids for 24 h at 25 torr, and weighing the dried material. This measured solubility for IA is in line with literature values of 8 to 9.5% w/v solubility in aqueous solutions [Dean 1992]. The addition and (complete or partial) solubilization of PDO and IA changed the measured pH of the solutions, as is shown in Figure 5.1. The 8 mg/mL of solubilized IA reduced the pH of DI water from 5.4 to 2.4 and the pH 7 PBS was reduced from 7.0 to 3.0. The completely soluble PDO did not significantly reduce the pH of the DI water solution. With the pH 7 PBS solution, PDO significantly increased the pH from 7.0 to approximately 7.6. The unexpected interaction between PDO and the PBS indicated that PBS should not be used further in the study.

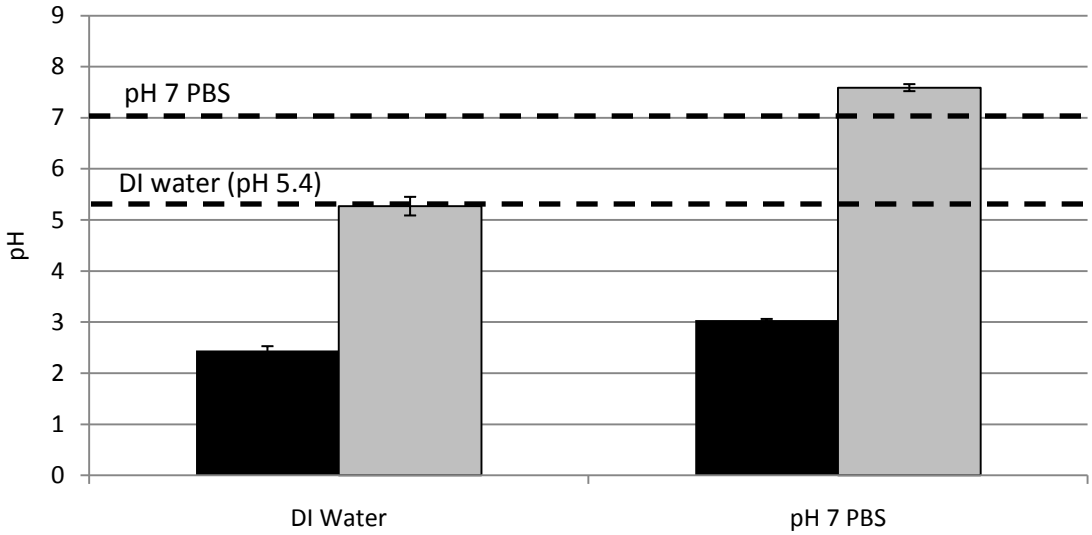

Figure 5.1: pH values for DI water and pH 7 PBS 72 h after the addition 1g of partially soluble IA (black columns) and completely soluble PDO (grey columns) was added to 10 mL of DI water. Each column represents the average pH for 3 samples with 95 % confidence interval error bars. Dashed lines indicaate the initial pH of the pH 7 PBS (pH 7, top dashed line) and DI water (pH 5.4, bottom dashed line).

5.4.2. Solution pH Analysis

The pHs of all solutions decreased as a function of time, and they approach an equilibrium value of pH 2.9 at 10,000 min, Figure 5.2 and 5.3. By 100 min, all solutions had become acidic, which will influence the degradation mechanisms present.

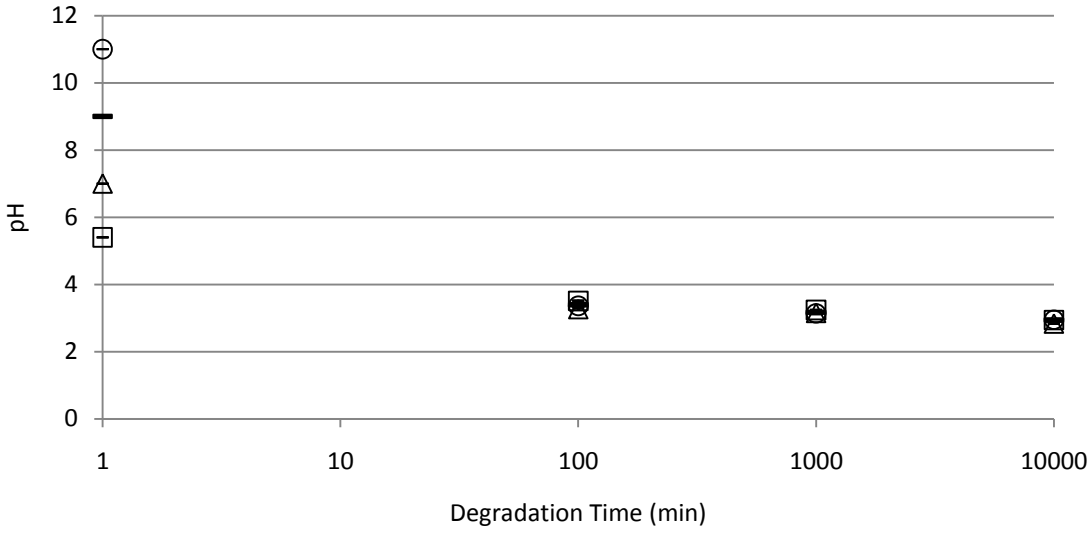

Figure 5.2: pH of solutions from PTI degradation experiment (0 to 10,000 min, 25 °C) for DI water and the pH 7, 9, and 11 KOH aqueous solutions (□ DI; △ pH 7; -- pH 9; ○ pH 11). Error bars represent 95% confidence intervals for 3 replicates.

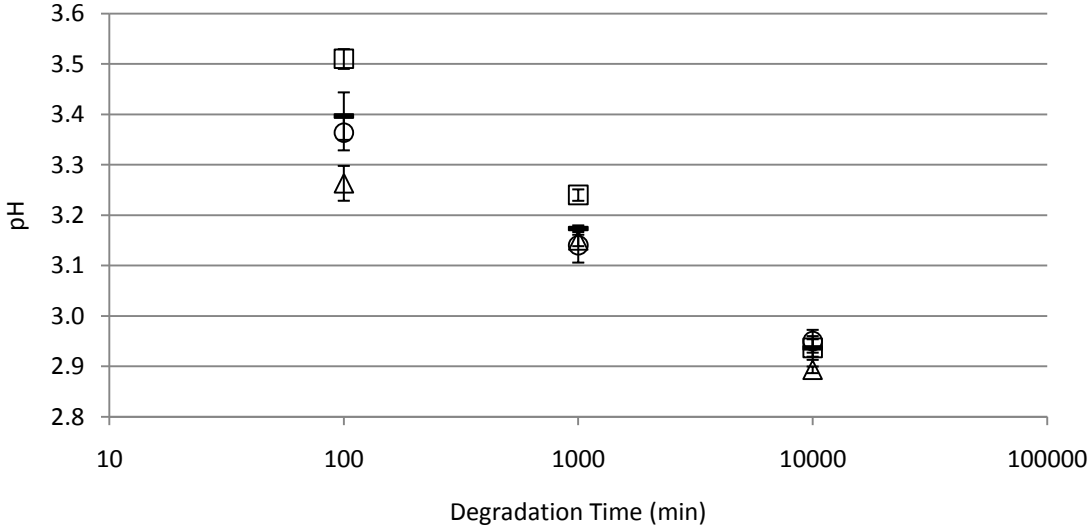

Figure 5.3: pH of solutions from PTI degradation experiment (0 to 10,000 min, 25 °C) for DI water and the pH 7, 9, and 11 KOH aqueous solutions (□ DI; △ pH 7; -- pH 9; ○ pH 11). Error bars represent 95% confidence intervals for 3 replicates.

5.4.3. Gravimetric Analysis

PTI was hydrolytically degraded in aqueous KOH solutions (pH 7, 9, and 11), DI water (pH 5.4), and an 'air' control (no liquid) at 25 °C for 100 to 10,000 min. Samples will be referred to by their initial conditions pH 7, 9, or 11, DI, or Air in discussing the results. The wet sample weights , over all times, showed only minimal deviations from the initial weights (Figure 5.4). At 10,000 min, the samples showing the most wet weight change were those degraded in pH 7 and pH 11 solutions and they had lost only ~0.15% of their initial weight. Since there is no reason to believe the procedure was flawed, there are two possible reasons for the lack of weight loss: (1) there is no mass loss and system is not degrading, and (2) the system is experiencing degradation and/or diffusion of degradation products out of the polymer with an equal influx of water replacing the lost polymer mass. Reason 1 is debunked by examining the dry weight loss data. As can be seen in Figure 5.5, there is over 20% weight loss of the dried material at 10,000 min for the DI water sample. In Figure 5.5, the dry weight loss percentage is plotted as a function of degradation time. Air did not vary 0% change from initial mass for 100 to 10,000 min. In the first 100 min, there is a significant reduction in dry weight of PTI by 1 to 3 wt.% for all samples, and the weight loss continued for all samples through 10,000 min. At 10,000 min, the samples in DI water and pH 11 had lost approximately 21% and 7%, respectively, of their initial mass. Reason 2 can reasonably explain the lack of weight loss in the wet samples and the differences (dramatic in some samples) between the wet and dry weight loss. We know that we have low Mw material in the PTI sample and that IA is partially soluble and PDO is completely soluble in aqueous solutions. Whether the mass loss in the dry samples is due to degradation and diffusion of the degradation products out of the sample or the simple diffusion of low Mw material will be discussed in the GPC section of the paper.

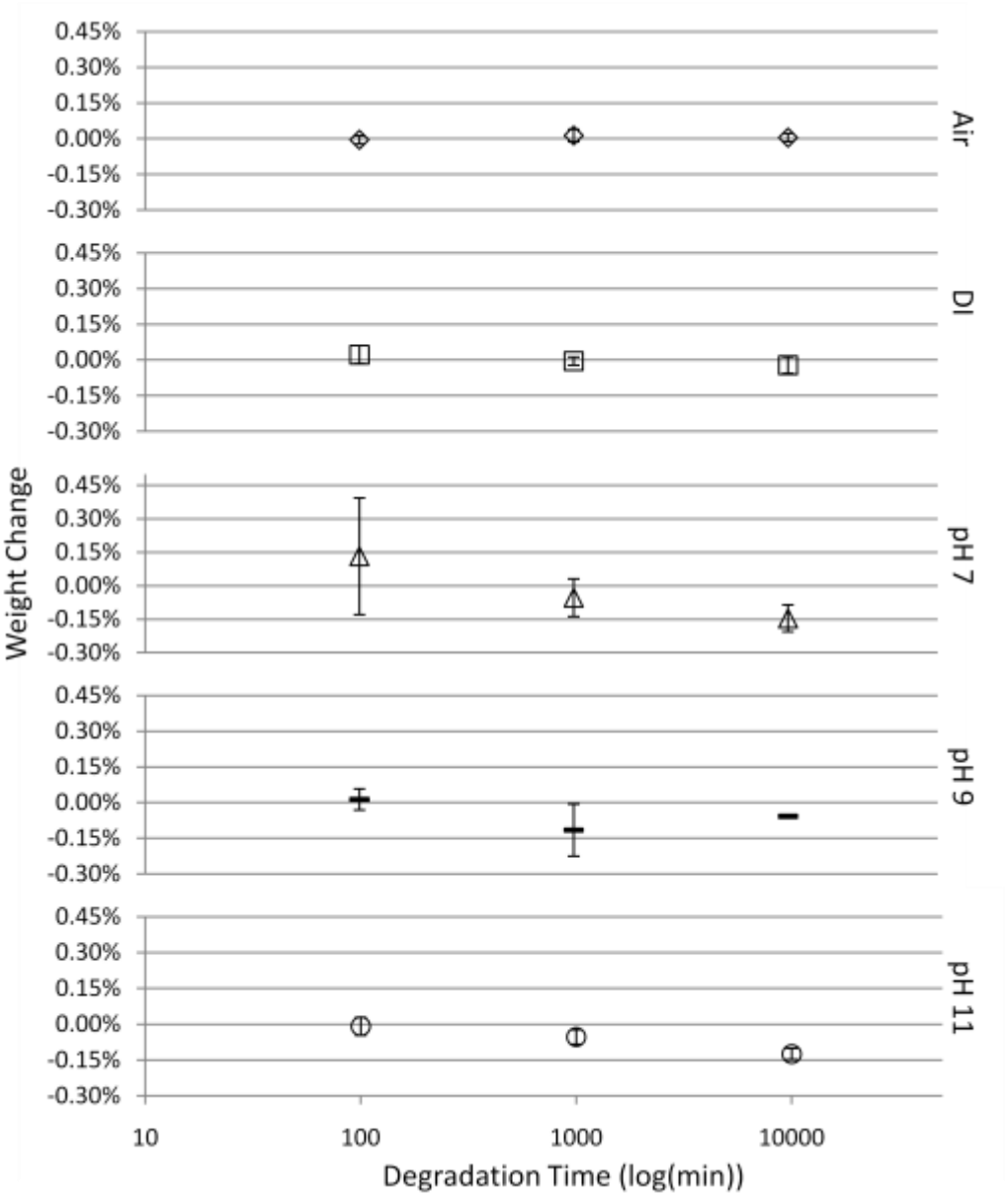

Figure 5.4: Percent weight change as a function of aging time for PTI when wet (◇: air; □ DI water; △ pH 7; -- pH 9; ○ pH 11). Error bars represent 95% confidence intervals for 3 replicates.

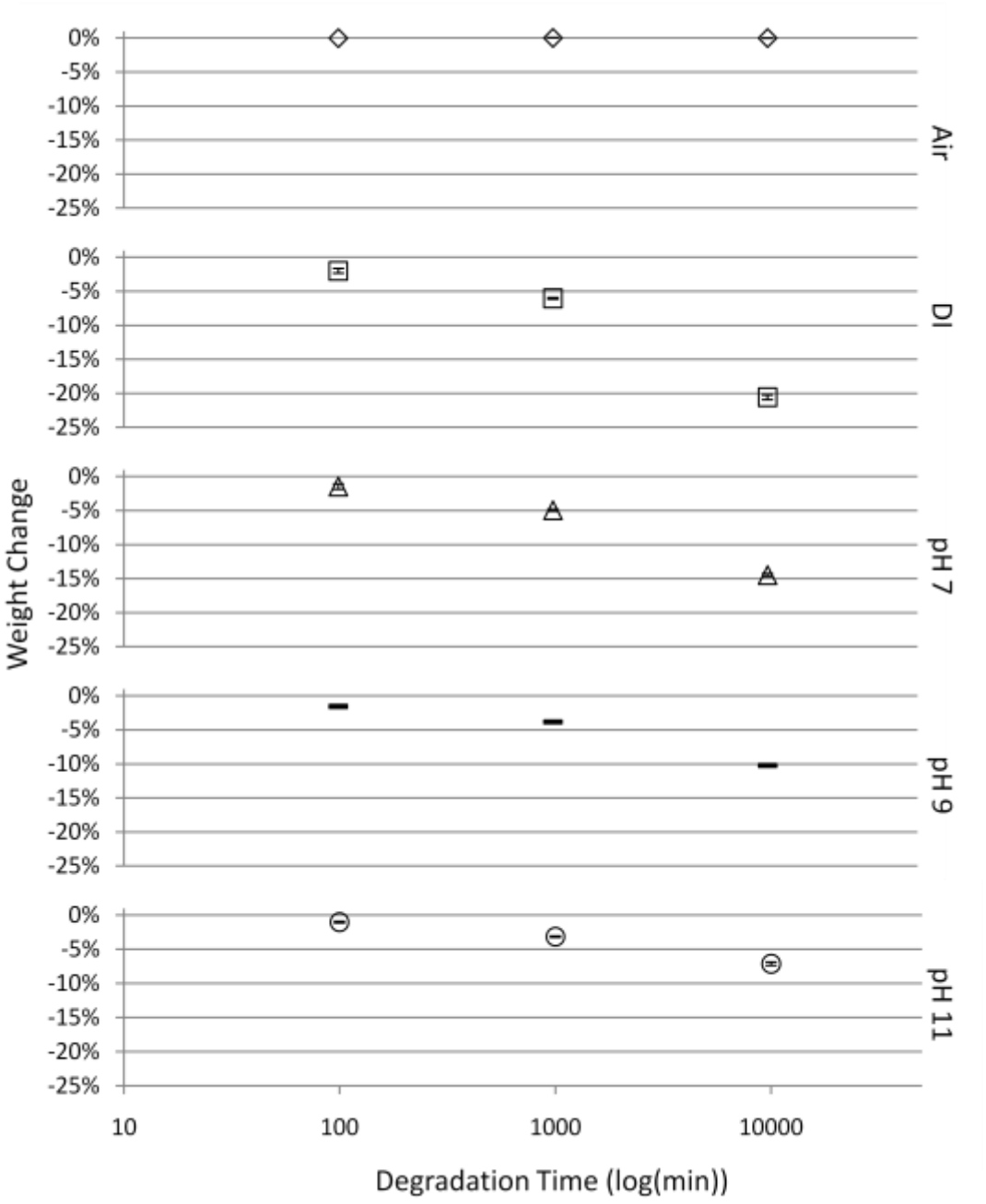

Figure 5.5: Percent weight change as a function of aging time for PTI after drying in air (◇ air; □ DI water; △ pH 7; ⎓ pH 9; ○ pH 11). Error bars represent 95% confidence intervals for 3 replicates.

There is a correlation between starting pH and final weight loss that can be explained considering whether the hydrolysis is base-mediated or acid-catalyzed. Acid-catalyzed ester hydrolyses predominately follow the $A_{AC}2$ and $A_{AL}1$ mechanisms with the $A_{AC}2$ mechanism being the dominate mechanism of the two and complete hydrolysis will occur with an excess of water (Figure 5.4a,b). In the base-mediated ester hydrolyses, the $B_{AC}2$ mechanism is the dominate mechanism that requires a basic aqueous solution (Figure 5.4c). The $A_{AC}1$ and $A_{AL}2$ mechanisms do exist, but they are rarely observed and are considered to be have only minor impacts on ester hydrolysis. Therefore, the $A_{AC}1$ and $A_{AL}2$ mechanisms will not be discussed further in reference to PTI degradation. Similarly, the $B_{AC}1$, $B_{AL}1$, and $B_{AL}2$ reaction mechanism do exist but are considered to be minor contributors to ester hydrolysis. So they will not be discussed further. The pH 11 and pH 9 samples were expected to follow with $B_{AC}2$ mechanism initially (Figure 5.4c) and then change to the $A_{AC}2$ and $A_{AL}1$ mechanisms as the aqueous solution became more acidic due to the presence of degradation products with acid end groups. It was unknown which mechanisms would drive degradation in the pH 7 solution. For DI water (pH 5.4), degradation was expected to be driven by the $A_{AC}2$ and $A_{AL}1$ mechanisms.

(a)

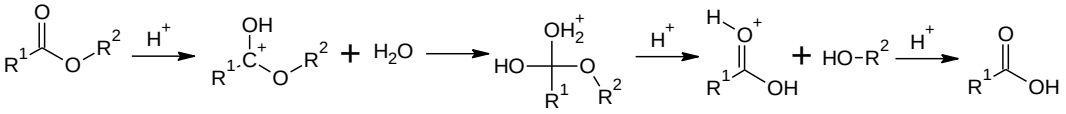

(b)

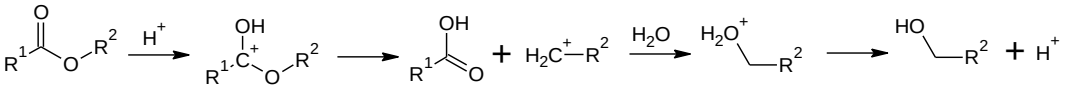

(c)

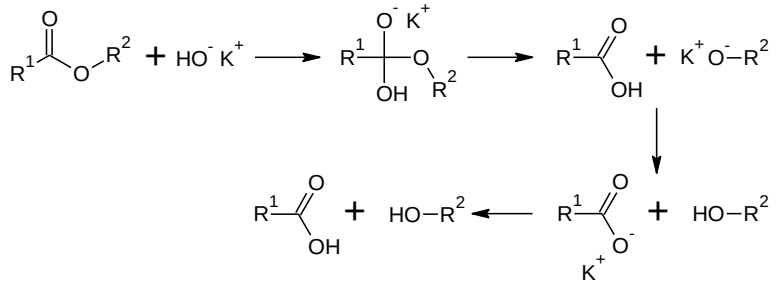

Figure 5.6: Ester hydrolysis reaction mechanisms: (a) $A_{AC}2$, (b) $A_{AL}1$, and (c) $B_{AC}2$.

The basic solutions, pH 11 and pH 9, had the least weight loss at approximately 7 wt.% and 10 wt.%, respectively (Figure 5.4). In contrast, the solution with the lowest pH (DI water, initial pH 5.4) had the largest weight loss at ~21 wt.%. pH 11 and pH 9 converted from based mediated ester hydrolysis to acid catalyzed hydrolysis in the first 100 min of aging, but could not obtain the same weight loss of DI water (21 wt.%). This may be impacted by the presence of K^+ ions in the pH 9 and pH 11 solutions that can produce stable carboxylate anions upon ester cleavage (instead of the carboxylate acid) that would compete with the $A_{AC}2$ and $A_{AL}1$ mechanisms of degradation through interference with the protonation of the carbonyl. Therefore, the system is prevented from becoming auto-catalytic through the production of acid

from the initial degradation. Since degradation is inhibited, less material is lost from the samples and this is indeed the trend seen in the dry weight loss data.

The change in dry weight appears minimal in the initial 100 h; however, when the dry weight change data is examined along with the weight change rate (Figure 5.7), the initial 100 min there is a 1 to 3 wt.% dry weight reduction that corresponds to a weight change rate of between 0.02 and 0.06 mg/min. The rate of weight loss decreased as a function of degradation time and is approaching zero at 10,000 min. If the system was autocatalytic, the rate of degradation would have increased as a function of time. There was no acceleration of degradation rate over time, and PTI is not affected by autocatalytic hydrolysis as the number of end groups present in the polymer increase with degradation.

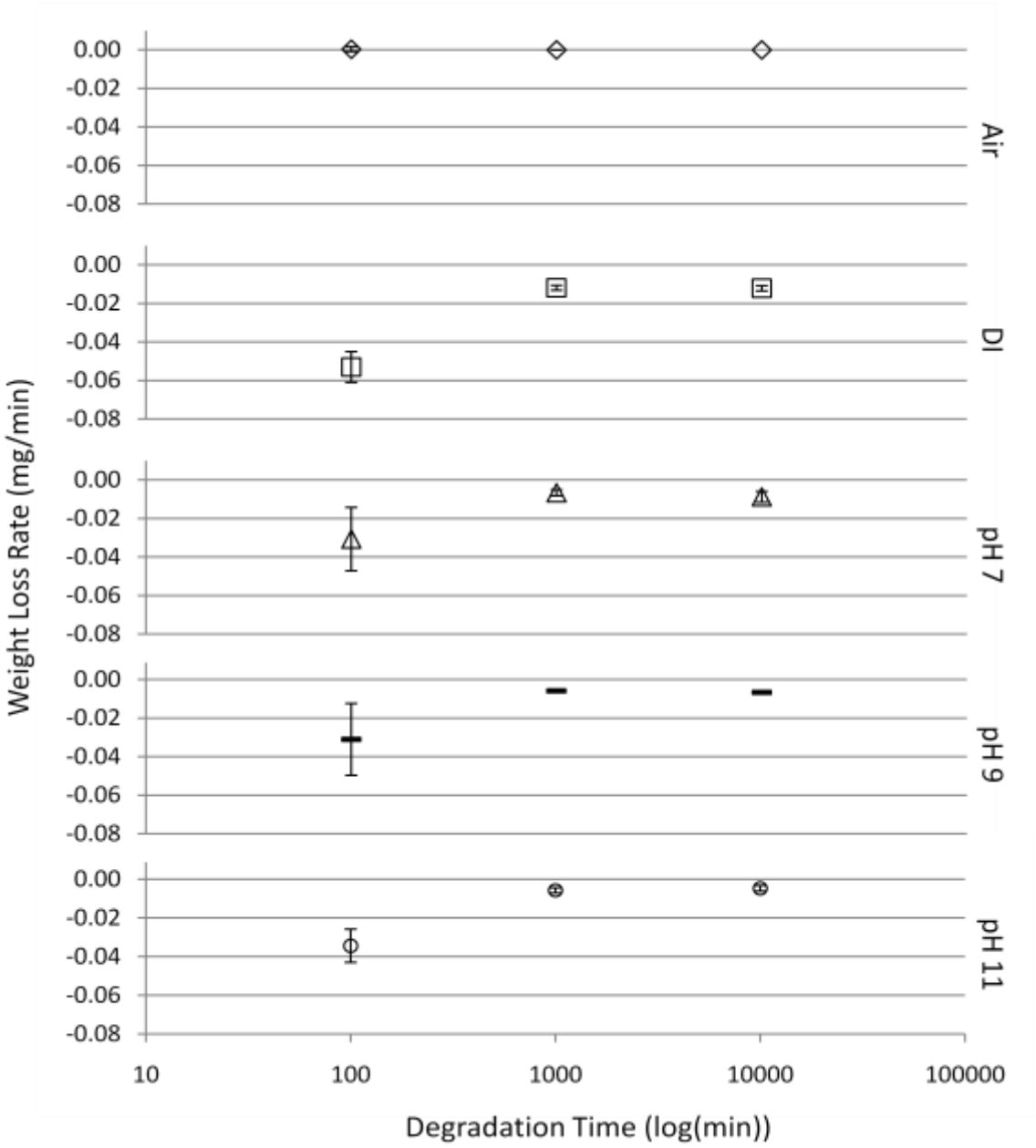

Figure 5.7: Weight loss rate as a function of aging time for PTI (◇ air; □ DI water; △ pH 7; -- pH 9; ○ pH 11). Error bars represent 95% confidence intervals for 3 replicates.

5.4.4. Diffused Reflectance Infrared Fourier Transform Spectroscopy

DRIFT was performed on one sample from each degradation time / solution combination. A representative PTI DRIFT spectrum can be seen in Figure 5.8. The area of interest is the carbonyl stretch region from 1900 to 1500 cm^{-1}. Changes in carbonyl peak location and size qualitatively indicates the formation of carboxylic acid and the ester degradation. PHRs of ester carbonyl were calculated to quantitatively show functional group conversion. Before PHRs could be calculated, the carbonyl peaks had to be deconvoluted and the individual peaks identified. Seven peaks were identified in the 1900 to 1500 cm^{-1} wavenumber range (Figure 5.9): 1586 cm^{-1} carboxylate anion carbonyl stretch (1), 1639 cm^{-1} vinylidine stretch (2), 1673 cm^{-1} trans-substituted alkenes or tri-/quad-substituted alkenes stretch (3), 1704 cm^{-1} dimerized carboxylic acid carbonyl stretch (4), 1744 cm^{-1} ester carbonyl stretch (5), 1786 cm^{-1} cyclic anhydride carbonyl symmetric stretch (6), and 1822 cm^{-1} cyclic anhydride carbonyl asymmetric stretch (7).

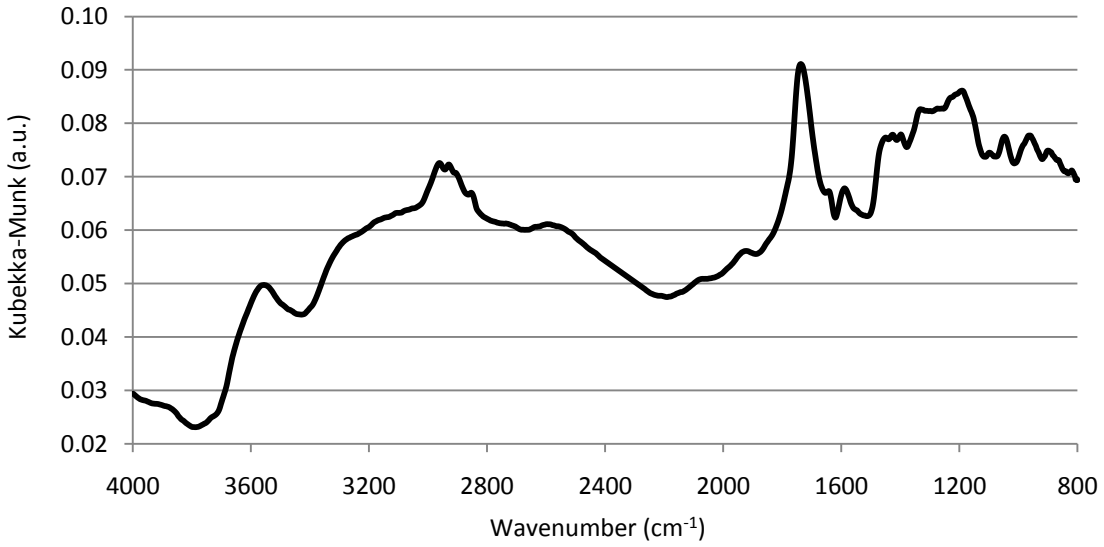

Figure 5.8: Representative DRIFT spectrum of degraded PTI powder (1,000 min, pH 7) mixed at 5 wt.% with KBr.

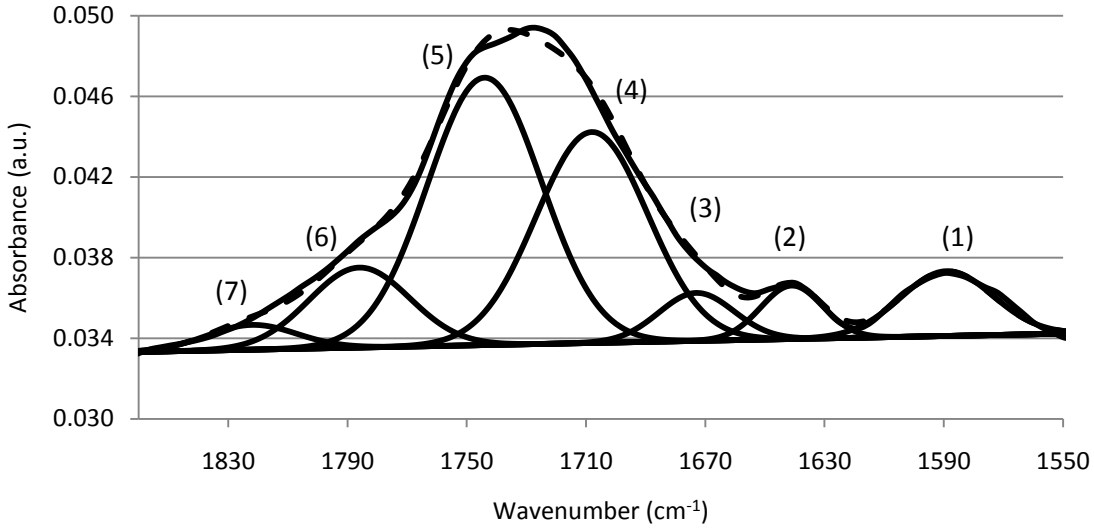

Figure 5.9: Carbonyl peak fit of a DRIFT spectrum for degraded PTI (air, 1,000 min). The identified subpeaks are 1592 cm^{-1} carboxylate anion carbonyl stretch (1), 1639 cm^{-1} vinylidine stretch (2), 1673 cm^{-1} trans-substituted alkenes or tri-/quad-substituted alkenes stretch (3), 1704 cm^{-1} dimerized carboxylic acid carbonyl stretch (4), 1744 cm^{-1} ester carbonyl stretch (5), 1786 cm^{-1} cyclic anhydride carbonyl symmetric stretch (6), and 1822 cm^{-1} cyclic anhydride carbonyl asymmetric stretch (7). Dashed line is the composite spectrum from addition of the individual peaks.

The DRIFT FTIR data is single data points making it difficult to draw conclusion, but there are definite trends observed. With degradation, it is expected that the ester carbonyl PHR (5) will decrease and the carboxylic acid carbonyl PHR (4) will increase. As shown in Figure 5.10, the measured PHR for the ester carbonyl did decrease as a function of degradation time for all samples, except the air control. DI had the largest decrease in ester carbonyl over 100 to 10,000 min from ~2.7 to ~2.0 PHR following $A_{AC}2$ and $A_{AL}1$ mechanisms for ester hydrolysis in acidic solutions with excess water. pH 7 had a significant decrease in ester carbonyl's PHR of ~0.5 from 100 to 10,000 min following $A_{AC}2$ and $A_{AL}1$ mechanisms. The degradation of pH 7 esters could have been hindered by K^+ in solution. KOH was added to DI water to obtain a pH 7 solution. The amount of KOH necessary to adjust the pH 7 to the correct initial pH was minimal, and does not appear to have greatly affected the degradation by stabilization of carboxylate

anions. pH 9 and pH 11 had the highest ester carbonyl concentrations at 10,000 min. Both of these samples had to transition from a base-mediated dominated degradation mechanism, $B_{AC}2$, to a acid-catalyzed dominated degradation mechanisms, $A_{AC}2$ and $A_{AL}1$, and had the highest K^+ concentrations. The base-mediated ester hydrolyses is driven to completion by the formation of stable carboxylate anions due to acid-base interaction, specifically K^+ ions being present. In comparison, the acid catalyzed ester hydrolyses id driven to completion by the presence of excess water. As the solutions become acidic due to the increased presence of carboxylic acid (as ester degraded), the K^+ ions do not leave the solution, but continue to stabilize the carboxylate anions as the acid-catalyzed degradations mechanisms become dominant. The K^+ ions hinder the dominate $A_{AC}2$ and $A_{AL}1$ mechanisms by interfering with the carbonyl protonation. An initially acidic solutions leads to the greater ester bond degradation when compared to initially basic solutions that have counter ions that can stabilize the carboxlyate anion.

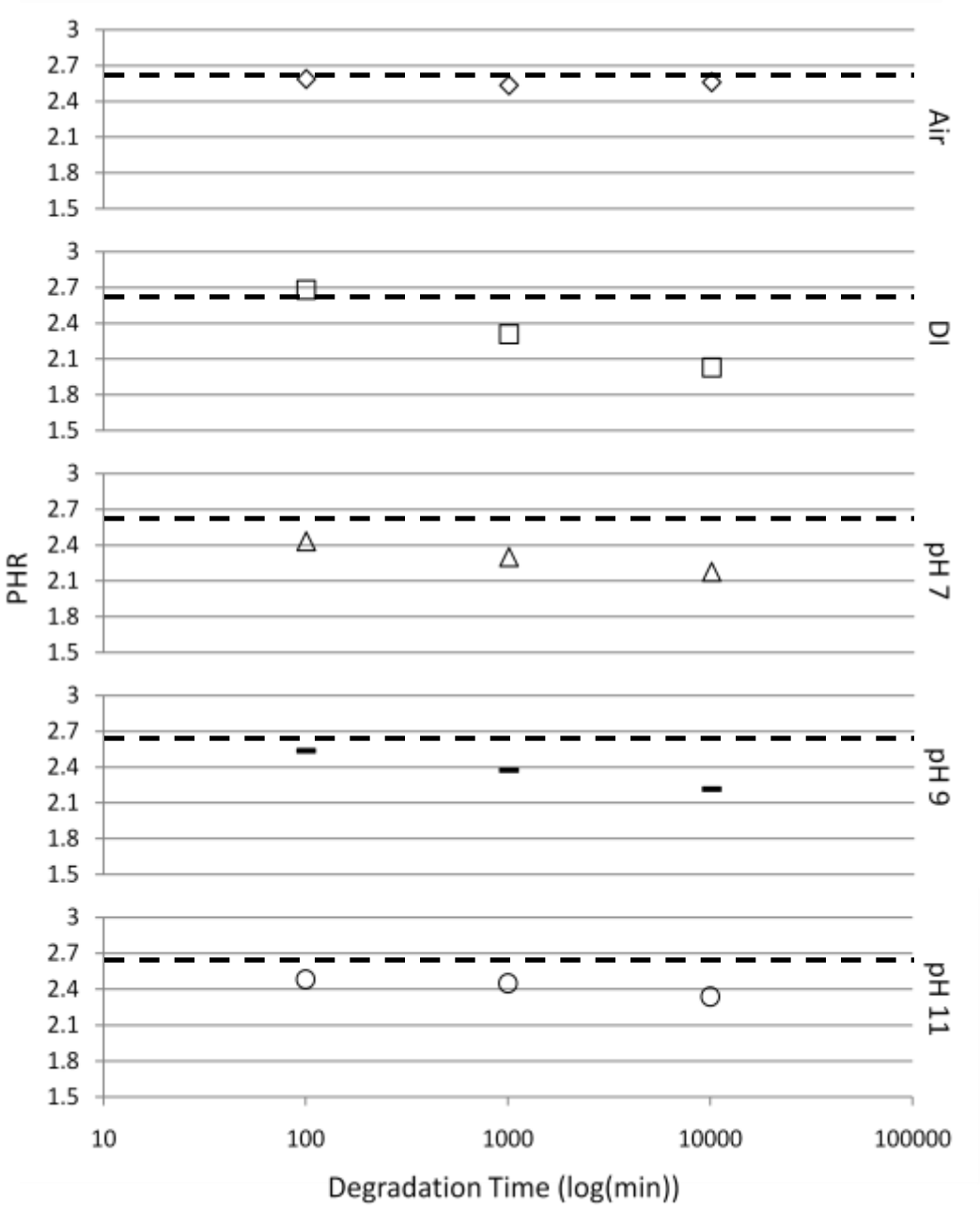

Figure 5.10: PHR change for 1744 cm^{-1} peak, ester carbonyl, as a function of aging time for PTI (◇: air; □: DI water; △: pH 7; --: pH 9; ○: pH 11). Error bars represent 95% confidence intervals for 3 replicates. Dashed line represents neat material before grinding.

With ester degradation, there is a corresponding increased in carboxylic acid PHR in all the samples, except the air control (Figure 5.11). For all solutions by 100 min, degradation was following the $A_{AC}2$ and $A_{AL}1$ reaction mechanisms and producing carboxylic acids. DI water and pH 7 had the greatest increase in carboxylic acid carbonyl PHR with increased aging time, both increased from ~1.9 to ~2.5, which was expected due to DI water and pH 7 having the greatest decrease in ester carbonyl PHR 100 to 10,000 min. pH 11 and pH 9 had the least increase carboxylic acid carbonyl PHR with increasing aging time, both increased from ~1.9 to ~2.1. The carboyxlate anion PHR was expected to increase with the carboxylic acid PRH from 100 to 10,000 min, except for air contol, which had no change with increased aging time (Figure 5.12). For DI and pH 7, the carboxylate anion decreased with increased aging time, which was unexpected. The carboxylate anion could be converting to a carboxylic acid and increasing the carboxylic acid PHR, or it could be diffusing into the solution for DI water and pH 7. pH 12 and pH 9 have relatively constant carboxylate anion carbonyl PHR, 0.5 and 0.3, respectfully. The K^+ ion, through acid-base interaction, is stabilizing the carboxylate anion in pH 12 and pH 9.

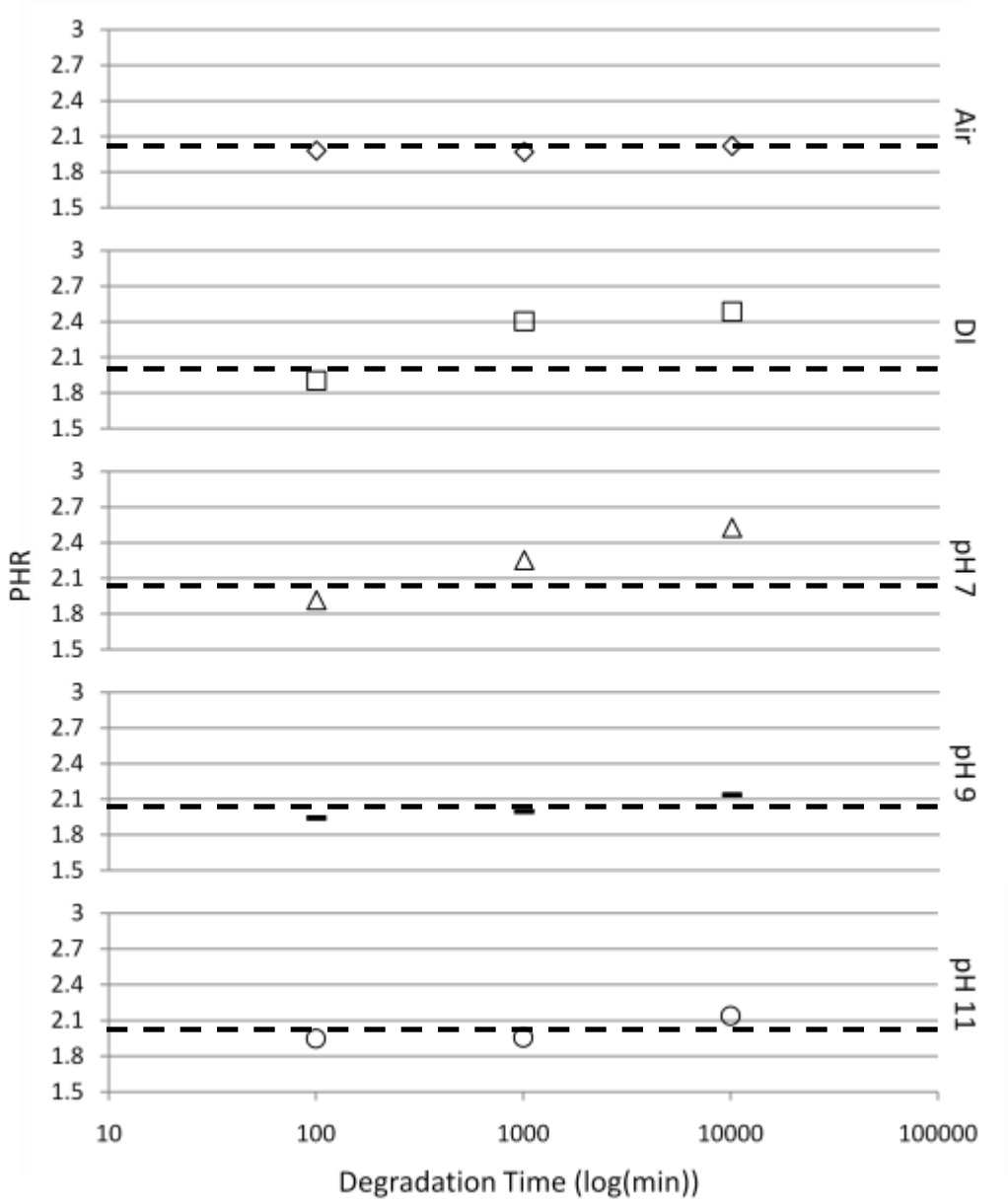

Figure 5.11: PHR change for 1704 cm^{-1} peak, carboxylic acid carbonyl, as a function of aging time for PTI (◇: air; □: DI water; △: pH 7; ╍: pH 9; ○: pH 11). Error bars represent 95% confidence intervals for 3 replicates. Dashed line represents neat material before grinding.

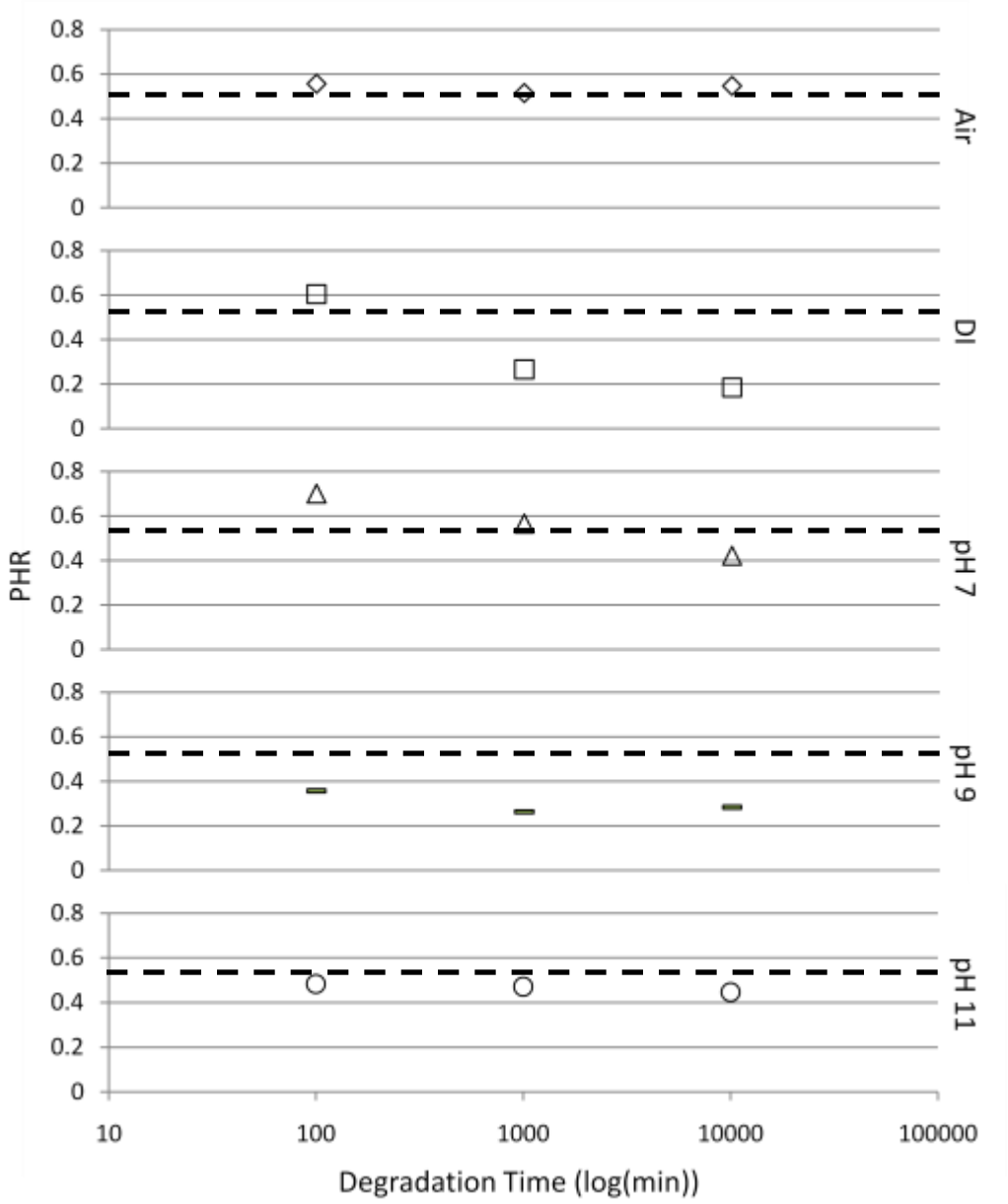

Figure 5.12: PHR change for 1586 cm^{-1} peak, carboxylate anion, as a function of aging time for PTI (◇: air; □: DI water; △: pH 7; ╍: pH 9; ○: pH 11). Error bars represent 95% confidence intervals for 3 replicates. Dashed line represents neat material before grinding.

5.4.5. Gel Permeation Chromatography (GPC)

PTI exhibited significant degradation from 100 to 10,000 min as shown by the weight change, FTIR spectroscopy analysis, and aqueous phase pH discussed above. Gel permeation chromatography (GPC) was used to monitor the Mw in the solid and solution, and provided information on the Mw distribution as measured by the polydispersity index (PDI). With PTI, the Mw will be skewed to lower values due to PTI being only partially soluble in tetrahydrofuran, GPC effluent. PTI did initially have a bi-modal Mw distribution. The higher Mw polymer was above 10,000 Da and will be refered to as HMw. The lower Mw polymer was below 10,000 Da and will be refered to as LMw. The PTI air control LMw and PDI did not deviate from the starting materials LMw and PDI, 1379 ± 9 Da and 1.61 ± 0.17 (Figure 5.13 and 5.14). During the initial 100 min, DI water and pH 7, 9, and 11 LMw increased by ~100 Da when compared to the air control. The increase in LMw is due to the diffusion of polymer into the solution, and this diffusion causes the pH of all solution to become acidic (Figure 5.2). There was no change in PTI's LMw from 100 to 1,000 min for all solutions. From 1,000 min to 10,000min, the molecular weights of DI water, and pH 7, 9, and 10 solutions Mw decreased by 50 to 200 Da as hydrolytic degradation occurs and LMw material diffuse into the aqueous phase. For pH 11, the LMw decreased from 1500 to 1425 Da, pH 9 LMw decreased from ~1475 to ~1375 Da, pH 7 LMw decreased from ~1457 to ~1330 Da, and DI water decreased from ~1490 to ~1270 Da from 1,000 to 10,000 min. pH 11 solution had least impact on PTI with LMw decreasing by ~75 Da, the least of all solids in aqueous solution. The degradation for pH 9 and pH 11 starts off as $B_{AC}2$ in the first 100 min and converts to $A_{AC}2$ and $A_{AL}1$ as the surrounding solution becomes acidic (Figure 5.2). pH 11 and pH 9 hydrolyses was inhibited by the presence of K^+ ions that stabilized the carboxylate anions. Once there are a significant number of carboxylic acid end groups present, as shown by the increase in PHR of carboxylic acids at longer degradation time, $A_{AC}2$ and $A_{AL}1$

degradations mechanisms can overcome the carboxylate anion stabilization effects and proceed to products for pH 11. With increasing initial solution acidity and reduction in K^+ ion, the reduction in LMw increases.

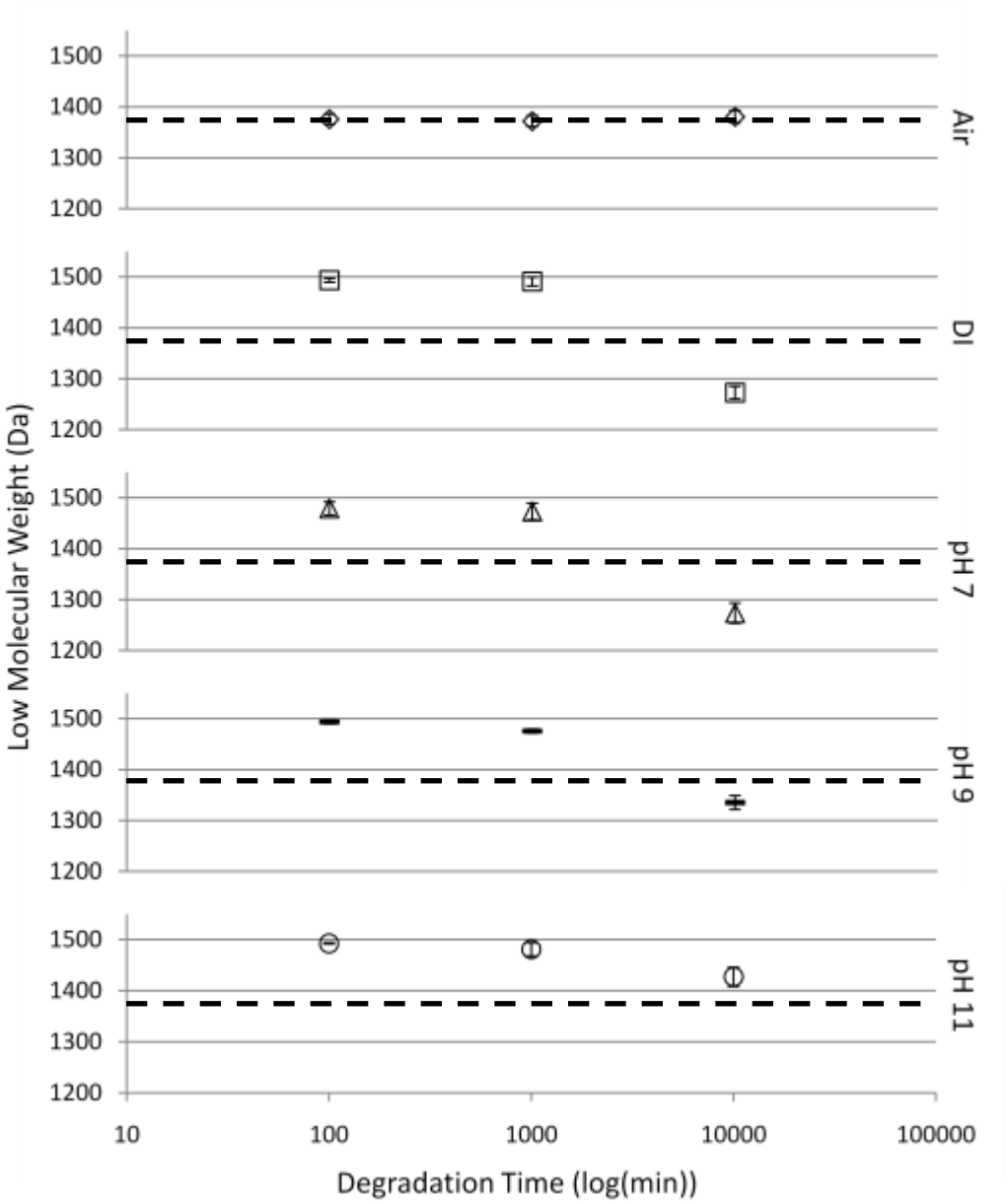

Figure 5.13: Degraded solid phase low Mw as a function of aging time for PTI (◇: air; □: DI water; △: pH 7; ╌: pH 9; ○: pH 11). Error bars represent 95% confidence intervals for 3 replicates. Neat PTI: 1,379 ± 9 Da (with 1.78 ± 0.05 PDI, DP 16.0 ± 0.1). Dashed line represents neat material before grinding.

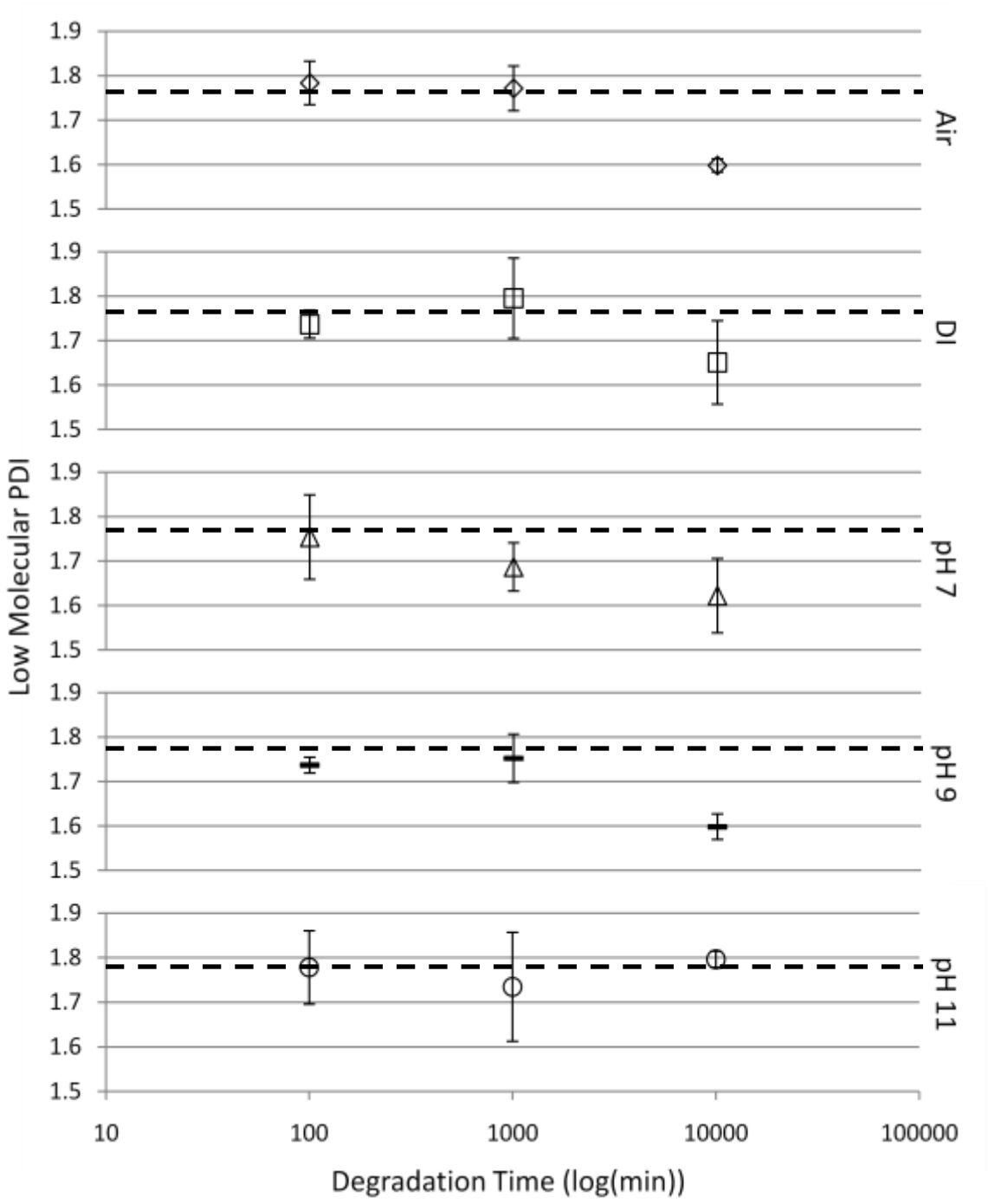

Figure 5.14: Low Mw solid phase PDI as a function of aging time for PTI (◇: air; □: DI water; △: pH 7; ⋯: pH 9; ○: pH 11). Error bars represent 95% confidence intervals for 3 replicates. Dashed line represents neat material before grinding.

The PDI for DI water and pH 7, 9, and 11 trends were not as systematic as the Mw trends (Figure 5.14). Air does appear to decrease from ~1.77 to ~1.6 at 1,000 to 10,000 min, but it is still with the confidence interval of the neat material, 1.71 ± 0.17 PDI. It is not believed that this is degradation of air control because it was not accompanied by a decrease in sample weight, change in the FTIR, or a change in the Mw. For DI and pH 9 from 100 to 1,000 min, the PDIs appear to increase from ~1.73 to ~1.8 and ~1.73 to ~1.76. The increase in PDI with no change in Mw from 100 to 1,000 min shows that degradation is occurring, and the degradation products have not diffused out of the polymer leading to an increase in PDI. From 1,000 to 10,000, DI and pH 9 PDI reduce from ~1.8 and ~1.76 to ~1.65 and ~1.6, respectively. pH 7 did not experience a increase in PDI as a function of aging time. From 100 to 10,000 min, pH 7 PDI decreased from 1.75 to 1.62. pH 11 had no apparent dependence on PDI. No relation between PDI and any other factor could be determined.

For PTI in the aqueous fraction, the Mw decreased for all solutions with increasing time, Figure 5.14. pH 7, 9, and 11 had their initial pH adjusted with KOH, and this does appear to affect the size of molecule that can dissolve into aqueous solution. The initial acidity or K^+ ions concentration of the solution does appear to be a driving factor in hydrolytic degradation of PTI. At 10,000 min, pH 11 solutions had the lowest Mw PTI at ~450 Da, and the pH 11 solution had the greatest change in Mw, ~175 Da, from 100 to 10,000 min. When the amount of material dissolved in solution is taken into account based the dry weight loss, the DI Water (~20 wt.%) Mw may be shifted higher due higher due to increased diffusion of material out of the solid state. With decreasing PTI dissolved in solution from DI to pH 11 based on change in dry weight of ~20wt.% to ~7wt.%, the Mw in solution decrease from 600 to 425 Da. There are two reasons for the Mw to be higher in DI than pH 11. The first reason is that there is more material diffusing

out of the polymer, and this increases the Mw for DI. The second reasons are that the more dilute the ester bonds are in aqueous solution; the higher the reaction rate for $A_{AC}2$ and $A_{AL}1$.

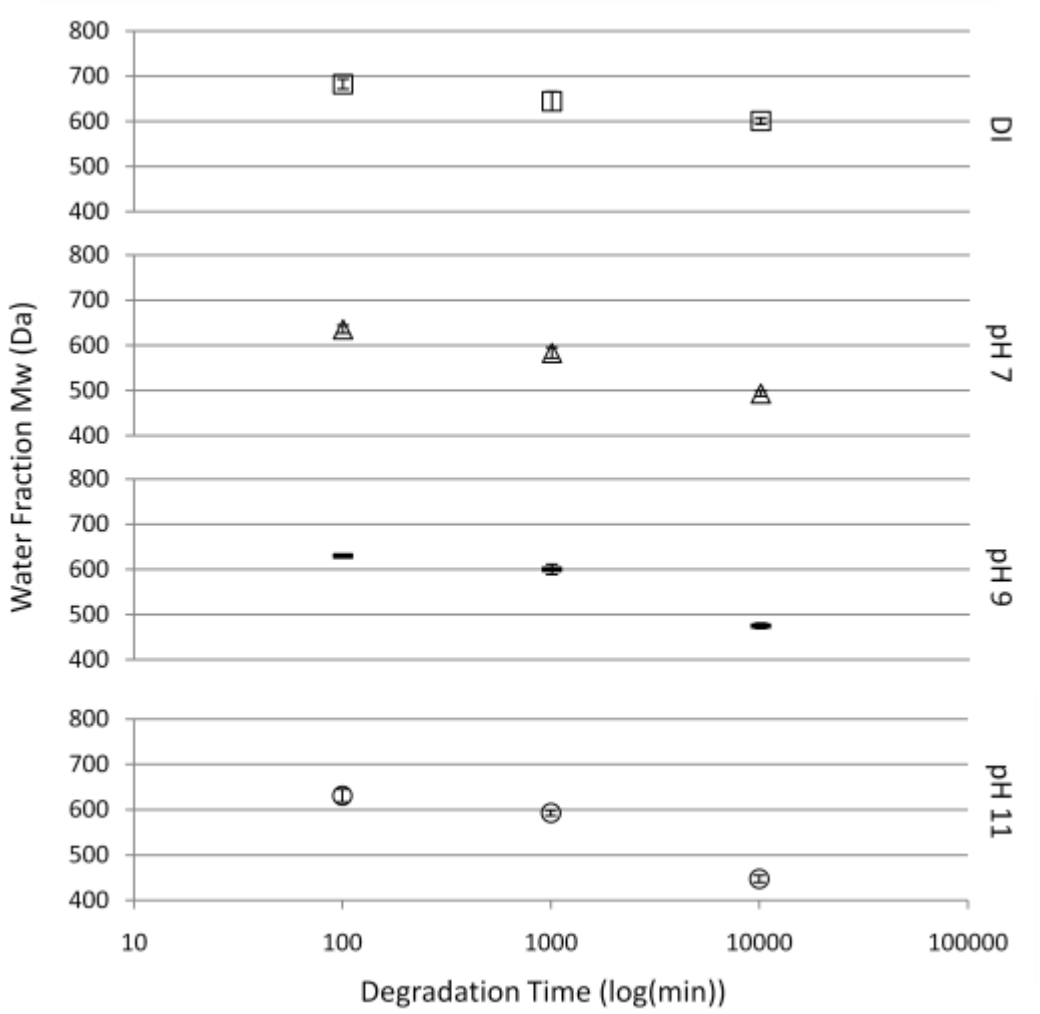

Figure 5.15: Aqueous phase Mw as a function of aging time for PTI (◇: air; □: DI water; △: pH 7; ╍: pH 9; ○: pH 11). Error bars represent 95% confidence intervals for 3 replicates. Dashed line represents neat material before grinding.

Solution PDI values for PTI do not show significant variation until 10,000 min, Figure 5.16. The PDI's have the same characteristic distribution based on the initial pH of the solution as the solutions Mw's have at 10,000 min. PTI in pH 11 solutions has the lowest PDI (~1.1) and the lowest Mw (~450 Da), and PTI in DI water (pH 5.4) has the highest PDI (~2.1) and highest Mw (~600 Da) at 10,000 min. The GPC system is only calibrated down to a Mw of 240 (approximately 3 monomers repeat units), which cuts off any Mw below this point making for a artificially low PDI. When examining the PDI and Mw in conjunction, DI does degrade PTI through both $A_{AC}2$ and $A_{AL}1$. Diffusion does impact both the Mw and increases the PDI of polymer in solution. Degradation is occurring in DI water, but due to significant amount of PTI that is dissolving out of the solid into the solutions (~20% dry weight loss at 10,000 min), the degradation in solution cannot equal Mw's seen in pH 11 at 10,000 min. pH 11 solution PDIto have a PDI decrease from ~1.3 to ~1.1 with Mw going from ~625 to ~450 Da, the material dissolving into solution being hydrolytic degradation through $A_{AC}2$, and $A_{AL}1$ mechanisms. PTI in pH 9 solution is also being degraded with PDI stable at ~1.35 and a decrease in Mw of ~150 Da. With PTI in pH 7 solution, degradation is taking place, but not to the extent of pH 9 or 11 solutions due to increased PTI in solution, 14 wt.% loss from the solid to the solution. With decreased acidity of the initial solutions and the addition of counter ions, PTI hydrolytic degradation has a larger impact as the $A_{AC}2$ and $A_{AL}1$ mechanism have higher reaction rates with more dilute solutions.

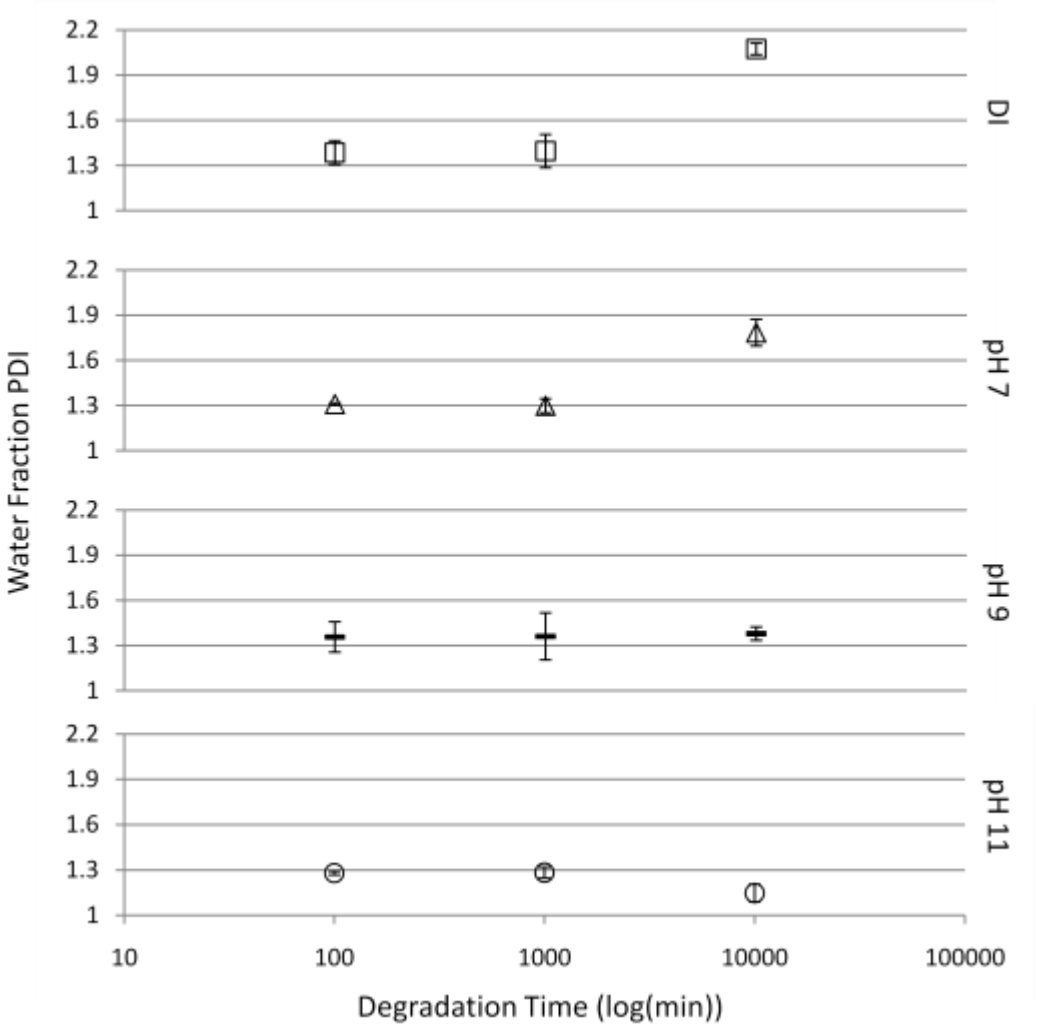

Figure 5.16: Aqueous phase PDI as a function of aging time for PTI (◇: air; □: DI water; △: pH 7; ╌: pH 9; ○: pH 11). Error bars represent 95% confidence intervals for 3 replicates. Dashed line represents neat material before grinding.

PTI initially had a bi-modal molecular weight distribution due to having both step and chain growth polycondensation reactions during polymerization. Having the bi-modal Mw weight distribution allows for the determination of the effects of Mw on hydrolytic degradation. In the initial 100 min, Figure 5.17, the high molecular weight material, from now on referred to as HMw, is lower than the control, but only statically significantly for pH 9. At 1,000 min, all samples in solution are significantly different than the Air control and have reduced in Mw. The

lower Mw material did not show any significant change in Mw at 1,000 min. After 1,000 min, the HMw was not detected, and it is assumed that the HMw has degraded to a point at which it is indistinguishable from the lower Mw material.

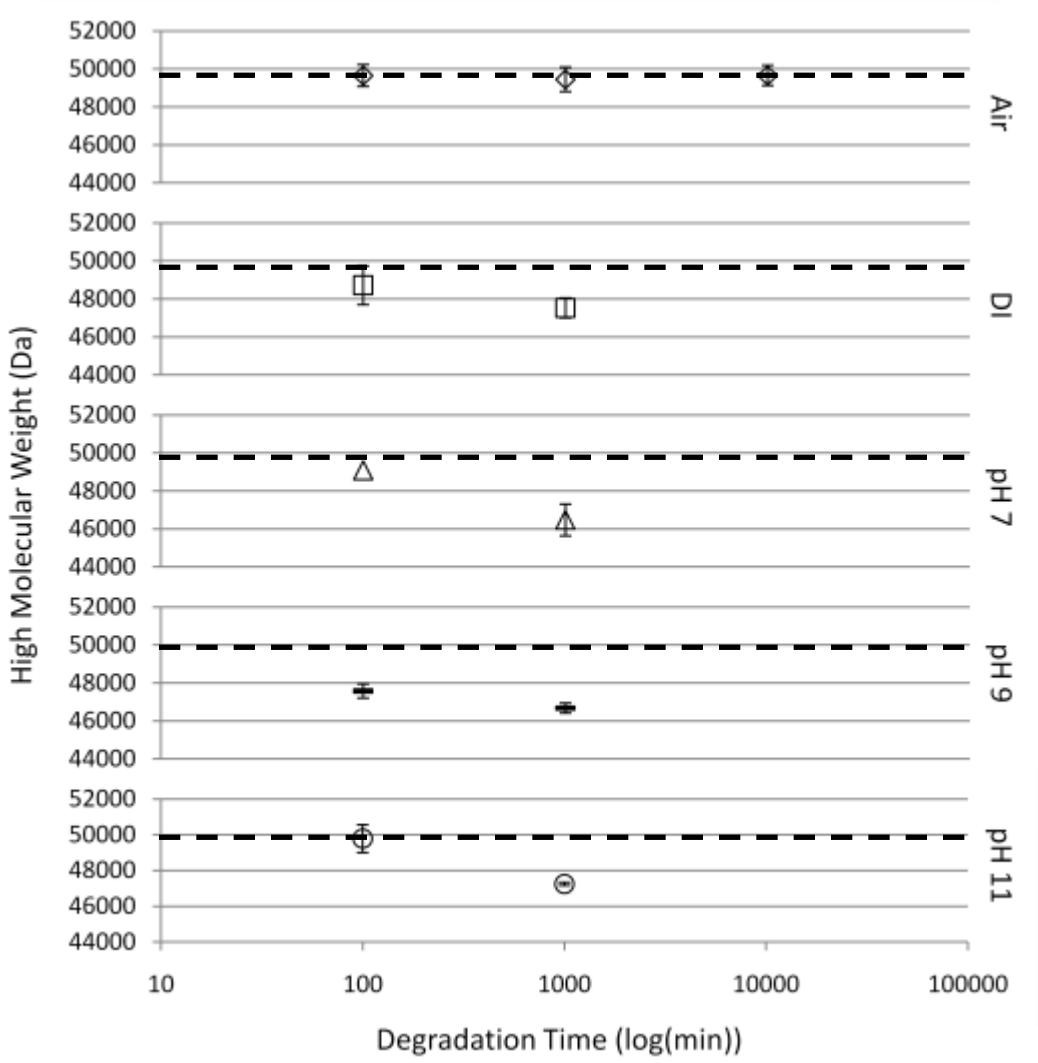

Figure 5.17: Solid phase high Mw as a function of aging time for PTI (◇: air; □: DI water; △: pH 7; ▫: pH 9; ○: pH 11). Error bars represent 95% confidence intervals for 3 replicates. PTI neat: 50,650 ± 2,953 Da (with 1.71 ± 0.17 PDI, DP 588.9 ± 1.4, 1.5 ± 0.2 wt.%). Dashed line represents neat material before grinding.

Examining the PDI during the first 1,000 min, Figure 5.18, the PDI did not change. This gives evidence that the HMw is not experiencing random chain session and is experiencing end chain session. If the HMw was experiencing random chain session, a broadening of the PDI would have occurred. Hydrolytic degradation is preferentially degrading the HMw with end chain session.

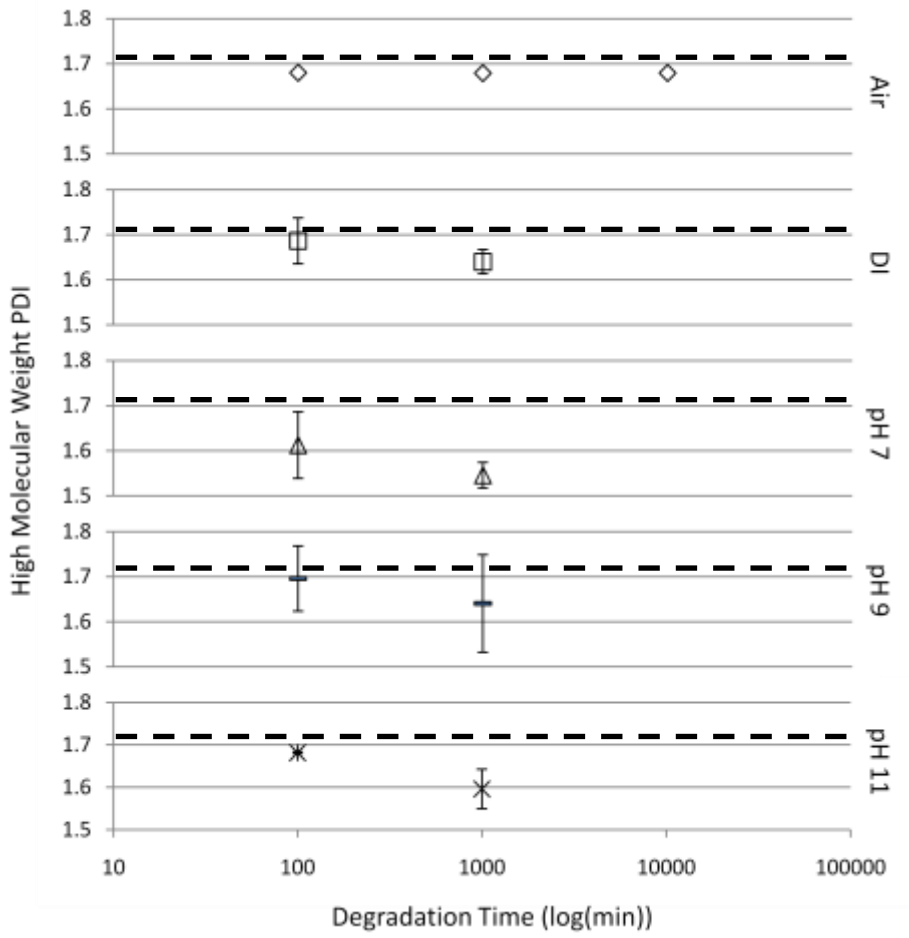

Figure 5.18: Solid phase high Mw PDI as a function of aging time for PTI (◇: air; □: DI water; △: pH 7; ⎓: pH 9; ○: pH 11). Error bars represent 95% confidence intervals for 3 replicates. PTI neat: 50,650 ± 2,953 Da (with 1.71 ± 0.17 PDI, DP 588.9 ± 1.4, 1.5 ± 0.2 wt.%). Dashed line represents neat material before grinding.

The HMw concentration increased in the first 1,000 min before it was degraded to where it was indistinguishable from the lower Mw material. The HMw area on the GPC trace increased for all samples except Air from 100 to 1,000 min, Figure 5.19. During the same time period, there was a significant decrease in the dry weight of the samples, Figure 5.4. The low Mw material is diffusing out of PTI, which was postulated earlier, while the HMw is too large to diffuse out of PTI. The diffusion of low Mw into solution increases HMw concentration in first 1,000 min.

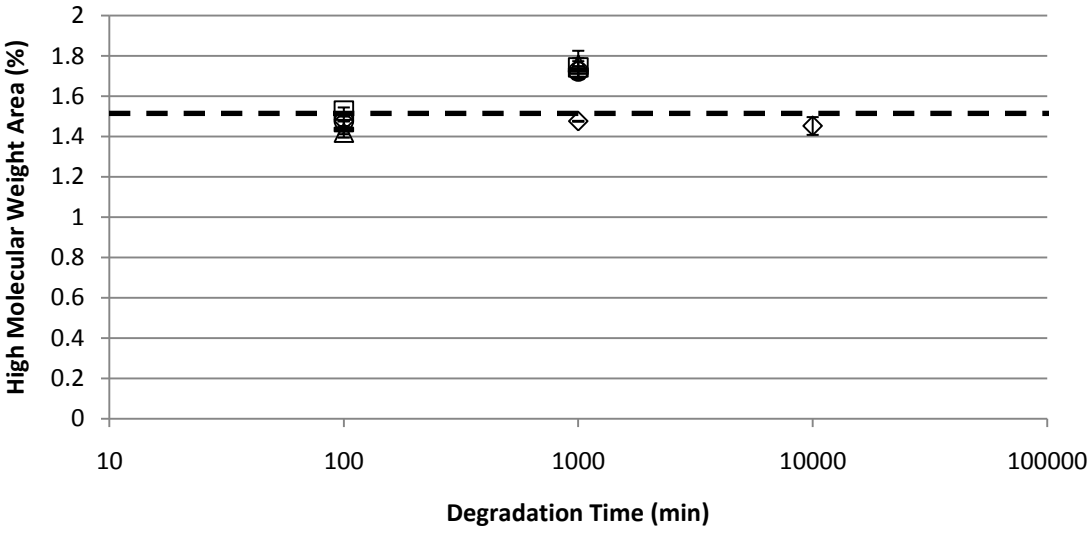

Figure 5.19: Solid phase high Mw area as a function of aging time for PTI (◇: air; □: DI water; △: pH 7; ╍: pH 9; ○: pH 11). Error bars represent 95% confidence intervals for 3 replicates. PTI neat: 50,650 ± 2,953 Da (with 1.71 ± 0.17 PDI, DP 588.9 ± 1.4, 1.5 ± 0.2 wt.%). Dashed line represents neat material before grinding.

5.4.6. Differential Scanning Calorimetry

PTI exhibits no glass transition or melting temperature between -90 °C (minimum DSC temperature) and 212 °C (the temperature where 5 wt.% loss is measured). Since X-ray diffraction was not performed and the melting enthalpy for 100% crystalline PTI is unknown, the cold crystallization enthalpies are used to monitor PTI's crystallinity. The crystallinity trends downwards as a function of increasing degradation time for all samples (Figure 5.20). At 100 min, all samples have reduced their cold crystallization enthalpy by a maximum of 50 J/g from the air control. It is suggested that there are small crystalline structures that can be readily degraded or diffused out of PTI in the first 100 min, and the larger crystals do not experience degradation until after 1,000 min. Further investigation using x-ray diffraction and DSC is needed of changes in crystalline structure need to be undertaken to fully understand the changes in crystalline concentration.

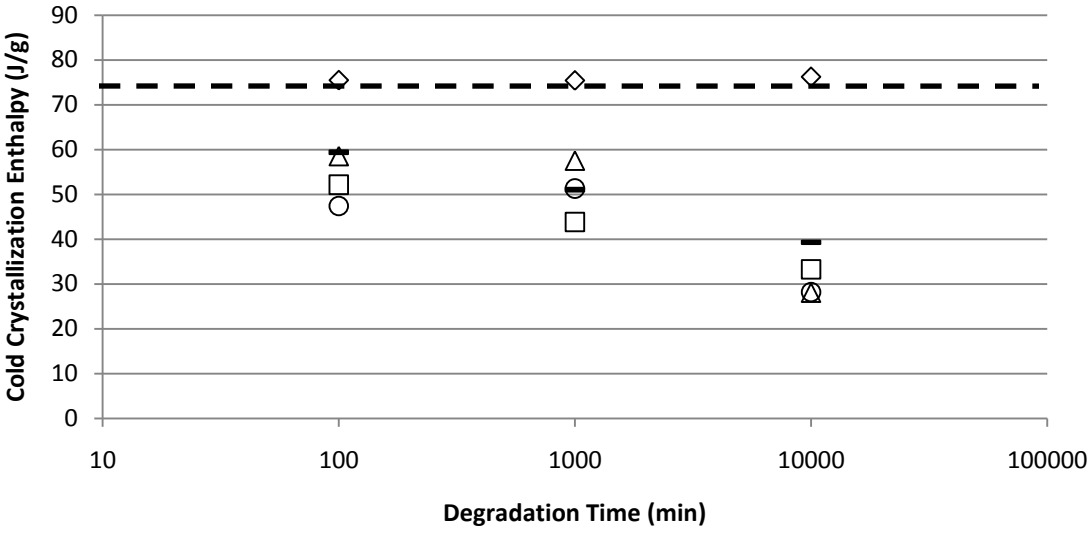

Figure 5.20: Crystallization enthalpy as a function of aging time for PTI (◇: air; □: DI water; △: pH 7; ⎓: pH 9; ○: pH 11). Error bars represent 95% confidence intervals for 3 replicates. Dashed line represents neat material before grinding.

5.5. Conclusions

Hydrolytic degradation of PTI should not be performed in PBSs due to PDO interaction with PBS, and it should be performed in pH adjust DI water. PTI weight while wet showed that there was weight loss to diffusion, and it was not more the 0.5 wt.% over 10,000 min for DI water and pH 7, 9, and 11 KOH solutions. The pH of the solution surrounding PTI decreased to a pH of 2.9 and was independent of starting pH. The PTI dry weights had a maximum decrease of ~21 wt.% with DI water and a minimum decrease of ~7 wt.% with pH 11 at 10,000 min. It was determined by the weight dependence on initial pH that K^+ ion was stabilizing the carboxylate anion through acid-base interaction interfering with the $A_{AC}2$ and $A_{AL}1$ mechanisms. 1744 cm-1, ester carbonyl, PHR decreased with aging time with PTI in DI water having the largest PHR decrease of 0.7 and pH 11 having smallest increase of 0.2. 1704 cm-1, carboxylic acid, PHR increased with aging time with PTI in DI water having the largest PHR increase of 0.6 and pH 11 having smallest increase of 0.3. FTIR confirmed that K^+ ion interfered with $A_{AC}2$ and $A_{AL}1$ mechanisms reducing the ester hydrolysis of polymer with higher concentrations of K^+ ions. GPC showed that in the initial 100 min, all samples in solvent increase in Mw as low Mw material dissolves into the aqueous phase reducing the surrounding solution pH. This showed that diffusion has a significant impact on degradation by removing low Mw material from the solid phase and into the aqueous phase. Mw showed a dependence on aging time and K^+ ion concentration. pH 11 with the highest concentration of K^+ ions and at 10,000 min had the highest Mw of ~1450 Da. In contrast, DI water with the lowest concentration of K^+ ions and at 10,000 min had the lowest Mw of ~1275 Da. GPC also showed that the high Mw polymer, Mw greater than 10,000 Da, degraded to a point where it was not distinguishable from low Mw polymer at 10,000 min. The cold crystallization enthalpy was shown by DSC to decrease by as

much as 50 J/g for PTI at 10,000 min. It was demonstrated that PTI is hydrolytically degradable under varied pH and time conditions.

5.6. Recommended Future Work

Further work needs be done on the effects of ions on hydrolytic degradation by using different ions, such as sodium and calcium, and at varied concentrations. Temperature dependent hydrolytic degradation experiments needs to be completed. Thermal analysis needs to be utilized to monitor changes in thermal properties and to give further insight into the degradation mechanism. Hydrolytic degradation at elevated temperatures and at very short times needs to be examined. To prove that PTI is completely renewable, biological degradation experimental studies needs to be undertaken.

5.7. Acknowledgements

Completion of this work in a timely manner would not have been possible without undergraduate researchers Erin Smith, Mitch Wall, Zach Wynne, and Phillip Jamison. Some TGA and DSC experiments were completed by Kimberly Ivey of Clemson University.

5.8. References

Bruckner, R., “Nucleophilic Substitution Reactions on the Carboxyl Carbon (except through Enolates),” in Advanced Organic Chemistry, Elsevier, New York, 221-270, 2002.

Catiker, E., Gumusderelioglu, M., Guner, A., “Degradation of PLA, PLGA homo- and Copolymers in the Presence of Serum Albumin: A Spectroscopic Investigation,” Polymer International, 49, 728-734, 2000.

Chu, C. C., “Hydrolytic Degradation of Polyglycolic Acid: Tensile Strength and Crystallinity Study,” Journal of Applied Polymer Science, 26, 1727-1734, 1981.

El-Hadi, A., Schnabel, R., Straube, E., Muller, G., Henning, S., “Correlation between degree of Crystallinity, Morphology, Glass Temperature, Mechanical Properties and Biodegradation of Poly(3-hydroxyalkanoate) PHAs and their Blends,” Polymer Testing, 21, 665-674, 2002.

Hill, S. P., de Oca, H. M., Klein, P. G., Ward, I. M., Rose, J., Farrar, D., “Dynamic Mechanical Studies of Hydrolytic Degradation in Isotropic and Oriented Maxon B,” Biomaterials, 27, 3168-3177, 2006.

Hofmann, D., Entrialgo-Castano, M., Kratz, K., Lendlein, A., “Knowledge-Based Approach towards Hydrolytic Degradation of Polymer-Based Biomaterials,” Advanced Materials, 21, 3237-3245, 2009.

Hoglund, A., Odelius, K., Hakkarainen, M., Albertsson, A.-C., “Controllable Degradation Product Migration from Cross-Linked Biomedical Polyester-Ethers through Predetermined Alterations in Copolymer Composition,” Biomacromolecules, 8, 2025-2032, 2007.

Li, H., Wang C., Bai, F., Yue, J., Woo, H.-G., “Living ring-Opening Polymerizaiton of L-Lactide Catalyzed by Red-Al,” Organometallics, 23, 1411-1415, 2004.

Neffe, A. T., Tronci, G. Alteheld, A. Lendlein, A., “Controlled Change of Mechanical Properties during Hydrolytic Degradation of Polyester Urethane Networks,” Macromolecular Chemistry and Physics, 211, 182-194, 2010.

Nostrum, C. F. v., Veldhuis, T. F. J., Bos, G. W., Hennink, W. E., “Hydrolytic Degradation of Oligo(Lactic Acid): A Kinetic and Mechanistic Study,” Polymer, 45, 6779-6787, 2004.

Oyama, H. T., Tanaka, Y., Kadosaka, A., “Rapid Controlled Hydrolytic Degradation of Poly(L-Lactic Acid) by Blending with Poly(Aspartic Acid-co-L-Lactide),” Polymer Degradation and Stability, 94, 1419-1426, 2009.

Roe, R. J., “Methods of X-Rau and Neutron Scattering in Polymer Science,” Mark, J. E., ed., Oxford University Press, Oxford, 2000.

Saha, S. K., Tsuji, H., "Effects of Molecular Weight and Small Amounts of D-Lactide Units on Hydrolytic Degradation of Poly(L-Lactic Acid)s," Polymer Degradation and Stability, 91, 1665-1673, 2003.

Satchell, D. P. N., Satchell, R. S., "Mechanistic Aspects. Recent Developments Concerning Mechanisms of Acylation by Carboxylic Acid Derivatives," in Supplement B: The Chemistry of Acid Derivatives, Vol. 2, John Wiley & Sons, Ltd., Hoboken, New Jersey, 747-802, 1992.

Saunders, J. H., Dobinson, F., "The Kinetics of Polycondensation Reactions," in Comprehensive Chemical Kinetics, Vol. 15, Bamford, C. H., Tippers, C. F. H., American Elsevier, New York, 473-581, 1976.

Shirahase, T., Komatsu, Y., Tominaga, Y., Asai, S., Sumita, M., "Miscibility and Hydrolytic Degradation in Alkaline Solution of Poly(L-Lactide) and Poly(Methyl Methacrylate) Blends," Polymer, 47, 4829-4844, 2006.

Smith, M., March, J., "Aliphatic Substitution: Nucleophilic and Organometallic," in March's Advanced Organic Chemistry, 6th ed., Wiley-Interscience, Hoboken, New Jersey, 425-656, 2007.

Vasanthan, N., Ly, O., "Effect of Microstructure on Hydrolytic Degradation Studies of Poly(L-Lactic Acid) by FTIR Spectroscopy and Differential Scanning Calorimetry," Polymer Degradation and Stability, 94, 1364-1372, 2009.

Vert, M., Li, S., Garreau, H., Mauduit, J., Boustta, M., Schwach, G., Engel, R., Coudane, J., "Complexity of the Hydrolytic Degradation of Aliphatic Polyesters," Die Angewandte Makromolekulare Chemie, 247, 239-253, 1997.

CHAPTER 6

CONCLUSIONS

6.1. PTM Conclusions

6.1.1. PTM Preliminary Catalyst and Temperature Screening

Aluminum chloride, iron(III) chloride, tin(II) chloride, and zinc chloride showed no significant difference in yield over the reaction temperature range of 125 to 175 °C with a reaction time of 24 h studied when no vacuum or stirring of reaction mixture was applied. Gravimetric yields varied between 5-59 wt.% with maximum yields occurring between 135 and 165 °C, likely bounded by the melt temperature of MA and the onset of thermal degradation. The polymer formed using aluminum chloride as the catalyst demonstrated the highest ester carbonyl concentration based on FTIR peak height ratios (PHR) with the ester carbonyl peak (1726 cm^{-1}) at a 10.5 PHR and the cyclic ester carbonyl (1749 cm^{-1}) at a 5.7 PHR. Based on catalyst cost and environmental impact and ester concentration in the polymer product, aluminum chloride was chosen as the catalyst for continued study in the synthesis of polyesters from renewable monomers.

6.1.2. PTM Copolymerization Expanded Study

Aluminum chloride was then used as the catalyst to study the synthesis of a linear PTM copolymer using melt polycondensation with vacuum and stirring over the 125-175 °C reaction

temperatures range and 2-16 h reaction time range. PTM yields displayed a strong dependence on reaction time and temperature. Over reaction temperature range studied, 125-175 °C, the maximum yield was obtained between 145 and 155 °C with a gravimetric yield ~78±5 wt.%. A maximum yield of ~77±20 wt.% was obtained from polymerizations at 155 °C for 2 h, but this reaction condition was considered to be unstable. Based on the large yield variations, the system was determined to be in a non-equilibrium state. More consistent gravimetric yields (76±5 wt.%) were obtained at 4 h and 155 °C. Linear and cyclic esters were identified in PTM using FTIR with carbonyl peaks corresponding to the linear and cyclic esters identified at 1726 cm^{-1} and 1749 cm^{-1}, respectively. Consistent with the yield data, when the full range of reaction temperatures was examined the maximum ester concentration was found for the 155 °C / 4 h PTM samples. With the reaction temperature held constant at 155 C, and increased reaction time resulted in a gradual increase in both the linear and cyclic ester carbonyls with yield decreasing from 155 to 175 °C. One of the projects goals was to maximize yield, and it was found that gravimetric yield was maximized at 155 °C and 4 h with a moderate ester concentration. NMR confirmed that PTM contained both ester and ether bonds, but due to user fees was not further used in quantifying ester and ether bond content as a function of reaction time and temperature. FTIR and NMR confirmed that PTM is a linear polyester, but could not confirm PTM ester cyclic structure. XPS showed that PDO was being added preferentially versus MA by comparison of theoretical and experiential atomic concentrations of oxygen and carbon. Using GPC, PTM was found to have a bi-modal molecular weight distribution due to simultaneous step- and chain-growth polycondensation. Step-growth polymerization dominated resulting in a low Mw component (below 10 kDa) and yields below 99.5%. The high Mw component in PTM (~35 kDa) was produced by chain-growth polymerization and was left as a mixture with the low Mw component in the PTM product. The low Mw component (~1.4 kDa)

accounted for >95 wt.% of the product and limits the physical properties making PTM unacceptable as a standalone, load-bearing polymer. If separated, high Mw PTM could be used for degradable films for packaging limited shelf life items, such as produce and meat. The low Tg (-57 °C) and Tm (30 °C) measured for PTM do not make it useful in most commercial applications, but it may have use in specialty applications such as sensors or biomedical applications. Thermal analysis did not identify any crystalline portion of PTM and the combination of backbone chemistry and low Mw allowed PTM to be very susceptible to hydrolytic degradation.

6.1.3. PTM Hydrolytic Degradation

Two hydrolytic degradation studies were performed on PTM. The first study lasted 672 h with the fluid exchanged every 24 h and investigated the 2 to 12 pH range. Phosphate buffer solutions were used for the pH 4, 7, and 10 solutions. The pH 2 and pH 12 solutions were comprised of HCl and KOH in DI water, respectively. PTM showed a 50-90 weight loss during the study with no significant difference in weight loss measured as a function of pH. FTIR spectroscopy did not provide insight into the degradation mechanism or into the lack of weight loss variation between the different pH solutions. Using GPC, the 'high' Mw was found to be completely degraded after 168 h in all solutions, and the 'low' Mw did not vary significantly during 672 h aging time. By exchanging the fluid every 24 h, the degradation products were not allowed to accumulate in the fluid and so equilibrium was not reached. Through the periodic removal of the degradation products, the ester hydrolysis reaction was shifted to the right. A relatively constant PTM concentration gradient was maintained that led to higher rates of degradation and diffusion of the degradation products into the aqueous phase. Increased PTM

diffusion into the aqueous phase minimized pH effects on chemical structure and molecular weight.

The second hydrolytic study was performed at 25 °C using KOH/DI water for pH 7, 9, and 11 solutions and DI water (pH 5.4) for 10,000 min without the fluid being exchanged. Weight loss was seen for all of the aqueous solutions with a trend of increased weight loss at decreased pH. The PTM sample lost ~21 wt.% in the pH 11 KOH/DI solution and in DI water (pH 5.4) lost ~37 wt.% at 10,000 min. The measured pH of all solutions (initially pH 5.4-11) were acidic (pH ~6) by 10 min and continued to decrease to a pH ~ 4 at 10,000 min. Therefore, $A_{AC}2$ and $A_{AL}1$ were the dominate ester hydrolysis mechanisms after 10 min. FTIR spectroscopy showed cyclic and linear ester concentrations decreased for all solutions with DI water having the largest decrease. GPC indicated that the low Mw component of the PTM samples in all of the solutions experienced a decrease in Mw ranging between ~250 Da (pH 11 KOH/DI solution) and ~800 Da (DI water). By comparing yield, FTIR, and GPC results, K^+ ions were found to interfere with the $A_{AC}2$ and $A_{AL}1$ ester hydrolysis mechanisms by stabilization carboxylate anions through acid-based interaction. The carboxylate anion stabilization limited PTM degradation in pH 11 and pH 9 KOH/DI water.

6.1.4. PTM Overall Conclusions

PTM was produced by the melt polycondensation of PDO with MA using the catalyst aluminum chloride catalyst, vacuum, and stirring. The maximum yield (~78±5 wt.%) was obtained at the reaction conditions of 155 °C and 4 h with the product having a bimodal Mw of ~1.4 and ~34 kDa. PTM is a linear polymer composed of ester and ether backbone bonds. The low melting point, ~29 °C, and glass transition, -57 °C, make it useful for specialty applications or as a plasticizer. PTM is susceptible to hydrolytic degradation up to 50 wt.% over a wide range of

pH in only ~1 wk. So, PTM could be considered for short term (less than a week) and non-load bearing applications. Potential uses include a plasticizer for other renewable polymers, sensor applications, and drug delivery.

6.2. PTI Conclusions

6.2.1. PTI Copolymerization

PDO and IA were melt polycondensed with aluminum chloride catalyst, vacuum, and stirring. The polycondensation was performed over the 125-175 °C reaction temperature and 2-32 h reaction time ranges. A maximum gravimetric yield of 78±8 wt.% was obtained at 16 h and 155 °C. A single ester carbonyl peak was identified at 1743 cm^{-1}, corresponding to a linear ester, and its PHR was found to be a maximum at 16 h and 155 °C. With increased reaction temperature, vinylidine (1639 cm^{-1}) concentration reduced as the vinylidine was saturated by an alcohol to form branches by Ordelt saturation mechanism. NMR confirmed that PTI was branched, and XPS showed that PDO and IA monomers were added to PTI in a 1:1 molar ratio based on carbon and oxygen atomic concentrations. Branching decreased PTI solubility in tetrahydrofuran artificially lowering the Mw determined by GPC. A bi-modal molecular weight distribution was found for PTI. Step-growth polymerization produced PTI with a Mw of 0.5 to 1.5 kDa and chain-growth polymerization produced PTI with a Mw of 25 to 45 kDa at 125-175 °C and 2-32 h. An unexpected cold crystallization temperature was found at ~160 °C by DSC, and affects the hydrolytic degradation of PTI.

6.2.2. PTI Hydrolytic Degradation

PTI hydrolytic degradation was performed at 25 °C for 10,000 min with pH 7, 9, 11 KOH/DI water solutions and DI water (pH 5.4). Although the solutions started at different pH values, all aqueous solutions had a measured pH of ~3.4 by 100 min degradation such that only the $A_{AC}2$ and $A_{AL}1$ ester hydrolysis mechanisms applied for all solutions. PTI showed a maximum weight loss of 21 wt.% at 10,000 min in DI water. DRIFT FTIR spectral analysis indicates that all of the PTI samples had a decreased ester concentration with increased degradation time. The DI water sample had the largest ester PHR decrease (0.7) and the pH 11 KOH/DI water sample had the lowest ester PHR decrease (0.2). Mw loss over 10,000 min increased from ~75 Da at pH 11 to ~250 Da at pH 5.4 (DI water). Like PTM, the K^+ ion interferes with the $A_{AC}2$ and $A_{AL}1$ ester hydrolysis mechanisms in PTI by stabilization of the carboxylate anions through acid-based interactions. This study found that PTI degradation was a function of ion concentration, but not pH.

6.2.3. PTI Overall Conclusions

PTI is a low Mw, branched copolymer. Due to branching, PTI is a rigid to elastomeric material with possible load bearing application. The maximum yield, 78 ±8 wt.%, and ester concentration were obtained at 155 °C and 16 h reaction conditions. For the THF-soluble PTI material, the measured Mw was ~1±0.1 kDa and ~38±2 kDa. A cold crystallization temperature was found at ~160 °C that decreased with degradation time. PTI is hydrolytically degradable, but to a lesser extent than PTM due to branching and crystallization and showed a maximum weight loss of 22 wt.% after 10,000 min. Potential applications for PTI include packaging material, disposable utensils and tableware, indoor furniture (in dry climates), and many other applications requiring a stiff, degradable material.

CHAPTER 7

RECOMMENDATIONS FOR FUTURE WORK

Chapter 7 discusses the work that can be done to further understand PTM and PTI and novel ideas for contining efforts in the development of degradable, renewable polymers and polymer composites.

7.1. Polymerization

The synthesis and characterization efforts presented here for PTM and PTI provide a strong foundation for continued research in the area of bioplastics. Polymerizations at reaction temperatures below 125 °C and reaction temperatures longer than 16 h (PTM) and 32 h (PTI) may improve the Mw and yield based on preliminary experiments that have been completed. It would be interesting to investigate heterogeneous catalysts and enzyme-based catalysts and their effect on the chemistry, yield, and Mw of the polymer product. For PTI, the use of protecting groups on the carbon double bond with post-polymerization removal followed by cross-linking would allow for PTI to have a better controlled Mw and crosslink density, and therefore tunable properties. For both PTM and PTI, the chain growth reaction mechanism should be further maximized to give novel high Mw bioplastics. To maximize chain growth polymerization, an initiator will have to be used in a solvent, and the modification of the monomers may be necessary to achieve the high reactivity required for chain-growth polymerization where transesterification is suppressed. Additionally, a method of

polymerization that should be explored is the use of green solvents, such as ionic liquids, as the medium during polycondensation. This method might prove to be the easiest method to obtain high Mw by increasing the rate of removal of water through distillation during the reaction.

7.2. Characterization

In the GPC characterization, a refractive index (RI) detector was used with poly(styrene) calibration standards, so only a relative molecular weights were obtained. A GPC with triple detection (RI, viscometry, and light scattering) and/or the use of a more polar calibration standard would provide a more accurate determination of Mw. For PTI, determination of branching using techniques that were not available, such as solid state NMR and small angle neutron scattering, would provide better insight into the chemical structure. Further work into the thermal characterization of both polymers need to be performed to better understand the impacts of reaction conditions, compression molding, extrusion, and hydrolytic degradation on the glass transition, melting, and crystallization temperatures. The tensile strength, Young's modulus, Poisson's ratio, hardness, compressive strength, and impact strength of both PTM and PTI need to be determined.

7.3. Degradation

Hydrolytic degradation was performed on both PTM and PTI, but the use of KOH in the basic aqueous solutions appears to have influenced the degradation mechanisms. Other counter ions, such as Mg^{2+}, Ca^{2+}, and metal ions, may give different results and further study is needed. The influence of higher temperatures, greater than 30 °C, on hydrolytic degradation was not studied, and would be an important parameter in the processing and degradation of these materials in landfills or composting. In addition to temperature, for processing (e.g.,

extrusion, blow molding, and compression molding) the impacts of pressure and shear would also need to be studied. Biological degradation under aerobic and anaerobic conditions should to be carried out for PTI and PTM to determine if these polymers are biodegradable.

7.4. Green Composites

The reinforcement of PTI, PTM, or a blend of PTI and PTM with natural fibers would likely improve the mechanical properties of the polymers and yield an all-green composite. The interface between PTM and PTI and the surface of natural fiber should be explored and may require modification of the fiber surface to obtain the best properties. In addition, the effects of fiber aspect ratio, length, weight fraction, type, and orientation should be investigated to determine the range of composite properties that can be obtained, and so the potential applications.

APPENDIX A

PROCEDURES

A.1. General Polymerization Procedure for Bioplastics project

A.1.1. Materials (this is a list of materials for a single polymerization reaction; it can be duplicated to fit needs)

- Alcohol monomer (glycerol 98% or 1,3-propanediol 98%)
- Acid monomer (malonic acid 98%, itaconic acid 98%, or fumaric acid 98%)
- Catalyst (aluminum chloride 99%, iron (III) chloride 99%, tin (II) chloride 99%, or zinc chloride 99%)
- 1 x 100 mL round bottom flask with 24/40 neck
- 2 large septum for 24/40 necked flask
- 1 x 0.75” magnetic stir bar
- 1 silicone oil bath rated to at least 180 °C
- 3 barb to luer lock fittings
- 4 x 18 gauge needles
- Tubing rated for up to 200 °C and vacuum (at least 2 ft)
- 1 x 500 ml round bottom flask with 24/40 neck (condenser)
- 1 x 24/40 vacuum adapter
- 1 small insulated cooler for ice bath
- Liquid nitrogen
- Dual bank manifold set-up for vacuum and dry nitrogen
- Dry nitrogen gas cylinder
- 3 spatulas
- 1 disposable glass pipette and bulb
- 2 glass 100 mL beakers

- Denver APX-100 Analytical balance
- Weigh dishes

A.1.2. Procedure

Before you start to prepare for the polymerization, calculate the amount of each monomer and catalyst that will be used. This procedure is for initially 50 g of monomers, scale to your needs.

1. Set oil bath at desired temperature.
2. Put liquid nitrogen into liquid nitrogen trap on vacuum manifold system.
3. Put a septum on the top of the 500 mL round bottom flask.
4. Place 500 mL round bottom into ice bath.
5. Connect tubing to vacuum manifold.
6. Run tubing to condenser.
7. Put a luer lock fitting on the end of the tubing running from the vacuum manifold.
8. Put a 18 gauge needle on the end of tubing with luer lock fitting.
9. Put the needle into the septum on top of 500 mL vacuum flask.
10. Take a second piece of tubing and put luer lock fitting and 18 gauge needle on both ends and put one end into the 500 mL round bottom flask.
11. Using the analytical balance, weigh the 100 mL round bottom flask, stir bar, acid monomer, and alcohol monomer using the spatula and pipette with bulb.
12. Put stir bar, acid monomer, and alcohol monomer in flask.
13. Put a septum onto the 100 mL round bottom flask.

14. Connect the 100 mL round bottom flask to the other end of the piece of tubing running from the 500 mL flask.
15. Put a second needle into the 100 mL round bottom flask that vents to the atmosphere.
16. Purge the system with dry nitrogen for 5 min, while not in the oil bath.
17. Weigh out appropriate amount of catalyst with 5% extra to allow for deactivation during transfer to round bottom flask.
18. Turn off nitrogen purge, remove the 2nd needle in the 100 mL round bottom, and turn on vacuum. The reaction set-up should look like Figure A.1 after the 2nd needle is removed and vacuum is turned on.
19. Put catalyst into 100 mL round bottom flask and remove needle that vents to atmosphere.
20. Put flask under vacuum and place flask into oil bath.
21. Leave flask in oil bath for predetermined reaction time.
22. When reaction time is complete, remove flask from oil bath and remove needle that connects the flask to the vacuum system.
23. Place flask into ice water to cool for 10 min to quench the reaction.

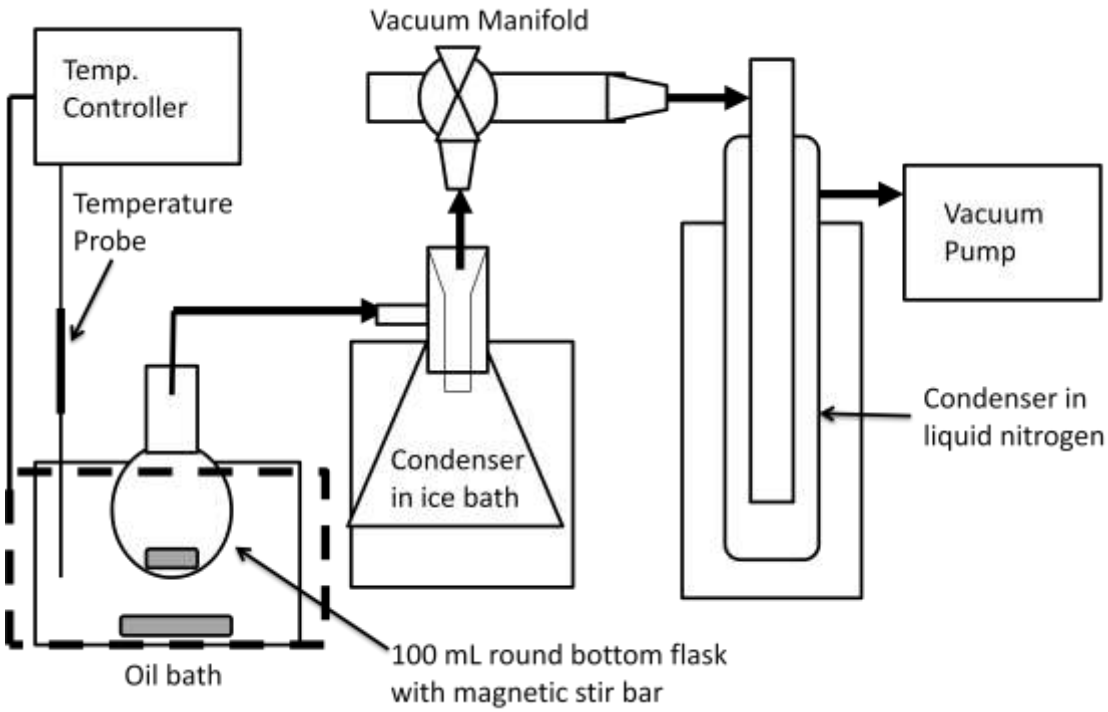

Figure A.1: General polymerization reaction set-up connected to vacuum system with 100 mL round bottom flask charged with ~50 g of monomer.

A.2. General Polymer Purification Procedure for Bioplastics project

A.2.1. Materials (this is a list of materials for a single polymerization reaction; it can be duplicated to fit needs)

- Buchner funnel
- Erlenmeyer flask with 24/40 ground glass joint
- 24/40 Vacuum adapter
- Grade 40 Whitman ashless filters of appropriate size to fit Buchner funnel
- Aspirator
- 500 or 1,000 mL griffin beaker (dependent on amount and type of polymer to be purified)

- Reacted polymer in 100 mL round bottom flask
- 98%+ chloroform
- 98% diethyl ether
- Petri dish top and bottom
- Denver APX-100 Analytical balance
- Magnetic stir plate
- Vacuum system with liquid nitrogen trap
- Vacuum oven
- Spatulas

A.2.2. Procedure

1. Assemble Buchner funnel, Erlenmeyer, and vacuum adapter.
2. Connect to aspirator.
3. Weigh out 4 filters of appropriate size to fit Buchner funnel.
4. Weigh petri dish top and bottom separately.
5. Put 50 mL of chloroform into 100 mL round bottom flask that has polymer in it.
6. Allow to dissolve polymer (it will not dissolve the entire polymer).
7. Pour out chloroform into griffin beaker.
8. Using a spatula, remove polymer still in round bottom flask.
9. If necessary, repeat steps 4-7 to remove all polymer.
10. Take stir bar from round bottom flask and put it into the griffin beaker.
11. Once all polymer is out of round bottom flask, pour diethyl ether into griffin beaker to make a 5:1 to 10:1 solution of diethyl ether to chloroform.

12. Place griffin beaker on stir plate and stir vigorously for at least 10 min to allow for polymer to precipitate (may take up to an hour).
13. Put a filter into Buchner funnel.
14. Turn on water to aspirator.
15. Carefully pour diethyl ether/chloroform/polymer solution through filter.
16. Change filter as needed (it will normally take all 4 filters to filter once, but at times it will take up to 12, depending on polymer).
17. Keep filters separate from purified polymer as they have a tendency to become entrapped in polymer during drying.
18. Once the solution has been filtered, dispose of the solution in the harmful hazardous waste container.
19. Put the filters and purified polymer into vacuum oven.
20. Put liquid nitrogen into vacuum system liquid nitrogen trap.
21. Close the vacuum oven and turn on the vacuum.
22. Pull maximum vacuum.
23. Leave polymer in vacuum oven for at least 24 h at room temperature.
24. Increase temperature in vacuum oven to 40 °C and leave polymer under elevated temperature and vacuum for at least 24 h (this should be extended if there is more than 60 g of polymer in the vacuum oven at the same time or if the polymer appears to still be partially solubilized after 48 h. To determine if polymer is still losing solvent and needs to be dried longer, periodically weigh the petri dish with polymer and continue drying until the dish is losing minimal weight).
25. After polymer has had solvent removed, weigh petri dish with polymer.

A.3. Compression Molding Procedure

A.3.1. Materials

- Polymer
- Hot gloves
- Spatula
- Shims or mold
- 2 x aluminum plates 12” x 12”
- Silicon release spray

A.3.2. Procedure

1. Turn on the power to the compression molder by switch on the wall to the right of the instrument.
2. Turn on the instruments main power with the red switch on the right hand side of the instrument.
3. Turn on the power to the hydraulic pumps by switching the right rocker switch on the instrument panel to on.
4. Turn on the power the heated platen by switching the left rocker switch on the instrument panel to on.
5. Set the temperature to the upper and lower platen use their individual controllers by pressing the right most button on each temperature controller once.
6. Use the up and down buttons to set the temperature.
7. Press the right most button again to confirm set point

8. To set pressure, switch to manual mode by pressing “man” on the right control panel.
9. Then press “set” 3 times to get to force setting in pounds.
10. Use the up and down arrows to select appropriate force.
11. Press “man” to confirm.
12. Allow platen and mold to come to equilibrium.
13. Place material in mold.
14. Press the two large green buttons at the same time and hold until pressure is reached.
15. Let press sit until time is complete.
16. Press red button and remove mold.
17. Turn on the water at the spigot on the right wall.
18. Cool the mold to room temperature.
19. Carefully remove sample from mold once cooled.

A.4. GPC Procedure

Water GPC system with a Water 2414 refractive index detector, Waters 1515 isocratic HPLC pump, Waters 717plus autosampler, column heater, Waters Styragel HR 5E, 4E and guard column. The system is run at 0.3 mL/min of Optima tetrahydrofuran at 30 °C. The GPC should always be running in recycle mode at 0.1 mL/min of tetrahydrofuran (THF).

A.4.1. To start the GPC

1. Turn on the computer, auto-sampler (switch on front), column heater (switch on back), isocratic pump (switch on left side), and refractive index detector (RID) (switch on front).
2. Once the computer is on, start the Breeze software (it will take the software 5 min to start).

3. Turn on solvent recycle by pressing “shift” than “3/recycle” on the RID front control panel.
4. Set the temperature to 30 °C by pressing “Temp” on the RID control panel, and then type 30 in the cell for the detector and column heater.
5. On the Breeze software, open the correct experimental set-up by going to “View Method”. Then go to file menu and select open. Open the appropriate experimental file.
6. Set the flow rate to 0.1 ml/min by going to the panel on the screen that shows flow rate and pressure (this should always be on the screen). Click on the flow rate and set to 0.1 mL/min.
7. The system is now set in stand-by state.

A.4.2. Sample Preparation

1. The GPC is setup to run THF, so the samples will be dissolved in Optima THF.
2. Weigh out 4 to 8 mg of sample (ask your supervisor which weight use because it will be sample dependent due to different Mw materials have different responses).
3. Add 4 mL of Optima THF to make the samples concentration to be between 1 and 2 mg/mL.
4. Let the samples dissolve for 4 to 24h (Longer solution times are better. If the sample is not dissolving, put samples into sonication bath for extended period of time.).
5. Get a clean, 1 mL, snap vials (enough for all of your samples), a disposable needles, and a glass syringe for the next steps.
6. Get 2 beakers and put just enough Optima THF in one to rinse the syringe 3 times between each sample, and use the 2nd beaker for waste.

7. Put a clean needle on the syringe.
8. Rinse the syringe and needle three times with Optima THF.
9. Draw your sample out of vial.
10. Carefully remove the needle from the syringe with the sample in the syringe.
11. Put a syringe filter on the syringe.
12. Slowly depress the plunger to push the sample though the filter and into a clean vial.
13. Dispose of the filter and the needle (the needle goes into a sharp container).
14. Repeat steps 7 through 12 for each sample.

A.4.3. Running Samples

1. Get the carousel out of the auto-sampler by opening the door on the front of the auto-sample and wait until the auto-sampler releases the carousel.
2. Put 2 vials with pure optima THF into slots 1 and 2 (These are needed to equilibrate the system before running samples because the system will increase flow rate from 0.1 mL/min to 0.3 mL/min at the start of running and there will be non-equilibrium conditions due to this.).
3. Put the 1 mL, snap vials into slots starting at 3, and keep track of which slot which sample is in the carousel.
4. Put the carousel back into the auto-sampler and close the auto-sampler's door.
5. Go to the Breeze program and open the "Sample Queue."
6. The first column is slot number, and the second column is sample name. Put your sample names into the second column.
7. The third column is function, select broad sample from the drop down list on this column.

8. Fourth column is the method, and select the correct method from the drop down menu on this column.
9. In the next 2 columns, set the run time to 32 min and the injection volume to 30 µL.
10. Once this has been done for all samples, click on run in lower left hand corner.
11. The program will prompt for a set name, enter the sample sets name.
12. Click run.
13. Ensure that flow rate increases to 0.3 mL/min and that recycle turns off when the first blank runs. (This happens when the computer has been on too long).
14. If the flow rate does not increase and/or recycle does not turn off, click stop in the lower left hand corner and select stop immediately.
15. Save your sample set by going to the file menu and selecting “save sample set.”
16. Close the program and turn off the GPC by switching the 4 switches on the GPC system to off.
17. Restart the GPC by following the “To start GPC procedure” above and then repeat the above steps except open your sample set by going to file menu and “open sample set”.

A.4.4. Analysis of Data

1. During or once the sample set is completed, go to “Find Data” window.
2. Go to channels tab and click “Update” on the top tool bar.
3. The completed runs should be showing, highlight the samples to be analyzed.
4. Right click and then click “Review” (this will take you to the “View Data” window).
5. To manually integrate the peaks, zoom in on the peak of interest by left clicking on the GPC trace and making a box around the peak of interest.
6. Left click at the start of the peak and drag to end of peak.

7. If more than one peak, repeat step 6 for multiple peaks.
8. To quantify the peak, go to the top tool bar and find the 8th button from the right. Click this button, and the peaks retention time will change to the molecular point.
9. To view Mw, Mn, and other properties, go to the 3rd button from the right on the top tool bar and click it.

A.4.5. Export Data (Mw, Mn and other parameters)

1. Go to “Find Data.”
2. Click on the “Results Tab.”
3. Highlight the samples of interest
4. Right click and select “Export Data.”
5. There are several export methods, select “Exporting 2.”
6. The data will export to Eport file on the desktop

A.4.6. Export Raw Data (Chromatogram)

1. Go to “Find Data.”
2. Click on the “Channels” tab.
3. Highlight data of interest.
4. Click on “Database” on the file menu bar
5. Click “Export.”
6. A window will appear and click “By-Pass Export Methods.”
7. Select a file to save the data to.
8. Click “Export.”

A.4.7. GPC Calibration

This is a relative calibration using polystyrene standards:

1. Prep calibration standards by following “Sample Preparation” method above.
2. Run the samples following the “Running Samples” method above, except change function from broad sample to broad standard.
3. Once the standards have been run, got to “Find Data” and highlight the standards.
4. Right click on standards and select “Alter Sample” this will open the alter sample window.
5. Highlight the standards in the alter sample window.
6. Got to “Edit” in the tool bar above the samples and select “Components,” and this will bring up the components editor window
7. Click on “Current Sample” tab at the bottom of components editor widow
8. Go to the “Moments” tab
9. Enter the Mw, Mn, and Mp into the correct cells (The Mw, Mn, and Mp can be found on the standards).
10. Once all of the standards components have been entered, click “Ok” at the bottom of the components editor window.
11. Click save in the alter sample window and then “Ok.”
12. Highlight the standards in the “Find Data” window.
13. Right click on the highlighted standards and select “Review.”
14. Manually integrate the peaks by left clicking start of the peak on the GPC trace and dragging to the end of the peak.
15. Then click the 7th button from the left on the upper tool bar (calibrate button)
16. Repeat for all standards.

17. To save the calibration, go to file menu then scroll over “Save” and click on “Calibration.”
18. The calibration is now complete and saved.

A.4.8. Trouble shooting procedures

Drifting base line (contaminants absorbed on the column or in the detector):

1. Next to the pump flow rate there are three buttons, click the middle button.
2. Follow the directions given by the software.
3. Max flow rate is 0.5 mL/min for purging the auto-injector and RID.
4. If this does not stabilize the base line, change out all of the solvent in the THF reservoir on the left side of the GPC and purge the system.
5. If this does not work, increase the detector and column temperature by 5 °C and repeat.
6. Repeat the temperature increase to a maximum of 70 °C if needed.
7. If increasing temperature does not work, back flow the columns and repeat purging of system.
    a. Backflow the columns, by reversing the columns orientation to the flow with only one column in-line at a time.
    b. Loosen the nuts on both ends of each column, remove the columns not to be backflowed, and seal there ends.
    c. Put one column in with the flow direction arrow on the column pointing against the flow of the system.
    d. Purge the system.
    e. Repeat for all 3 columns.

A.5. FTIR Procedures

On a Thermo Electron corporation Nicolet 6700 FT-IR with a helium-neon laser, mercury-cadmium-telluride (MCT) detector or deuterated triglycine sulfate (DTGS) detector, with Pike VeeMax II for external reflectance or attenuated total reflectance spectroscopy, Pike EasyDiff for diffused reflectance infrared Fourier transform spectroscopy, or Thermo Electron universal sample holder for transmission spectroscopy using Omnic 8.1.10 software (copyright 1992-2009, Thermo Fisher Scientific Inc.).

A.5.1. Clearing Water from Drip Leg

1. Ensure the wash sink is clear of glassware.
2. Get ear plugs for everyone in the lab
3. Go the yellow handle valve above the GPC that is on the main compressed airline for the lab.
4. Close the yellow handle valve.
5. Slowly open on the red handle valve directly below it.
6. Compressed air, with any water that had pooled in the drip leg, will now flow into the wash sink.
7. When the compressed air shows no indication of water, close off the red handled valve and open on the yellow handled valve.

A.5.2. Filling Liquid Nitrogen Dewar on MCT Detector

1. On the left side of the instrument, open the front most circular lid above where the detectors are located in the instrument.
2. Remove the black plug.

3. Put in the funnel with a metal stem and expanded polystyrene spacer gently into where the black plug was located.
4. Carefully pour a small amount of liquid nitrogen into the funnel and allow the funnel and dewar to cool for 2 min.
5. Gently pour liquid nitrogen into the dewar until it over flows.
6. Let the funnel warm up while in the dewar to avoid breaking it when taking it out.
7. Remove the funnel, and carefully replace black plug.
8. Gently replace lid to original position, but do not push down on the lid until the rubber gasket has come to room temperature.
9. Once rubber gasket is up to room temperature, press lid into place.

A.5.3. Transmission FTIR

1. Put the transmission accessory into the accessory bay on the FTIR.
2. Close the hood on the instrument.
3. Empty the drip leg for the purge gas
    a. Ensure the wash sink is clear of glassware.
    b. Get ear plugs for everyone in the lab
    c. Go the yellow handle valve above the GPC that is on the main compressed airline for the lab.
    d. Turn off the yellow handle valve.
    e. Turn on the red handle valve directly below it.
    f. Compressed air will now flow into the wash sink.
    g. When the compressed air becomes clear, turn off the red handled valve and turn on the yellow handled valve.

4. Purge the FTIR for at least 20 min.
5. While FTIR purges, open Omnic program on the FTIR computer.
6. Go to “Collect” on the upper menu under “Experimental Setup.”
7. Click “open” in the experiment setup window to open saved experimental files.
8. If there is no saved experimental files for current sample set, go to the “Collect” tab.
9. Input number of scans, resolution, and set format to absorbance on the left side of the window.
10. In the file handling area of the same window on the upper right side, input your initials and check both “save automatically” and “save interferograms.”
11. In the background handling section below file handling area, click on either “Collect background before every sample” or “Collect background after every sample.”
12. Go to “Bench” tab in the experimental setup window.
13. Set “Sample Compartment” to Main
14. Set “Detector” to either “DTGS TEC” or “MCT High D*.”
15. Set “Beam Splitter” to “XT-KBr.”
16. Select appropriate source for your samples under “Source.” The standard choice is “IR.” The “IR - Turbo” should be avoided because it can significantly reduce the He-Ne laser’s life span, the “IR – Rest” is for when the instrument is not in use for extended periods of time, and “White light” is for probing low wavelengths.
17. Set “Accessory” to match the accessory in the accessory compartment.
18. Set the range of wavenumbers to be scanned (usually left at default values).
19. Adjust gain (1 to 8) and aperture (32 to 74) to obtain a signal between 5 and 8. If the signal values cannot be reduced to appropriate levels, put in a physical screen (A-D) on

the inside of the left side of the sample chamber where the beam exits the sample chamber.

20. Before taking data, always go to the “Diagnostic” tab in the experimental setup window and click on the “Align” button to maximize signal.
21. Save the experimental file.
22. Close the experimental setup window.
23. Take a background with no sample by hitting “Ctrl + B.”
24. If background has a low concentration of water, save the background by going to file menu and save. The background needs to be retaken every 30 min to 1 hr.
25. Open the experimental setup window again.
26. Go to the collect tab, and under “Background Handling” click “Use specific background file:” and load the previously taken background.
27. Click “Save” and then “Ok.”
28. Find the appropriate transmission crystal (KBr or KRS-5 round disk crystals).
29. Gently apply a thin layer of sample to crystal.
30. Put crystal into universal sample holder.
31. Carefully load the universal sample holder into the FTIR by opening the window on the hood and sliding the holder into the transmission accessory.
32. Allow the system to purge 2 to 10 min after loading sample.
33. Take the sample spectrum by hitting “Ctrl + S”
34. If the sample has noticeable water interference, at the end of taking the spectrum, click “More Scans” and not “Add to Window” when prompted. If the spectrum is satisfactory, click “Add to Window” when prompted.

A.5.4. Attenuated Total Reflectance - FTIR

1. Put the variable angle ATR/ER accessory into the accessory bay on the FTIR with the removable flanges on the instrument in place where the IR beam enters and exits the sample chamber.
2. Plug in the purge line for the accessory into the back of the sample compartment.
3. Put either the Zn-Se or Ge crystal on to the ATR/ER accessory
4. Set the accessory's angle to 60°.
5. Purge the FTIR for at least 20 min.
6. While FTIR purges, open Omnic program on the FTIR computer.
7. Go to collect on the upper menu and experimental setup
8. Click "open" in the experiment setup window to open saved experimental files.
9. If there is no saved experimental files for current sample set, go to the "Collect" tab.
10. Input number of scans, resolution, and set format to absorbance on the left side of the window.
11. In the file handling area of the same window on the upper right side, input your initials and check both "save automatically" and "save interferograms"
12. In the background handling section below file handling area, click on either "Collect background before every sample" or "Collect background after every sample."
13. Go to bench tab in the experimental setup window.
14. Set "Sample Compartment" to Main
15. Set "Detector" to either "DTGS TEC" or "MCT High D*."
16. Set "Beam Splitter" to "XT-KBr."
17. Select appropriate source for your samples under "Source." The standard choice is "IR." The "IR - Turbo" should be avoided because it can significantly reduce the He-Ne laser's

life span, the “IR – Rest” is for when the instrument is not in use for extended periods of time, and “White light” is for probing low wavelengths.

18. Set “Accessory” to match the accessory in the accessory compartment.
19. Set the range of wavenumbers to be scanned (usually left at default values).
20. Adjust gain (1 to 8) and aperture (32 to 74) to obtain a signal between 5 and 8. If the signal values cannot be reduced to appropriate levels, put in a physical screen (A-D) on the inside of the left side of the sample chamber where the beam exits the sample chamber.
21. Before taking data, always go to the “Diagnostic” tab in the experimental setup window and click on the “Align” button to maximize signal.
22. Save the experimental file.
23. Close the experimental setup window.
24. Take a background with no sample by hitting “Ctrl + B.”
25. If background has a low concentration of water, save the background by going to file menu and save. The background needs to be retaken every 30 min to 1 hr.
26. Open the experimental setup window again.
27. Go to the collect tab, and under “Background Handling” click “Use specific background file:” and load the previously taken background.
28. Click “Save” and then “Ok.”
29. Gently apply a thin layer of sample to the crystal.
30. Take the sample spectrum by hitting “Ctrl + S”
31. If the sample has noticeable water interference, at the end of taking the spectrum, click “More Scans” and not “Add to Window” when prompted. If the spectrum is satisfactory, click “Add to Window” when prompted.

A.5.5. External Reflectance - FTIR

1. Put the variable angle ATR/ER accessory into the accessory bay on the FTIR with the removable flanges on the instrument in place where the IR beam enters and exits the sample chamber.
2. Plug in the purge line for the accessory into the back of the sample compartment.
3. Put a cover on top of the accessory with a hole that is slightly smaller than the sample to be analyzed.
4. Purge the FTIR for at least 20 min.
5. While FTIR purges, open Omnic program on the FTIR computer.
6. Go to collect on the upper menu and experimental setup
7. Click “open” in the experiment setup window to open saved experimental files.
8. If there is no saved experimental files for current sample set, go to the “Collect” tab.
9. Input number of scans, resolution, and set format to absorbance on the left side of the window.
10. In the file handling area of the same window on the upper right side, input your initials and check both “save automatically” and “save interferograms”
11. In the background handling section below file handling area, click on either “Collect background before every sample” or “Collect background after every sample.”
12. Go to bench tab in the experimental setup window.
13. Set “Sample Compartment” to Main
14. Set “Detector” to either “DTGS TEC” or “MCT High D*.”
15. Set “Beam Splitter” to “XT-KBr.”

16. Select appropriate source for your samples under “Source.” The standard choice is “IR.” The “IR - Turbo” should be avoided because it can significantly reduce the He-Ne laser’s life span, the “IR – Rest” is for when the instrument is not in use for extended periods of time, and “White light” is for probing low wavelengths.
17. Set “Accessory” to match the accessory in the accessory compartment.
18. Set the range of wavenumbers to be scanned (usually left at default values).
19. Adjust gain (1 to 8) and aperture (32 to 74) to obtain a signal between 5 and 8. If the signal values cannot be reduced to appropriate levels, put in a physical screen (A-D) on the inside of the left side of the sample chamber where the beam exits the sample chamber.
20. Before taking data, always go to the “Diagnostic” tab in the experimental setup window and click on the “Align” button to maximize signal.
21. Save the experimental file.
22. Close the experimental setup window.
23. Take a background with no sample by hitting “Ctrl + B.”
24. If background has a low concentration of water, save the background by going to file menu and save. The background needs to be retaken every 30 min to 1 hr.
25. Open the experimental setup window again.
26. Go to the collect tab, and under “Background Handling” click “Use specific background file:” and load the background previously collected and saved.
27. Click “Save” and then “Ok.”
28. Gently apply a thin layer of sample to the crystal.
29. Take the sample spectrum by hitting “Ctrl + S”

30. If the sample has noticeable water interference, at the end of taking the spectrum, click "More Scans" and not "Add to Window" when prompted. If the spectrum is satisfactory, click "Add to Window" when prompted.

A.5.6. Diffused Reflectance Infrared Fourier Transform (DRIFT) Spectroscopy

1. Put the DRIFT accessory into the accessory bay on the FTIR.
2. Close the hood on the instrument.
3. Purge the FTIR for at least 20 min.
4. Prepare the DRIFT sample:
    a. Make 2% to 5% concentration of sample in KBr power.
    b. Grind the sample and powder together.
    c. Find the DRIFT sample preparation kit where FTIR components are kept.
    d. Using the "small cup," put the cup into the sample preparation disk (two large, black, plastic disks used to hold the cup steady while loading sample).
    e. Carefully pour sample into sample cup
    f. Using a razor (very sharp), make the sample come even to the top of the cup by carefully scraping away excess sample, while at the same time making sure that the sample is flat as possible.
    g. Put sample cup into DRIFT sample holder (holder holds one sample and one background sample).
    h. Load a second sample cup with pure KBr powder for a background.
    i. Carefully put sample holder into DRIFT accessory by opening hold and inserting sample holder onto rail.
    j. Put the control sample into line with the beam.

5. While FTIR purges, open Omnic program on the FTIR computer.
6. Go to collect on the upper menu and experimental setup
7. Click “open” in the experiment setup window to open saved experimental files.
8. If there is no saved experimental files for current sample set, go to the “Collect” tab.
9. Input number of scans, resolution, and set format to “Kubelka-Munk” on the left side of the window.
10. In the file handling area of the same window on the upper right side, input your initials and check both “save automatically” and “save interferograms”
11. In the background handling section below file handling area, click on either “Collect background before every sample.”
12. Go to bench tab in the experimental setup window.
13. Set “Sample Compartment” to Main
14. Set “Detector” to either “DTGS TEC” or “MCT High D*.”
15. Set “Beam Splitter” to “XT-KBr.”
16. Select appropriate source for your samples under “Source.” The standard choice is “IR.” The “IR - Turbo” should be avoided because it can significantly reduce the He-Ne laser’s life span, the “IR – Rest” is for when the instrument is not in use for extended periods of time, and “White light” is for probing low wavelengths.
17. Set “Accessory” to match the accessory in the accessory compartment.
18. Set the range of wavenumbers to be scanned (usually left at default values).
19. Adjust gain (1 to 8) and aperture (32 to 74) to obtain a signal between 5 and 8. If the signal values cannot be reduced to appropriate levels, put in a physical screen (A-D) on the inside of the left side of the sample chamber where the beam exits the sample chamber.

20. Before taking data, always go to the “Diagnostic” tab in the experimental setup window and click on the “Align” button to maximize signal.
21. Save the experimental file.
22. Close the experimental setup window.
23. Take the background of pure KBr by hitting “Ctrl + S.”
24. Once background is completed, Omnic will prompt for taking sample. Do not click on “take sample spectrum” until after sample is moved in line with the IR beam.
25. To move the sample into the IR beam path, open the sliding window on the hold and slide sample holder to move sample into path of the beam.
26. Let the chamber purge for 2 to 10 min.
27. Click “take sample spectrum”
28. If the sample has noticeable water interference, at the end of taking the spectrum, click “More Scans” and not “Add to Window” when prompted or repeat taking control and sample with adjusted purge times. If the spectrum is satisfactory, click “Add to Window” when prompted.

A.5.7. Peak Height Ratio (PHR)

1. Open spectrum or spectra to be analyzed by going to file menu then open.
2. Open the peak height tool by clicking on it in the lower left hand corner of the screen.
3. Find the C-C scissoring peak at ~1465 cm^{-1} and click on it.
4. On the screen should be a vertical line with a box at its top indicating the peak that you clicked on, adjust this until it is centered on ~1465 cm^{-1}.
5. Adjust the baseline by moving the inverted triangles on the horizontal line until the base line is level with the background.

6. Record the peak height. This height is the denominator of the PHR.
7. Click on the peak of interest and adjust the vertical line to center on the peak and the baseline to be level.
8. Record the height. This height is the numerator of the PHR.
9. Repeat steps 7 and 8 for all peaks of interest.
10. Maintain the same peak positions and base line position for all spectrum of interest.

A.5.8. Peak Resolve

1. Select spectrum of interest.
2. Zoom in on area of interest for peak fit.
3. Go to the Analyze drop down menu and click on “Peak Resolve.”
4. A new window will open up with the spectrum of interest, check boundaries to ensure correct area is being peak fitted.
5. Go to the Find Peaks tool bar change the peak shape from Voigt to Gaussian.
6. Set the sensitivity to High and the FWHM to a value of 30 in the Find Peaks tool bar.
7. Click on “Find Peaks” on the Find Peaks tool bar.
8. Click on the “Peaks” button on the left side of the window.
9. An Edit Peaks window will appear with all peaks listed with their position, height, and FWHM.
10. If the peaks position or FWHM need to be adjusted, constrained, or fixed, double click on the peak.
11. A new Edit Peak window appears, in this window the peak shape can be adjusted, and all of the parameters can be adjusted, constrained, or fixed by clicking on the boxes and inputting adjustments and containments.

12. Close the Edit Peak window for a single peak by right clicking “Ok.”
13. Close the Edit Peak window for all peaks by right clicking “Ok.”
14. Click on “Fit Peaks” located on the right side of the window in the Fit Peaks tool bar.
15. If peak positions or other peak parameters are unacceptable, adjust the peaks by following steps 8 through 14.
16. Once fitting is acceptable, print the fitted spectrum by clicking on “Print” on the left side of the window.
17. Click on “Peaks” and in the Edit Peaks window, click on “Clipboard.”
18. Open and Excel window and paste the peaks parameters into that window.
19. Repeat for all spectrum of interest.

A.6 Contact Angle

Analysis was run on a Krüss EasyDrop DSA100 using Drop Shape Analysis software for Windows (DSA version 1.90.0.14, copyright 1997-2003, Krüss).

A.6.1. Level Instrument

Periodically the instrument needs to be checked for level.

1. Find a small level
2. Put the level where the sample would be placed
3. Adjust the feet of the EasyDrop to obtain level.
4. Rotate the level in multiple directions to ensure the EasyDrop is completely level.

A.6.2. Installing the syringe and needle

1. Find one of the Hamilton syringe and attach either a red needle for sessile drops or a green needle for pendent drops.
2. Flush the needle several times with the fluid that will be used to make drops.
3. Fill the needle.
4. Open Drop Shape Analysis software.
5. Go to the DSA Device Control Panel and the “Dosing” tab
6. Set the dosing control to continous with the button that has “Contin” on it.
7. Adjust the position of the plunger holder up or down using the dosing controls up and down arrows (the arrows are reversed to the direction that the plunger moves).
8. Once plunger holder is in the correct position, put the syringe into the syringe holder and the plunger into the plunger holder, carefully.
9. Using the dosing control, depress the plunger until fluid comes out the needle.

A.6.3. Static Contact Angle

Before running experimental samples, the below procedure should be done with HPLC water on standards (PTFE, LDPE, EAA, PGFE).

1. Place sample on sample stage.
2. Use environmental chamber if elevated temperatures are needed.
    a. Remove sample stage cover
    b. Put environmental chamber on stage with windows facing the camera and light.
    c. Set temperature of chamber using recirculation bath.
3. Open Drop Shape Analysis software.
4. Go to file menu and open “FG window.”

5. Click on the “Live Video Feed” button (10th button from the right, picture of video camera on button)
6. Increase illumination strength by going to the DSA device control panel and “Imaging” tab.
7. Increase illumination strength to 32.
8. Zoom the camera out by spinning the zoom on the camera to 0.7.
9. Loosen thumb screw on backside of syringe holder to lower needle into frame.
10. Tighten the thumb screw once needle is in frame.
11. Go to DSA device control panel and the “Dosing” tab.
12. Set dosing method to “Volume” and set volume to 5 µL.
13. Press the up area to dispense 5 µL of fluid.
14. Using the z-direction dial on the sample holder, slowly raise the sample until it just touches the drop.
15. Lower the sample platform using the z-direction dial.
16. Zoom on the sample using the zoom dial on the camera until the drop almost fills the FG window feed.
17. Focus on the drop using the camera’s focus.
18. Take a still of the drop using the “Snap” button on the tool bar (9th button from the right, has a picture of a camera on the button).
19. Right click on the FG window, go to drop type, and click on “Sessile Drop.”
20. Right click on the FG window, go to drop subtype, and click on “Normal Sessile Drop.”
21. Right click on FG window and make sure “Auto Detect Substrate” is unchecked.
22. Right click on the FG window, go to baseline type, and click on “Linear.”

23. Click on the baseline shown in FG window, adjust up and down using up and down arrow keys, and adjust tile using left and right arrow keys. The baseline should intersect the drop where the drop meets the substrate.
24. Go to file menu and open “Result Window.”
25. Right click on FG window, go to contact angle using, and select appropriate fitting method.
26. Highlight results and copy.
27. Paste into excel file.
28. Right click on FG window and save picture of drop.

A.7. Simultaneous Thermogravimetric Analysis and Differential Scanning Calorimetry (SDT)

Analysis was performed on a TA Instruments SDT Q600 using Advantage for Q series (Version 2.8.0.394, Thermal Advantage Release 5.1.2, copyright 2001-2009, TA Instruments-Waters LLC) and analysis was performed on TA Instruments Universal Analysis 2000 software for Windows 2000/XP/Vista (version 4.7A, build 4.7.0.2, copyright 1998-2009, TA Instruments-Waters LLC).

1. Open furnace by going to control panel on SDT, press furnace button, set to open, and hit apply.
2. Take two Pt pans and, carefully, put on cantilever balance. The rear pan is a reference and front pan is for the sample.
3. Close the furnace using the SDT control panel.
4. Open Q600 SDY controller by clicking on the Q600 SDT icon in the TA Instrument Explorer window.

5. Tare the weight of the pans by clicking on the tare button that looks like an old fashion counter weight balance button on the top tool bar.
6. Open the furnace using the SDT control panel.
7. Remove the front Pt pan.
8. Put it on the balance and tare the weight.
9. Weigh out ~5 mg of sample into pan.
10. Put the sample Pt pan back onto cantilever balance.
11. Close the furnace.
12. In the middle section, click on the summary tab.
13. Under Procedure Summary, set mode to SDT Standard and Test to Ramp.
14. In Sample Information, enter a sample name, Pan type to PT, enter any additional comments, set the data file name, and check network drive.
15. Go to the Procedure tab.
16. Under method, check Use Current.
17. Set final temperature to 300 ^{o}C.
18. Next add Ramp at 5 ^{o}C/min.
19. Go to Notes tab
20. Set Mass Flow Control Settings to #1-Nitrogen and a flow rate of 50 mL/min.
21. Click run in the upper left hand corner.

A.8. Modulated Differential Scanning Calorimetry (DSC)

Analysis was performed on a TA Instruments DSC Q2000 using Advantage for Q series (Version 2.8.0.394, Thermal Advantage Release 5.1.2, copyright 2001-2009, TA Instruments-Waters LLC) and analysis was performed on TA Instruments Universal Analysis 2000 software for

Windows 2000/XP/Vista (version 4.7A, build 4.7.0.2, copyright 1998-2009, TA Instruments-Waters LLC).

1. Weigh a T-Zero pan and lid.
2. Weigh out 5 mg of sample.
3. Put sample into T-Zero pan and put lid on pan.
4. Put the Black T-Zero cupped die into the upper part of the press.
5. Put the pan with sample and lid into the Black T-Zero lower die.
6. Put die into press.
7. Press the pan to seal pan.
8. Put pan into auto sampler of DSC
9. Open Q2000 DSC controller by clicking on the Q2000 DSC icon in the TA Instrument Explorer window.
10. In the middle section, click on the summary tab.
11. Under Procedure Summary, set mode to Standard and Test to Custom.
12. In Sample Information, enter a sample name, enter the pan number (position in auto sampler), set Pan type to Tzero Aluminum, check pan mass, enter a sample size and pan mass, enter any additional comments, set the data file name, and check network drive.
13. Go to the Procedure tab.
14. Under method, click on editor.
15. Add equilibrate at -90 ^{o}C
16. Next add Data storage On.
17. Next add Ramp at 5 ^{o}C/min to 220 ^{o}C.
18. Finally add Data storage Off.
19. Go to Notes tab

20. Set Mass Flow Control Settings to #1-Nitrogen and a flow rate of 50 mL/min.
21. To add another sample repeat steps 1-8, then append a new run in the left most window, and repeat steps 12 – 18.
22. Click run in the upper left hand corner.

A.9. Nuclear Magnetic Resonance

On a Buckner 300 NMR with Topspin 2.0 using deuterated chloroform.

A.9.1. Sample Preparation

1. Weigh out 5 mg of sample.
2. Put into NMR tube.
3. Fill tube 3/4th full with deuterated chloroform.
4. Let it dissolve for 24 h.
5. If it does not dissolve, sonicate for 4 h.

A.9.2. NMR Procedure

1. Left click on username and type the password for account (dependent on user)
2. Click on TOPSPIN 2.0
3. In pink command line, type ej and hit enter to eject sample holder.
4. Insert sample into sample holder.
5. Type ij to inject sample holder.
6. Type edc and hit enter to make new file.
7. Enter sample name and click ok.
8. Type rpar and hit enter.

9. Click on parameter set to select proton or other type of NMR.
10. Left click on copy all.
11. Type gpro and press enter and wait for program to finish.
12. Type lock and press enter.
13. Chose the deuterated chloroform from solvent list and click ok.
14. Type ii and press enter and wait for program to finish.
15. Type rsh and press enter.
16. Click on most recent set of shim data.
17. Type ns 1 and press enter.
18. Type rga and enter.
19. Type zg and enter and wait for acquisition to finish.
20. Type efp for spectrum to appear.
21. Type apk for automatic phase and data quality analysis
22. If data looks bad, click on BSMS control window and click on the shim tab.
23. Shim Z1, Z2, X, and Y.
24. Type zg.
25. Type efp and ensure line ship is better.
26. Type ns and enter the number of scans, which have to be a multiple of 8.
27. Type zg and hit enter.
28. Wait for acquisition to be completed.
29. Type efp.
30. Type apk.
31. Data acquisition is complete and saved. Insert new sample at this time or reinsert standard.

32. Reinsert standard.
33. Click file.
34. Click exit.
35. Click exit and hit ok,
36. Click on start and log off.

A.10. X-Ray Photoelectron Spectroscopy

This procedure is to be used for PHI 1600 ESCA with Perkin-Elmer dual anode source x-ray source, 04-548, Perkin-Elmer Omni III lens, 72-366S, Perkin-Elmer ion pump, Perkin-Elmer specimen manipulator, 10-325, Perkin-Elmer instrument console, 40-710, Perkin-Elmer dual x-ray source control, 32-096, Perkin-Elmer x-ray supply, 20-040, Perkin-Elmer DGC III digital gauge controller, and Perkin-Elmer spherical capacitor energy analyzer, 10-360, with PHI Surface Analysis Software for windows version 3.0 copyright 1994 Physical electronics Inc.

A.10.1. Sample preparation

1. Sample needs to be put under vacuum for an extended period of time to remove all solvents and volatiles from the sample.
2. If the sample is a polymer film or Si wafer, mount sample on sample puck using copper hold downs.
3. If sample is a powder, compress sample into a small disk and use sample covers to hold sample in place.
4. If sample is too small to use sample covers or hold downs, copper or carbon tape can be use to hold sample in place, but this is not recommended.

A.10.2. Sample loading into XPS main chamber

1. On sample entry chamber, close red and black valves.
2. Open green valve to bring chamber to atmospheric pressure.
3. Remove cover from sample entry chamber.
4. Using puck tongs, place sample puck into sample holder.
5. Replace cover and ensure it is seated properly.
6. Close green valve.
7. Turn on main roughing pump that is connected to the black valve.
8. Open black valve.
9. Using the Varian Multi Gauge on the right side of the XPS, pump the entry chamber to 2 x 10^{-2} Torr.
10. Once 2 x 10^{-2} Torr is reached, close black valve and open red valve.
11. Pump down entry chamber to 1 x 10^{-4} Torr and then wait 1 h.
12. After pumping down entry chamber, open gate valve separating entry chamber and main chamber of the XPS.
13. If main chamber increases above 1 x 10^{-7} Torr (seen on the Perkin-Elmer Digital Gauge Control III), immediately close gate valve and continue to pump down entry chamber. Otherwise proceed with steps below.
14. Slide the sample over sample hold in main chamber.
15. Align main chamber sample holder using X and Y controls on the right side of XPS main chamber.
16. Raise main chamber sample holder using Z control on the right side of the XPS main chamber.
17. Remove sample holding arm from main chamber by sliding it out.

18. Close gate valve.
19. Allow pressure in main chamber to go below 9 x 10^{-9} Torr before attempting to turn on X-ray beam.

A.10.3. Starting X-ray source

If at any time during the following procedure the pressure increases above 5 x 10^{-8} Torr, the XPS will interlock fault, and the procedure has to be restarted from the beginning.

1. Turn on the heat exchanger on the far right side of the XPS.
2. Turn on the power to the X-ray supply (bottom panel on right side of XPS).
3. Turn on the power to the X-ray source control (top panel on right side of XPS).
4. On the X-ray source control, select source 1 and switch to Int.
5. On the X-ray source control, under filament energize, push Mg button.
6. On the X-ray source control, under parameter display/control, push HV button.
7. Press large, red, high voltage button on X-ray source control panel.
8. On the X-ray supply panel, turn the high voltage control until the parameter display/control on the X-ray source control reads 0.5 kV.
9. Continue increasing voltage by 0.5 kV every 1 to 2 min until 8 kV is reached.
10. Once 8 kV is reached, increase voltage by 0.1 kV every 1 to 2 min until 8.5 kV is reached. At 8.3 kV, the instrument has reached a high enough voltage as to cause instant death if an electrical component is touched.
11. At 8.5 kV, increase voltage by 0.5 kV every 1 to 2 min until 12 kV is reached and stop increasing voltage.

12. On the X-ray source control panel, under parameter display/control, push the Mg button to bring display the current power.
13. Using the up and down arrows under the parameter display/control, increase the power by 1 W every 1 to 2 min until 8 W is achieved and the X-ray source is now active.
14. At 8 W, let the instrument rest for 5 min to allow the X-ray source to achieve equilibrium.
15. After 5 min, increase power by 1 W every 1 to 2 min until 12 W is achieved.
16. Once 12 W is achieved, increase power to 25 W and every 1 to 2 min increase by 25 W until 200 W is achieved.
17. Under parameter display/control on the X-ray source control panel, push the HV button.
18. Increase voltage by 0.5 kV until 15 kV is achieved, and the system is now at maximum working voltage.
19. Under parameter display/control on the X-ray source control panel, push the Mg button.
20. Increase power by 25 W every 1 to 2 min until 300 W is achieved.
21. X-ray source is now at working power and voltage, push the card rack power button the power control panel on the left side of the instrument.
22. Turn on Fostec light (white box on XPS desk).
23. Using the built in 10X microscope, using X, Y, and Z control bring the area of interest on the sample into focus.
24. Open PHI CMA XPS software on the computer.
25. Go to file menu and select dir.
26. Select directory and input a 5 character sample name.
27. Click ok.

28. Go to Acquire on the menu bar and select survey.
29. Specify upper binding energy and range (normally upper binding energy is 1100 eV and range is 1100 eV).
30. Set step size to 0.5 eV, time/step to 10 ms, and 10 repeats.
31. Got Execution on menu bar and select start acquisition.
32. Once data acquisition is complete, got to file menu and save file as ASCII.
33. Go to Acquire on the menu bar and select Multiplex.
34. Add regions such as C1, O1, and Si1 in reference to the chemical elements of interest from survey scan for high resolution scan. Adjust regions range as needed.
35. Set step size to 0.2 eV, time/step to 50 ms, and repeats to 15.
36. Got Execution on menu bar and select start acquisition.
37. Once data acquisition is complete, got to file menu and save file as ASCII.
38. Repeat steps 22-37 for additional spots and samples.
39. To turn off instrument, on the X-ray source control panel, switch Int switch to Ext.
40. Under parameter display/control on the X-ray source control panel, push HV button.
41. On the X-ray supply panel, turn the high voltage control left until 0 kV is read off of X-ray source control.
42. X-ray source is now off; push the card rack power button the power control panel on the left side of the instrument.
43. Turn off the X-ray source control, X-ray supply, and heat exchanger.
44. Open the gate valve between the entry chamber and the main chamber and remove the sample.
45. Using a Fat 16 formatted flash drive, transfer files to flash drive to analyze on CasaXPS.

A.10.4. Sudden loss of ion pump during operation

1. To turn off instrument
2. On the X-ray source control panel, switch Int switch to Ext.
3. Under parameter display/control on the X-ray source control panel, push HV button.
4. On the X-ray supply panel, turn the high voltage control left until 0 kV is read off of X-ray source control.
5. X-ray source is now off; push the card rack power button on the power control panel on the left side of the instrument.
6. Turn off the X-ray source control, X-ray supply, and heat exchanger.
7. Push the electronics power button on the power control panel to turn off the electronics.
8. Turn ion pump to off on the ion pump control panel (left side of instrument, bottom panel).
9. Push main power on/reset on power control panel.
10. Push the electronics power button on the power control panel to turn on the electronics.
11. On the digital gauge control III panel on the right side of the XPS, push 1 and then 3.
12. If pressure is above 5×10^{-5} Torr, open the gate valve to the sample entry chamber and remove the sample out of the main chamber.
13. Then use the turbo pump to pump down the main chamber with the gate valve open.
14. Once 5×10^{-5} Torr is reached, close the gate valve and follow the steps below.
15. Turn the ion pump to start on the ion pump control panel and wait 2 min.
16. Turn the ion pump to run on the ion pump control.

A.10.5. Analysis with CasaXPS

This procedure is to be used with CasaXPS version 2.2.88, copyright 1999-2004 Neal Fairley.

1. Start CasaXPS software.
2. Under file menu, click on “Convert and Merge.”
3. Select survey and high resolution scans to be analyzed.

For Survey Spectrum

4. Open “Element Library” by pressing F10.
5. Go to “Periodic Table” tab in element library window.
6. Select elements in the spectrum or click find peaks in periodic table tab.
7. Click on create regions in periodic table tab.
8. Open “Quantification Parameters” by pressing F7.
9. Under the “Regions” tab in the quantification parameters window, adjust R.S.F. to values for PHI 1600 XPS found in Moulder, J. F., Stickle, W. F., Sobol, P. E., Bomben, K. D., Handbook of X-Ray Photoelectron Spectroscopy, Perkin-Elmer Corporation, Eden Prairie, MN, 1992, 253.
10. Adjust regions on spectrum to each element.

For High Resolution Spectrum

11. For high resolution scans, open “Quantification Parameters” by pressing F7.
12. Click on create in the quantification parameters’ “Regions” tab.
13. Under the regions tab in the quantification parameters window, adjust R.S.F. to values for PHI 1600 XPS found in Moulder, J. F., Stickle, W. F., Sobol, P. E., Bomben, K. D., Handbook of X-Ray Photoelectron Spectroscopy, Perkin-Elmer Corporation, Eden Prairie, MN, 1992, 253.
14. Adjust region on spectrum for to include the peaks for the element.

15. Click on the “Components” tab in the quantification parameters window.
16. Click on create to “Create” peaks under spectrum peak.
17. Unclick “Use RMS” under components tab.
18. Click on “Fit Components” button until Chi^2 does not change.
19. If the peaks full width, half max (FWHM) differ by more than 10%, constrain them by editing the fwhm Constr. cells and adjust the fwhm cells, normally to 1.5-1.8 or 1.6-2.0, to values that fall within the FWHM constraints.
20. If peaks are within 0.8 eV, either reduce the number of peaks present or constrain the peaks position by editing Pos. Constr. cells and adjust peak positions to fall within constraints.
21. Repeat fitting components, step 18, if steps 19 and/or 20 were followed.
22. Open “Processing” by pressing F8.
23. Go to “Smoothing” tab in spectrum processing window.
24. Click on apply 3 times (or more if necessary, peaks may be loss if repeated too many times).
25. Go to quantification parameters’ “Components” tab and repeat step 18.
26. Peaks may need to be added or subtracted at this point based on fitting and literature values.
27. Repeat steps 19 through 25 until a reasonable fit is achieved based on literature and Chi^2.
28. Once an acceptable peak fitting is achieved, the spectrum may need to shifted to allow C 1s C-C/C-H peak to fall at 285 eV.
29. Shift the peaks by going to spectrum processing window’s “Calibration” tab.
30. Put in measured value of reference peak and correct position of peak.

31. Under adjust in the same tab, check both “Regions” and “Components.”

32. Click apply.

33. Record peak positions, FWHM, and area.

APPENDIX B

EXAMINATION OF STANNOUS OCTOATE AS A CATALYST

B.1. Introduction

An alternative (non-metal halide) catalyst was attempted for poly(trimethylene malonate) (PTM) and poly(trimethylene itaconate) (PTI) for comparative purposes. Stannous octoate has been extensively researched and has been used in the production of poly(lactic acid) and poly(glycolic acid) [Okada 2002, Jerome 2008, Sun 2002, Church 2003, Helminen 2003, John 1996, Storey 2001, Teramoto 2004]. PTM and PTI were polymerized with stannous octoate at 4 and 16 h, respectively, with the following reaction conditions: 155 °C, 1:100 catalyst:monomer molar ratio, 1:1 acid:alcohol molar ratio, vacuum, and stirring.

B.2. Experimental Materials and Methods

Reagents. 1,3-Propane diol (PDO, 98%, Sigma Aldrich), itaconic acid (IA, 99%, VWR), tetrahydrofuran (Fisher Scientific, Optima grade, +99.9%), stannous octoate (VWR, 99%), chloroform (VWR, 98%), and diethyl ether (VWR, >99%) were used as received.

Polymerization

Copolymerization of 1,3-propanediol (PDO), malonic acid (MA), and itaconic acid (IA). The melt polycondensation of 1,3-propanediol (PDO) and malonic acid (MA) to form PTM and ,3-propanediol (PDO) and itaconic acid (IA) to form PTI were performed in a 100 mL round bottom flask (charged with ~ 50 g monomer) for 4 h (PTM) and 16 h (PTI) at 155 °C and 25 torr with mixing using a magnetic stir bar. Stannous octoate was used as the catalyst and an initial 1:100 catalyst:monomer molar ratio was utilized for all reactions.

Polymer separation. To remove the catalyst and excess monomer, at room temperature the reaction products were dissolved in chloroform and then poured into diethyl ether. Precipitated polymer was then filtered using Whitman (grade 40) filter paper. For each reaction, this separation procedure was repeated until precipitated polymer could no longer be visually

detected on the filter surface. The filtered polymer was dried in a vacuum oven at 15 torr and 20 °C for 24 h and then weighed.

Characterization

The polymers were characterized by transmission FTIR spectroscopy using a Thermo Electron 6700 instrument purged with dry air. Samples were either smeared or solution cased with THF onto potassium bromide crystals. Gravimetric product yields were calculated using the limiting monomer to determine theoretical yields based on complete conversion. The recovered polymer weight was divided by the theoretical weight and then converted to percent yield. A Waters gel permeation chromatograph (GPC) with RI detector, 4E and 5E (polystyrene-divinylbenzene, 4.6 x 300 mm) Styragel® columns, 0.3 mL/min THF effluent, and a 10-point polystyrene calibration was used to determine molecular weights and polydispersities.

B.3. Results and Discussion

PTM and PTI polymerized with stannous octoate had gravimetric yields significantly lower than PTM and PTI polymerized using aluminum chloride (detailed in Chapters 2 and 3). Using stannous octoate, the gravimetric yields were 21.2 ±1.3 wt.% for PTM, and 26.6 ±2.1 wt.% for PTI. At the same reaction conditions, when aluminum chloride was used as the catalyst, PTM and PTI had gravimetric yields of approximately 75 and 77 wt.%, respectively. So, stannous octoate was not able to achieve gravimetric yields comparable to aluminum chloride for PTM and PTI under the same reaction conditions.

The chemical structure of PTM and PTI polymerized with stannous octoate was examined using transmission FTIR spectroscopy. Representative spectra are shown in Figure B.1. The spectra have noticeable differences from PTM and PTI polymerized with aluminum chloride (see Chapters 2 and 3 for details). Spectral differences in the carbonyl region, 1500 to

1900 cm^{-1}, were the most interesting and so the carbonyl region for PTM and PTI was peak fit to identify and quantify individual peaks.

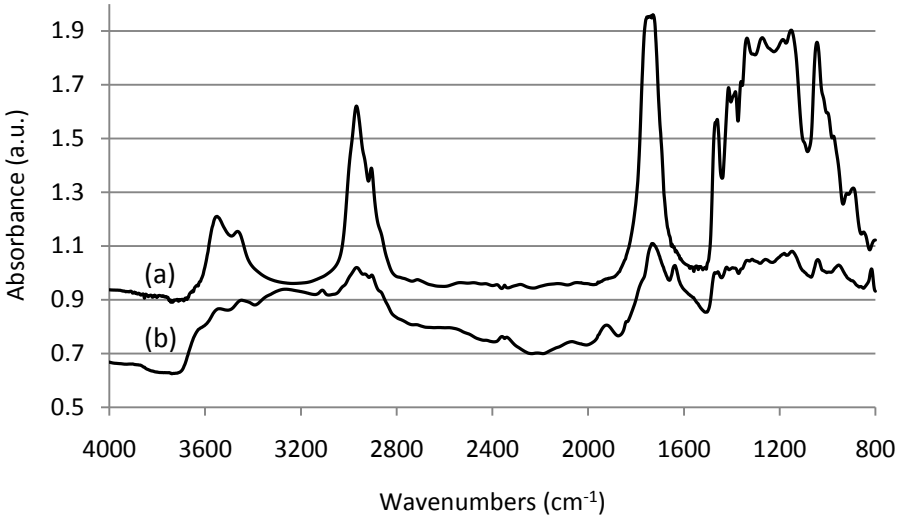

Figure B.1: Transmission FTIR spectra for (a) PTM (155 °C, 4 h) and (b) PTI (155 °C, 16 h) using stannous octoate as the catalyst.

For PTM, four major peaks of interest were identified: 1702 cm^{-1}, carboxylic acid carbonyl stretch; 1726 cm^{-1}, high Mw ester carbonyl stretch; 1749 cm^{-1}, low Mw ester carbonyl stretch; 1753 cm^{-1}, cyclic ester carbonyl stretch (Figure B.2). Two additional peaks were also identified for a trans- or tri/quad-substituted alkene C=C stretch (1675 cm^{-1}) and vinylidine stretch (1640 cm^{-1}). PTM monomers do not contain unsaturated bonds, and it is not known how alkene bonds were formed. Peak height ratio (PHR) values were calculated for PTM polymerized with stannous octoate, and these PHR values were significantly lower than PTM polymerized with aluminum chloride. The two major ester carbonyl peaks, 1726 and 1749 cm^{-1}, had PHRs of 1.8 ±0.2 and 2.1 ±0.3, respectively, that were significantly lower than PTM polymerized with aluminum chloride (~3.7 and ~4.5 PHRs).

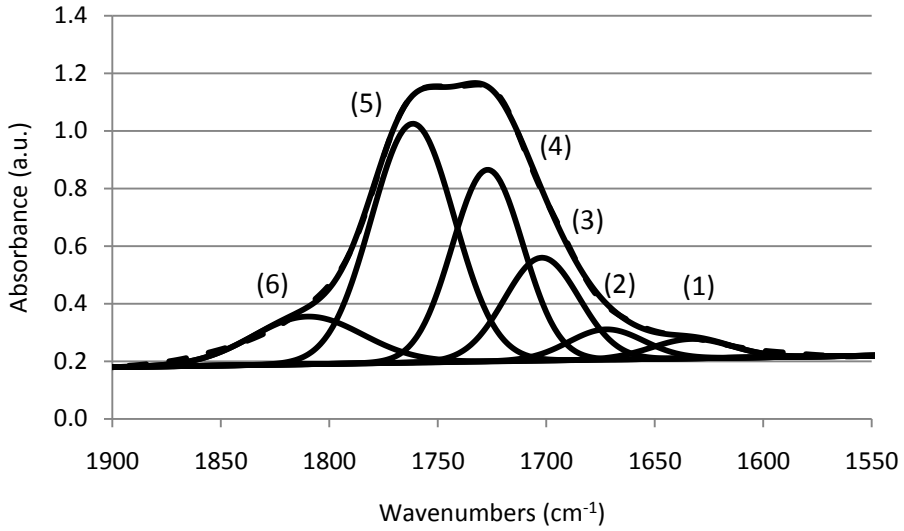

Figure B.2: Transmission FTIR spectrum from 1820 cm^{-1} to 1650 cm^{-1} for PTM polymerized with stannous octoate. Peak fitting (standard error of composite spectrum to experimental spectrum, 4.36) revealed six peaks: (1) 1640 cm^{-1}, vinylidine C=C stretch; (2) 1675 cm^{-1}, trans-, tri-, or quad-substituted alkenes stretch; (3) 1702 cm^{-1}, carboxylic acid carbonyl stretch; (4) 1726 cm^{-1}, high Mw ester carbonyl stretch; (5) 1749 cm^{-1}, low Mw ester carbonyl stretch; (6) 1753 cm^{-1}, cyclic ester carbonyl stretch.

For PTI, six peaks were identified in the carbonyl region (Figure B.3): 1587 cm^{-1}, carboxylate anion carbonyl stretch; 1639 cm^{-1}, vinylidine stretch; 1704 cm^{-1}, dimerized carboxylic acid carbonyl stretch; 1744 cm^{-1}, ester carbonyl stretch; 1786 cm^{-1}, cyclic anhydride carbonyl symmetric stretch; 1822 cm^{-1}, cyclic anhydride carbonyl asymmetric stretch. PTI made with stannous octoate and aluminum chloride had these same carbonyl peaks. However, the ester carbonyl PHR at 1744 cm^{-1} decreased from 3.8 ±0.2 to 1.5 ±0.2 when changing from alumunium chloride to stannous octoate. This demonstrates a lower ester concentration in PTM produced using stannous octoate versus aluminum chloride. The vinyldine PHR for stannous octoate has a significantly greater PHR (1.7 ±0.2) than aluminum chloride (1.3 ±0.1). There is evidently greater vinyldine saturation (via Ordelt saturation) with aluminum chloride; therefore, more branching is expected in PTM polymerized with aluminum chloride than stannous octoate.

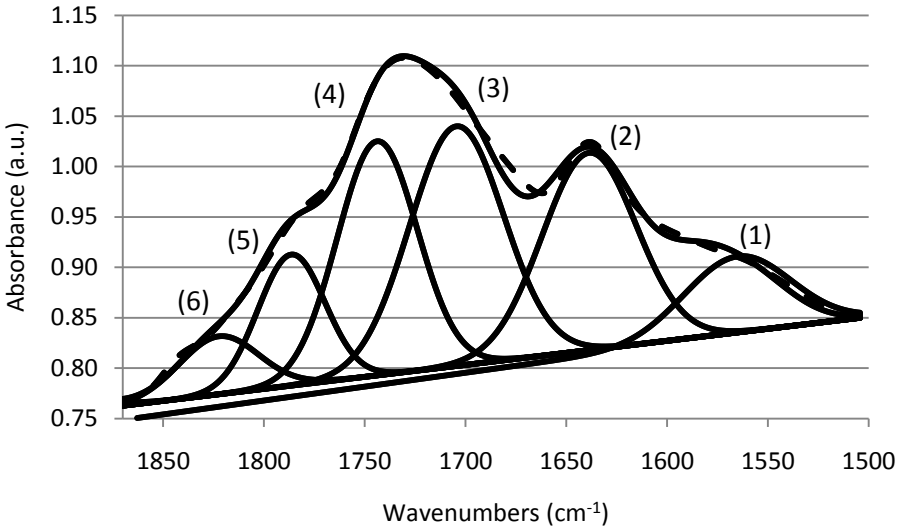

Figure B.3: Representative DRIFT spectrum from 1520 to 1860 cm^{-1} for PTI polymerized with stannous octoate. Peak fitting (standard error 3.21) revealed 6 peaks: 1587 cm^{-1} carboxylate anion carbonyl stretch (1), 1639 cm^{-1} vinylidine stretch (2), 1704 cm^{-1} dimerized carboxylic acid carbonyl stretch (3), 1744 cm^{-1} ester carbonyl stretch (4), 1786 cm^{-1} cyclic anhydride carbonyl symmetric stretch (5), and 1822 cm^{-1} cyclic anhydride carbonyl asymmetric stretch (6).

GPC was used to determine the molecular weight (Mw) and polydispersity index (PDI) for PTM and PTI polymerized with stannous octoate. The Mw for PTM produced with stannous octoate was 1,388 ±42 Da, which was the same as PTM polymerized with aluminum chloride (~1,400 Da and ~37,000 Da). PTM polymerized with aluminum chloride had a bi-modal weight distribution, but when stannous octoate was used only a single mode was found. PTI produced with stannous octoate did show a bi-modal Mw distribution (13,223 ±1468 Da and 3,076 ±146 Da). The lower PTI Mw was 3X that of aluminum chloride (~1,000 Da), and the higher PTI Mw was less than half that of aluminum chloride (~37,000 Da). Stannous octoate was not able to did facilitate the chain-growth polycondensation mechanism for PTM. For PTI, stannous octoate increased the Mw of the lower Mw fraction and decreased Mw for the higher Mw fraction when compared to PTI polymerized with aluminum chloride.

PTI polymerized with stannous octoate had a Mw of ~3,000 Da for the lower Mw faction, which accounts more than 95 wt.% of PTI and is 3X greater than PTI polymerized with aluminum chloride. It would be expected that PTI polymerized with stannous octoate would be hard, brittle material like PTI polymerized with aluminum chloride final product. PTI polymerized with stannous octoate was a waxy solid, which was unexpected. Differences in the physical appearance of the two PTI materials may be due to differences in the branching and cross-linking densities, and could be determined using solid state NMR or small angle neutron scattering. Even though PTI polymerized with stannous octoate had a higher Mw, it had a lower effective Mw that PTI polymerized with aluminum chloride due to a reduction in branching and cross-linking as shown by the increase in vinyldine PHR with FTIR.

B.4. Conclusions

For PTM and PTI polymerizations, stannous octoate was not as effective as a catalyst as aluminum chloride based on gravimetric yield and FTIR. For both polymers, gravimetric yields with stannous octoate were approximately a third of those obtained when using aluminum chloride. The ester concentration, important in hydrolytic degradation, was found to be reduced by half for both PTI and PTM in the polymers formed using stannous octoate.

B.5. Recommendations for Future Work

PTM and PTI polymerizations using heterogeneous or supported catalyst should be attempted. Polycondensation in solvents, such as ionic liquids, is another route to high molecular weight polymers and should be attempted with PTM and PTI to increase their Mw.

B.6. References

Catiker, E., Gumusderelioglu, M., Guner, A., "Degradation of PLA, PLGA homo- and Copolymers in the Presence of Serum Albumin: A Spectroscopic Investigation," Polymer International, 49, 728-734, 2000.

Church, A. C., Smith, J. A., Pawlow, J. H., Wagener, K. B., "Nontraditional Step-Growth Polymerization: ADMET," in Synthetic Methods in Step-Growth Polymers, John Wiley & Sons, New York, 431-526, 2003.

Dean, J. A., Lange's Handbook of Chemistry, 14th ed., McGraw-Hill, Inc., 7.42-7.71, 1992.

Dell'Erba, R., Martuscelli, E., Musto, P., Ragosta, G., "Unsaturated Polyester Resins: a Study of the Mechanism and kinetics of the Curing Process by FTIR Spectroscopy," Polymer Networks and Blends, 7(1), 1-11, 1997.

Gulmine, J. V., Akcelrud, L., "FTIR Characterization of Aged XLPE," Polymer Testing, 25, 932-942, 2006.

Helminen, A., O., Korhonen, H., Seppala, J.V., "Crosslinked Poly(ester anhydride)s Based on Poly(ε-caprolactone) and Polylactide Oligomers," Journal of Polymer Science: Part A: Polymer Chemistry, 41, 3788-3797, 2003.

Jerome, C., Lecomte, P., "Recent Advances in the Synthesis of Aliphatic Polyesters by Ring-Opening Polymerization," Advanced Drug Delivery Reviews, 60, 1056-1076, 2008.

John, G., Tsuda, S., Morita, M., "Synthesis and Modification of New Biodegradable Copolymer: Serine/Glycolic Acid Based Copolymers," Journal of Polymer Science Part A: Polymer Chemistry, 35(10), 1901-1907, 1996.

Okada, M., "Chemical Synthesis of Biodegradable Polymers," Progress in Polymer Science, 27, 87-133, 2007.

Silverstein, R. M., Blassler, G., C., Morrill, T. C., Spectrometric Identification of Organic Compounds, 5th ed., John Wiley & Sons, Inc., Hoboken, NJ, 102-133, 1991.

Storey, R. F., Sherman, J. W., "Novel Synthesis of (Carboxylic Acid)-Telechelic Poly(ε-Caprolacton)," Polymer Preprints, 42(2), 2001.

Sun, J., Shi, W., Chen, D., Liang, C., "The Ring-Opening Polymerization of D,L-Lactide Catalyzed by New Complexes of Cu, Zn, Co, and Ni Schiff Base Derived from Salicylidene and L-Aspartic Acid," Journal of Applied Polymer Chemistry, 86, 3312-3315, 2002.

Sutton, d., Durand, R., Shuai, X., Gao, J., “Poly(D,L-Lactide-co-Glycolide)/Poly(Ethylenimine) Blend Matrix System for pH Sensitive Drug Delivery,” Journal of Applied Polymer Science, 100, 89-96, 2006.

Teramoto, N., Kogure, H., Kimura, Y., Shibata, M., “Thermal Properties and Biodegradability of the copolymers of L-Lactide, ε-Caprolactone, Ethylene Glycol Oligomer with Maleate Units and their Crosslinked Products,” Olymer, 45, 7927-7933, 2004.

Zhou, Y., Wy, G.-L., Zhou, R.-X., Liu, Z.-L., “Synthesis and Properties of Novel Aliphatic Poly(Carbonate-Esters)s,” European Polymer Journal, 45, 1868-1872, 2009.

APPENDIX C

COPOLYMER FROM GLYCEROL AND FUMARIC ACID

C.1. Introduction

Glycerol (GLY) and fumaric acid (FA) are both multi-functional monomers that are readily found in biomass, and they were reacted to form a novel bioplastic, poly(glycolic fumarate) (PGF). Glycerol is a tri-alcohol that is a by-product of bio-fuel production, and fumaric acid is a di-acid with a carbon double bond between the 2^{nd} and 3^{rd} carbon. The reaction of these two monomers under melt polycondensation conditions produces a highly branched and cross-linked polymer. Inherently the glycerol promotes branching with its tri-ol structure, and FA promotes branching though opening of the carbon double bond via Ordelt saturation [Brioude 2007, Zhange 2005, Chen2008]. Ordelt saturation is defined as the electrophilic addition of a hydroxyl group to a carbon double bond. Under acidic conditions, a double bond can be saturated by an alcohol group leading to polymer branching and possible formation of an infinite network [Fardet 1982-B, Zetterlund 2002]. The degree of saturation is dependent on the acidity, temperature, and alcohol concentration of the reaction mixture and can lead to a 10 to 20% reduction of the C-C double bonds under thermodynamically-controlled conditions [Fardet 1982-A, Fardet 1982-B, Zetterlund 2002]. In addition to Ordert saturation kinetics, the melt polycondensation of GLY and FA can follow four reaction pathways. The $A_{AC}1$ and $A_{AC}2$ mechanisms start with the acid and proceeding to an ester with the loss of a low Mw byproduct [Satachell 1992, Smith 2007, Bruckner 2002, Saunders 1976]. The $A_{AC}2$ mechanism is considered to be the dominant mechanism [Satachell 1992, Smith 2007, Bruckner 2002, Saunders 1976]. While the $A_{AL}1$ and $A_{AL}2$ mechanisms have been theorized, the $A_{AL}2$ mechanism has not been observed to occur during polycondensation reaction [Satachell 1992, Smith 2007, Bruckner 2002, Saunders 1976]. The $A_{AC}2$ and $A_{AL}1$ mechanisms dominate, and the $A_{AC}1$ and $A_{AL}2$ mechanisms occur to lesser degrees. Refer to Chapter 2 and 3 for further discussion of reaction mechanisms. GLY and FA were reacted under melt polycondensation conditions to produce a

highly branched and cross-linked polymer at a single reaction temperature, 155 °C, and time, 22 h, while examining variation in the alcohol (GLY) to acid (FA) monomer ratio.

C.2. Experimental Materials and Methods:

Reagents. Glycerol (GLY, 99%, Figure C.1) and chloroform (98%) were used as received from VWR. Fumaric acid (FA, 98%, Figure C.1), $AlCl_3$ (98%), and diethyl ether (>99%) were used as received from Sigma-Aldrich.

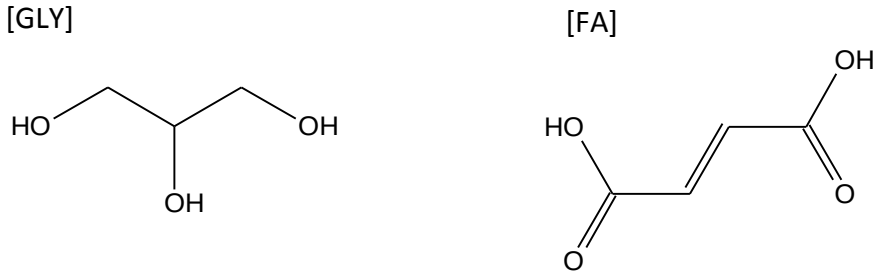

Figure C.1: Monomer chemical structures for glycerol (GLY) and fumaric acid (FA).

Copolymerization of glycerol (GLY) and fumaric acid (FA). The melt polycondensation of GLY and FA to form PGF was investigated using a 100 mL round bottom flask for 22 h at 155 °C and 25 torr with mixing using a magnetic stir bar. A charge of ~50 g monomer and an initial 100:1 M/C ratio was utlized for all reactions with the alcohol:acid molar ratio varied at 0.1:0.9, 0.25:0.75, 0.5:0.5, 0.75:0.25, and 0.9:0.1.

Polymer separation. Excess monomer and catalyst were removed from the reaction products at room temperature by dissolving in chloroform and then poured into diethyl ether to precipitate the polymer. For each reaction, precipitated polymer was filtered using Whitman (grade 40) filter paper. This separation procedure was repeated until precipitated polymer

could no longer be visually identified in the ether phase. The filtered polymer was dried in a vacuum oven at 15 torr and 20 °C for 24 h and weighed.

Characterization. A PHI 1600 Electron Scanning Chemical Analysis (ESCA) instrument with PHI 10-360 spherical detector and achromatic Mg K_α X-ray source (300 W, 15 kV) was used to gather additional information on the chemical composition and repeat unit structure. Survey and high resolution spectra were collected with PHI Surface Analysis software (v3.0, ©1994, Physical Electronics Inc.) and analyzed with CasaXPS software (v2.2.88). The C-H peak in the carbon high resolution scan was shifted to 285 eV as a standard reference. PGF was also characterized by attenuated total reflectance-Fourier transform infrared (ATR-FTIR) spectroscopy using a Thermo Electron 6700 instrument purged with dry air. A Pike VeeMax II accessory with a 60 ° zinc-selenide crystal was used for ATR-FTIR. Gravimetric product yields were calculated using the limiting monomer to determine theoretical yields based on complete conversion. The recovered polymer weight was divided by the theoretical weight and then converted to percent yield.

C.3. Results and Discussion

A series of PGF copolymers were produced at constant reaction conditions (155 °C for 22 h with vacuum and stirring) by changing the comonomer molar ratios. Alcohol molar fractions of 0.1, 0.25, 0.5, 0.75, and 0.9 were examined. Variation of alcohol molar fraction resulted in PGF with gravimetric yields of 90 wt.% and 98 wt.% for 0.75 to 0.25 alcohol monomer fractions (Figure C.2). These PGF copolymers were insoluble in common solvents as was expected due to the extensive branching and cross-linking. (No swelling of PGF was observed in toluene, dimethylfuran, tetrahydrofuran, dichloromethan, chloroform, acetone, methanol, and ethanol after X h.) FA has an easily accessible double bond allowing for Ordelt

saturation and therefore more extensive branching and cross-linking. The degree of branching and cross-linking could not be determined with available equipment MSU.

At 0.9 alcohol molar fraction the product was not a solid, but instead a liquid and indicates a low molecular weight product. At high alcohol content conditions, the reduced acidity of the reaction mixture and lack of carbon double bonds significantly reduced the formation of polymer branches and cross-links and resulted in a lower effective Mw. The product of the 0.1 GLY fraction reaction produced a solid with a gritty texture and that appeared to contain crystalline FA.

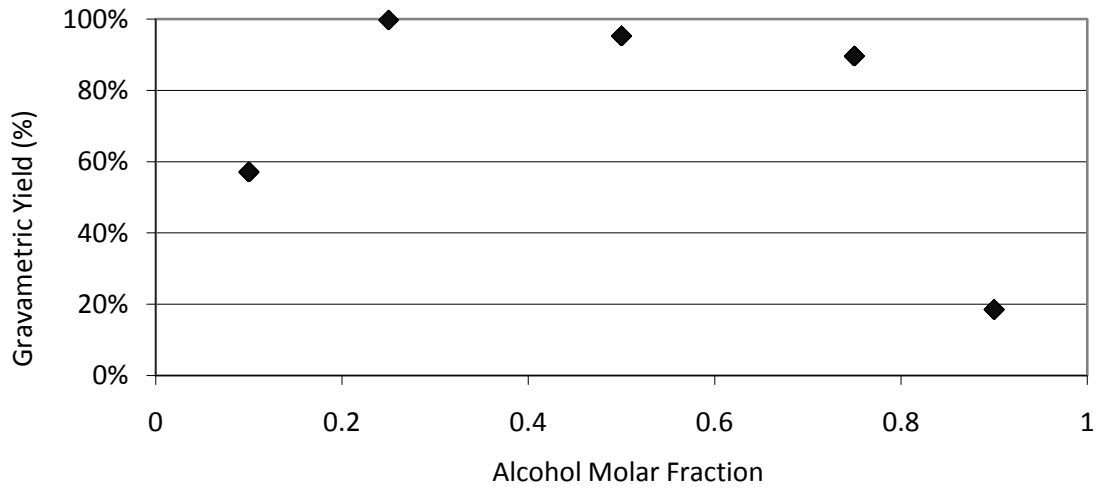

Figure C.2: Dependence of PGF gravimetric yield on alcohol molar fraction ($AlCl_3$ catalyst, 22 h, 155 °C). Plotted data represents single experiments.

PGF was examined using ATR-FTIR to determine the functional groups present. Figure C.3 shows the FTIR spectrum for PGF with 0.5 alcohol molar fraction. The peak at ~1720 cm^{-1} indicates the presence of carbonyl, Figure C.3. The carbonyl stretch region, 1580 to 1850 cm^{-1}, was further resolved by peak fitting to determine the types of carbonyls present, Figure C.4. Four peaks were identified: 1645 cm^{-1}, alkene stretch; 1695 cm^{-1}, dimerized carboxylic acid carbonyl stretch; 1729 cm^{-1}, ester carbonyl stretch [Dell'Erba 1997, Silverstein 1991, Dean 1992,

Caitker 2000, Sutton 2006, Gulmine 2006, Zhou 2009]; 1760 cm^{-1}, cyclic ester carbonyl stretch [Dell'Erba 1997, Silverstein 1991]. The FA carboxylate groups reacted with the GLY alcohol groups to preferentially form ester bonds through the $A_{AL}2$ and, $A_{AL}1$ mechanisms.

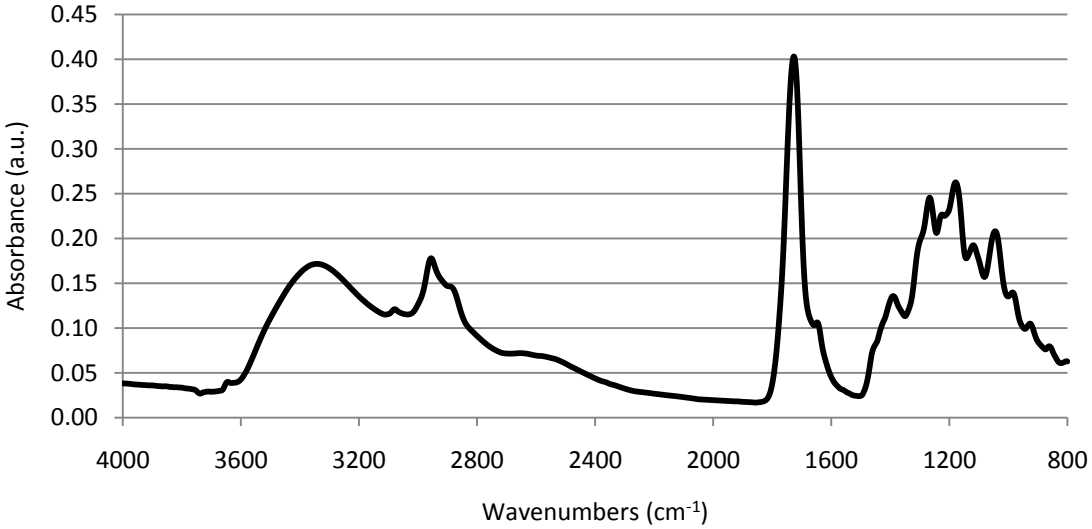

Figure C.3: Representative ATR-FTIR spectrum for PGF ($AlCl_3$, 22 h, 155 C, 1:1 acid:alcohol molar ratio).

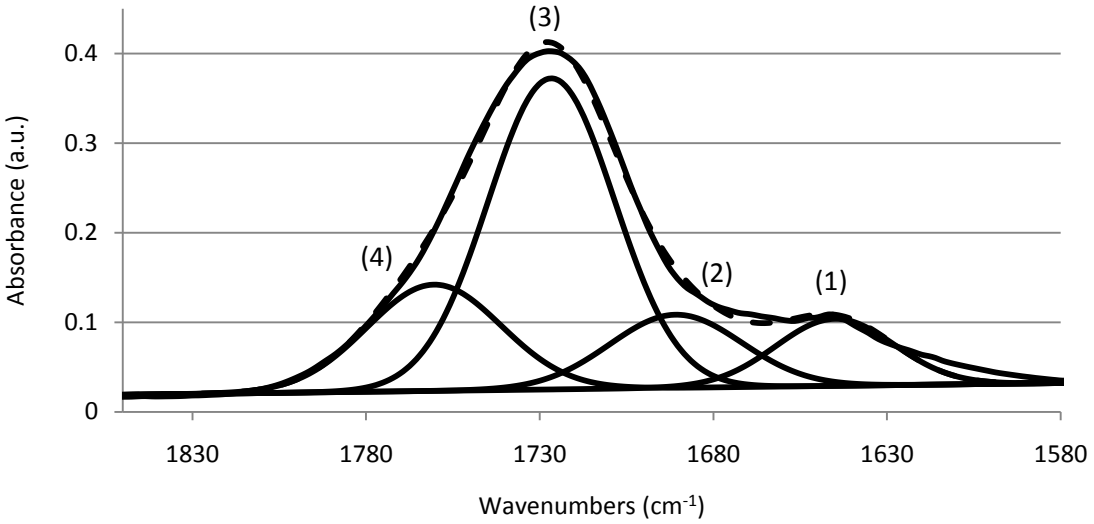

Figure C.4: Representative ATR-FTIR spectrum of PTM from 1850 cm^{-1} to 1580 cm^{-1} with peak fitting (standard error 4.10). Four major peaks of interest were identified: (1) 1645 cm^{-1}, alkene stretch, (2) 1695 cm^{-1}, dimerized carboxylic acid carbonyl stretch, (3) 1729 cm^{-1}, ester carbonyl stretch, and (4) 1760 cm^{-1}, cyclic ester carbonyl stretch. The dash line represents the composite curve of the fitted peaks

The PGF products were also characterized with XPS in order to provide additional insight into the chemical structure of PGF. Only oxygen and carbon were found in the survey scan of PGF (Table 1). The atomic composition of PGF was not statistically different than theoretical calculations based on carboxylate groups reacting only with alcohol groups through $A_{AC}2$ and $A_{AL}1$ mechanisms (Table C.1). From the close match between experimental and theoretical data, the PGF appears to be an alternating copolymer.

Table C.1: Theoretical and experimental carbon and oxygen atomic concentrations in PGF (22 h, $AlCl_3$, 155° C, 1:1 acid:alcohol ratio) as determined by XPS with 95% confidence intervals.

Atomic Percent	Theoretical	Experimental
Carbon	56.8 %	57.6 % ±1.2 %
Oxygen	43.2 %	42.4 % ±1.2 %

As is shown in Figure C.5, the C 1s high resolution peak was peak fit and contributions from C-H at 285 eV (~55 % area), C-O at 286.5 eV (~8 % area), and C=O at 289.2 eV (~37 % area) were identified [Sabbatini 1996, Louette 2006 69-73, Louette 2006 38-43, Cossement 2006, Nanse 1997]. C-O concentration (~8% area) was significantly lower than the theoretical predictions (30% area), and the C=O concentration (~37% area) was significantly higher than the theoretical predictions (20% area). It is unknown why the theoretical and experimental concentrations are different, and without data replication, few conclusions can be drawn.

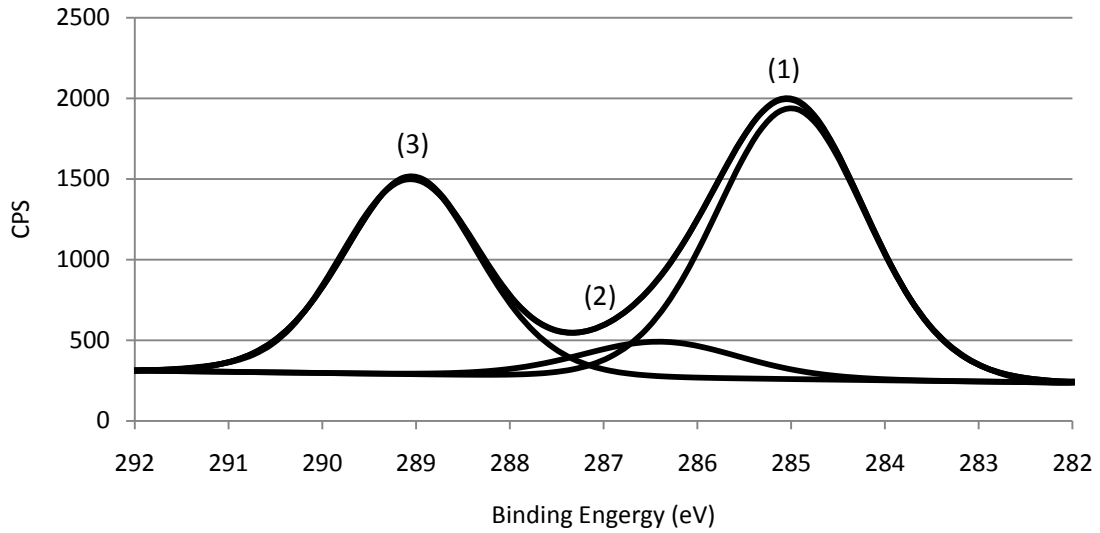

Figure C.5: High resolution XPS C 1s spectrum of PGF (22 h, $AlCl_3$, 155° C) with peaks identified as (1) C-H at 285 eV (~55 % area), (2) C-O at 286.5 eV (~8 % area), and (3) C=O at 289.2 eV (~37 % area). The original and composite peak spectra are shown, but they are indistinguishable.

C.4. Conclusions

PTG is a unsaturated, copolymer from GLY and FA with ester bonds in the backbone. The insolubility of PGF indicates it is likely a highly branched polymer. Transmission FTIR showed that alkene and ester bonds are present in PGF. GLY and FA were evidently added in a 1:1 molar ratio as demonstrated by the XPS atomic concentration of oxygen and carbon with C-H, C-O, and C=O the only function groups contained in PGF.

C.5. Recommended Future Work

Branching and cross-linking densities for PGF needs to be determined by solid-state NMR and small angle neutron scattering. The effects of reaction temperature and time on PGF studied to determine if the chemical structure can be controlled with alternative reaction conditions.

C.6. References

Brioude, M. d. M., Guimaraes, D. H., Fiuza, R. d. P., Prado, L. A. S. d. A., Boaventura, J. S., Jose, N. M., "Synthesis and Characterization of Aliphatic Polyesters from glycerol, by-Products of biodiesel Production, and Adipic Acid," Materials Research, 10(4), 335-339, 2007.

Catiker, E., Gumusderelioglu, M., Guner, A., "Degradation of PLA, PLGA homo- and Copolymers in the Presence of Serum Albumin: A Spectroscopic Investigation," Polymer International, 49, 728-734, 2000.

Chen, Q.-Z., Bismarck, A., Hansen, U., Junaid, S., Tran, M. X., Harding, S. E., Nadire, N. A., Boccaccini, A. r., "Characterization of a Soft Elastomer Poly(Glycerol Sebacate) Designed to Match the Mechanical Properties of Myocardial Tissue," Biomaterials, 29, 47-57, 2008.

Cossement, D., Gouttebaron, R., Cornet, V., Viville, P., Hecq, M., Lazzaroni, R., "PLA-PMMA blends: A Study by XPS and ToF-SIMS," Applied Surface Science, 252, 6636-6639, 2006.

Dean, J. A., Lange's Handbook of Chemistry, 14th ed., McGraw-Hill, Inc., 7.42-7.71, 1992.

Dell'Erba, R., Martuscelli, E., Musto, P., Ragosta, G., "Unsaturated Polyester Resins: a Study of the Mechanism and kinetics of the Curing Process by FTIR Spectroscopy," Polymer Networks and Blends, 7(1), 1-11, 1997.

Fradet, A., Marechal, E., "Kinetics and Mechanisms of Polyesterification I. Reactions of Diols with Acids," Advances in Polymer Science, 43, 51-142, 1982-A.

Fradet, A., Marechal, E., "Study on Models of Double Bond Saturation During the Synthesis of Unsaturated Polyesters," Makromolekulare Chemie, 183, 319-329, 1982-B.

Gulmine, J. V., Akcelrud, L., "FTIR Characterization of Aged XLPE," Polymer Testing, 25, 932-942, 2006.

Louette, P., Bodino, F., Pireaux, J.-J., "Poly(dimethyl siloxane) (PDMS) XPS Reference Core Level and Energy Loss Spectra," Surface Science Spectra, 12, 38-43, 2005.

Louette, P., Bodino, F., Pireaux, J.-J., "Poly(methyl methacrylate) (PMMA) XPS Reference Core Level and Energy Loss Spectra," Surface Science Spectra, 12, 69-73, 2005.

Nanse, G., Papirer, E., Fioux, P., Moguet, F., Tressaud, A., "Fluorination of Carbon Blacks. An X-Ray Photoelectron Spectroscopy Study. Part II. XPS Study of a Furnace Carbon Black treated with Gaseous Fluorine at Temperatures below 100 °C. Influence of the Reaction Parameters and of the Activation of the Carbon Black on the Fluorine Fixation," Carbon, 35(3), 371-388, 1997.

Sabbatini, L., Zambonin, P. G., "XPS and SIMS Surface Chemical Analysis of some Important Classes of Polymeric Biomaterials," Journal of Electron Spectroscopy and Related Phenomena, 81, 285-301, 1996.

Satchell, D. P. N., Satchell, R. S., "Mechanistic Aspects. Recent Developments Concerning Mechanisms of Acylation by Carboxylic Acid Derivatives," Supplement B: The Chemistry of Acid Derivatives, Vol. 2, John Wiley & Sons, Ltd., Hoboken, New Jersey, 747-802, 1992.

Saunders, J. H., Dobinson, F., "The Kinetics of Polycondensation Reactions," in Comprehensive Chemical Kinetics, Vol. 15, Bamford, C. H., Tippers, C. F. H., American Elsevier, New York, 473-581, 1976

Silverstein, R. M., Blassler, G., C., Morrill, T. C., Spectrometric Identification of Organic Compounds, 5th ed., John Wiley & Sons, Inc., Hoboken, NJ, 102-133, 1991.

Smith, M., March, J., "Aliphatic Substitution: Nucleophilic and Organometallic," in March's Advanced Organic Chemistry, 6th ed., Wiley-Interscience, Hoboken, New Jersey, 425-656, 2007.

Sutton, d., Durand, R., Shuai, X., Gao, J., "Poly(D,L-Lactide-co-Glycolide)/Poly(Ethylenimine) Blend Matrix System for pH Sensitive Drug Delivery," Journal of Applied Polymer Science, 100, 89-96, 2006.

Zetterlund, P. B., Weaver, W., Johnson, A. F., "Kinetics of Polyersterification: Modeling of the Condensation of Maleic Anhydride, Phthalic Anhydride, and 1,2-propylene Glycol," Polymer Reaction Engineering, 10(1-2), 41-57, 2002.

Zhang, H., He, Y., Li, S., Xiaobo, L, "Synthesis and Hydrolytic Degradation of Aliphatic Polyesteramides Branched by glycerol," Polymer Degradation and Stability, 88, 309-316, 2005.

Zhou, Y., Wy, G.-L., Zhou, R.-X., Liu, Z.-L., "Synthesis and Properties of Novel Aliphatic Poly(Carbonate-Esters)s," European Polymer Journal, 45, 1868-1872, 2009.

APPENDIX D

THERMAL DEGRADATION OF POLY(TRIMETHYLENE MALONATE)

D.1. Introduction

In addition to the biological and hydrolytic degradation mechanisms discussed in Chapters 1 through 5, polymers are subject to thermal degradation as well. A limited view of thermal degradation under real-world conditions is gained from studying the impact of elevated temperature without any increased pressure or shear. PHAs have been shown to exhibit increased rates of thermal degradation at the temperatures encountered during typical polymer processing [Harrison 2006, Bordes 2009, Zou 2009]. Thermal degradation of PHAs, such as PLA, have been shown to lead to decreases in Mw and mechanical properties and can be attributed to random main-chain scission [Carrasco 2006, Signori 2009]. Other minor pathways also contribute to thermal degradation, including depolymerization, oxidative degradation, and transesterification [Signori 2009, Carrasco 2006, Zou 2009, Liu 2006]. To fully understand the degradation effects due to thermal processing, chemical structure, molecular weight, and thermal properties need to be studied as a function of the elevated temperatures and pressures that are typically used in post-polymerization processing.

D.2. Experimental Materials and Methods

Reagents. 1,3-Propane diol (PDO, 98%, Sigma Aldrich), itaconic acid (IA, 99%, VWR), $AlCl_3$ catalyst (98%, Sigma Aldrich), tetrahydrofuran (Fisher Scientific, +99.9%, Optima grade), chloroform (VWR, 98%), and diethyl ether (VWR, >99%) were used as received.

Copolymerization. Polymerizations were performed in a 100 mL round bottom flask (charged with ~ 50 g monomer) for 4 h at 155 °C and 25 torr with mixing using a magnetic stir bar. Initially, a 1:100catalyst:monomer molar ratio with 1:1 alcohol:acid molar ratio was added to the reaction vessel.

Characterization. The polymer was characterized by transmission FTIR spectroscopy using a Thermo Electron 6700 instrument purged with dry air. Samples were either smeared or solution cast with THF onto potassium bromide crystals. A Waters gel permeation chromatograph (GPC) with RI detector, 4E and 5E (polystyrene-divinylbenzene, 4.6 x 300 mm) Styragel® columns in series, 0.3 mL/min THF effluent, and a 10-point polystyrene calibration was used to determine molecular weights and polydispersities.

Compression Molding. PTM was compression molded into a 2.54 x 2.54 x 0.316 cm sheet using a 15 ton press hydraulic press at the following conditions: 1,000 psi / 70 °C for 10 min, 10,000 psi / 70 °C for 10 min, 1,000 psi / 210 °C for 30 min, and 10,000 psi / 210 °C for 30 min.

D.3. Results and Discussion

FTIR spectra of compression molded PTM had the same peaks as the neat material (refer to Chapter 2) in the 1500 to 1850 cm^{-1} wavenumber range. The dimerized carboxylic acid carbonyl (1702 cm^{-1}), linear ester carbonyl (1726 cm^{-1}), and cyclic ester carbonyl (1749 cm^{-1}) were peak fit and the PHR calculated, using 1465 cm^{-1} as the reference peak. The carboxylic acid PHR, 1702 cm^{-1}, of compression molded PTM maintained a value of 1.0 ±0.2 that was statistically the same as neat PTM's PHR of 1.1 ±0.2, and the linear ester carbonyl (1726 cm^{-1}) PHR of compression molded PTM maintained a PHR of approximately 3.7 (Figure D.1). There was a significant decrease in the cyclic ester carbonyl (1749 cm^{-1}) PHR of compression molded PTM from 4.6 ±0.3 for neat PTM to approximately 1.5 (Figure D.1). FTIR did not provide insight into the degradation mechanism and only showed that the cyclic ester concentration decreases with compression molding.

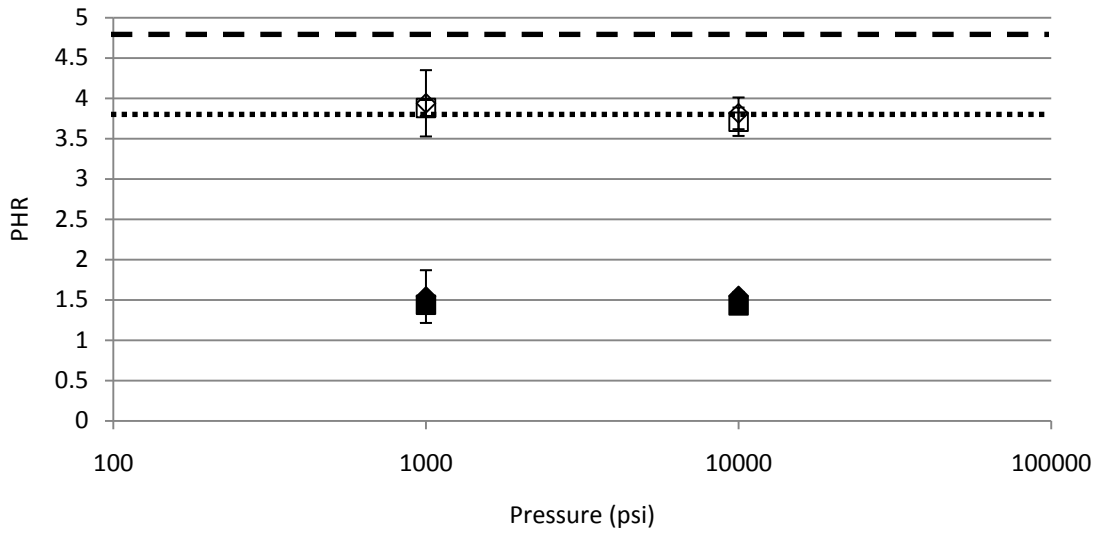

Figure D.1: Linear ester carbonyl, 1726 cm^{-1}, and cyclic ester carbonyl, 1749 cm^{-1}, PHR for PTM compression molded at 70 °C for 10 min (□, 1726 cm^{-1}; ■, 1749 cm^{-1}) and at 210 °C for 30 min (◇, 1726 cm^{-1}; ◆, 1749 cm^{-1}). The dotted line is the neat material's 1726 cm^{-1} PHR, and The dashed line is the neat material's 1749 cm^{-1} PHR.

To determine changes in molecular weight (Mw) and polydispersity index (PDI) of PTM due to compression molding, gel-permeation chromatography was used. The compression molded Mw increased from ~1,600 Da for neat PTM to ~2,200 Da after compression molding (Figure D.2). The increase in Mw can be contributed to PTM partially liquefying and flowing out of the mold making any conclusion about degradation effects on Mw difficult. The amount of PTM that liquefied was not quantified. With an increase in pressure from 1,000 to 10,000 psi, PTM's Mw decreased from ~2,200 to ~2,100 Da (Figure D.2). The decrease in Mw with increasing pressure could be contributed to degradation, but it is inconclusive due to material liquefying and flowing out of the mold during compression molding. The PDI did change from 1.8 ±0.2 for the neat PTM to 2.2 ±0.1 for compression molded PTM with no dependence on compression molding parameters. The increase in PDI indicates that the material was thermally degraded during compression molding.

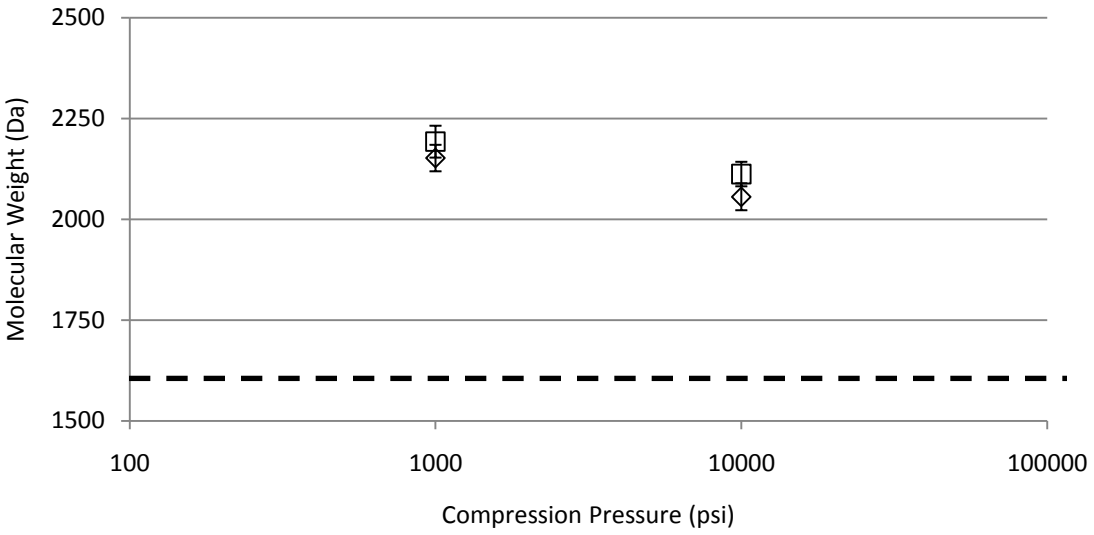

Figure D.2: Molecular weight dependence on pressure for compression molded PTM (□, PTM compression molded at 70 °C for 10 min; ◇, PTM compression molded at 210 °C for 30 min). Dashed line represents the GPC-determined Mw of neat PTM.

D.4. Conclusions

The increase in PDI indicates that PTM does thermally degrade during compression molding. Ester carbonyl PHR and PDI showed no dependence on compression molding pressure or temperature. Mw did show a dependence on pressure, but it cannot be clearly contributed to degradation due to material liquifying and leaving the mold during compression molding. Compression molding of PTM does significantly alter the chemical composition based on FTIR and Mw and PDI based on GPC, but more work is needed.

D.5. Recommended Future Work

Shearing at elevated temperatures and pressures is encountered during polymer extrusion, a common method of molding plastics. PTM extrusion needs to be attempted and PTM degradation during extrusion needs to be examined.

D.6. References

Bordes, P., Hablot, E., Pollet, E., Averous, L., “Effect of Clay Organomodifiers on Degradation of Polyhydroxyalkanoates,” Polymer Degradation and Stability, 94, 789-796, 2009.

Carrasco, F. Dionisi, D., Martinelli, A., Majone, M., “Thermal Stability of Polyhydroxyalkanoates,” Journal of Applied Polymer Science, 100, 2111-2121, 2006.

Harrison, G. M., Melik, D. H., “Application of Degradation Kinetics to the Rheology of Poly(hydroxyalkanoates),” Journal of Applied Polymer Science, 102, 1794-1802, 2006.

Liu, Z., Zou, Y., Li, W., Cao, G., Chen, W., “Kinetics of Thermo-Oxidative and Thermal Degradation of Poly(D,L-Lactide) (PDLLA) at Processing Temperature,” Polymer Degradation and Stability, 91, 3259-3265, 2006.

Signori, F., Coltelli, M.-B., Bronco, S., “Thermal Degradation of Poly(lactic acid) (PLA) and Poly(butylenes adipate-co-terephthalate) (PBAT) and Their Blends upon Melt Processing,” Polymer Degradation and Stability, 94, 74-82, 2009.

Zou, H., Yi, C., Wang, L., Liu, H., Zu, W., “Thermal Degradation of Poly(Lactic Acid) Measured by Thermogravimetry Couple to Fourier Transform Infrared Spectroscopy,” Journal of Thermal Analytical Calorimetry, 97, 929-935, 2009.

APPENDIX E

ALTERNATIVE MONOMER AND CATALYST RATIO

E.1. Introduction

For poly(trimethylene malonate) (PTM) and poly(trimethylene itaconate) (PTI), the alcohol to acid monomer ratio and the catalyst concentration were varied to determine which monomer ratio or catalyst concentration would produce a bioplastic with superior physical or mechanical properties. It has been shown that the use of an excess of alcohol monomer at the inception of the reaction leads to maximum yield [Fardet 1982, Bacaloglu 1998, Tserki 2006, Takasu 2006, Fu 2003, and Flory 1946]. The addition of the excess alcohol monomer is often necessary due to the volatilization of the alcohol monomer at elevated reaction temperatures and subsequent loss of the monomer [Fardet 1982, Bacaloglu 1998, Tserki 2006, Takasu 2006, Fu 2003, and Flory 1946]. In addition using increased alcohol molar concentration to compensate for loss of material during the reaction, the variation of alcohol molar concentration is used to control the molecular weight of the polymer [Fardet 1982, Kuchanov 2004]. To the knowledge of the author, there is a lack of research in exploring a wide range alcohol to acid molar concentration in polycondensation reactions. In addition to varying the monomer ratio, the catalyst ratio was varied to examine the effects on yield and molecular weight. In previous bioplastics syntheses, a 1:100 catalyst to monomer molar ratio was used to ensure a reaction. It is not uncommon to see catalyst concentrations at 1:1,000 to 1:10,000 in polymerizations that achieve high yields and moderate molecular weights through polycondensation reactions [Okada 2002, Jerome 2008, Sun 2002, Helminen 2003, John 1996, Storey 2001]. Lower catalyst concentrations minimize side reactions and are more economical [Kajiyama 2003, Moon 2000, Sodergard 1998, Dobrzynski 2002]. A high catalyst concentration can insure a faster reaction, but has a higher economic cost and can promote side reactions producing impurities and reducing the molecular weight and yield of the final product. An examination of the alcohol to acid monomer and catalyst to monomer molar ratios for PTM and

PTI is necessary in order to optimize these polycondensation reactions for yield and molecular weight.

E.2. Experimental Materials and Methods

Reagents. 1,3-Propane diol (PDO, 98%, Sigma Aldrich), $AlCl_3$ catalyst (98%, Sigma Aldrich), chloroform (VWR, 98%), and diethyl ether (VWR, >99%) were used as received.

Copolymerization of 1,3-propanediol (PDO), malonic acid (MA), and itaconic acid (IA). Polymerizations were performed in a 100 mL round bottom flask (~ 50 g monomer) for 4 h (PTM) or 16 h (PTI) at 155 °C and 25 torr with mixing using a magnetic stir bar. A 1:100, 1:1,000, and 1:10,000 catalyst:monomer molar ratio with 1:1 alcohol:acid molar ratio for PTM polymerizaiton. Alcohol:acid molar ratio of 0.9:0.1, 0.75:0.25, 0.5:0.5, 0.25:0.75 and 0.1:0.9 with 1:100 catalyst:monomer molar ratio for both PTM and PTI polymerization.

Polymer separation. Excess monomer and catalyst were removed from the reaction products by dissolving in chloroform and then poured into diethyl ether. Precipitated polymer was then filtered using Whitman (grade 40) filter paper. For each reaction, this separation procedure was repeated until precipitated polymer could no longer be visually identified. The filtered polymer was dried in a vacuum oven at 15 torr and 20 °C for 24 h and then weighed.

Characterization. The PTM polymers were characterized by transmission FTIR spectroscopy using a Thermo Electron 6700 instrument purged with dry air. PTI polymers were characterized by diffused reflectance infrared Fourier transform (DRIFT) spectroscopy with a Pike EasyDiff accessory and samples mixed with KBr powder at 3 wt.%. Gravimetric product yields for both PTM and PTI polymers were calculated using the limiting monomer to determine theoretical yields based on complete conversion. The recovered polymer weight was divided by the theoretical weight and then converted to percent yield. A Waters gel permeation

chromatograph (GPC) with RI detector, 4.6 x 300 mm 4E and 5E Styragel® columns, 0.3 mL/min THF effluent, and a 10-point polystyrene calibration was used to determine molecular weights and polydispersities.

E.3. Results and Discussion

E.3.1. Poly(trimethylene malonate) (PTM)

The alcohol to acid molar concentration's affect on yield was in-line with literature. Maximum yields were obtained between 0.5 to 0.75 alcohol molar fraction with significant decreases in yield occurring at low (0.1, 0.25) and high (0.9) alcohol molar fractions (Figure E.1). As expected, optimized yields of PTM required equal alcohol to acid monomer molar ratios or an excess of alcohol.

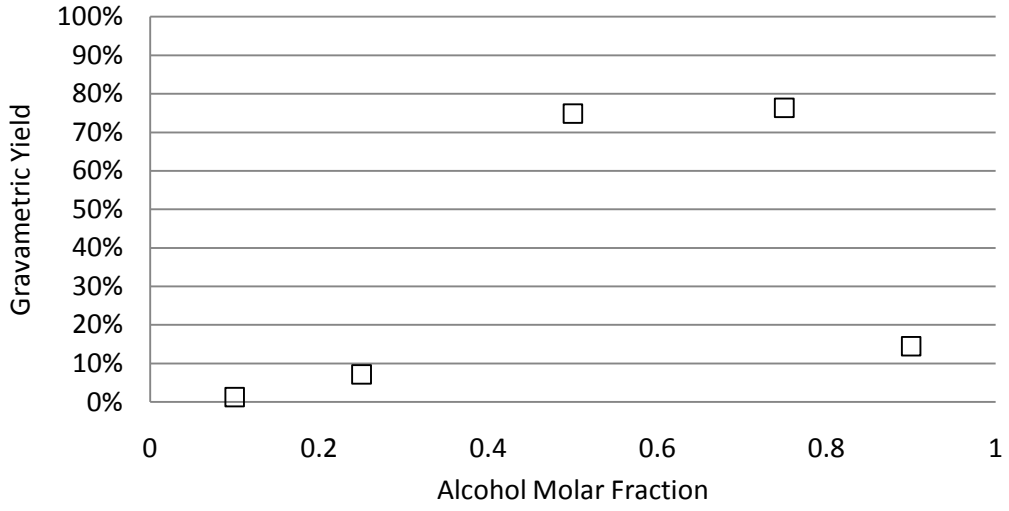

Figure E.1: Effect of alcohol molar fraction catalyst concentration on gravimetric yield for PTM (155 °C, 4 h, 1:100 catalyst:monomer molar ratio). The data presented is single data points.

Catalyst concentration also showed a dramatic effect on PTM yields (Figure E.2). As the catalyst:monomer molar ratio was decreased from 1:100 to 1:1,000, the yield decreased by ~ 70%. There is a significant decrease in catalyst effectiveness with decrease in catalyst concentration. This was not unexpected as the catalyst is deactivated over time during the reaction, so a higher catalyst concentration allows the reaction to proceed for longer times. The yield did increase from 1:1,000 to 1:10,000 for an unknown reason that was not further investigated. It should be noted that a 1:10 catalyst:monomer molar ratio reaction was attempted. It was a violent reaction and tripped the safety pressure release on the reaction vessel. The reaction vessel attained positive pressure at 1:10 concentration as the vacuum could not be maintained.

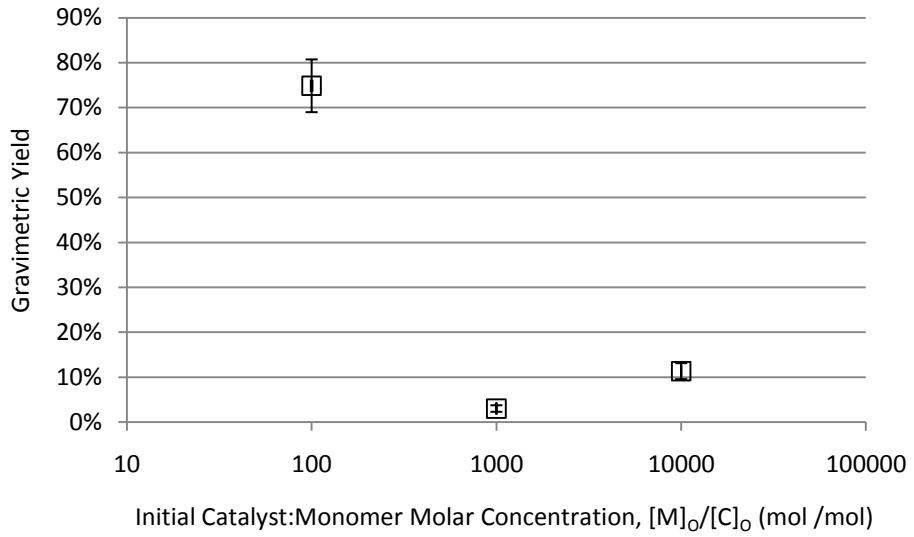

Figure E.2: Catalyst:monomer molar concentration affect on PTM (155 °C, 4 h) gravimetric yield.

E.3.2. Poly(trimethylene itaconate) (PTI)

The alcohol molar fraction was varied from 0.1 to 0.9 with gravimetric yields varying from ~22 to ~77 wt.% as seen in Figure E.3. The maximum yield was achieved at 0.5 alcohol molar fraction. It was expected that the maximum yield would be found near 0.5 alcohol molar

fraction, but it was expected that yield would remain near the maximum yield with 0.75 alcohol molar fraction like PTM as the higher alcohol concentration would facilitate polycondensation.

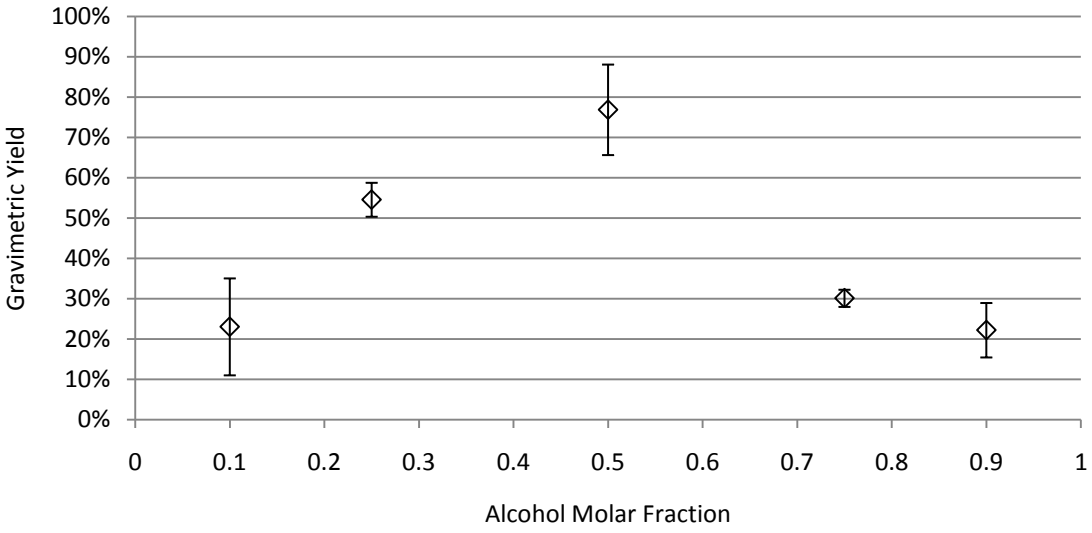

Figure E.3: Effect of alcohol molar fraction catalyst concentration on gravimetric yield for PTI (155 °C, 16 h, 1:100 catalyst:monomer molar ratio). Bars indicate 95% confidence intervals.

Diffused reflectance infrared Fourier transform (DRIFT) spectroscopy was performed on one sample from each alcohol molar fraction. The spectra can be seen in Figure E.4. Seven peaks/regions (Figure E.4) showed significant change: (1) ~3676 cm^{-1}, carboxylic acid free O-H stretch; (2) 3600 – 3000 cm^{-1}, alcohol O-H stretch; (3) 3000 – 2750 cm^{-1}, C-H stretch; (4) 2750 – 2450 cm^{-1}, ketone and aldehyde O-H stretch; (5) ~1720 cm^{-1}, carbonyl stretch; (6)~1580 cm^{-1}, caboxylate anion stretch; (7) 1100 – 950 cm^{-1}, primary alcohol C-O stretchand carboxylic acid C-O stretch [Dell'Erba 1997, Silverstein 1991, Dean 1992, Caitker 2000, Sutton 2006, Gulmine 2006, Zhou 2009]. As the alcohol molar fraction decreases, the peaks related to IA's carboxylic acid increased or shifted, peaks (1), (5), and (7). The carboxylic acid O-H stretch (1) becomes prominent with higher acid content, the carbonyl (5) shifts to a lower wavenumber as the

carboxylic acid of IA increases in concentration, and the carboxylic acid C-O stretch (7)shifts to a lower wavenumber as it goes from being dominated by PDO's C-O to IA's carboxylic acid C-O. The carboxylate anion carbonyl stretch (6) shifts to a higher wavenumber with decreaseing alcohol molar fraction. This shift is theorized to be due to increased intermolecular forces because of higher concentration of carboxylic acid. It appears that the C-H stretch increases with increasing alcohol molar fraction, but without peak height ratio, this cannot be confirmed. With increasing acid molar fraction, it does appear that ketone and aldehyde functional groups are being formed by the appearance of peaks in region (4). It is known that aldehydes and ketones can form under acidic conditions, though the exact reaction mechanism that is occurring during PTI polymerization is not known [Smith 2007]. The functional groups in PTI can be controlled by varying the alcohol molar fraction.

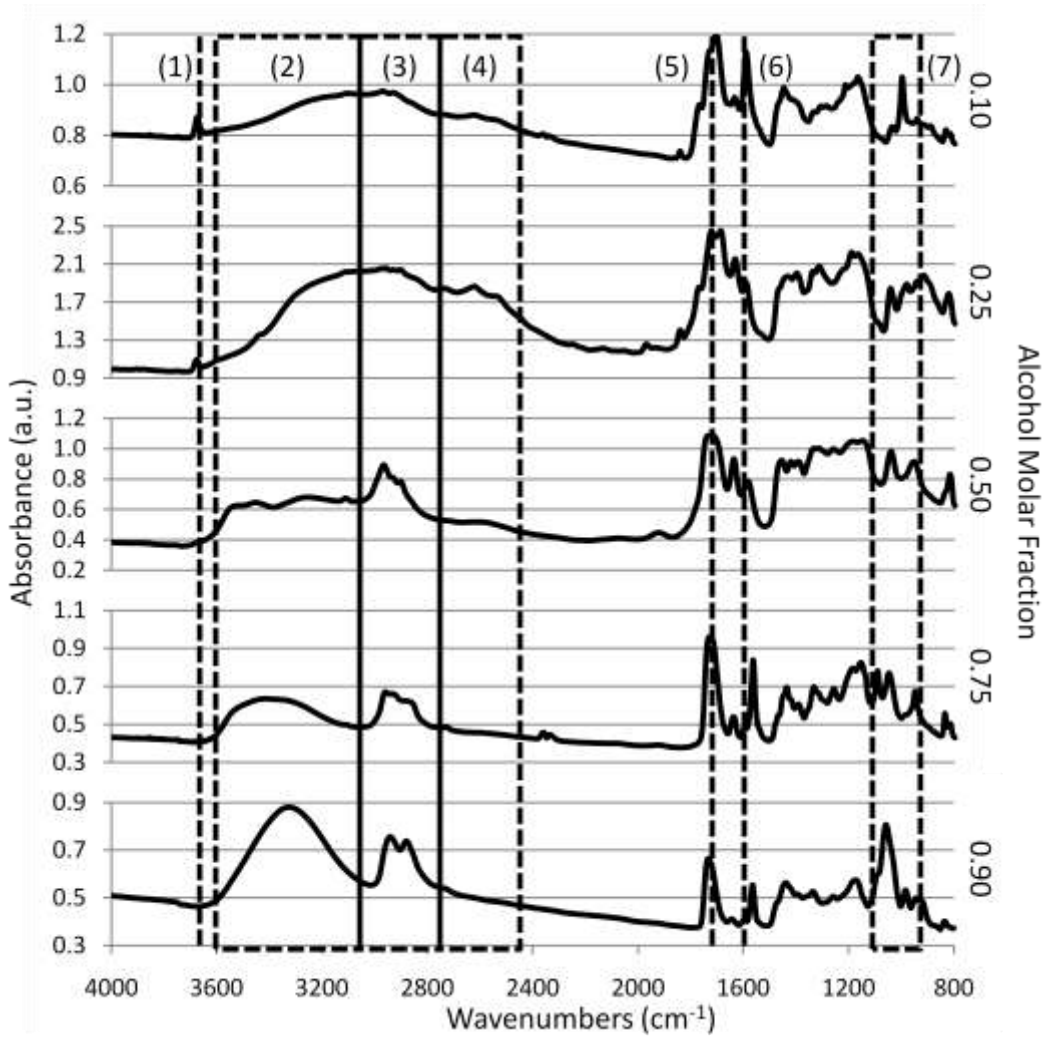

Figure E.4: Representative PTI DRIFT spectrum with seven peaks/regions showing significant change: (1) ~3676 cm^{-1}, carboxylic acid free O-H stretch; (2) 3600 – 3000 cm^{-1}, alcohol O-H stretch; (3) 3000 – 2750 cm^{-1}, C-H stretch; (4) 2750 – 2450 cm^{-1}, ketone and aldehyde O-H stretch; (5) ~1720 cm^{-1}, carbonyl stretch; (6)~1580 cm^{-1}, caboxylate anion stretch; (7) 1100 – 950 cm^{-1}, primary alcohol C-O stretch.

GPC was attempted on all PTI alcohol molar fraction samples. PTI with 0.25 and 0.1 alcohol molar fraction was only slightly soluble in tetrahydrofuran, and the material that was solubilized was below significantly 450 Da, the GPC calibration lower limit. The Mw of 0.25 and 0.1 alcohol molar fraction material could not be determined due its low Mw. The lack of solubility is likely due to increased branching and cross-linking of PTI with increased IA concentration that could not be quantified with equipment available at MSU. As the alcohol

molar fraction increased from 0.5 to 0.9, the Mw decreased from ~1300 Da to ~610 Da with the yield decreasing from 77 to 22 wt.%. With increasing alcohol molar fraction, it was expected that the yield and Mw would decrease because there was a lower concentration of acid groups for the alcohol groups to react with and form ester bonds.

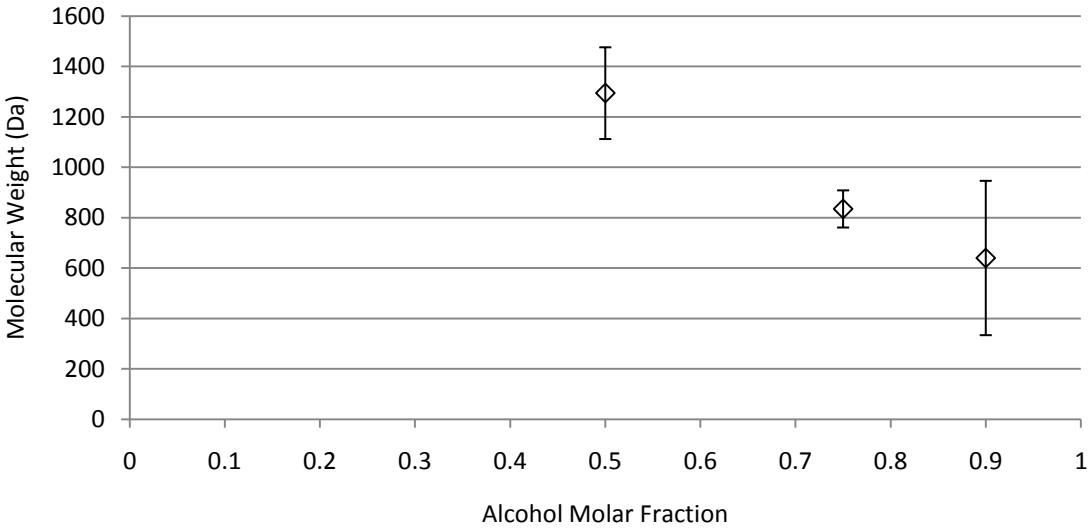

Figure E.5: PTI Mw versus alcohol molar fraction (155 °C, 16 h, $AlCl_3$) with 95% confidence intervals.

E.4. Conclusions

PTM gravimetric yield showed a strong dependence on alcohol molar fraction and catalyst:monomer molar concentration. An alcohol molar fraction from 0.5 to 0.75 and 1:100 catalyst:monomer molar concentration should be used to achieve maximum yield. For PTI, a alcohol molar fraction of 0.5 should be used to achieve maximum gravimetric yield and maximum detectable Mw. With increasing alcohol molar fraction, PTI chemical structure significantly changes, and PTI branching and cross-linking makes it partially insoluble in tetrahydrofuran.

E.5. Recommended Future Work

Chemical structure and Mw need to be determined for PTM with varied alcohol molar fraction and catalyst:monomer molar concentration. For PTI, catalyst:monomer molar concentration needs to be varied to determine if a lower catalyst concentration could be used to achieve the same chemical struture, Mw, and gravimetric yield.

E.6. References.

Bacaloglu, R., Fish, M., Biesiada, K., "Kinetics of Polyesterification of Adipic Acid," Polymer Engineering and Science, 36(6), 1014-1022, 1996.

Catiker, E., Gumusderelioglu, M., Guner, A., "Degradation of PLA, PLGA homo- and Copolymers in the Presence of Serum Albumin: A Spectroscopic Investigation," Polymer International, 49, 728-734, 2000.

Dean, J. A., Lange's Handbook of Chemistry, 14th ed., McGraw-Hill, Inc., 7.42-7.71, 1992.

Dell'Erba, R., Martuscelli, E., Musto, P., Ragosta, G., "Unsaturated Polyester Resins: a Study of the Mechanism and kinetics of the Curing Process by FTIR Spectroscopy," Polymer Networks and Blends, 7(1), 1-11, 1997.

Dobrzynaski, P., Kasperczyk, J., Janeczek, H., Bero, M., "Synthesis of Biodegradable Glycolide/L-Lactide Copolymers using Iron Compounds as Initiators," Polymer, 43, 2595-2601, 2002.

Flory, P. J., "Fundamental Principles of Condensation Polymerization," Chemical Review, 39, 137-197, 1946.

Fradet, A., Marechal, E., "Study on Models of Double Bond Saturation During the Synthesis of Unsaturated Polyesters," Makromolekulare Chemie, 183, 319-329, 1982.

Fu, H., Kulshrestha, A. S., Gao, W. Gross, R. A., "Physical Characterization of Sorbitol or Glycerol Containing Aliphatic Copolyesters Synthesized by Lipase-Catalyzed Polymerization," Macromolecules, 26, 9804-9808, 2003.

Gulmine, J. V., Akcelrud, L., "FTIR Characterization of Aged XLPE," Polymer Testing, 25, 932-942, 2006.

Helminen, A. O., Korhonene, H., Seppala, J. V., "Crosslinked Poly(ester anhydride)s based on Poly(ε-caprolactone) and Polylactide Oligomers," Journal of Polymer Science: Part A: Polymer Chemistry, 41, 3788-3797, 2003.

Jerome, C., Lecomte, P., "Recent Advances in the Synthesis of Aliphatic Polyesters by Ring-Opening Polymerization," Advanced Drug Delivery Reviews, 60, 1056-1076, 2008.

John, G., Tsuda, S., Morita, M., "Synthesis and Modification of New Biodegradable Copolymer: Serine/Glycolic Acid Based Copolymers," Journal of Polymer Science Part A: Polymer Chemistry, 35(10), 1901-1907, 1996.

Kajiyama, t., Taguchi, T., Kobayashi, H., Kataoka, K., Tanaka, J., "Synthesis of High Molecular Weight Poly(α,β-malic acid) for Biomedical use by Direct Polycondensation," Polymer Degradation and Stability, 81, 525-530, 2003.

Kuchanov, S., Slots, H., Stroeks, A., "Development of a Quantitative Theory of Polycondensation," Progress in Polymer Science, 29, 563-633, 2004.

Moon, S, I,. Lee, C. W., Miyamtot, M., Kimura, Y. Melt Polycondensation of L-Lactic acid with Sn(II) Catalysts Activated by Various Proton Acids: A Direct Manufacturing Route to High Molecular Weigh Poly(L-lactic acid), Journal of Polymer Science, Part A: Polymer Chemistry, 38, 1673-1679, 2000.

Okada, M., Okada, Y., Tao, A., Aoi, K., "Biodegradable Polymers Based on Renewable Resources: Polyesters Composed of 1,4:3,6-Dianhydroheitol and Aliphatic Dicarboxylic Acid Units," Journal of Applied Polymer Science, 62, 2257-2265, 1996.

Silverstein, R. M., Blassler, G., C., Morrill, T. C., Spectrometric Identification of Organic Compounds, 5th ed., John Wiley & Sons, Inc., Hoboken, NJ, 102-133, 1991.

Smith, M., March, J., "Aliphatic Substitution: Nucleophilic and Organometallic," in March's Advanced Organic Chemistry, 6th ed., Wiley-Interscience, Hoboken, New Jersey, 425-656, 2007.

Sodergard, A., Stolt, M., "Ring-Opening Polymerization of L-lactide by Means of Different Iron Compounds," Macromolecular Symposium, 130, 393-402, 1998.

Storey, R. F., Sherman, J. W., "Novel Synthesis of (Carboxylic Acid)-Telechelic Poly(ε-Caprolacton)," Polymer Preprints, 42(2), 2001.

Sun, H., Chen, S., Yao, Y., Shen, Q., Yu, K., "Homoleptic Lanthanide Metallocenes and their Derivatives: Syntheses, Structural Characterization and their Catalysis for Ring-Opening Polymerization of ε-Caprolactone," Applied Organometallic Chemistry, 20, 310-314, 2006.

Sutton, d., Durand, R., Shuai, X., Gao, J., "Poly(D,L-Lactide-co-Glycolide)/Poly(Ethylenimine) Blend Matrix System for pH Sensitive Drug Delivery," Journal of Applied Polymer Science, 100, 89-96, 2006.

Takasu, A., Oishi, Y., Iio, Y., Inai, Y., Hirabayashi, Y., "Synthesis of Aliphatic Polyesters by Direct Polyesterificaiton of Dicarboxylic Acids with Diols under Mild conditions Catalyzed by Reusable Rare-Earth Triflate," Macromolecules, 36, 1772-1774, 2003.

Tserki, V., Matzinos, P., Pavlidou, E., Panayiotou, C., "Biodegradable Aliphatic Polyesters. Part II. Synthesis and Characterization of chain Extended Poly(Butylene Succinate-co-butylene Adipate)," Polymer Degradation and Stability, 91, 377-384, 2006.

Zhou, Y., Wy, G.-L., Zhou, R.-X., Liu, Z.-L., "Synthesis and Properties of Novel Aliphatic Poly(Carbonate-Esters)s," European Polymer Journal, 45, 1868-1872, 2009.

APPENDIX F

PTM KINETIC MODELING

F.1. Introduction

Flory provided the first major contribution for the probabilistic modeling of polycondensation reactions based on step growth polymerization conditions. His work is based on the general kinetic equation

$$-\frac{d[COOH]}{dt} = k[COOH]^m[OH]^n$$

where t = time, k = reaction constant, m & n = reaction order, [COOH] = concentration of carboxylic acid groups, and [OH] = concentration of alcohol groups [Flory 1953 79-82, Fradet 1982, Odian 1991]. When [COOH] = [OH] Flory's general kinetic equation for polycondensation reaction becomes

$$-\frac{dC}{dt} = k_d C^d$$

where C = concentration of end groups, d = reaction order, and k_d = reaction constant. Flory then defined the extent of reaction, p, as

$$p = \frac{N_0 - N}{N_0}$$

where N_O = initial concentration of end groups and N = final concentration of end groups [Flory 1953 79-82, Fradet 1982, Odian 1991]. Flory's model failed to take into account the loss of water. Szabo-Rathy later showed that if water loss is not accounted for that the rate constant can be in error by 15 - 35 % [Szabo-Rathy 1971].

The use of a simple model that takes into account the dominant reactions usually suffices to describe the system. A modification of Flory's fundamental principle by Szabo-Rethy accounts for water and increases the model's accuracy [Fradet 1982]. In Szabo-Rethy's modified Flory model

$$\overline{DP_n} = \frac{1}{1-p'} = \frac{\overline{M_n} - 1}{mean\ \ segment\ \ weig\ ht}$$

where DP_n = degree of polymerization based on number average molecular weight and M_n = number average molecular weight and

$$p' = 1 - \left[\frac{1}{(1 - 0.018C_0)\frac{1}{1-p} + 0.018C_0} \right]$$

where p‘ = conversion corrected for water and C_0 = initial concentration of functional groups [Szabo-Rathy 1971].

Taking Flory’s general kinetic equation and integrating over time produces

$$(n-1){C_0}^{n-1} k_n t = \left[\frac{1}{1-p}(1 - 0.018C_0) + 0.018C_0 \right]^{n-1} - 1 .$$

The kinetic rate constant, k_n, is defined by the Arrhenius equation (Equation F.7) with A = pre-exponential factor, E_a = activation energy, R = gas constant, and T = temperature (in Kelvin).

$$k_n = Ae^{-E_a / RT}$$

Using Flory’s modified equation and Arrhenius equation, the reaction order, pre-exponential factor, and activation energy can be determined for PTM copolymerizaiton using Excel® and Excel®’s Solver to minimize squared sum of the residuals by varying A, E_a, and n.

F.2. Results and Discussion

Flory’s modified equation and Arrhenius equation was fit to the experimental data of extent of reaction (p’) vs reaction time and temperature and the reaction order was found to be 2 with A and E_a 8.5 x 10^3 ±0.4 x 10^3 L·mol^{-1}·s^{-1} and 15.005 ±0.001 kJ·mol^{-1}, respectively. The

squared sum of the residuals from fitting this data was 0.012. Flory showed that if the reaction order was 3 the system was uncatalyzed, and if the system was catalyzed, the reaction order would be 2 [Flory 1952]. Since for our system the reaction order found to be 2, it shows that aluminum chloride catalyzed the system. Furthermore, the experimental A and E_a vales are in the same range ($A = 2 \times 10^2$ to 6×10^6 $L \cdot mol^{-1} \cdot s^{-1}$, Ea = 10 to 80 $kJ \cdot mol^{-1}$) as other polycondensation reactions of linear, saturated diols and diacids [Fradet 1982].

Experimental and theoretical extent of reaction (p') never varied more than 5% from each other, as shown in Figures F.1 and F.2, over a range of reaction temperature (125 to 175 °C) and reaction time (2 to 16 h) with aluminum chloride at 1:100 catalyst:monomer molar ratio and 1:1 acid:alcohol monomer molar ratio. The theoretical extent of reaction was consistently greater than the experimental extent of reaction and is likely due to a failure to account for the reverse reaction or side reactions.

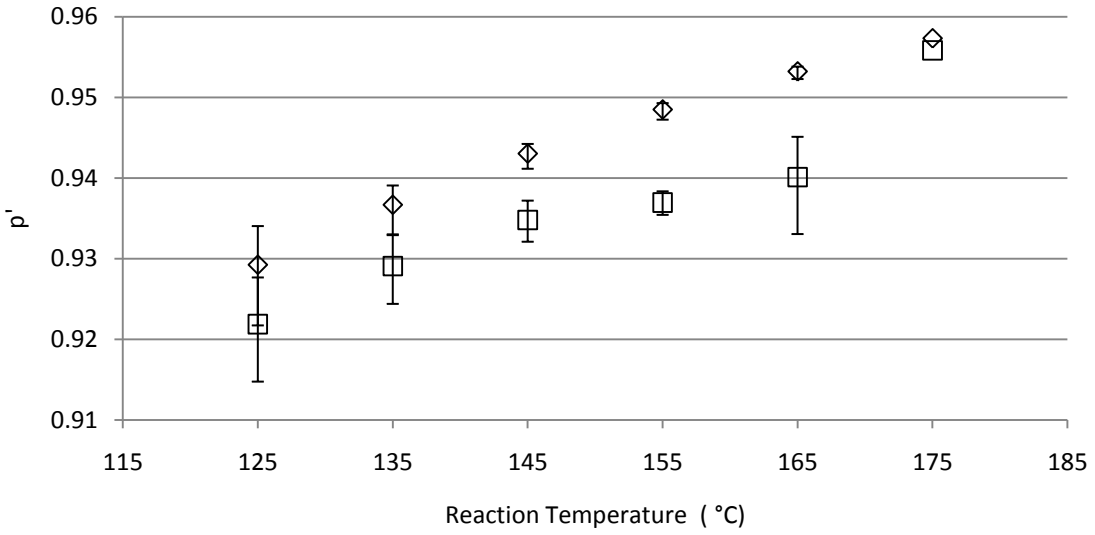

Figure F.1: Theoretical (◇) using modified Flory's extent of reaction and general kinetic equation and experimental (□) extent of reaction versus reaction temperature for PTM made with aluminum chloride at 155 °C with bars representing 95% confidence interval.

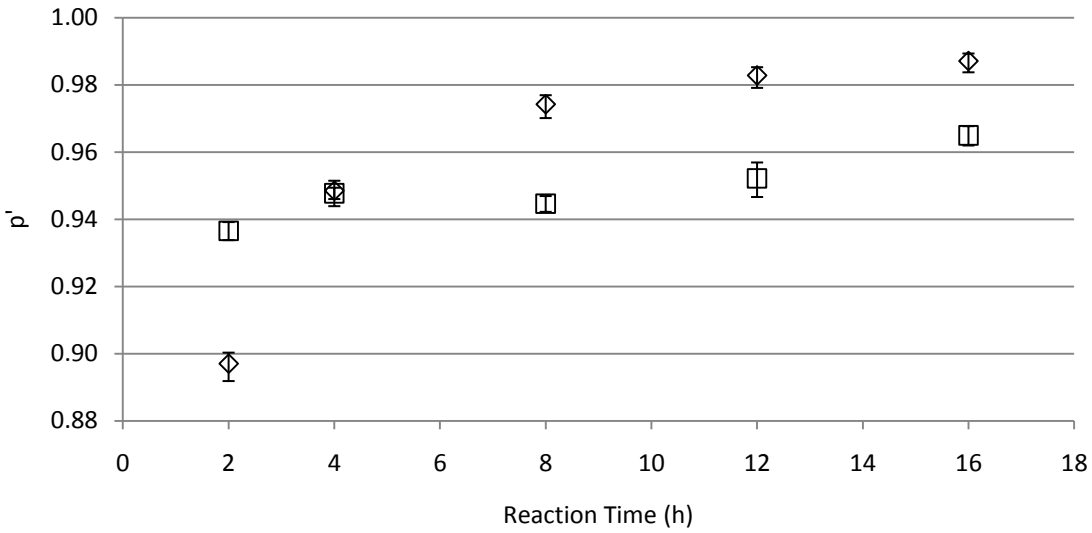

Figure F.2: Theoretical (◇) using modified Flory's extent of reaction and general kinetic equation and experimental (□) extent of reaction versus reaction time for PTM made with aluminum chloride at 155 °C with bars representing 95% confidence interval.

F.3. Conclusions

The polymerizaiton of 1,3-propanediol and malonic acid are well modeled by Flory's kinetic models that were modified by Szabo-Rathey for water loss of water and polycondensation. Using this modified polycondensation model, PTM can be shown to be catalyzed by aluminum chloride and follow 2nd order reaction kinetics. The values of A and Ea are similar to other polycondensation reactions of linear, saturated diols and acids.

F.4. Recommended Future Work

The model used can be extended to include the reverse reaction in order to increase accuracy, and it can be modified to include parameters for branching in order to model PTI. The use of programs that allow for a higher level of mathematics, would allow for a more rigious model that includes infinite sums or partial differential equations.

F.5. References

Flory, P. J., Principles of Polymer Chemistry, Cornell University, 29-36, 1953.

Fradet, A., Marechal, E., "Kinetics and Mechanisms of Polyesterification I. Reactions of Diols with Acids," Advances in Polymer Science, 43, 51-142, 1982.

Odian, G., Principles of Polymerization, 3rd ed., John Wiley & Sons, New York, 41-197, 1991.

Szabo-Rethy E., "Comment on the Calculation Methods of Kinetics of Polyesterification Reactions," European Polymer Journal, 7, 1485-1499, 1971.

APPENDIX G

PTM ATOMIC FORCE MICROSCOPY

G.1. Introduction

To examine the surface of PTM, atomic force microscopy (AFM) was attempted in both air and water environments.

G.2. Experimental Methods and Materials

PTM (155 °C, 4 h, $AlCl_3$) was synthesized as described in Chapter 2 and compression molded (1,000 psi, 30 °C, 10 min) following the procedure in Chapter 4. A Veeco Icon AFM instrument with ScanAsyst and Peak Force Tapping™ was used with a silicon nitride cantilevers with silicon tips, k~ 0.4 N/m and tip radius = 5-10 nm. Technique used was Peak Force TappingMode (ScanAsyst) with Quantitative Nanomechanical Mapping (QNM)..

G.3. Results and Discussion

A dry PTM sample was scanned using Peak Force Tapping™ and showed that PTM had an uneven surface (Figure G.1), with a maximum height differential of 600 nm over a 25 μm^2 area. A drop of distilled water was then placed between the sample and the scanning tip and scanning resumed. There was difficulty in capturing an AFM image of PTM in a water environment due to the continuous swelling of PTM during 30-45 minutes of scanning (Figure G.2). The behavior of the PTM sample in an aqueous environment showed the material to by hydroscopic and to swell significantly over a 30-minute time span. The swelled PTM sample still showed a relatively rough surface structure.

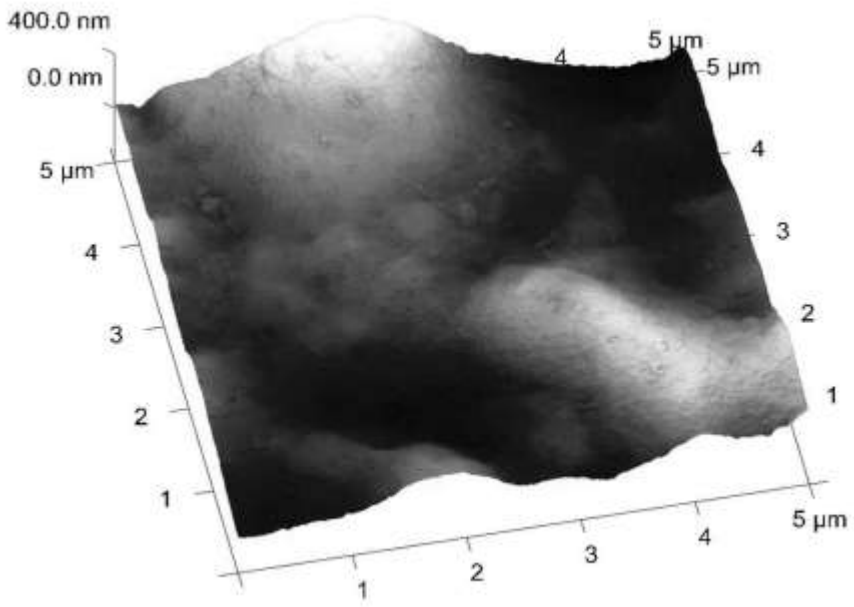

Figure G.1: Peak Force Tapping™ AFM scan of a compression molded PTM (155 °C, 4 h, $AlCl_3$) coupon in an air environment.

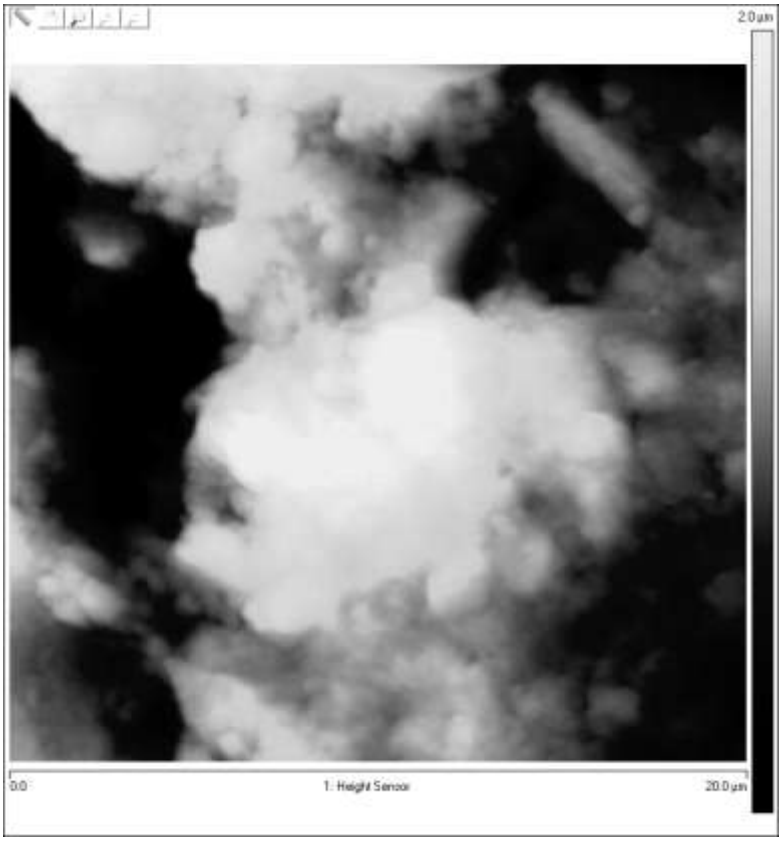

Figure G.2: AFM height scan (20 x 20 µm) of PTM (155 °C, 4 h, $AlCl_3$) swollen with water.

G.4. Conclusions

PTM has an uneven surface in both the dry and wet states and is hygroscopic. AFM showed that PTM is hygroscopic, and it is theorized with this information that PTM is absorbing water to replace the mass lost via degradation, resulting in no gross weight change over the 10,000 min duration of the degradation study.

G.5. Recommended Future Work

A study of PTM swelling needs to be performed to determine the weight and volume change of PTM when exposed to water.